COMPREHENSIVE FUNCTIONAL INVESTIGATION OF THE HUMAN TRANSLOCATOR PROTEIN 18 KDA (TSPO) IN A NOVEL CELLULAR KNOCKOUT MODEL – ON THE TRAIL OF THE ENIGMA

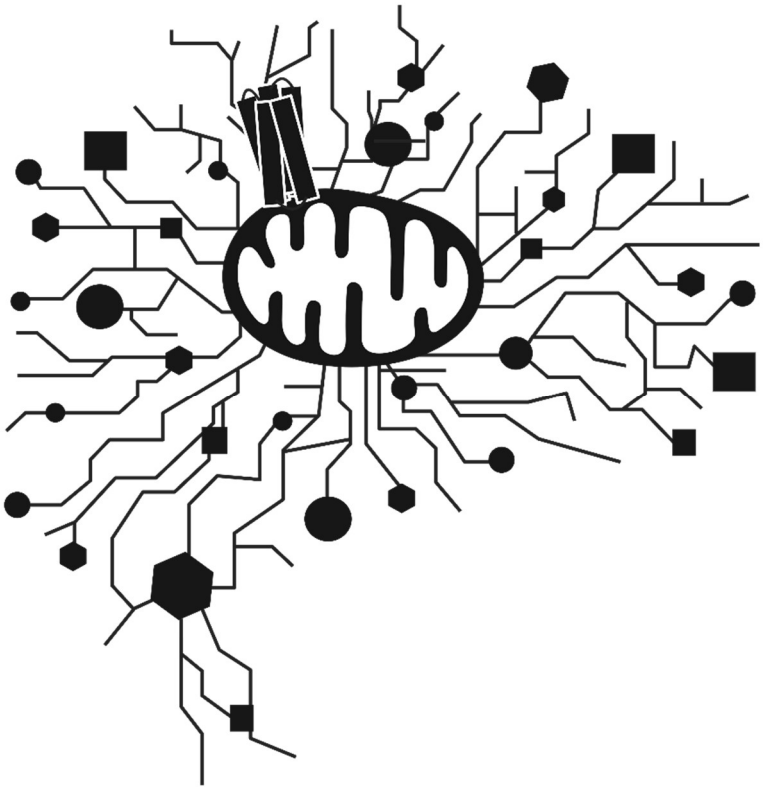

DISSERTATION

ZUR ERLANGUNG DES DOKTORGRADES

DER NATURWISSENSCHAFTEN (DR. RER. NAT.)

DER FAKULTÄT FÜR BIOLOGIE UND VORKLINISCHE MEDIZIN

DER UNIVERSITÄT REGENSBURG

vorgelegt von

Stefanie Bader

aus

Eckernförde

im Jahr

2023

Cover logo inspired by Gulcin Pekkurnaz, UCSD

Das Promotionsgesuch wurde eingereicht am:
06. Juli 2023

Die Arbeit wurde angeleitet von:
Prof. Dr. rer. nat. Christian Wetzel

Unterschrift:

Table of contents

Abstract

The translocator protein 18 kDa (TSPO), initially characterised in 1977 as a peripheral binding receptor for benzodiazepines, is an evolutionarily conserved outer mitochondrial protein ubiquitously expressed in almost all cell types, albeit in a tissue- and cell-specific manner. Physiological expression within the brain is relatively weak. However, pathological conditions, such as Alzheimer's disease, multiple sclerosis, and cancer, can lead to upregulated TSPO expression, implying a role for TSPO in the pathophysiology of neurodegenerative, neuroinflammatory, and neoplastic diseases (Ammer et al., 2020; Rupprecht et al., 2010). Although TSPO is considered a multifunctional protein associated with various aspects of mitochondrial physiology, its precise role in mitochondrial homeostasis and its mechanisms of action remain elusive.

This study aimed to analyse the effect of TSPO on the regulation of mitochondrial metabolism in a human cellular model. Therefore, using the CRISPR/Cas9 technology, TSPO knockout (KO) and control (CTRL) variants of human induced pluripotent stem cells (hiPSCs), reprogrammed from primary adult skin fibroblasts, were generated.

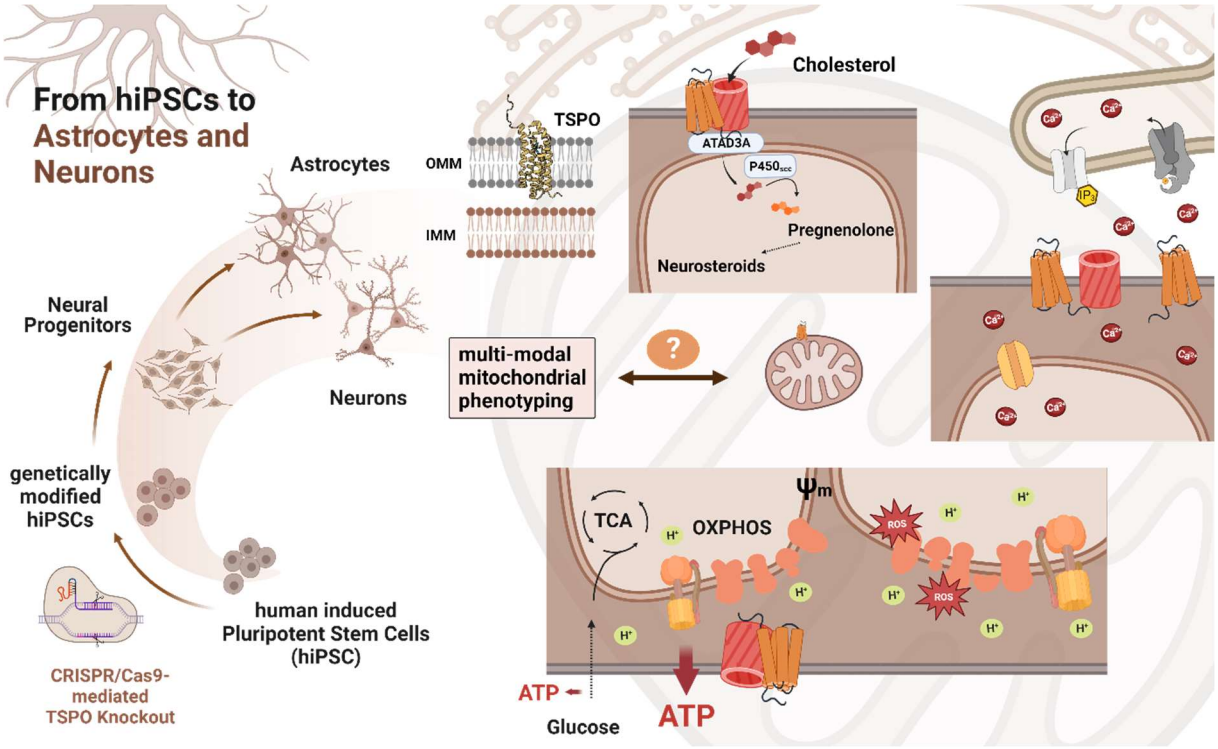

Figure 1: Graphical abstract

In a multimodal phenotyping approach, parameters of cellular and mitochondrial functions were investigated and compared in neural progenitor cells, astrocytes, and neurons differentiated from hiPSC CTRL and KO cell lines. In those different cell types, the bioenergetic profile, as well as the mitochondrial membrane potential (MMP) and the Ca^{2+} homeostasis was assessed. Furthermore, oxidative stress, mitochondrial content, and cell size were evaluated.

Functional characterisation of TSPO KO cells, as compared to CTRL cells, revealed altered Ca^{2+} levels in the cytosol and mitochondria, a depolarised MMP, and increased levels of reactive oxygen species (ROS), indicating an unbalanced redox state and oxidative stress. While the mitochondrial content seemed to be unchanged, the mitochondrial DNA copy number was significantly decreased in mitochondria devoid of TSPO. Notably, TSPO deficiency was accompanied by reduced expression of the voltage-dependent anion channel (VDAC). Respirometry experiments favoured the possible role of TSPO in regulating the bioenergetic status of the cell, as mitochondrial respiration and glycolysis were significantly reduced along with the deletion of TSPO protein expression. Interestingly, across all cell types, TSPO-KO cells were significantly smaller in size.

Moreover, a significant decrease in the protein expression of TSPO and the TSPO-associated protein VDAC1 in a human cellular model of depression was observed, suggesting a potential link between TSPO and the pathomechanism of mitochondrial dysfunction in depression.

Taken together, these findings point consistently towards the impairment of mitochondrial function in TSPO KO cells, contributing to the understanding of the multifaceted role of TSPO and setting the stage for further investigations to unravel the underlying mechanisms and its involvement in various physiological and pathological processes.

Zusammenfassung

Das Translokatorprotein 18 kDa, erstmals 1977 als peripherer Benzodiazepin-Rezeptor beschrieben, ist ein evolutionär konserviertes Protein der äußeren Mitochondrienmembran. Obwohl ubiquitär in allen Geweben exprimiert, variieren die Expressionslevel gewebe- und zellspezifisch. Die physiologische Expression im Gehirn ist vergleichsweise schwach. Neurodegenerative, neuroinflammatorische, sowie neoplastische Erkrankungen können jedoch einen pathologischen Anstieg der TSPO-Expression zur Folge haben, was auf eine TSPO-spezifische Rolle in der Pathophysiologie dieser Krankheiten hinweist. Wenngleich TSPO als Schlüsselprotein funktional mit verschiedenen Aspekten des mitochondrialen Metabolismus in Verbindung gebracht wird, sind die genauen Funktionen und Wirkmechanismen von TSPO weiterhin unklar.

Im Rahmen dieser Arbeit sollte der Einfluss von TSPO auf die Regulation des mitochondrialen Metabolismus in einem humanen Zellmodell analysiert werden. Dazu wurde ein CRISPR/Cas9-vermittelter TSPO-Knockout in hiPSCs generiert, die aus primären adulten Fibroblasten reprogrammiert wurden. Um eine multimodale Analyse eines klar definierten TSPO-defizienten Phänotyps in verschiedenen Zellarten zu ermöglichen, wurden neurale Vorläuferzellen, Astrozyten und Neurone aus TSPO-Knockout und Kontroll-Stammzellen differenziert. Es wurde das bioenergetische Profil, sowie das MMP und die Ca^{2+} Homöostase untersucht. Zudem wurden ROS Level, Mitochondriengehalt und die Zellgröße analysiert.

Die funktionale Charakterisierung der TSPO-KO Zellen zeigte im Vergleich zu Kontroll-Zellen veränderte mitochondriale und zytosolische Ca^{2+}-Spiegel, ein depolarisiertes MMP und Hinweise auf oxidativen Stress innerhalb der Zellen. Während die Anzahl an Mitochondrien unverändert erschien, konnte eine verringerte mitochondriale DNA *copy number* in Mitochondrien ohne TSPO beobachtet werden. Zudem, ging der Verlust der TSPO-Expression mit einer verringerten Expression des spannungsabhängigen Anionenkanals VDAC1 einher.

Respirometrische Analysen lassen eine mögliche modulatorische Rolle von TSPO auf den bioenergetischen Status der Zelle vermuten, da die mitochondriale Atmung, sowie die Glykolyse in Folge der TSPO-Deletion nachweislich reduziert waren. Interessanterweise waren die Knockout-Zellen aller untersuchten Zelltypen deutlich kleiner.

Darüber hinaus wurde eine signifikante Abnahme der Proteinexpression von TSPO und des TSPO-assoziierten Proteins VDAC1 in einem zellulären humanen Depressionsmodel beobachtet, was auf eine mögliche Verbindung zwischen TSPO und den Pathomechanismen von mitochondrialer Dysfunktion bei Depression hindeuten könnte.

Zusammenfassend deuten diese Ergebnisse auf eine Beeinträchtigung der mitochondrialen Funktion in TSPO-KO-Zellen hin. Dies trägt zum besseren Verständnis der vielschichtigen Rolle von TSPO bei und bildet eine Grundlage für weitere Untersuchungen, um die zugrunde

liegenden Mechanismen und die Beteiligung von TSPO an verschiedenen physiologischen und pathologischen Prozessen aufzuklären.

1 Introduction

1.1 Mitochondria: organelles fundamental to life

Mitochondria are crucial organelles fundamental to life and health (Pizzorno, 2014) because of their essential roles in regulating several processes and pathways. They are the hubs of respiration and energy production; therefore, they are classically considered the 'powerhouse' of the cell (McBride et al., 2006). They produce more than 90% of the ATP required to maintain the vital functions of the cell (Marchi et al., 2012; Vyas et al., 2016). Besides their traditional roles as bioenergetic and biosynthetic centres, mitochondria exhibit numerous other functions, thus playing an important role in cellular signalling and homeostasis (Harvey, 2019; Nunnari & Suomalainen, 2012).

Mitochondria can transiently store calcium ions in the matrix and rapidly release Ca^{2+}, thereby serving as cytosolic Ca^{2+} buffers (Alberts, 2015; Nunnari & Suomalainen, 2012; Rossier, 2006). Mitochondria interact with the endoplasmic reticulum (ER), the primary site of Ca^{2+} storage, at mitochondria-associated membrane (MAM) contact sites, allowing for substantial Ca^{2+} exchange, thus playing an important role in Ca^{2+} signalling (Pizzo & Pozzan, 2007). In addition to Ca^{2+} flux regulation, mitochondria are involved in intracellular signalling by producing the majority of cellular reactive oxygen species (ROS) as byproducts of ATP synthesis. At low doses, ROS act as pivotal secondary messenger molecules that affect kinases, growth factors, and transcription factors (Harvey, 2019; R. A. J. Smith et al., 2012). Furthermore, they are involved in iron-sulphur cluster formation, fatty acid oxidation, and production of metabolic precursors for macromolecules such as lipids, proteins, DNA, and RNA (Alberts, 2015; Spinelli & Haigis, 2018). Mitochondria are sites of haem and steroid synthesis, and regulate cellular stress responses and apoptosis (McBride et al., 2006; Nunnari & Suomalainen, 2012; Zick et al., 2009).

Overall, mitochondrial function is complex and depends on its unique structure. These multifaceted organelles serve as integral components of numerous signalling cascades, regulating not only cellular metabolism, but also cell proliferation, redox states, innate immunity, and cell death (McBride et al., 2006). Therefore, it is not surprising that mitochondria are at the nexus of human health and diseases and that mitochondrial defects lead to pathological states. Accordingly, mitochondrial dysfunction has been identified as an early occurrence that contributes to the progression of various diseases, including diabetes (Kim et al., 2008), cancer (Porporato et al., 2018), multiple sclerosis (Barcelos et al., 2019), and neurodegenerative diseases (Johri & Beal, 2012; Stanga et al., 2020; Wu et al., 2019).

1.1.1 Mitochondrial structure and morphology

Mitochondria, classically depicted as solitary bean-shaped organelles, exist in a multitude of shapes and sizes. Their shapes range from fragmented spherical structures to tubular networks (McCarron et al., 2013; Serasinghe & Chipuk, 2017), highly dynamic by moving along the cytoskeleton via actin filaments or microtubules (Chan, 2006). Their numbers vary widely in different tissues and organs depending on metabolic demands, and can change in response to different physiological, pathological, and environmental conditions (Knez et al., 2016). Mitochondria exhibit heterogeneity in their structure and function, not only across different cell types (Lodish et al., 2021) but also within a single cell (Kuznetsov & Margreiter, 2009; Pekkurnaz & Wang, 2022). Furthermore, recent studies have suggested that even within a single mitochondrion, multiple distinct regions exist, which are responsible for different functions (D. M. Wolf et al., 2019). Mitochondrial structure and function are likely to be inextricably linked (Chan, 2006), and changes in mitochondrial morphology are accompanied by changes in metabolic activity to regulate cellular bioenergetics (P. Mishra & Chan, 2016). The relationship between size and function has revealed that metabolically active cells typically harbour elongated, network-like mitochondria, whereas small, spherical, and fragmented mitochondria are common in inactive cells (Westermann, 2012).

Mitochondria are complex organelles with unique ultrastructure. They are surrounded by two phospholipid bilayers, with an outer (OMM) and an inner (IMM) mitochondrial membrane, which differ in their composition and structure (Lodish et al., 2021). The space between them defines the intermembrane space (IMS), while the mitochondrial matrix is enclosed by the IMM (Pagliuso et al., 2018) (Fig. 2). Pore-forming integral membrane proteins, such as the voltage-dependent anion channel (VDAC) embedded in the OMM, allow for the exchange of metabolites, nucleotides, and ions and are able to form complexes with enzymatic or other functional proteins residing in the membrane, cytosol, or IMS compartment (Shoshan-Barmatz et al., 2017). Instead of cholesterol, the IMM contains cardiolipin (Schiaffarino et al., 2022), thus forming a diffusion barrier for ions and small molecules, and subsequently setting the structural barrier for the proton gradient required for ATP synthesis (Lodish et al., 2021).

The inner membrane is highly convoluted and forms long lamellar protrusions, the so-called cristae, into the mitochondrial matrix, resulting in a large increase in the surface area. The number of cristae depends on the metabolic activity of the cell (Kühlbrandt, 2015) and contains mitochondrial respiratory chain complexes, ATP synthase, and various carriers for metabolites (McBride et al., 2006). The matrix contains a complete genetic system, including mitochondrial ribosomes, the mitochondrial circular genome (mtDNA), numerous factors for maintaining, regulating, and expressing the genome (Alberts, 2015; Pfanner et al., 2019), and approximately 40% of mitochondrial proteins (Backes & Herrmann, 2017).

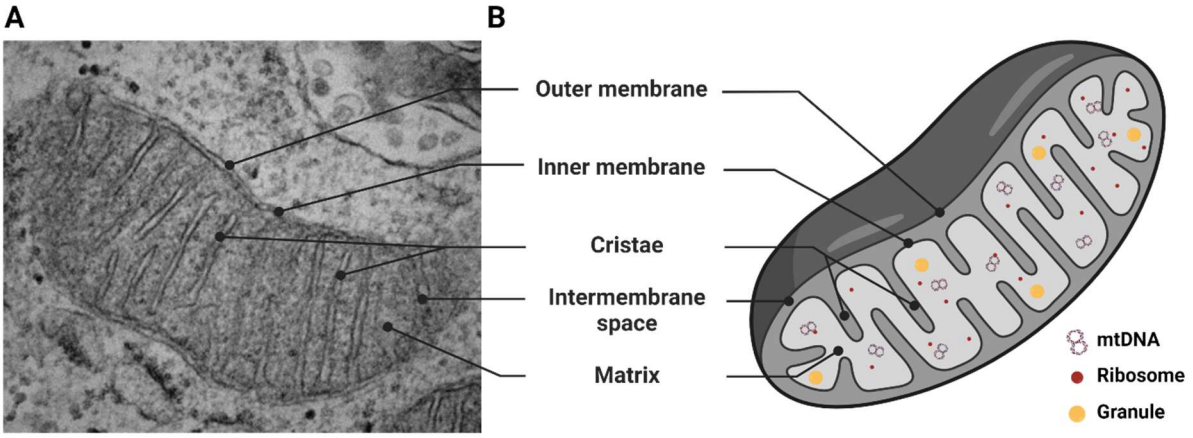

Figure 2: Mitochondrial structure. (A) Electron microscopy image illustrating one mitochondrion in cultured astrocytes. **(B)** Schematic illustration of mitochondrial architecture. Mitochondria are characterised by a double-membrane structure consisting of an outer and inner membrane. The OMM separates the mitochondria from the cytosol. It contains various porins and enzymes that regulate the exchange of nucleotides, ions, and metabolites involved in a wide range of metabolic processes. The IMM is highly impermeable to all molecules and forms many invaginations, the so-called cristae, that protrude into the matrix. These cristae enlarge the surface area and accommodate proteins required for the electron transport chain and many other chemical reactions that are essential for the mitochondria's varied functions. The two membranes generate two additional compartments: the intermembrane space between the two membranes and the mitochondrial matrix, encapsulated within the inner membrane containing mitochondrial DNA, ribosomes, and granules. Created with BioRender.com.

1.1.1.1 Mitochondrial dynamics: fusion and fission

Mitochondria are constantly changing organelles due to two opposing processes: fusion and fission, collectively known as mitochondrial dynamics (Serasinghe & Chipuk, 2017). These processes are responsible for creating the necessary variation in mitochondrial numbers, shapes, and structures (Chan, 2012), and help them adapt to environmental and physiological requirements (Alberts, 2015; H. Chen & Chan, 2009; Liesa et al., 2009). However, specific mitochondrial dynamics vary depending on physiological state, metabolic activity, and cell type (Pagliuso et al., 2018). Maintaining a balance between fusion and fission is crucial for cell survival and many physiological processes, including cell growth, death, and migration (Simula et al., 2017) as well as respiratory capacity, response to cellular stress, and mitophagy (Chan, 2012).

Fission involves the splitting of one large mitochondrion into smaller ones, allowing the isolation of defective mitochondria, partitioning and inheritance during mitosis, and distribution of transportable units along the cytoskeleton (Westermann, 2012). During fusion, two mitochondria join to generate extended mitochondrial networks, allowing functional complementation and exchange of mitochondrial contents (Serasinghe & Chipuk, 2017; Westermann, 2012), which are crucial for preserving mitochondrial function by stabilising mtDNA (Chan, 2012; H. Chen et al., 2010; Pagliuso et al., 2018). These processes serve as quality control mechanisms to protect the cell by allowing damaged and undamaged mitochondria to join, thereby diluting the damage or removing damaged parts, which can then be broken down by mitophagy (Chen & Chan, 2009; Ni et al., 2015) (Fig. 3).

To initiate mitochondrial fission, endoplasmic reticulum tubules wrap around the mitochondrial membrane and mark fission zones, leading to mitochondrial constriction (Friedman et al., 2011). GTPase dynamin-related protein 1 (DRP1) is responsible for inducing mitochondrial fission by translocating from the cytosol to the OMM fission sites, where it binds to several receptors, such as mitochondrial fission 1 protein (FIS1), mitochondrial fission factor (MFF), and mitochondrial dynamics proteins of 49 and 51 kDa (MID49/51) (P. Mishra & Chan, 2016), subsequently forming a polymeric constrictive ring-like structure around mitochondria (Archer, 2013; Trewin et al., 2018). Upon GTP hydrolysis, the DRP1 polymeric ring exerts pressure on the mitochondrial fission zone to further constrict the mitochondrion, followed by final scission into two separate organelles (Serasinghe & Chipuk, 2017).

In contrast, mitochondrial fusion involves both outer and inner membrane fusion and is regulated by three large GTPase proteins: mitofusin 1 (MFN1), mitofusin 2 (MFN2), and optic atrophy protein 1 (OPA1) (P. Mishra & Chan, 2016). During mitochondrial fusion, MFN1/MFN2 proteins dimerise and interact at the OMM between two adjacent mitochondria, exerting a pulling motion on each OMM and effectively merging them. After outer membrane fusion, OPA1 initiates inner membrane fusion depending on GTPase activity and GTP hydrolysis (Trewin et al., 2018).

By increasing their individual mitochondrial mass and mtDNA copy number, cells can further adapt to meet the changing energy demands for cellular growth, differentiation, and development (Scarpulla et al., 2012). However, since mitochondria cannot be created *de novo* (Westermann, 2010), mitochondrial biogenesis involves the augmentation and reconfiguration of existing networks via fusion and fission (Diaz & Moraes, 2008). Mitochondrial biogenesis is a complex process that requires the coordination of multiple pathways, including nuclear-mitochondrial communication, the expression and import of nuclear-encoded mitochondrial proteins, mtDNA amplification and mitochondrion-encoded gene translation, assembly of multi-subunit enzyme complexes, incorporation of mitochondrion-synthesised and imported membrane lipids, and regulation of mitochondrial dynamics and turnover (Diaz & Moraes, 2008; Westermann, 2010). The transcriptional co-activator peroxisome proliferator-activated receptor γ co-activator 1α (PGC-1α) is considered the master regulator of mitochondrial biogenesis and expression of nuclear-encoded mitochondrial proteins (Srivastava, 2017). PGC-1α upstream modulates two important transcription factors, nuclear respiratory factors 1 and 2 (NRF1 and NRF2), which activate the nuclear transcription of mitochondrial genes (Diaz & Moraes, 2008; Scarpulla, 2006) and subsequently activate mitochondrial transcription factor A (TFAM), further driving the transcription and replication of mtDNA (Sanchis-Gomar et al., 2014).

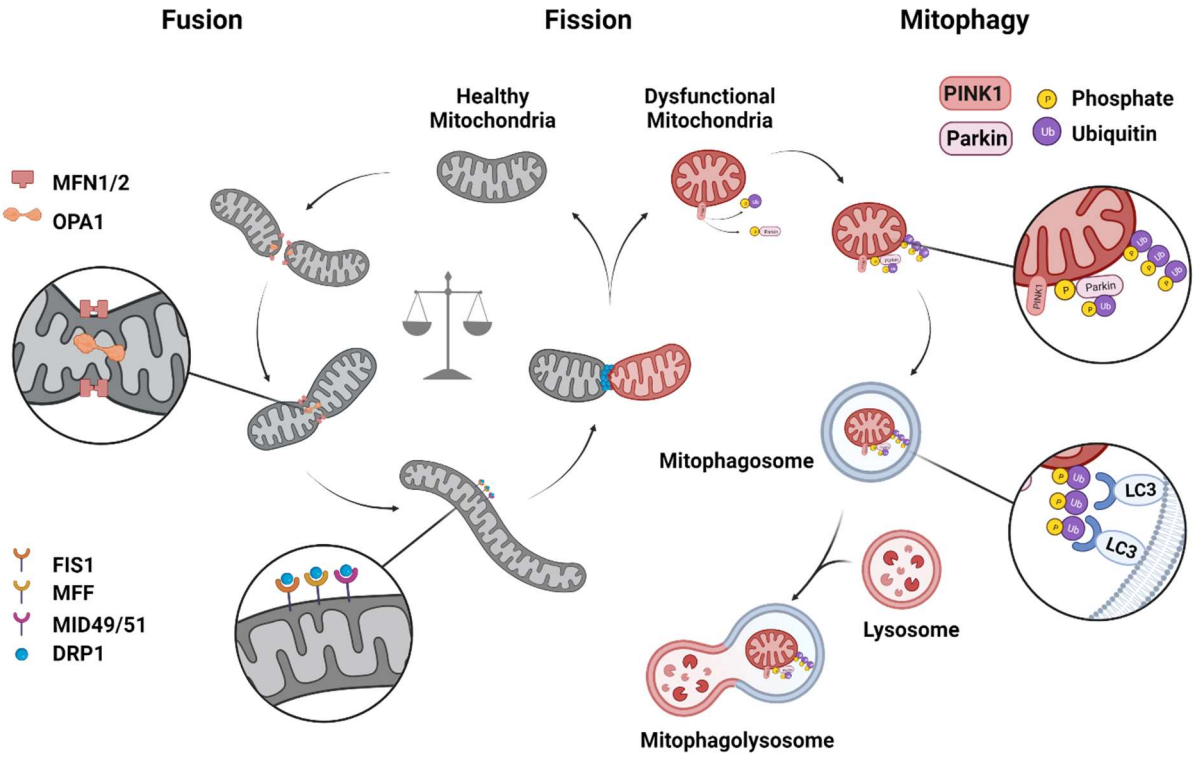

Figure 3: Mitochondrial dynamics. Mitochondrial morphology is maintained by a balance between fusion and fission. Mitochondrial fusion is mediated by the GTPases mitofusin 1 and 2 (MFN1/2) and optic atrophy protein 1 (OPA1), resulting in an interconnected, healthy mitochondrial network. Mitochondrial fission leads to mitochondrial fragmentation, which depends on dynamin-related protein 1 (DRP1). Fragmented dysfunctional mitochondria are cleared via mitophagy. Upon loss of mitochondrial membrane potential, PTEN-induced kinase 1 (PINK1) accumulates on the OMM, where it phosphorylates ubiquitin molecules and the E3 ubiquitin ligase parkin. Activated parkin further promotes ubiquitination of specific substrates in the outer membrane. Poly-ubiquitin chains are subsequently recognised by autophagy adaptor proteins, which bind to microtubule-associated protein 1 light chain 3 (LC3) on the growing phagophore adjacent to the mitochondria, resulting in the engulfment and degradation of damaged mitochondria. Created with BioRender.com.

1.1.1.2 mtDNA copy number and replication

Mitochondria are the only organelles that contain their own genomes other than the nucleus. This double-stranded genome, which consists of 16,569 base pairs in humans, is maternally inherited and encodes a small number of genes, including 13 polypeptide subunits of the electron transport chain (ETC), 22 transfer RNAs (tRNA), and two ribosomal RNAs (rRNA) (Diaz & Moraes, 2008). Most of these genes are located on the guanine-rich heavy strand (H-strand), whereas only some genes are encoded by the cytosine-rich light strand (L-strand) (Fig.4). mtDNA lacks an intron-exon structure and the only non-coding regions, the largest being the displacement-loop or D-loop, regulate mtDNA replication, transcription, and translation (Diaz & Moraes, 2008; Falkenberg, 2018). However, the vast majority of mitochondrial proteins are encoded by nuclear DNA (Ferramosca, 2020). Therefore, mitochondrial structure and function are controlled by both genomes and intergenomic communication is essential for adequate functioning (Herst et al., 2017).

Single or multiple mtDNA molecules are arranged in nucleoprotein complexes, which are referred to as nucleoids, and anchored to the IMM facing the mitochondrial matrix (Herst et al.,

2017). The amount of mtDNA in each cell typically ranges from 10^3 to 10^5 copies, which can vary depending on the type of cell (Filograna et al., 2021).

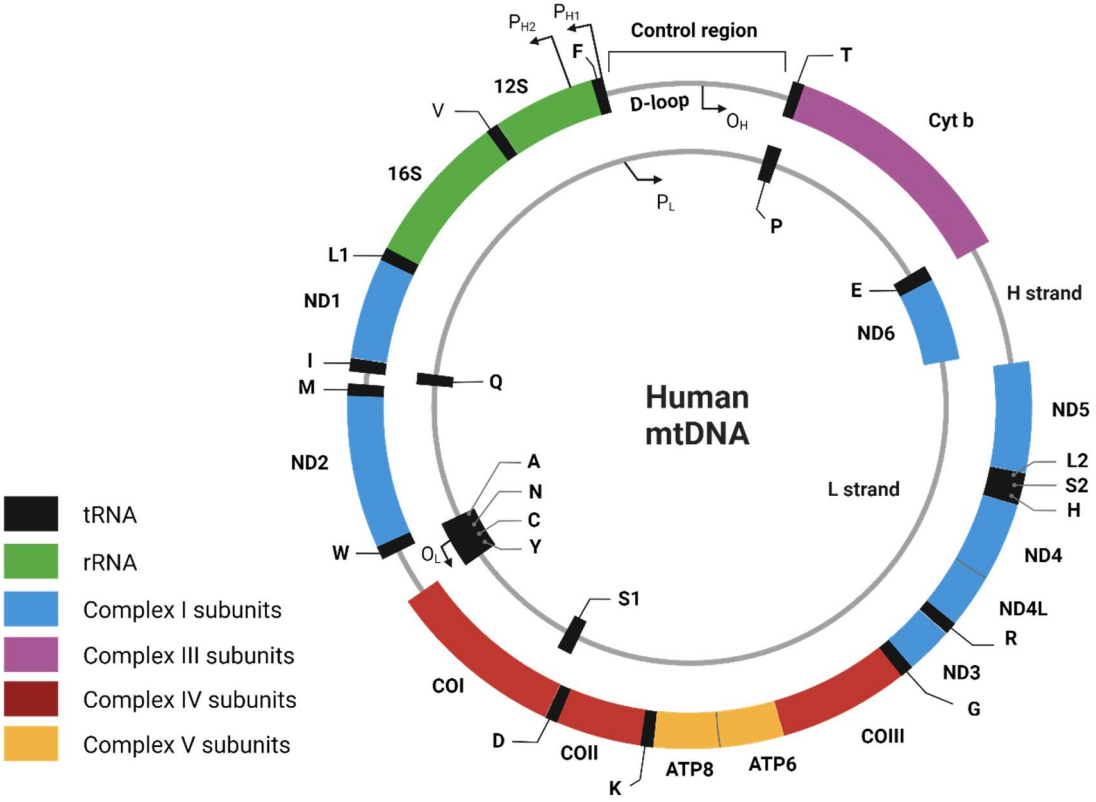

Figure 4: Human mitochondrial DNA. The 16,569 bp long circular human mitochondrial genome (mtDNA) with genes and control regions labelled. Adapted from Picard, Wallace, & Burelle; 2016. Created with BioRender.com.

To maintain the mtDNA copy number, the import of numerous nuclear-encoded proteins is necessary, which govern maintenance, replication, transcription, RNA maturation, and mitochondrial translation. The mitochondrial replisome complex orchestrates the replication of the mitochondrial genome independent of nuclear DNA replication and consists of the unique heterodimeric DNA polymerase γ (POLγ), which is only present in mitochondria, the DNA helicase TWINKLE, and the mitochondrial single-stranded DNA-binding protein (mtSSB) (Falkenberg et al., 2007; Filograna et al., 2021). Because POLγ is unable to use double-stranded DNA as a template, TWINKLE moves along with POLγ at the replication fork to catalyse the unwinding of mtDNA in the 5' to 3' direction. Unlike nuclear DNA replication, mtDNA replication proceeds continuously on both strands without the formation of Okazaki fragments. To coordinate the DNA synthesis of both strands, mtDNA features a dedicated origin of DNA replication on each strand, and replication is initiated at the heavy-strand origin (O_H) without simultaneous synthesis of the complementary L-strand. The long stretches of single-stranded DNA formed at the replication fork are stabilised by mtSSB, which also promotes the helicase activity of TWINKLE. Once the replisome machinery has synthesised two-thirds of the mtDNA, replication at the origin of the light strand starts (O_L) (Gustafsson et al., 2016).

Mutations in mtDNA have been linked to the aging process (A. L. M. Smith et al., 2022; Zapico, 2013) as well as various disorders (Malik & Czajka, 2013), including neurodegenerative diseases such as Parkinson's and Alzheimer's disease (Coskun et al., 2012). This could be attributed to the close proximity of mtDNA to the ETC, the main site of ROS production, inefficiency of DNA repair mechanisms, and the absence of introns and histones that protect mtDNA from oxidative stress (H. Lin et al., 2011). Altered mtDNA levels or mutations may contribute to increased oxidative stress and inflammation, leading to impaired oxidative phosphorylation (A. L. M. Smith et al., 2022). Thus, mtDNA copy number alterations have recently been used as biomarkers to study various disorders associated with mitochondria (Koller et al., 2020; Mei et al., 2015; Memon et al., 2017).

1.1.1.3 Mitochondrial clearance by mitophagy

When mitochondrial damage exceeds the ability of mitochondrial repair mechanisms, mitophagy is used to eliminate the entire organelle (Rong et al., 2021), resulting in a decline in mitochondrial mass (Benischke et al., 2017; Doblado et al., 2021). Mitophagy is a selective degradation process of damaged mitochondria, which plays a crucial role in maintaining mitochondrial quality and cellular homeostasis to ensure optimal cellular fitness (Ma et al., 2020). However, mitophagy is not only important for the clearance of damaged mitochondria, but also for ensuring optimal cellular energy production, regulating steady-state mitochondrial turnover, and fine-tuning of mitochondrial numbers (King & Plun-Favreau, 2017). The clearance of mitochondria in mammals involves the activity of the PINK1/parkin mitophagy pathway (Fig. 3), which identifies damaged mitochondria through the accumulation of PINK1 after mitochondrial membrane depolarisation (Ashrafi & Schwarz, 2015; Greene et al., 2012). Under normal conditions, PTEN-induced putative protein kinase 1 (PINK1) is imported into the IMS and undergoes proteasome-mediated degradation (Greene et al., 2012; Ma et al., 2020). However, upon loss of mitochondrial membrane potential, PINK1 stabilises and accumulates in the outer mitochondrial membrane (Narendra et al., 2010). PINK1 kinase activity is activated by an unknown mechanism of autophosphorylation (Aerts et al., 2015; Okatsu et al., 2012), which in turn phosphorylates parkin, an E3 ubiquitin ligase of mitochondria (Burté et al., 2015; Kondapalli et al., 2012), and ubiquitin (Ub) chains present on the OMM, serving as a platform for parkin recruitment and activation through direct binding (Kane et al., 2014; Tang et al., 2017; Wauer et al., 2015). This leads to a feed-forward amplification loop, resulting in more PINK1-mediated phospho-ubiquitin and recruitment of more parkin onto the OMM (Ordureau et al., 2014). Activated Parkin ubiquitinates various proteins on the mitochondrial surface, such as VDAC (Geisler et al., 2010), MFN2 (Tanaka et al., 2010), and Miro (Liang et al., 2015), which arrest the movement and fusion of damaged mitochondria (Ashrafi & Schwarz, 2015; Wang et al., 2011). Subsequently, ubiquitin-binding autophagy receptors, such as optineurin

or p62/SQSTM1, are recruited to damaged mitochondria (Geisler et al., 2010; Lazarou et al., 2015) and bridge ubiquitinated mitochondria to autophagosomal microtubule-associated chain 3B (LC3), directing them to proteasomal degradation and paving the way for autophagic engulfment and mitophagic digestion (Evans & Holzbaur, 2020).

1.1.2 Mitochondrial bioenergetics in a nutshell

For the development of cellular structures, cell differentiation, and cell growth, the conversion of organic molecules from the environment into ATP, the energy currency of the cell, is crucial. Aerobic respiration in mitochondria involves multiple interconnected pathways that converge to ultimately provide electrons to the ETC (Duchen, 2000). Mitochondria play a fundamental role in regulating metabolic pathways, and the tight control of their dynamics and functions is essential for sustaining an adequate energy balance (Nasrallah & Horvath, 2014). They contain the enzymatic machinery required for the final oxidation of carbohydrates, fatty acids, and proteins, resulting in the generation of energy in the form of ATP. Carbohydrates are broken down in the cytosol by glycolysis, and enter the mitochondria in the form of pyruvate. Pyruvate dehydrogenases inside the mitochondria decarboxylate pyruvate to form acetyl-CoA, which can subsequently enter the tricarboxylic acid (TCA) cycle, where it is oxidised to form CO_2. Alternatively, fatty acids are converted to acetyl-CoA in the mitochondria via fatty acid oxidation (FAO), while various enzymes catabolise amino acids into TCA cycle intermediates. The electrons generated in the TCA cycle are transferred to NAD^+ and FAD^+ to generate high-energy electron carriers, nicotinamide adenine dinucleotide (NADH) and flavin adenine dinucleotide ($FADH_2$), respectively, which are then re-oxidised in the ETC to produce ATP via oxidative phosphorylation (OXPHOS).

Table 1: Overview of the main mitochondrial metabolic pathways. The main processes and the needed energy sources and energy outputs are described.

Metabolic pathway	Process	Energy Source	Energy Output
Tricarboxylic acid cycle	Oxidation of acetyl-CoA to release stored energy	Acetyl-CoA; NAD^+; FAD^+; GDP	CoA; NADH; $FADH_2$; GTP
Oxidative phosphorylation	Redox reactions in the ETC, leading to energy release to produce ATP	NADH, $FADH_2$, ADP, O_2	NAD^+; FAD^+; H_2O; ATP
Fatty acid oxidation	Catabolic breakdown of fatty acids to generate acetyl-CoA	Cn-acyl-CoA, FAD^+, NAD^+; CoA	Cn-2-acyl-CoA, $FADH_2$; NADH, acetyl-CoA

1.1.2.1 Oxidative phosphorylation

The most important process of energy production in aerobic organisms is ATP generation by oxidative phosphorylation, the primary task of the mitochondria (Duchen, 2000)

During OXPHOS, electrons from the reducing equivalents NADH and $FADH_2$, generated during TCA cycle activity, FAO, and glycolysis, are transferred to molecular oxygen to form ATP. This successive electron transfer through a series of redox reactions is accomplished by an electron transport chain consisting of four multienzyme electron carriers located in the inner mitochondrial membrane (Fig. 5).

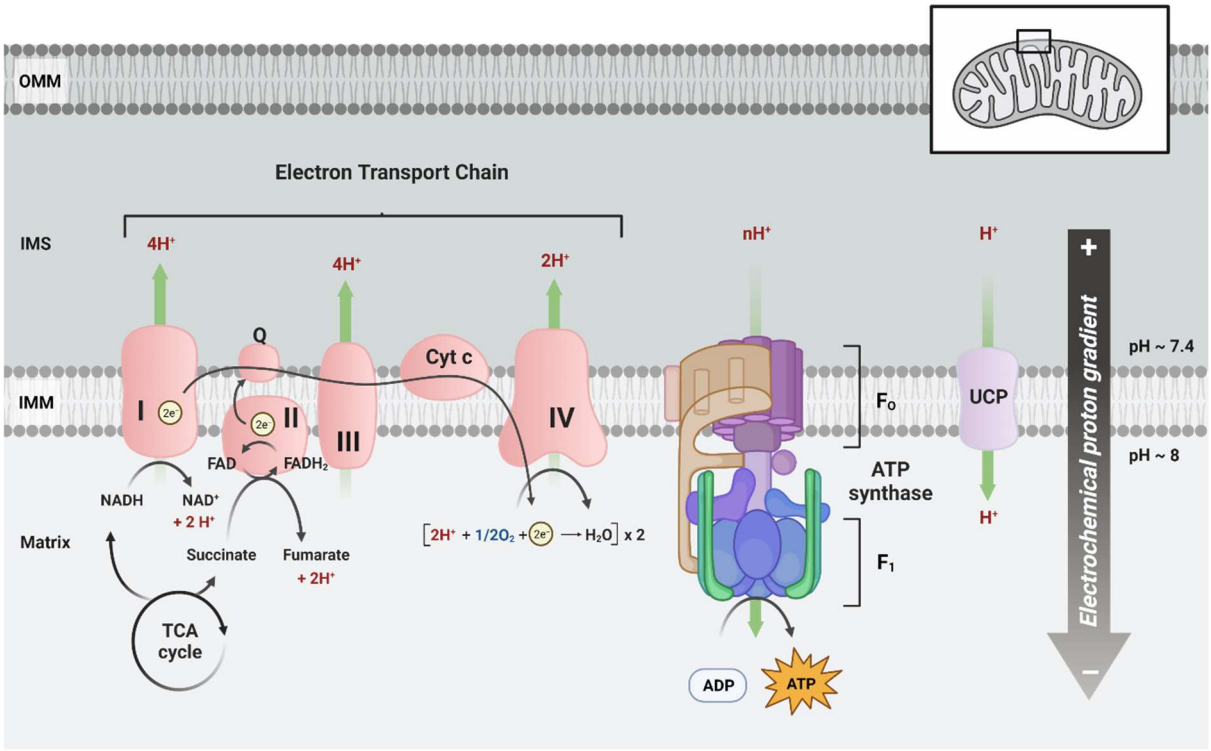

Figure 5: Schematic representation of mitochondrial oxidative phosphorylation. The reducing equivalents NADH and $FADH_2$, derived from the breakdown of carbohydrates and lipids, donate electrons (e^-) to complex I and complex II, respectively. The electrons are then transferred in a series of redox reactions until they reach molecular oxygen (O_2), which is the final electron acceptor, resulting in the formation of water. As electrons move through the electron transport chain, energy is released, which is used by complexes I, III, and IV to transport protons (H^+) from the mitochondrial matrix into the IMS against an electrochemical gradient to create a proton motive force. This proton motive force can drive the production of ATP via the reflux of protons through complex V (ATP synthase). Created with BioRender.com.

Each complex has a higher standard reduction potential than the electron donors, with molecular oxygen (O_2) as the final electron acceptor having the highest standard reduction potential, ultimately driving ETC and restoring the NAD^+ and FAD^+ pools. Complexes I and II accept electrons from NADH and $FADH_2$, respectively, and transfer them to the lipid-soluble electron carrier coenzyme Q and further to complex III. Electron flow continues through complex IV and finally ends with the reduction of O_2 to form water. The energy generated by electron flow across different complexes is used to pump protons (H^+) from the matrix into the IMS against their concentration gradient through the action of complexes I, III, and IV. This H^+

transport creates a pH gradient across the inner membrane, with a high pH in the matrix and lower pH in the IMS. A voltage gradient also develops across the inner membrane, generating a membrane potential (Δψm≈150mV).

The adenine nucleotide translocator (ANT) transports the generated ATP molecules in exchange for ADP into the cytosol, where it is available for all energy-dependent processes (Alberts, 2015; Chandel, 2015; Lodish et al., 2021).

Table 2: Characterisation of ETC complexes embedded in the IMM.

ETC complex	Enzyme	Mechanism
Complex I	NADH dehydrogenase	Oxidises NADH by transferring two electrons to coenzyme Q, while pumping four H^+
Complex II	Succinate dehydrogenase	Oxidises $FADH_2$ by transferring two electrons to coenzyme Q
Q	Ubiquinone/ubiquinol	Electron transfer to complex III
Complex III	Cytochrome c reductase	Electron transfer to cytochrome c and releasing four H^+ into the IMS
Complex IV	Cytochrome c oxidase	Oxidises cytochrome c by transferring its electrons to O_2, reducing it to H_2O and pumping two additional H^+
Complex V	ATP synthase	Δφm drives the molecular rotor and phosphorylates ADP to ATP

1.1.2.2 Redox homeostasis and oxidative stress

The mitochondrial electron transport chain is the main source of reactive oxygen species within a cell. The majority of mitochondrial ROS are produced when electrons leak from complex I and form highly reactive superoxide (O_2^-) by one-electron reduction of molecular oxygen (Balaban et al., 2005; Chandel, 2015; Murphy, 2009). Complex I-mediated O_2^- production is regulated by the NADH/NAD^+ ratio and the rate of reverse electron transport (RET), which occurs when reduced ubiquinone transfers electrons back through complex I to flavin mononucleotides. While the NADH/NAD^+ ratio is influenced by ATP demand and the activity of the ETC, RET is driven by a high ubiquinol/ubiquinone ratio alongside a high proton-motive force (Murphy, 2009). Additionally, complex III is capable of generating O_2^-, which is greatly amplified upon the addition of antimycin A, a complex III inhibitor (Murphy, 2009; Quinlan et al., 2011). Both complexes can leak electrons into the mitochondrial matrix, whereas only complex III can leak electrons into the IMS (Muller et al., 2004).

To prevent damage, cells possess robust ROS-detoxifying enzymes as well as non-enzymatic antioxidants such as glutathione, ascorbic acid, and uric acid (Mirończuk-Chodakowska et al., 2018; Murphy, 2009; Nimse & Pal, 2015). O_2^- is dismutated into the more stable hydrogen

peroxide (H_2O_2) by superoxide dismutase (SOD) enzymes. In the mitochondrial matrix, manganese-dependent SOD2, and in the cytosol and IMS SOD1, a copper- or zinc-dependent enzyme catalyses this reaction (Kowaltowski et al., 2009). To maintain cellular redox balance, H_2O_2 is further deactivated by antioxidant enzymes such as catalase, glutathione peroxidase (GPx), and peroxiredoxins (Kowaltowski et al., 2009; Mailloux, 2018). Moreover, cytochrome c exhibits antioxidant properties itself and can scavenge O_2^- (Pasdois et al., 2011). Additionally, ROS can activate mitochondrial uncoupling proteins (UCP) to help dissipate the proton gradient, thereby limiting ROS production through a negative feedback loop (Brand et al., 2004; St-Pierre et al., 2006).

When mitochondrial ROS excessively accumulate and exceed the antioxidative capacity of a cell, oxidative stress causes damage to macromolecules such as proteins, lipids, and mtDNA, eventually resulting in mitochondrial dysfunction. This can lead to a process known as the vicious cycle of further ROS production and further mitochondrial dysfunction, exacerbating the damage caused by ROS (Ma et al., 2020).

In contrast, low levels of ROS play key roles as secondary messengers in cell signalling and homeostasis, and regulate various biological processes, such as the immune response (West et al., 2011), autophagy, proliferation, migration, and cell differentiation (Holmström & Finkel, 2014; Rhee, 2006; Scherz-Shouval et al., 2007; Sena & Chandel, 2012; West et al., 2011). H_2O_2 can diffuse through membranes and primarily act as a signal by affecting the activity of proteins. This causes reversible oxidation of redox-sensitive thiol groups, thereby altering protein function by changing its binding interactions, lifetime, and subcellular localisation (Holmström & Finkel, 2014; Sena & Chandel, 2012), and subsequently modifying cross-talk between the mitochondria and the nucleus (Holmström & Finkel, 2014; Murphy, 2009). Furthermore, peroxiredoxins have been shown to relay H_2O_2-derived oxidising equivalents to transcription factors or kinases such as MAPK (Barata & Dick, 2020). Interestingly, the MAPK signalling pathway leads to the transcription of PGC-1α, which is involved in the expression of antioxidants and mitochondrial biogenesis (Gureev et al., 2019), thereby enabling an optimal balance between ROS and mitochondrial function (St-Pierre et al., 2006).

1.1.2.3 Calcium homeostasis

Calcium is a key signalling molecule involved in a wide range of cellular processes, including nuclear transcription, cell dynamics, oxidative energy metabolism, neuronal synaptic transmission, and neurotransmitter exocytosis (Berridge, 2012; Bravo-Sagua et al., 2017). Therefore, tight regulation of low-resting cytosolic Ca^{2+} levels and Ca^{2+} signalling is essential for maintaining cellular homeostasis (Bagur & Hajnóczky, 2017).

Mitochondria are multifunctional organelles that contribute to cell signalling through sophisticated communication mechanisms (Gottschalk et al., 2018), with Ca^{2+} uptake being

one of the most important processes involved (Cerella et al., 2010). They are intracellular Ca^{2+} stores that act as Ca^{2+} buffers (Romero-Garcia & Prado-Garcia, 2019) at privileged contact sites with the ER, known as the MAM and the plasma membrane (Szymański et al., 2017), thereby regulating fluctuations in cytosolic levels and playing an important role in cytosolic Ca^{2+} homeostasis.

Ca^{2+} influx proceeds quite unrestricted across the OMM through the cation-selective open VDAC conformation (Pavlov et al., 2005); therefore, cytosolic and IMS concentrations are at equilibrium (Serrat et al., 2022). However, the uptake of free Ca^{2+} into the mitochondrial matrix is driven by the negative membrane potential Δψm of healthy mitochondria (Duvvuri & Lood, 2021) and is strictly regulated via facilitated diffusion across the IMM by the mitochondrial Ca^{2+} uniporter holocomplex (MCU_{CX}), a Ca^{2+}-selective channel. Therefore, the transport of Ca^{2+} into the mitochondria is not directly coupled with the import or export of any other ion (Kamer & Mootha, 2015).

MCU_{CX} is composed of several proteins, including the pore-forming proteins MCU and MCUB, the essential MCU regulator (EMRE), the mitochondrial calcium uniporter regulator 1 (MCUR1), and the mitochondrial calcium uptake proteins 1, 2, and 3 (MICU1-3), which modulate the complex activity (J. Mishra et al., 2017; Pallafacchina et al., 2021). MCU is the Ca^{2+} permeant pore of the complex; however, co-expression with MCUB completely abolishes MCU currents, thereby suppressing the channel activity (Mammucari et al., 2017). MICU1-3 are localised to the IMS and exhibit a gatekeeper function that regulates channel opening. While MICU1 acts as both an inhibitor and cooperative activator of MCU by controlling the Ca^{2+} threshold and facilitating mitochondrial Ca^{2+} uptake at high Ca^{2+} concentrations, MICU2 directs channel closure, inhibiting Ca^{2+} influx at low resting cytosolic Ca^{2+} concentrations (De Stefani et al., 2015). MICU3 is predominantly expressed in the CNS, acting as an activator of the channel and increasing Ca^{2+} uptake (Patron et al., 2019).

Ca^{2+} within the mitochondrial matrix plays a crucial role in oxidative metabolism. It improves the kinetics of multiple TCA cycle enzymes including pyruvate dehydrogenase, isocitrate dehydrogenase, α-ketoglutarate dehydrogenase, and succinate dehydrogenase. Ca^{2+} ions bind to and activate the regulatory subunits of these enzymes, leading to increased rates of substrate oxidation and electron transfer, which ultimately results in increased production of NADH and FADH2. This in turn enhances the efficiency of OXPHOS and maintains the proton gradient across the IMM, resulting in increased ATP production and efficient cellular metabolism (Dejos et al., 2020; Griffiths & Rutter, 2009; McCormack et al., 1990). However, excessive Ca^{2+} overload can be detrimental, leading to the collapse of Δψm and the release of pro-apoptotic proteins into the cytosol, thereby inducing apoptosis (S. Zhang et al., 2022).

Ca^{2+} efflux from the mitochondrial matrix is primarily mediated by two saturable pathways: the $Na^+/Ca^{2+}/Li^+$ exchanger (NCLX), which extrudes calcium in exchange for sodium or lithium

ions, and the H^+/Ca^{2+} (HCX) exchanger, which actively transports Ca^{2+} for 2 H^+ (Takeuchi et al., 2015). Another mechanism involves the mitochondrial permeability transition pore (mPTP). Under pathological conditions, mPTP is involved in cell death regulation, as its long-lasting or irreversible opening results in the loss of Δψm and swelling, eventually leading to cell death via necrosis. Transient opening of the mPTP, however, plays a role in Ca^{2+} efflux and may also be involved in ROS signalling, as brief opening of the mPTP causes transient mitochondrial depolarisation and a short burst of ROS production (Kinnally et al., 2011; Wacquier et al., 2020).

Overall, strict regulation mediated by the interplay of various proteins is crucial to prevent Ca^{2+} overload as well as Ca^{2+} depletion by maintaining matrix Ca^{2+} concentrations while enabling dynamic mitochondrial Ca^{2+} signalling (Pathak & Trebak, 2018), since calcium deregulation can cause cell damage or even cell death (Cerella et al., 2010).

1.2 Translocator protein 18 kDa: a multi-faceted mitochondrial protein

The translocator protein 18 kDa (TSPO) was initially discovered in 1977 as a peripheral binding site for diazepam when investigators attempted to identify endogenous receptors for benzodiazepines, one of the most widely used drugs for treating patients with anxiety, convulsions, or insomnia (Braestrup et al., 1977; Braestrup & Squires, 1977; Davies & Huston, 1981).

TSPO has long been referred to as the peripheral-type benzodiazepine receptor (PBR) to distinguish it from the 'central' benzodiazepine receptor (CBR), which is associated with the γ-aminobutyric acid type A ($GABA_A$) receptor (Austin et al., 2013; Papadopoulos et al., 2006; Selvaraj & Stocco, 2015) forming an essential complex for inhibitory neurotransmission in the central nervous system (CNS) (Bergman, 1986; Casellas, 2002; Goldschen-Ohm, 2022; Saano, 1988). CBR and PBR have been reported to be distinct proteins that differ not only pharmacologically and structurally, but also in tissue distribution and cellular and subcellular localisation (Casellas, 2002; Marangos et al., 1982), with CBR primarily expressed in the plasma membrane of neurons (Guilarte, 2019). In comparison, TSPO/PBR is mainly found in glial cells in the CNS (Casellas, 2002; Papadopoulos et al., 2006; Rupprecht et al., 2010). Subcellularly, TSPO is primarily located in the OMM (Frison et al., 2017), especially clustered at outer and inner membrane contact sites (Lacapère & Papadopoulos, 2003; Papadopoulos et al., 2006; Rone et al., 2012; Rupprecht et al., 2010), but has also been observed in MAMs, the ER, and the plasma membrane (Loth et al., 2020).

TSPO belongs to a conserved family of widely distributed membrane proteins (Papadopoulos et al., 2006) that are expressed across the whole mammalian body but in a tissue- and cell-type-specific manner (Frison et al., 2017). In particular, steroid-synthesising tissues and

secretory glands, such as the adrenals and gonads, exhibit high expression levels (Austin et al., 2013; Selvaraj & Stocco, 2015). However, it is also present in other peripheral tissues, including the lungs, kidneys, heart, and skin (Anholt et al., 1985; Gavish et al., 1999).
Under physiological conditions, TSPO expression within the CNS is relatively low and restricted mainly to microglia and reactive astrocytes (Casellas, 2002); however, it is also found in the endothelium and neurons (Notter et al., 2021).
Pathological conditions such as Alzheimer's disease, multiple sclerosis, and cancer can lead to upregulated TSPO expression levels in affected tissues, implying a role for TSPO in the pathophysiology of neurodegenerative, neuroinflammatory, and neoplastic diseases (Arbo et al., 2015; Casellas, 2002; Rupprecht et al., 2010; Selvaraj & Stocco, 2015).

1.2.1 Evolution and molecular structure

The human *TSPO1* gene encodes a sequence of four exons of nuclear DNA on the long arm of chromosome 22 (22q13.31) (Austin et al., 2013), showing a high degree of conservation throughout the evolution from bacteria to humans (Papadopoulos et al., 2006). The *TSPO* sequence shows a high degree of interspecies homology (M. Jaremko et al., 2015) and is phylogenetically widespread from archaea and bacteria to insects and vertebrates. However, it is not ubiquitous and TSPO genes are absent in *E. coli* and *Saccharomyces cerevisiae* (Hiser et al., 2021; M. Jaremko et al., 2015).
Both human and mouse *Tspo* genes translate to a protein consisting of 169 amino acids with 81% sequence identity (Notter et al., 2021; Selvaraj et al., 2015). The bacterial sequence of the tryptophan-rich sensory protein (TspO) from *Rhodobacter sphaeroides* shares 33.5% sequence homology (Austin et al., 2013; Selvaraj et al., 2015), and TSPO homologues can also be found in plants, such as *Arabidopsis thaliana* (Papadopoulos et al., 2006).
TSPO expression is regulated at multiple levels and sequence examination of the *TSPO* promoter region has revealed a GC-rich region containing binding sites for specificity proteins 1, 3, and 4 (SP1, SP3, and SP4) (Batarseh et al., 2012). Sequences in the promoter region that bind to the v-ets erythroblastosis virus E26 oncogene homologue (ETS) and activator protein 1 (AP1) have also been reported to drive basal *TSPO* gene transcription (Giatzakis et al., 2007; Giatzakis & Papadopoulos, 2004), thus providing strong evidence that the PKCε-ERK1/-AP1/STAT3 signalling pathway mainly induces TSPO expression by upregulating ETS and SP1/SP3 transcription factors (Ammer et al., 2020; Batarseh et al., 2008, 2010). Additionally, non-transcription factor-mediated gene regulation of *TSPO* via natural antisense transcripts has been demonstrated. Seven intron-based short interspersed repetitive elements B2 (SINE B2) reside at the *TSPO* locus. Within intron 3, one of these elements drives the expression of a transcript that overlaps with exon 3, thereby functioning as a natural antisense transcript. This antisense transcript directly targets *TSPO* mRNA and represses TSPO

expression via complementary base pairing (Fan & Papadopoulos, 2012). However, the precise mechanisms regulating *TSPO* transcription remain unclear (Batarseh et al., 2010).

TSPO is a small 18 kDa integral membrane protein that contains numerous hydrophobic tryptophan residues distributed throughout the sequence and forms five α-helical amphipathic transmembrane domains (TM1-TM5) (M. Jaremko et al., 2015; Joseph-Liauzun et al., 1998). This tightly packed helical bundle spans the lipid bilayer of the OMM in a right-handed clockwise TM1-TM2-TM5-TM4-TM3 (viewed from the cytosol) order (Ł. Jaremko et al., 2014) (Fig. 6).

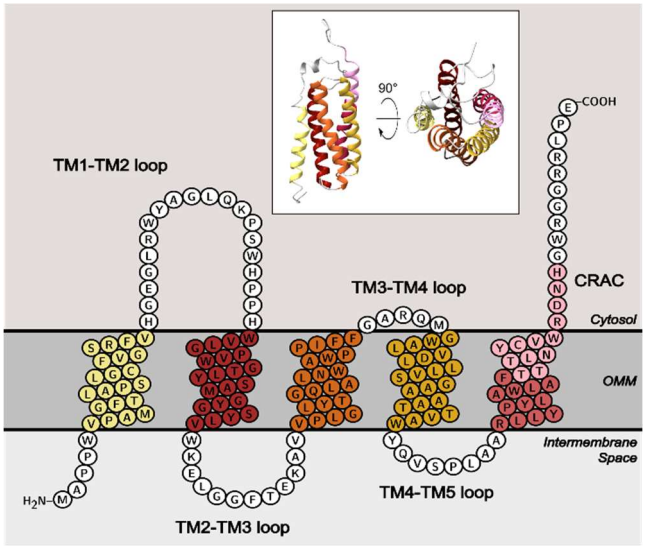

Figure 6: Topological model of human TSPO. TSPO consists of 169 amino acids that form five α-helical transmembrane domains (TM1-TM5) spanning the lipid bilayer. On the cytosolic side, TSPO features a TM1-TM2 loop, a TM3-TM4 loop, and a long, flexible C-terminal tail. At this cytoplasmic carboxy end within transmembrane helix 5 (TM5), the conserved cholesterol recognition amino acid consensus (CRAC) domain (pink) was identified as a high-affinity binding site for cholesterol. As intramitochondrial components, TSPO exhibits a short N-terminus and TM2-TM3 and TM4-TM5 loops. Topology model of full-length human TSPO was generated using PROTTER. *Inset:* View of the TSPO monomer, perpendicular and parallel to the membrane plane created with Chimera.

A five amino acid short intramitochondrial N-terminus and a 14 amino acid long flexible C-terminal tail (V. Milenkovic et al., 2015) flank the pentahelical structure of TSPO. Topological analysis also revealed several hydrophilic loop regions connecting the individual TM domains (Joseph-Liauzun et al., 1998): a TM3-TM4 and a TM1-TM2 loop on the extramitochondrial side and the TM4-TM5 and TM2-TM3 loops as intramitochondrial components (M. Jaremko et al., 2015). The long TM1-TM2 loop (LP1) near the C-terminus also forms a small, flexible α-helix ($\alpha_{1,2}$), which stabilises upon binding of the TSPO ligand PK11195 (Ł. Jaremko et al., 2014) to the hydrophobic pocket formed by the five transmembrane helices. This $\alpha_{1,2}$ helix forms a lid to stabilise ligand binding in the fluid-filled centre of the protein (Frison et al., 2017; M. Jaremko et al., 2015). TSPO interacts with a variety of endogenous ligands and metabolites, such as cholesterol, porphyrins, phospholipase A2 and diazepam-binding inhibitor (DBI) (Veenman et al., 2016) and also provides a target structure for many small synthetic molecules with significant in vivo efficacy (Ł. Jaremko et al., 2015).

At the cytoplasmic carboxy end, near the transmembrane helix TM5, a conserved cholesterol recognition amino acid consensus (CRAC) domain (amino acid residues 147-159) was identified as a binding site with nanomolar affinity for cholesterol (M. Jaremko et al., 2015; H. Li & Papadopoulos, 1998), suggesting TSPO as a membrane-associated cholesterol transport protein (Krueger & Papadopoulos, 1990; Lacapère et al., 2001). However, 3D structural NMR analyses showed that, contrary to previous assumptions of TSPO transporting cholesterol through the interior core (Lacapère et al., 2001; Rupprecht et al., 2010), the CRAC domain does not form a tunnel-like pore for cholesterol binding and translocation. Moreover, the amino acid side chains essential for cholesterol binding are localised outside the TSPO structure and point away from the interior of the protein towards the membrane (Frison et al., 2017; Ł. Jaremko et al., 2014; M. Jaremko et al., 2015).

Additionally, the extramitochondrial C-terminus comprises a strong positive charge, whereas the components of the receptor within the IMS are equally positively and negatively charged. These differentially charged regions may be important for the recognition and interaction of endogenous ligands and proteins with TSPO (Ł. Jaremko et al., 2014).

TSPO has been reported to exist in monomer, dimer, and oligomer states, as multiple bands have been detected by western blotting using TSPO polyclonal antisera (Delavoie et al., 2003). However, studies using a rabbit monoclonal antibody could detect only a single 18 kDa band (Morohaku et al., 2013). Electron microscopy (EM) structure and crystallographic studies have revealed that bacterial TSPO forms a highly stable dimer (Guo et al., 2015; Korkhov et al., 2010; R. Lin et al., 2015), whereas NMR structural analysis of murine TSPO (mTSPO) has revealed a monomer (Ł. Jaremko et al., 2014). However, residue-specific analysis showed that mTSPO exists in a dynamic monomer-dimer equilibrium in the membrane. It has been shown that cholesterol binding to mTSO changes the structure across the protein, shifting the dynamic equilibrium towards the monomer (Jaipuria et al., 2017).

Therefore, further investigations are required to gather more experimental evidence regarding TSPO oligomerisation and complex formation. In particular, the interaction with VDAC1 appears to be important for a mechanistic understanding.

1.2.2 The many functions of TSPO

Since its discovery in 1977, the structural and functional properties of TSPO have been a topic of active research, and TSPO has attracted great interest because of its variety of associated biological functions and potential therapeutic implications (Casellas, 2002).

However, despite over 40 years of extensive investigation and in-depth pharmacological and biochemical studies, the functions of TSPO remain unclear and controversial (Casellas, 2002; Notter et al., 2021).

Its localisation in the outer membrane of mitochondria, a multifunctional organelle itself, underscores its importance in cell physiology and at the crossroads of critical pathways of mitochondrial homeostasis and signalling (Frison et al., 2017; Gatliff & Campanella, 2012; Nutma et al., 2021; Selvaraj & Stocco, 2015). The evolutionarily conserved sequence from bacteria to humans further supports its functional significance. TSPO is considered a multifunctional protein involved in a wide array of cellular and mitochondrial functions that are essential for human health (Nutma et al., 2021). Nevertheless, its precise role in various physiological and pathophysiological contexts and its specific mechanisms of action remain elusive. TSPO has been demonstrated to be involved in cholesterol transport, thereby affecting mitochondrial steroid synthesis in general (Barron et al., 2018; Owen, Fan, et al., 2017; Papadopoulos et al., 2015) as well as the synthesis of neurosteroids in neuronal cells (Bader et al., 2019; Da Pozzo et al., 2012; Germelli et al., 2021; Owen, Fan, et al., 2017; Papadopoulos et al., 2018; Selvaraj & Tu, 2016; L. Wolf et al., 2015).

Moreover, TSPO participates in Ca^{2+} homeostasis (Gatliff et al., 2017; Gatliff & Campanella, 2012; V. M. Milenkovic et al., 2019), mitochondrial respiration, and bioenergetics (Banati et al., 2014; G.-J. Liu et al., 2017; V. M. Milenkovic et al., 2019). Other TSPO-associated functions include the regulation of oxidative stress, generation of ROS, mitophagy (Gatliff et al., 2014), and beta-oxidation of fatty acids (Tu et al., 2016), thereby affecting downstream cellular processes, such as proliferation, survival, and apoptosis (Papadopoulos & Lecanu, 2009; Rupprecht et al., 2010; Veenman, et al., 2007), and network functions, such as GABAergic neurotransmission and related higher brain functions (Rupprecht et al., 2010).

Additionally, TSPO is thought to play a role in the pathophysiology of neuroinflammation, neurodegeneration, and neoplasia, as its expression is increased in the context of diseases such as Parkinson's disease, multiple sclerosis, and various tumours (V. Milenkovic et al., 2015; Rupprecht et al., 2010).

1.2.2.1 TSPO and (neuro-) steroid synthesis

Steroid hormones, cholesterol-derivates with crucial biological functions involved in cellular signalling and hormonal control (Costa et al., 2018) are produced through *de novo* steroidogenesis, mainly in the adrenal cortex, gonads, and placenta. Additionally, a range of neurosteroids are synthesised in the brain (Schiffer et al., 2019). These endogenous neuromodulators, as well as neuroactive steroids produced in peripheral organs but acting on the CNS, are able to rapidly alter neuronal excitability and structural plasticity (Da Pozzo et al., 2012; Porcu et al., 2016).

As a first step, steroid synthesis involves the conversion of cholesterol to pregnenolone, the precursor of all steroid hormones. This conversion is catalysed by a specific isoform of cytochrome P450 (cholesterol side-chain cleavage enzyme P450scc), which is located on the

matrix side of the IMM (Frison et al., 2017; Miller, 2013). As cholesterol is highly lipophilic and cannot readily traverse the OMM to the IMM through the aqueous IMS, intracellular transport machinery is required to facilitate its import as the rate-limiting step of steroidogenesis (Costa et al., 2020). This process is thought to be carried out by a multimeric protein complex called the transduceosome, which includes the mitochondrial proteins TSPO, VDAC1 and ATPase family AAA domain-containing protein 3A (ATAD3A), and cytoplasmic steroidogenic acute regulatory protein (StAR) (Fig. 7). These proteins work together to enable cholesterol translocation into the mitochondrial matrix (Aghazadeh et al., 2015; A. Midzak & Papadopoulos, 2016; A. S. Midzak et al., 2011; Miller, 2013).

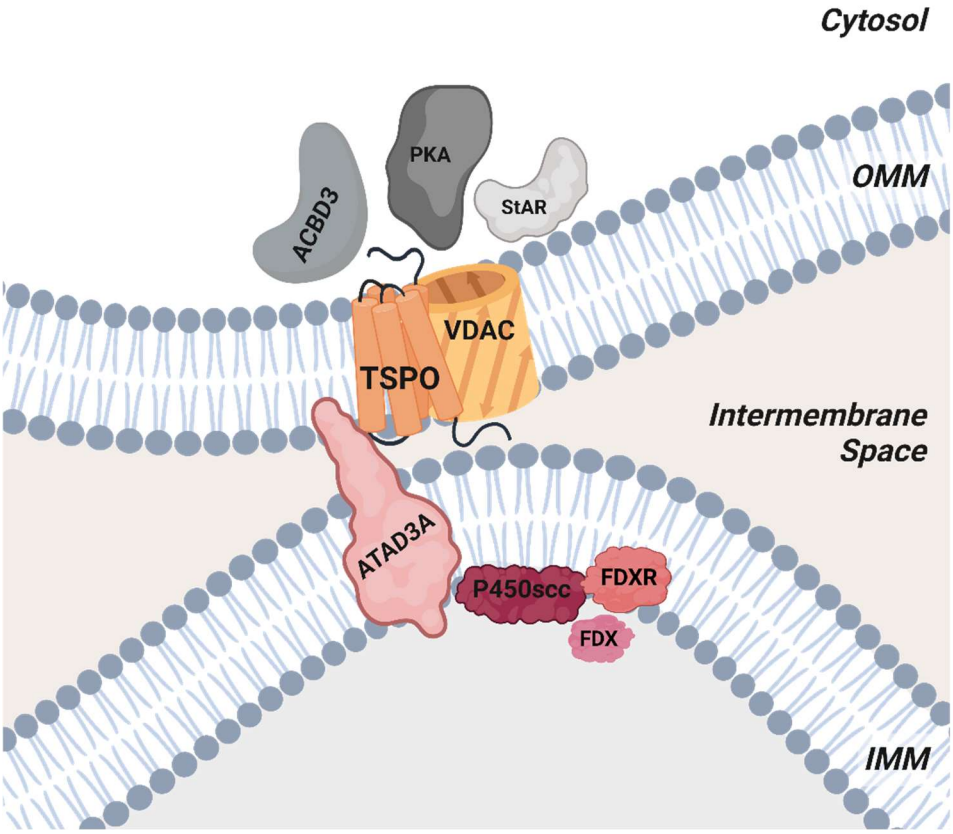

Figure 7: Mitochondrial cholesterol import and metabolism machinery. The transduceosome is composed of cytoplasmic (StAR, ACBD3, PKA, coloured gray), OMM (TSPO and VDAC, coloured orange), and IMM (ATAD3A, coloured red) proteins. Upon hormonal stimulation, the individual components of the transduceosome non-covalently assemble and transduce the resultant cAMP signal for cholesterol translocation into the mitochondria. However, the detailed molecular mechanism underlying cholesterol import remains largely unknown. Once cholesterol is imported into the mitochondria, the metabolon of the IMM (CYP11A1, FDX, and FDXR, coloured red) catalyzes the conversion of cholesterol to pregnenolone, the precursor of all steroids, including neurosteroids Adapted from Midzak & Papadopoulos, 2016. Created with BioRender.com.

Although the precise molecular mechanisms of cholesterol import are not yet fully understood, it is believed that the individual components of the transduceosome assemble in response to hormonal stimulation and cholesterol translocation is initiated via StAR in response to cAMP signalling (Aghazadeh et al., 2015; A. Midzak & Papadopoulos, 2016; A. S. Midzak et al., 2011; Miller, 2013). StAR is located in the cytoplasm, acts as a cholesterol shuttle, binds to cholesterol, and moves it to the OMM. VDAC is thought to interact with other proteins and

anchor TSPO and StAR to facilitate cholesterol transfer from the cytoplasm to the mitochondrial matrix. ATAD3A is also thought to play a role in transduceosome function. The N-terminal region of ATAD3A is localised within the OMM, whereas the C-terminus can be found in the matrix, effectively bridging the two membranes to form a contact site (Rone et al., 2012). It has also been proposed that ATAD3A acts as a scaffold to help organise other components of protein complexes and regulate their activity (Arguello et al., 2021).

Once inside the mitochondria, cholesterol is converted to pregnenolone, and subsequently different steroids are synthesised in a tissue-dependent manner. In the brain, glial cells and neurons produce neurosteroids such as progesterone, dehydroepiandrosterone (DHEA), and allopregnanolone. Neurosteroids have been shown to be involved in a variety of physiological and behavioural functions, such as mood, anxiety and cognition (Da Pozzo et al., 2012; Engel & Grant, 2001; Garcia-Segura & Melcangi, 2006). By modulating the activity of neurotransmitter receptors, such as GABA and NMDA receptors, they exhibit anxiolytic, antidepressant, and antipsychotic effects (Da Pozzo et al., 2012; Porcu et al., 2016; Rupprecht et al., 2001; Rupprecht, Wetzel, et al., 2022).

The role of TSPO in the regulation of steroid synthesis, including its possible involvement in CNS diseases and dysfunction, has been extensively studied and characterised (Batoko et al., 2015; Rupprecht, Wetzel, et al., 2022; Selvaraj & Stocco, 2015). Owing to its ubiquitous expression, particularly in steroidogenic tissues (Papadopoulos et al., 2006; Rupprecht et al., 2010; Selvaraj et al., 2015), and its early discovery as a high-affinity cholesterol-binding protein (H. Li & Papadopoulos, 1998), TSPO has long been considered essential for mitochondrial cholesterol translocation (Batoko et al., 2015; Selvaraj et al., 2015). Several studies have provided evidence that TSPO is crucial for steroid production and plays an essential role in viability and fertility. The link between TSPO and steroid synthesis was established in two important studies, demonstrating that the binding of synthetic TSPO ligands induced steroid hormone production in both Y1-adrenocortical (Mukhin et al., 1989) and MA-10-Leydig tumour cells (Krueger & Papadopoulos, 1990; Papadopoulos et al., 1990). To further confirm the contribution of TSPO, the endogenous TSPO ligand DBI was used to promote steroid production in steroidogenic cells (Garnier et al., 1993; Papadopoulos et al., 1991). Subsequent experiments have also revealed that TSPO is essential for steroidogenesis, as the inhibition of TSPO expression via gene knockdown (Hauet et al., 2005) or gene disruption (Papadopoulos, Amri, Li, et al., 1997) in rat Leydig cells led to a reduction in steroid production. These findings confirmed the involvement of TSPO in steroidogenesis and suggested that TSPO acts as a channel that mediates mitochondrial cholesterol import (Gatliff & Campanella, 2016). As a result of this expanding understanding of its function, PBR was renamed translocator protein to better reflect its role in cellular physiology (Papadopoulos et al., 2006; Rupprecht et al., 2010).

However, recent studies have contradicted these initial findings and have shown that TSPO is not involved in steroid synthesis (Selvaraj et al., 2015). Conditional TSPO knockout ($TSPO^{\Delta/\Delta}$) in mouse Leydig cells did not affect testosterone production in vivo (Morohaku et al., 2014). In contrast to a previous report that described TSPO knockout mice as early embryonically lethal (Papadopoulos, Amri, Boujrad, et al., 1997), global knockout of TSPO ($TSPO^{-/-}$) did not result in any alterations in viability, fertility, or steroid-producing ability (Banati et al., 2014; Tu et al., 2014).

Moreover, steroidogenic human adrenocortical cells, which hardly express endogenous TSPO, produce steroid hormones (Tu et al., 2014). These conflicting results have led to a re-examination of the biological role of TSPO in steroidogenesis and its significance in health and disease (Tu et al., 2014).

Nevertheless, recent studies have shown that TSPO is specifically involved in neurosteroid synthesis in murine (Bader et al., 2019; L. Wolf et al., 2015) and human microglial cells (Germelli et al., 2021), which increased after stimulation with specific TSPO ligands (Germelli et al., 2021; L. Wolf et al., 2015). Consistently, the essential contribution of StAR and TSPO in promoting neurosteroidogenesis has been demonstrated in astrocytes, the main steroidogenic cells of the CNS (Costa et al., 2020). In particular, a study conducted on primary rat hypothalamic astrocytes revealed that PKA-mediated phosphorylation of StAR and TSPO was essential for promoting neurosteroid synthesis after hormonal treatment (C. Chen et al., 2014). Another study using an astrocytic model showed that stimulation of TSPO with synthetic ligands increased the expression level of the mitochondrial form of StAR, an indicator of protein activation (Costa et al., 2020; Santoro et al., 2016).

1.2.2.2 TSPO as a regulator of mitochondrial and cellular homeostasis

TSPO is associated with various aspects of mitochondrial physiology and a significant hypothesis relates these putative functions to the interaction between TSPO and VDAC (Frison et al., 2017). VDAC exhibits both ion selectivity and voltage dependence, enabling mitochondrial function and energy supply. In the open state (high conductance), VDAC transports organic anions, ATP, ADP, inorganic phosphate (P_i), and respiratory substrates. While in the closed state (low conductance), the channel is permeable to smaller cations such as K^+, Na^+, and Ca^{2+} (Camara et al., 2017). Under physiological conditions, the cytoskeletal protein tubulin modulates VDAC function (Camara et al., 2017; Rostovtseva et al., 2008), whereas other proteins, including TSPO, can competitively bind to VDAC and may in turn modulate the tubulin-VDAC interaction. Thus, it is assumed that TSPO acts as a modulator of energy metabolism by altering VDAC permeability to ADP, ATP, and P_i (Gatliff & Campanella, 2012).

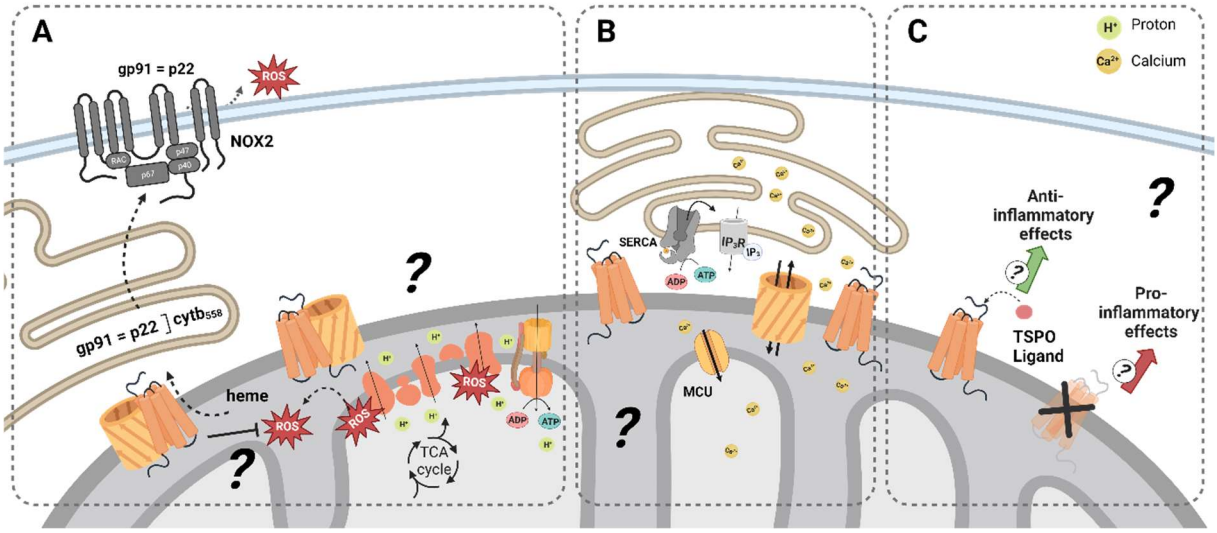

Figure 8 TSPO as a regulator of mitochondrial and cellular homeostasis. (A) TSPO Mitochondrial bioenergetics and redox homeostasis. The impact of TSPO loss on the oxygen consumption rate varies between cell types and may be due to differences in mitochondrial types and energetic status among cells. Interactions among TSPO, VDAC1, and NOX2 in the regulation of ROS generation and redox homeostasis have been proposed in several studies. However, the exact mechanisms of action remain unclear. **(B)** Calcium homeostasis. Various studies using specific TSPO ligands and TSPO deficiency models suggest a regulatory role of TSPO in mitochondrial Ca^{2+} homeostasis and cellular Ca^{2+} dynamics by modulating VDAC function. **(C)** Immunomodulation. Several findings suggest that TSPO is an immunomodulatory target and emphasise the potential of TSPO ligands as therapeutic interventions in neurodegenerative diseases, although further research is needed to understand their underlying mechanisms. Created with BioRender.com.

1.2.2.2.1 Bioenergetics and redox homeostasis

Several studies using the TSPO ligands PK11195 and Ro5-4864 have shown a dose-dependent reduction in oxygen consumption in the murine C1300 neuroblastoma cell line (Larcher et al., 1989) and an increase in the rate of stage IV respiration, and a decrease in the rate of stage III respiration in isolated mitochondria of rat kidneys, resulting in a significant reduction in the respiratory control rate due to TSPO binding (Hirsch et al., 1989). However, recent studies have shown no differences in the oxygen consumption rate (OCR) in isolated mitochondria from liver-specific $TSPO^{\Delta/\Delta}$ mice compared to the control group (Šileikytė et al., 2014). Similarly, the OCR of steroidogenic MA-10 Leydig cells, which highly express endogenous TSPO, did not differ from that of $TSPO^{\Delta/\Delta}$ MA-10 Leydig cells. Interestingly, they shift their substrate utilisation from glucose to fatty acids, with significantly higher mitochondrial FAO (Tu et al., 2016). In contrast, Banati et al. observed impaired basal mitochondrial respiration and significantly reduced ATP synthesis in TSPO-deficient murine microglial cells, suggesting reduced metabolic activity, and provided the first evidence of a regulatory role for TSPO in the energy metabolism of neural cells (Banati et al., 2014). TSPO knockdown in mouse BV-2 microglial cells also showed an influence of TSPO on the modulation of energy metabolism, with gene silencing of TSPO affecting several parameters of mitochondrial respiration but not the basal and maximal OCR (Bader et al., 2019). TSPO knockout in immortalised human microglia led to reduced basal and maximal oxygen consumption (V. M.

Milenkovic et al., 2019) and TSPO deficiency in primary mouse microglia inhibited mitochondrial oxidative phosphorylation and glycolysis, suggesting a general metabolic deficit in microglia (Yao et al., 2020). In contrast, TSPO overexpression in Jurkat cells resulted in increased ATP production and mitochondrial ETC gene transcription as well as elevated cell proliferation and motility (G.-J. Liu et al., 2017).

Various seemingly contradictory mechanisms have been proposed to explain the role of TSPO in redox homeostasis. One hypothesis states that TSPO, when associated with VDAC, induces ROS production, which can be reversed by knockdown of TSPO expression (Gatliff et al., 2014). Another study has suggested that TSPO overexpression could reduce mitochondrial ROS generation through an identical VDAC-dependent interaction (Joo et al., 2012, 2015). Consistent with this, the loss of TSPO in $TSPO^{\Delta/\Delta}$ Ma-10 Leydig cells resulted in increased ROS levels (Tu et al., 2016). Additionally, TSPO is thought to act on its own to neutralise ROS through the abundance of tryptophan residues in its structure, thereby protecting against oxidative stress (Guo et al., 2015). Furthermore, an association between TSPO and NADPH oxidase 2 (NOX2), the major source of ROS in the CNS, has been proposed to induce ROS production in primary mouse microglia. TSPO is assumed to act as a carrier for haeme, which is essential for $Cytb_{558}$, the catalytic core of NOX2 (Guilarte et al., 2016; Loth et al., 2020). An acute burst of ROS has been shown to cause an increase in TSPO levels, which can be reversed when a ROS scavenger is used. TSPO has been linked to the principal subunits of NOX2 in primary murine microglia, suggesting a regulatory role in the formation of $Cytb_{558}$ and the subsequent regulation of the expression level and activity of NOX2 and redox homeostasis in microglia (Loth et al., 2020). Cardiac-specific $TSPO^{\Delta/\Delta}$ mice, however, did not show any difference in the degree of ischaemia-reperfusion injury (Šileikytė et al., 2014), a pathology partially directed by myocardial NOX2 (Braunersreuther et al., 2013). Nevertheless, evidence of TSPO-NOX interaction has also been described in two independent studies. Galtliff et al. indicated TSPO-mediated Ca^{2+}-dependent activation of NOX5 in various cell types (Gatliff et al., 2017), whereas Wolf et al. postulated that TSPO is critical for Ca^{2+}-associated NOX1-mediated generation of extracellular ROS in retinal phagocytes (A. Wolf et al., 2020) (Fig 8A).

1.2.2.2.2 Mitochondrial calcium homeostasis

Ca^{2+} is a crucial intracellular messenger that plays a versatile role in the biochemistry and signalling pathways of the cell. Ca^{2+} levels within the cell are tightly regulated by steady-state Ca^{2+} influx and efflux. Diverse stimuli can lead to the release of Ca^{2+} from internal storage, such as the mitochondria and ER, or external sources, followed by its removal through a variety of mechanisms, including Ca^{2+} channels, transporters, pumps, and buffering proteins. This in turn results in the formation of intracellular signals. Ca^{2+} acts over a wide temporal and spatial range to regulate cellular processes, including enzyme activity, apoptosis, proliferation, gene

regulation, and metabolism (Berridge, 2012). Dysregulation of Ca^{2+} signalling can lead to cellular dysfunction and cell death and has been implicated in numerous diseases, including neurodegenerative disorders, cardiovascular diseases, and cancer (Modesti et al., 2021; Ureshino et al., 2019).

There is limited evidence for the role of TSPO in Ca^{2+} homeostasis; however, TSPO is assumed to be involved in maintaining cytoplasmic and mitochondrial Ca^{2+} levels. The interaction between TSPO and VDAC, the main Ca^{2+} channel in the OMM, may regulate changes in Ca^{2+} homeostasis. TSPO has been shown to interact with acyl-CoA binding domain-containing protein 3 (ACBD3), which forms a complex with the cAMP-dependent protein kinase PKA, subsequently regulating VDAC activity via phosphorylation (Gatliff et al., 2017). Previous studies have shown that TSPO ligands modulate the mitochondrial and cytoplasmic Ca^{2+} dynamics. Campanella et al. observed a new pharmacological effect of PK11195 on Ca^{2+} signalling and provided evidence for the possible regulation of apoptosis (Campanella, Szabadkai, et al., 2008). Moreover, studies focusing on the contribution of TSPO and its specific ligands to mitochondrial membrane permeability further suggest a potential role for TSPO in regulating mitochondrial Ca^{2+} homeostasis and sensitivity to apoptotic signals (Azarashvili et al., 2007, 2015; Krestinina et al., 2009). PK11195 treatment of the human colon tumor cell line HT-29 led to a rapid increase in intracellular Ca^{2+} concentration through transient mitochondrial Ca^{2+} efflux (Ostuni et al., 2007). Hong et al. suggested that the activation of TSPO by PK11195 is associated with reduced store-operated channel-mediated Ca^{2+} influx and subsequent modulation of cellular functions in human microglia (Hong et al., 2006). Although TSPO knockdown in BV-2 murine microglial cells did not affect basal cytoplasmic Ca^{2+} levels (Bader et al., 2019), knockout of TSPO in immortalised human microglia led to a significant Ca^{2+} increase, suggesting an important role of TSPO in regulating Ca^{2+} homeostasis (Bader et al., 2023; V. M. Milenkovic et al., 2019). Protoporphyrin IX (PPIX), a high-affinity TSPO ligand, reduced mitochondrial Ca^{2+} uptake in isolated rat heart mitochondria in a dose-dependent manner. In addition, PPIX affected VDAC function and decreased its conductance (Tamse et al., 2008). However, TSPO overexpression increased the intracellular Ca^{2+} concentration after exposure to IP_3 generating stimuli and pharmacological inhibition of Ca^{2+} retention by intracellular stores, thereby deregulating mitochondrial Ca^{2+} uptake capacity (Gatliff et al., 2017) (Fig. 8B).

Collectively, these findings indicate that TSPO may play a significant regulatory role in VDAC function, and consequently in the maintenance of mitochondrial Ca^{2+} homeostasis, as well as in the transport of ions and metabolites.

1.2.2.2.3 TSPO as a target for immunomodulation

The innate immune system, particularly microglia, is involved in neurodegenerative diseases, with neuroinflammation often preceding neuronal loss (Bae et al., 2014). Therefore, it is important to detect inflammatory processes during pre-symptomatic stages (Beckers et al., 2018). Positron emission tomography (PET) is a sensitive, non-invasive imaging technique used to investigate and quantify receptor and enzyme expression (Ory et al., 2014). A radiolabelled tracer for a protein overexpressed during neuroinflammation, such as TSPO, can be used as a diagnostic tool to monitor disease progression, as well as the effectiveness of anti-inflammatory therapies.

TSPO expression is increased in various neuropathologies such as Alzheimer's disease, multiple sclerosis, Parkinson's disease, major depressive disorder, and schizophrenia (Rupprecht et al., 2010). This altered expression correlates with the degree of damage (M.-K. Chen & Guilarte, 2008), and is often colocalised with activated microglia and reactive astrocytes (Lavisse et al., 2012; Werry et al., 2019). Thus, TSPO has been identified as a promising biomarker for neuroinflammation, and TSPO-PET radioligands allow localisation of damaged areas or active inflammatory processes (Ory et al., 2014).

In addition to their diagnostic use in visualising TSPO expression in vivo, several studies have demonstrated their ability to mitigate microglial reactivity and promote neuronal survival (Ferzaz et al., 2002; Ryu et al., 2005; Veiga et al., 2005). TSPO ligands are effective in treating neuroinflammation and degeneration in various disease models (Rupprecht et al., 2010). Some studies have considered increased TSPO expression in inflammatory tissue, even as an anti-inflammatory response and hence, making TSPO a potential disease-modifying gene and an attractive therapeutic target (Bae et al., 2014; S. A. Wolf et al., 2017).

TSPO interacts with several endogenous ligands such as cholesterol and porphyrins, and is a target structure for many small synthetic molecules with significant in vivo efficacy (Ł. Jaremko et al., 2015). Although synthetic TSPO ligands have primarily been developed for diagnostic imaging purposes, classical and newly developed ligands exhibit anti-inflammatory (Ryu et al., 2005; Santoro et al., 2016), immunosuppressive (Daugherty et al., 2013), neuroprotective (Soustiel et al., 2008; Veiga et al., 2005), regenerative (Girard et al., 2012), and anxiolytic (Rupprecht et al., 2009, 2010; Rupprecht, Wetzel, et al., 2022) activities.

Classical synthetic TSPO ligands, such as the isoquinoline carboxamide PK11195 and the benzodiazepine derivative Ro5-4864, which bind TSPO with nanomolar affinity, have been shown to exert neuroprotective and anti-inflammatory effects. Administration of Ro5-4864 not only reduced hippocampal amyloid-β accumulation and gliosis, thereby reducing behavioural impairment in younger mice, but also partially reversed the pathological condition in older mice in an Alzheimer's mouse model (Barron et al., 2018). Additionally, PK11195 treatment

improved behavioural and pathological disease outcomes in a late-stage Alzheimer's model by reducing both soluble and deposited amyloid-β (Christensen & Pike, 2018). In two other independent neurodegeneration models, Ro5-4864 prevented neuronal loss (Veiga et al., 2005), and increased neuronal survival and neurofilament network density (Soustiel et al., 2008). Ryu et al. showed that in a quinolinic acid-induced brain injury model, the TSPO antagonist PK11195 reduced pro-inflammatory cytokine production, microglial activation, and neuronal death (Ryu et al., 2005). Moreover, a recent study found that TSPO deficiency in primary microglia reduced their ability to phagocytose amyloid-β and increased the secretion of pro-inflammatory cytokines after stimulation with LPS or amyloid-β (H. Zhang et al., 2021).
Administration of another well-established TSPO ligand, the benzoxazine etifoxine, protected and improved symptomatic recovery in a mouse model of multiple sclerosis by reducing the expression of pro-inflammatory cytokines and peripheral immune cell infiltration in the spinal cord (Daugherty et al., 2013) as well as decreasing microglial reactivity and promoting neuronal survival, thereby exerting beneficial effects after intracerebral haemorrhage or traumatic brain injury (M. Li et al., 2017; Simon-O'Brien et al., 2016).
The TSPO agonist XBD173 (emapunil) is a selective and high-affinity second-generation ligand. It mediates anxiolytic and antidepressant effects in various experimental models without causing the side effect profile associated with conventional benzodiazepine derivatives (Kita et al., 2004; Rupprecht et al., 2009). In a mouse model of Parkinson's disease, treatment with XBD173 reduced the degeneration of dopaminergic neurones and improved motor function (Gong et al., 2019). Two studies have demonstrated the immunomodulatory and neuroprotective effects of XBD173 by reducing microglial reactivity, accumulation, and neurotoxicity as well as the expression of pro-inflammatory cytokines in BV-2 microglia (Karlstetter et al., 2014) and in a mouse model of light-induced retinal degeneration (Scholz et al., 2015). Additionally, XBD173 increased GABAergic neurotransmission by inducing neurosteroid synthesis and counteracted pharmacologically induced panic attacks in both rodents and humans (Rupprecht et al., 2009). Consistent with this, recent clinical studies on etifoxine reported anxiolytic effects similar to those of clonazepam, an established anxiolytic compound (Vicente et al., 2020). This might be attributed to the involvement of TSPO ligands in the synthesis of neurosteroids, which are known to modulate $GABA_A$ receptors and are also targeted by traditional anxiolytic drugs, such as benzodiazepines (Rupprecht, Wetzel, et al., 2022) (Rupprecht et al., 2022). Allopregnanolone, a potent $GABA_A$ receptor agonist, has been shown to have therapeutic effects in psychiatric conditions, such as anxiety, depression, and post-traumatic stress disorder (Rupprecht, Wetzel, et al., 2022; Schüle et al., 2014; Shang et al., 2020). Other than anxiolytic actions, some TSPO ligands have been found to exert antidepressant effects in various rodent models of depression (Gavioli et al., 2003; Kita et al., 2004; L.-M. Zhang et al., 2014). Shang et al. investigated the effects of the TSPO agonist, AC-

5216, on depression and memory in chronically stressed mice. They found that the TSPO ligand produced rapid antidepressant-like effects and improved memory performance in control mice, which was not observed in TSPO KO mice, indicating a TSPO-mediated anxiolytic action (Shang et al., 2020).

Taken together, TSPO has been widely used as a target for developing new diagnostic and therapeutic strategies due to its important role in cellular and systemic functions, as well as its involvement in various dysfunctions and diseases (Frison et al., 2017) and these findings highlight TSPO as an immunomodulatory target and emphasize the potential of TSPO ligands as pharmacological therapies in the treatment of neurological and psychiatric diseases, due to their anti-inflammatory and neuroprotective properties. However, the underlying mechanisms are still not fully understood (Fig. 8C).

1.3 Aim of the thesis

TSPO is associated with various aspects of mitochondrial metabolism. However, contradictory and controversial findings from decades of research since its discovery in 1977 impede the understanding of the physiological role of TSPO in steroid synthesis and its significance in maintaining mitochondrial homeostasis. Nevertheless, TSPO's unique characteristics, including its localisation in the outer mitochondrial membrane, evolutionary sequence conservation across species, and specific structural properties, support the assumption of an essential role in regulating cellular and mitochondrial functions. However, the precise involvement of TSPO in various physiological and pathophysiological contexts, as well as its potential therapeutic implications, remains yet to be fully elucidated.

Therefore, this thesis aimed to investigate the functional importance of TSPO using a novel human cellular TSPO knockout model, allowing experiments to be conducted in the presence and absence of TSPO. Using CRSIPR/Cas9 technology TSPO knockout variants of human induced pluripotent stem cells (hiPSCs) were generated and differentiated into neural progenitor cells (NPCs), astrocytes, and neurons, as TSPO function and physiological effects may vary in a tissue- and cell type-dependent manner. Subsequently, these different cell types were used to functionally characterise TSPO, with a main focus on mitochondrial phenotyping in TSPO knockout and control cells.

Accordingly, the present study investigated the involvement of TSPO in neurosteroid synthesis, calcium homeostasis, mitochondrial respiration, and other bioenergetic parameters, reflecting the functional integrity of mitochondria. Overall, these studies contribute basic cell biological knowledge towards understanding the putative role of TSPO as a hub in mitochondrial metabolism. Given the hypothesis that TSPO regulates mitochondrial homeostasis, understanding the molecular function and mechanisms of action of TSPO is indispensable as it may offer future therapeutic possibilities for mitochondria-related disorders.

2 Material and Methods

2.1 Material

2.1.1 Laboratory consumables and equipment

Table 3: Laboratory consumables

Consumable	Manufacturer
60µ-Dish (Ø 35 mm, high)	Ibidi GmbH; Gräfelfing; Germany
Cell culture plates	Corning Incorporated; Tewksbury, Massachusetts
CellTrics 50 µm cell strainer	Sysmex; Hamburg, Germany
Coverslips, glass (Ø 25 mm; Ø 12 mm)	VWR by Avantor; Radnor, Pennsylvania
Cryo vials 1.5 mL/2 mL	Sarstedt; Nümbrecht, Germany
Falcon tubes (15 mL, 50 mL)	Greiner Bio One; Kremsmünster, Austria
Falcon® 5mL Round Bottom Polystyrene Test Tube, with Cell Strainer Snap Cap	Omnilab; Bremen, Germany
Microplates 96-well (black bottom)	Greiner Bio One; Kremsmünster, Austria
Microplates 96-well (transparent)	Greiner Bio One; Kremsmünster, Austria
PCR tubes	Biozym; Hessisch Oldendorf, Germany
Pipette filter tips	Greiner Bio One; Kremsmünster, Austria
Pipette tips	Eppendorf; Hamburg, Germany
Reaction tubes (0.2 mL, 0.5 mL)	Sarstedt; Nümbrecht, Germany
Safe-lock reaction tubes (1.5 mL, 2, 5 mL)	Sarstedt; Nümbrecht, Germany
Seahorse XFp-Flux-Pack	Agilent Technologies; Santa Clara, California

Table 4:Laboratory equipment

Equipment	Manufacturer
5415R centrifuge	Eppendorf; Hamburg, Germany
Amaxa Nucleofector 1 Electroporation System	Amaxa biosystems; Köln, Germany
Chamber for coverslips (Ø 25 mm)	Warner Instruments; Hamden, Conneticut
FACS Celesta™	BD Biosciences; Franklin Lakes, New Jersey
Heracell 150 Incubator	Thermo Fisher Scientific; Carlsbad, California
Laminar Flow Hood	Thermo Fisher Scientific; Carlsbad, California
Megafuge 1.0 centrifuge	Heraeus; Hanau, Germany
Megafuge 2.0R centrifuge	Heraeus; Hanau, Germany
Mikro 220R centrifuge	Hettich; Tuttlingen, Germany
Mini-PROTEAN Tetra Cell running system	Bio-Rad; Hercules, California

Pipet controller accu-jet® pro	Brand; Wertheim & Grossostheim, Germany
Pipettes	Eppendorf; Hamburg, Germany
RotorGeneQ	Qiagen; Hilden, Germany
Seahorse XFp Flux Analyser	Agilent Technologies; Santa Clara, California
Sonoplus HD 3100	BANDELIN; Berlin, Germany
Tecan infinite F450 microplate reader	Tecan; Crailsheim, Germany
ThermoCycler GE Advanced D48	Bio-Gener; Hangzhou, China
Thermomixer CC	Eppendorf; Hamburg, Germany
Wet/Tank blotting system Mini Trans-Blot Cell	Bio-Rad; Hercules, California
VarioScan plate reader	Thermo Fisher Scientific; Carlsbad, California

2.1.2 Chemicals, reagents, and kits

Table 5: Chemicals and reagents

Chemical and reagent	Manufacturer
2-deoxy-D-Glucose	Biomol GmbH; Hamburg, Germany
Accutase	Gibco by Life Technologies; Carlsbad, California
Advanced DMEM/F12	Gibco by Life Technologies; Carlsbad, California
Ampicillin	Ratiophar; Ulm, Germany
Antimycin A	Biomol GmbH; Hamburg, Germany
Ascorbic acid (Vitamin C)	Carl Roth; Karlsruhe, Germany
Astrocyte Medium (ScienCell)	Provitro AG; Berlin, Germany
B-27 Plus Supplement	Thermo Fisher Scientific; Carlsbad, California
BbsI	New England Biolabs; Ipswich, Massachusetts
BrainPhys™ Neuronal Medium	STEMCELL Technologies; Vancouver, Canada
Citrate Buffer (pH 6)	ZYTOMED systems; Berlin, Germany
cOmplete,EDTA-free protease inhibitor (25x)	Merck; Darmstadt, Germany
CryoStor CS10	STEMCELL Technologies; Vancouver, Canada
Culture One Supplement	Thermo Fisher Scientific; Carlsbad, California
Cycloheximide	Sigma-Aldrich; St. Louis, Missouri
Cytosine arabinoside (Ara-C)	Biomol GmbH; Hamburg, Germany
Dibutyryl-cAMP (dcAMP)	STEMCELL Technologies; Vancouver, Canada
Dispase	STEMCELL Technologies; Vancouver, Canada
DMEM/F12	Gibco by Life Technologies; Carlsbad, California
DMSO	Sigma-Aldrich; St. Louis, Missouri

DPBS	Gibco by Life Technologies; Carlsbad, California
DPBS, calcium, magnesium	Gibco by Life Technologies; Carlsbad, California
FCCP	Biomol GmbH; Hamburg, Germany
FBS	Sigma-Aldrich; St. Louis, Missouri
Fluorescent Mounting Medium	Dako; Carpinteria, California
Fura-2/AM	Hölzel Biotec; Köln, Germany
Geltrex LDEC	Thermo Fisher Scientific; Carlsbad, California
Gentamycin	Gibco by Life Technologies; Carlsbad, California
Glucose	Carl Roth; Karlsruhe, Germany
GlutaMax (100x)	Gibco by Life Technologies; Carlsbad, California
H2DCFDA	Invitrogen by Life Technologies; Carlsbad, California
HBSS	Sigma-Aldrich; St. Louis, Missouri
Hoechst	Thermo Fisher Scientific; Carlsbad, California
Isopropyl alcohol	Carl Roth; Karlsruhe, Germany
ImmersolTM 518 F Immersion Oil	Carl Zeiss; Jena, Germany
JC-1	Invitrogen by Life Technologies; Carlsbad, California
Laminin	Sigma-Aldrich; St. Louis, Missouri
L-Glutamine	Sigma-Aldrich; St. Louis, Missouri
Matrigel	Corning Incorporated; Tewksbury, Massachusetts
MitoSOX Red	Invitrogen by Life Technologies; Carlsbad, California
MitoTracker Green	Invitrogen by Life Technologies; Carlsbad, California
mTeSR Plus Kit	STEMCELL Technologies; Vancouver, Canada
N2-Supplement	Thermo Fisher Scientific; Carlsbad, California
Neurobasal Medium	Gibco by Life Technologies; Carlsbad, California
Neurobasal Medium Plus	Gibco by Life Technologies; Carlsbad, California
Non-essential amino acids	Gibco by Life Technologies; Carlsbad, California
Normal goat serum	Thermo Fisher Scientific; Carlsbad, California
Oligomycin	Biomol GmbH; Hamburg, Germany
Opti-MEM	Gibco by Life Technologies; Carlsbad, California
Paraformaldehyde	Carl Roth; Karlsruhe, Germany
Penicillin-Streptomycin Solution	Sigma-Aldrich; St. Louis, Missouri
Pluronic 10% F127	Thermo Fisher Scientific; Carlsbad, California
Poly-L-ornithine solution	Sigma-Aldrich; St. Louis, Missouri
Protease Inhibitor Cocktail	Sigma-Aldrich; St. Louis, Missouri
Protein Marker IV, 10 – 170 kDa	VWR by Avantor, Radnor, Pennsylvania

PSC Neural Induction Supplement (50x)	Gibco by Life Technologies; Carlsbad, California
Puromycin	Carl Roth; Karlsruhe, Germany
Pyruvate	Sigma-Aldrich; St. Louis, Missouri
rH-BDNF	PreproTech; Rocky Hill, USA
rH-GDNF	PreproTech; Rocky Hill, USA
Rhod-2/AM	Hölzel Biotech; Köln, Germany
Y27632 ROCK-Inhibitor	STEMCELL Technologies; Vancouver, Canada
Rotenone	Biomol GmbH; Hamburg, Germany
Seahorse XF DMEM assay medium, pH 7.4	Agilent Technologies; Santa Clara, California
Sodium pyruvate	Gibco by Life Technologies; Carlsbad, California
T4 DNA Ligase	New England Biolabs; Ipswich, Massachusetts
T4 DNA Ligase Reaction Buffer (10x)	New England Biolabs; Ipswich, Massachusetts
T4 Polynucleotide Kinase	New England Biolabs; Ipswich, Massachusetts
TMRE	Biomol GmbH; Hamburg, Germany
Trilostane	Sigma-Aldrich; St. Louis, Missouri
STEMdiff Nural Progenitor Freezing Medium	STEMCELL Technologies; Vancouver, Canada
Triton X-100	Sigma-Aldrich; St. Louis, Missouri
Trypan Blue	Sigma-Aldrich; St. Louis, Missouri

Table 6: Kits

Kit	Manufacturer
CellTiter-Glo® Cell Viability Assay	Promega; Madison, Wisconsin
DNeasy Blood and Tissue	Qiagen; Hilden, Germany
Human Stem Cell Nucleofector™ Kit 2	Lonza; Basel, Switzerland
NucleoBond® XTRA Midi	MACHEREY-NAGEL; Düren, Germany
NucleoSpin® DNARapid Lyse	MACHEREY-NAGEL; Düren, Germany
NucleoSpin® Plasmid	MACHEREY-NAGEL; Düren, Germany
NucleoSpin® RNA Plus	MACHEREY-NAGEL; Düren, Germany
Pierce™ BCA Protein Assay	Thermo Fisher Scientific; Carlsbad, California
Pregnenolone ELISA	LDN, Nordhorn, Germany
QuantTech Reverse Transcription	Qiagen; Hilden, Germany
SuperSignal West Pico PLUS, Chemiluminescent Substrate	Thermo Fisher Scientific; Carlsbad, California
TakyonTM Rox SYBR® MasterMix dTTP Blue	Eurogene; Seraing, Belgium

2.1.3 Culture media and buffer composition

Table 7: Buffer and media

Buffer/Media	Composition
Cell Culture	
Astrocyte Freezing Medium	Astrocyte Medium 20% FBS 10% DMSO
Astrocyte Medium	Astrocyte Medium (ScienCell) 2% FBS 1% Astrocyte growth supplement
mTeSR Medium	mTeSR Plus Basal Medium mTeSR Supplement 50x 50 µg/mL Gentamycin
Neural Induction Medium (NIM)	Neurobasal Medium 2% Neural Induction Supplement 0.5% Penicillin/Streptomycin
Neural Expansion Medium (NEM)	48.75% Neurobasal Medium 48.75% Advanced DMEM/F12 2% Neural Induction Supplement 0.5% Penicillin/Streptomycin
Neuronal Medium	BrainPhys™ Neuronal Medium 1% B27 Plus 0.5% GlutaMax 0.5% non-essential amino acids 0.5% CultureOne 200 nM Ascorbic acid 20 ng/mL BDNF 20 ng/mL GDNF 1 mM dibutyryl-cAMP 50 U/mL Penicillin 50 µg/mL Streptomycin
Metabolic Assays	
ELISA Buffer	140 mM NaCl 5 mM KCL 1.8 mM $CaCl_2$ 1 mM $MgSO_4$ 10 mM Glucose 10 mM HEPES 0.1% BSA

Seahorse Assay Medium	1 mM Pyruvate 2 mM L-Gultamine 10 mM Glucose Seahorse XF DMEM assay medium, pH 7.4
Microscopy Techniques	
Antibody Buffer	0.1% Triton X-100 2% goat serum 1x PBS (pH 7.4)
Blocking Buffer	0.5% Triton X-100 10% goat serum 1x PBS (pH 7.4)
Ringer's Solution	140 mM NaCl 5 mM KCl 2 mM $CaCl_2$ 1 mM $MgCl_2$ 10 mM HEPES 5 mM Glucose pH 7.4
Protein Work (Western Blotting)	
1x Running buffer	25 mM TRIS 192 mM glycine 0.1% SDS pH=8.3
1x Transfer buffer	20 mM TRIS 150 mM Glycin pH 8.8
1x PBS	137 mM NaCl 10 mM Na_2HPO_4 2.7 mM KCL 2 mM KH_2PO_4
1x PBS-T	1x PBS 0.05% Tween-20
6x SDS loading buffer	250 mM Tris-HCL 30% [v/v] glycerol 10% [w/v] SDS 10 mM DTT 0.05% brophenol blue
SDS-PAGE separating gel (15%)	2.8 mL Aqua dest. 3.0 mL Separating gel buffer 5.9 mL 30 % Acrylamid 80 µL 10 % APS 8 µL TEMED

SDS-PAGE stacking gel (3.5%)	2.0 mL Aqua dest. 0.8 mL Stacking gel buffer 0.4 mL 30 % Acrylamid 16 µL 10 % APS 7 µL TEMED
Separating gel buffer	1.5 mM TRIS 0.4% SDS pH 8.8
5% Skimmed milk	5% [w/v] skimmed milk powder 1x PBS-T
Stacking gel buffer	0.5 M TRIS 0.4% SDS pH 6.8

2.2 Methods

2.2.1 Cell culture methods

2.2.2 Human induced pluripotent stem cells

The hiPSC line from healthy fibroblasts was generated prior to this study using non-integrating episomal plasmid vectors encoding KLF4, SOX2, L-MYC, LIN28, OCT3/4, and p53DD (pCXB-EBNS, pCE-hsk, pCE-hUL, pCE-hOCT3/4, and pCE-mp53DD (Addgene plasmid #41857, # 41814, # 41855, # 41813, and # 41856, gifted by Shinya Yamanaka)) using the Amaxa Nucleofactor (Lonza).

2.2.2.1 Culturing conditions

Undifferentiated human hiPSCs were cultured and maintained in mTeSR Plus medium supplemented with 50 µg/mL gentamycin on Matrigel-coated plates (8.7 µg/cm^2) under standard conditions (37°C, 5% CO_2). The medium was changed daily, and the cells were typically passaged at 70-80% confluency in a 1:3 split ratio. Areas of spontaneous differentiation, characterised by irregular cell morphology within a colony, were mechanically removed by aspiration.

2.2.2.2 Passaging, freezing and thawing procedure

For passaging, colonies were washed once with DMEM/F12, followed by incubation with 1 U/mL dispase for 5 to 7 min at 37°C. When the edges of the colonies started to detach, the dispase was removed and the cells were washed three times with DMEM/F12. An appropriate volume of mTeSR was added, and colonies were broken into small clusters using a 5 mL disposable glass pipette. After gentle mechanical detachment using a cell scraper, the disaggregated colonies were transferred immediately to a Matrigel-coated plate, placed in a 37°C incubator, and left undisturbed for the next 24 h to improve attachment.

For long-term storage, the cells were cryopreserved in liquid nitrogen using CryoStore CS10 freezing medium. hiPSCs were collected in small clusters in DMEM/F12, as described above, and pelleted by centrifugation for 5 min at 800 rpm. Subsequently, cells were taken up in freezing medium, carefully triturated two to three times to break up larger aggregates, and transferred into cryovials. The cells were immediately transferred to -80°C in an isopropanol freezing container to achieve a cooling rate of -1°C/min. After 24 h, the vials were transferred to liquid nitrogen and stored until further use.

Cryopreserved hiPSCs were thawed in a water bath at 37°C until a small fraction was still frozen. The cell suspension was quickly transferred dropwise into 5 mL of pre-warmed DMEM/F12 and spun down for 5 min at 800 rpm. After centrifugation, the supernatant was

aspirated and the colonies were resuspended in fresh mTeSR and seeded onto a Matrigel-coated plate.

2.2.3 CRISPR/Cas9-mediated TSPO knockout

To generate a model that would allow experiments to be performed in the presence or absence of TSPO, CRISPR/Cas9 gene editing was used to generate TSPO-deficient ($TSPO^{-/-}$) and control (CTRL) isogenic clones (three independent clones each) from a parental hiPSC line derived from a healthy donor. Thus, enabling a more profound analysis of TSPO function in mitochondrial homeostasis in human neural progenitors, astrocytes, and neurons.

2.2.3.1 Preparation of the CRISPR/Cas9-TSPO sgRNA plasmids

CRISPR/Cas9-TSPO sgRNA plasmids were prepared according to a previously published protocol (Ran et al., 2013). Therefore, two independent sgRNA-targeting sequences within exon 2 of the human TSPO gene were selected using the bioinformatics tool CRISPOR (http://crispor.tefor.net/, accessed on 27 November 2020). The sgRNA sequences were as follows: #116: 5`-TCCCGCTTTGTCCACGGCGAGGG-3`, and #126: 5`-TCCACGGCGAGGGTCTCCGCTGG-3`. The DNA sequences were separately cloned into the modified pSpCas9 (BB)-2A-Puro (PX459) V2.0 (Addgene plasmid #62988; Addgene, Teddington, UK) vector cAB03, using BbsI restriction sites. This vector, kindly provided by Dr. Emmanuel Nivet (Aix-Marseille Université, France (Arnaud et al., 2022)), contains the human EF1 alpha promoter instead of the CMV enhancer and drives the expression of the *Streptococcus pyogenes* Cas9, the puromycin resistance, and the chimeric sgRNA in mammalian cells.

For cloning, the target sequencing cloning protocol from ZhangLab was adapted. Briefly, oligonucleotide pairs were phosphorylated using T4 Polynucleotide Kinase and hybridised in a water bath by cooling from 95 to 18°C. The cAB03 vector backbone was linearised with BbsI for 30 min at 37°C and then ligated with the annealed oligonucleotides by incubating with T4 DNA Ligase overnight at 16°C. The ligation product was transformed into NEB® Stable Competent *E. coli* (C3040H) following the manufacturer's instructions. After incubation for 1 h at 30°C, the bacteria were inoculated onto ampicillin-containing LB agar plates (100 µg/mL) and incubated overnight at 37°C. The following day, bacterial colonies were picked and amplified overnight in ampicillin-containing LB medium (100 µg/mL). After miniprep extraction (NucleoSpin® Plasmid kit, MACHEREY-NAGEL), the presence of sgRNA in the plasmids of one or two bacterial colonies was confirmed by sequencing using the LKO1.S-F primer. A validated clone was then amplified, and its plasmid DNA was extracted by means of midiprep (NucleoBond® XTRA Midi kit, MACHEREY-NAGEL) and stored at -20°C.

2.2.3.2 Nucleofection

The Human Stem Cell Nucleofector Kit 2 (VPH-5022, Lonza) was used to transfer the cAB03 plasmid into undifferentiated hiPSCs. This method is based on electroporation. Cells were cultivated to a confluence of approximately 90%. For each nucleofection, a total amount of 1 million cells were required. One hour prior to electroporation, 10 µM of Rho-associated kinase inhibitor Y27632 (ROCK inhibitor) was added to the cells. The hiPSCs were then washed once with DMEM/F12 and incubated with Accutase for 8 to 10 min at 37°C to obtain very small colonies or single cells. The Accutase reaction was stopped by rapid addition of DMEM/F12 supplemented with 20% FBS. The cell suspension was gently resuspended with a 1000 µL pipette to avoid excessive pipetting to keep the cells intact. Single cells were collected, transferred into a Falcon tube containing 5 mL of prewarmed DMEM/F12, and centrifuged for 5 min at 800 rpm. During centrifugation, the cell number was estimated using a Neubauer cell-counting chamber under a light microscope IX70 (Olympus). The pellet was resuspended in DPBS at a final concentration of 1 million cells/mL. One millilitre of the cell suspension was transferred to a new Falcon tube and centrifuged at 800 rpm for 5 min. The cells were resuspended in 100 µL nucleofector mix containing 82 µL human stem cell nucleofector solution (Kit 2), 18 µL of supplement 1, and 4 µg of cAB03 plasmid DNA and electroporated with the Amaxa Nucleofector 1 Electroporation System (Amaxa Biosystems) using the program B-016. The electroporated cell suspension was then flushed into a Matrigel-coated well of a 6-well plate containing mTeSR medium supplemented with 10 µM ROCK inhibitor. Two nucleofections were performed for each of the sgRNAs. To define the best time period at which puromycin selection treatment had to be stopped, two additional wells containing cells electroporated without plasmids were used as a selection control. The next day, the medium was replaced with mTeSR supplemented with puromycin (0.5 µg/mL and 1 µg/mL for every two wells of each sgRNA and control, respectively) until all electroporated control cells died. Puromycin-resistant cells were maintained in mTeSR medium until clonal colonies were observed.

2.2.3.3 Clone isolation and screening

Individual colonies arising from a single cell after puromycin selection were manually picked under a light microscope ECLIPSE Ts2 (Nikon). Therefore, the colony was cut in half using a 200 µL pipette tip. One half was used for genomic DNA (gDNA) extraction, transferred individually into a 0.5 mL tube, and centrifuged at 13,000 rpm for 5 min. The other half was slightly dissociated, re-plated onto a Matrigel-coated well of a 24-well plate, and maintained in culture until validation for TSPO-KO.

For KO validation, gDNA was extracted from every picked colony using the DNeasy Blood and Tissue Kit (Qiagen). according to the manufacturer's instructions. Then, a 25 µL PCR reaction

was performed using 5 µL of the extracted gDNA and 20 µL of a PCR mix, the components and volumes of which are listed in Table 8, and specific primer sequences are listed in Table 9.

Table 8: Contents of PCR reaction mix

Component	Volume [µL]
forward primer	1
reverse primer	1
dNTP [10 mM each]	1
5x amplification buffer	5
Taq polymerase	0.125
ddH_2O	11.9

Table 9: Primer sequences used for knockout screening

Gene	5‘3‘-Primer Sequence		Manufacturer
TSPO-Exon2	forward	CTGGAAATGCGTTCACTCAG	Metabion; Planegg, Germany
	reverse	GCCTGGAGAAGACCCTCTGT	

2.2.3.4 hiPSC quality control: Genetic off-target screening

Potential off-target sites were analysed by direct DNA sequencing. The top five candidates were selected using the CRISPOR web tool (http://crispor.tefor.net/, accessed on 27 November 2020). Genomic DNA was isolated from iPSCs using a DNA RapidLyse Kit (MACHEREY-NAGEL), PCR amplification was performed around the five sites, and the PCR products were sequenced by Life Technologies, Regensburg. The primers used are listed in Table 10. Analyses of the sequenced DNA traces were performed using the Snapgene software (version 5.0.8).

Table 10: Primer sequences used for off-target screening

Off-Target	5‘3‘-Primer Sequence		Manufacturer
116-OFF#1	forward	CGCCTACCTCAATACACCCT	Metabion; Planegg, Germany
	reverse	CACCCTACTAGCTAGTCCCG	
116-OFF#2	forward	TAAGCTGCCTCTTACCCTGC	Metabion; Planegg, Germany
	reverse	GAGTCTTCAGGGCCTCACAT	
116-OFF#3	forward	GTGGCTTACAAACTGGGCTC	Metabion; Planegg, Germany
	reverse	CAGCGGGCATATACCTCTCT	
116-OFF#4	forward	CTCTTGGCTGTCCTGTCTCA	Metabion; Planegg, Germany
	reverse	GTGCCTGTTGTTGTGTGGAT	
116-OFF#5	forward	GCTCCTTTCCACCTTCCTCT	

	reverse	CTGCGTTCAAGAAATGGCCT	Metabion; Planegg, Germany
126-OFF#1	forward	CCCTGCCTGCTAAATCCAAT	Metabion; Planegg, Germany
	reverse	ATTGAGACTGTCGACGGAGG	
126-OFF#2	forward	TGTGTGAAGGACGAGGCTTT	Metabion; Planegg, Germany
	reverse	GTCTCGATCTCCTGACCTCG	
126-OFF#3	forward	CCAGACTCAACCTCAGCTGA	Metabion; Planegg, Germany
	reverse	AGAAAGCTCTGGGGTCAAGA	
126-OFF#4	forward	AATGATTACCGGGGCTTCCT	Metabion; Planegg, Germany
	reverse	ATGTAGTTGGCTGGCAGTCT	
126-OFF#5	forward	TCCCAGGTTCAAGCGATTCT	Metabion; Planegg, Germany
	reverse	TTCCTCAAAGATCCCAGGGG	

2.2.4 Neural progenitor cells

2.2.4.1 Neural induction, expansion and cryopreservation

NPCs were derived from hiPSCs following a monolayer culture method based on a previously published protocol (Yan et al., 2013). Undifferentiated cultures of hiPSCs were plated as small colonies onto Matrigel-coated culture plates at a density of 2-2.5x10^4 cells/cm². Approximately 24 h after splitting, the culture medium was switched to Neural Induction Medium (NIM) containing neurobasal medium and neural induction supplement (Life Technologies) and changed every other day until day 4 of neural induction. After day 4, the medium was changed daily as cells reached confluence. On day 7, the cells were detached and dissociated with Accutase by gently pipetting up and down after an incubation time of 5 min at 37°C. The cell suspension was passed through a 50 µm strainer and centrifuged at 800 rpm for 5 min. The cells were resuspended in Neural Expansion Medium (NEM) containing Neurobasal medium, Advanced DMEM/F12, and neural induction supplement, and seeded at a density of 0.5-1x10^5 cells/cm² on Geltrex-coated dishes (0.5 mg/mL). To prevent cell death after plating, NPCs younger than passage four were treated with 5 µM ROCK inhibitor overnight. Afterwards, NEM was changed every other day until cells reached confluence.

For passaging and expansion, NPCs were dissociated with Accutase as described above and maintained on Geltrex-coated plates at a density of 1x10^5 cells/cm² under standard culture conditions, with medium changes every other day. Dissociated NPCs were cryopreserved in STEMdiff Neural Progenitor Freezing Medium and stored at -196°C in liquid nitrogen. Cryopreserved NPCs were thawed in a water bath at 37°C and quickly transferred dropwise into 5 mL pre-warmed DMEM/F12. After centrifugation at 800 rpm for 5 min, the pellet was resuspended in fresh NEM and seeded onto a Geltrex-coated plate.

2.2.5 Astrocytes

2.2.5.1 Differentiation of astrocyte-like cells from NPCs

hiPSC-derived NPCs were differentiated into astrocytes according to a previously described protocol (Tcw et al., 2017). Briefly, NPCs were passaged with Accutase, as described above, and plated at 30,000 cells/cm² on Matrigel-coated plates (8.7 µg/cm²). The next day, NEM medium was exchanged for a commercially available astrocyte medium containing 2% FBS, 1% astrocyte growth supplement, and 1% penicillin/streptomycin (ScienCell). Full media changes were performed every 2-3 days during the 30 day-differentiation period and the cells were maintained under standard culture conditions (37°C, 5% CO_2). Upon confluence, 5 to 7 days after the initial seeding, the astrocytes were passaged onto new Matrigel-coated plates. Astrocytes between 31 and 60 days of differentiation were used in this study.

2.2.5.2 Passaging, freezing, and thawing procedures

For passaging on a weekly basis, astrocytes were washed once with DPBS without Ca^{2+} and Mg^{2+} and incubated with Accutase for 7 to 10 min at 37°C. Accutase treatment was stopped with DMEM/F12. The cells were then dissociated by carefully pipetting up and down and centrifuged at 800 rpm for 5 min. The cell pellet was resuspended in astrocyte medium and cell numbers were determined using a Neubauer cell counting chamber under a light microscope IX70 (Olympus). A total of $1.5x10^4$ to $3x10^4$ cells/cm² were seeded onto Matrigel-coated plates (3.5 µg/cm^2).

Between days 20 and 35 of differentiation, cells were amplified, stocked, and frozen. Therefore, astrocytes were passaged as described above. After centrifugation, a minimum of $5x10^5$ cells were resuspended in 1 mL of astrocyte freezing medium (astrocyte medium supplemented with 20% FBS and 10 % DMSO) and transferred into a cryovial. A controlled freezing rate of -1°C/min for successful cryopreservation was guaranteed using an isopropanol container. After 24 h at –80°C cells were stored in liquid nitrogen until use.

Cryopreserved astrocytes were thawed in a water bath at 37°C and quickly transferred dropwise into 5 ml of pre-warmed DMEM/F12. After centrifugation at 800 rpm for 5 min, the pellet was resuspended in fresh astrocyte medium and seeded onto a Matrigel-coated plate.

2.2.6 Neurons: Neuronal differentiation and cultivation

For neuronal differentiation, dissociated NPCs from passages 5 to 12 were plated onto coated imaging µ-dishes (Ibidi) at a density of 1 to $1.5x10^5$ cells/cm² and differentiated for 21 days. The dishes were coated with 20% poly-L-ornithine in sterile water for 4 h at room temperature, followed by overnight coating with laminin [10 µg/mL] in DPBS with Ca^{2+} and Mg^{2+} at 37°C. After 24 h, the medium was changed to BrainPhys™ Neuronal Medium supplemented with 1% B27 Plus, 0.5% GlutaMax, 0.5% non-essential amino acids, 0.5% Culture One, 200 nM

ascorbic acid, 20 ng/mL BDNF, 20 ng/mL GDNF, 1 mM dibutyryl-cAMP, 50 U/mL Penicillin, and 50 µg/mL streptomycin, and half of the medium was replaced every 2-3 days. Additionally, 4 µg/mL laminin was freshly added each time the medium was changed. The cells were maintained in a humidified incubator at 37°C and 5% CO_2.

2.3 Biochemical methods

2.3.1 Protein expression analysis

2.3.1.1 Cell lysis, protein isolation and sample preparation

For cell lysis, frozen cell pellets from 1 to 2x10^6 cells of the respective cell lines were thawed on ice and resuspended in 200-250 µL DPBS containing 1x protease inhibitor. For complete homogenisation, the samples were pulse-sonicated thrice for 20 s each on ice (BANDELIN Sonoplus HD 3100) at 15% amplitude. To determine the protein concentration of whole-cell lysates, a bicinoic acid assay (BCA) was performed using the Pierce™ BCA Protein Assay Kit (Thermo Fisher Scientific) according to the manufacturer's instructions and quantified with a VarioScan plate reader at 562 nm. The protein concentration was calculated using a BSA standard curve. The samples were prepared for SDS-PAGE or stored at –20°C until further use. Protein lysates were mixed with 6xSDS loading buffer and denatured for 5 min at 95°C. Treating the samples with SDS led to a negative charge in relation to the protein size.

2.3.1.2 SDS-polyacrylamide gel electrophoresis (SDS-PAGE)

Charged proteins were separated according to their molecular weights by SDS-PAGE. A total of 15 µg of protein per sample was resolved on a 12.5% or 15% separation gel, depending on the molecular weight of the protein of interest, and a 3.5% stacking gel. The samples were loaded together with a pre-stained molecular weight marker (PeqGold Protein Marker IV, VWR by Avantor). Electrophoresis was performed at a constant voltage of 140 V for approximately 90 min using a Mini-PROTEAN Tetra Cell running system (Bio-Rad).

2.3.1.3 Immunoblotting and protein transfer detection

Proteins separated by SDS gel electrophoresis were immobilised and transferred to a nitrocellulose membrane (AmershamTM Protran 0,45 NC, GE Healthcare Life Sciences) using the Wet/Tank blotting system Mini Trans-Blot Cell (Bio-Rad). Protein transfer was performed at a constant amperage of 200 mA for 150 min and cooled on ice during blotting. Subsequently, free binding sites on the nitrocellulose membrane were blocked with 5% non-fat dry milk in PBS containing 0.05% Tween (PBS-T) for 30 min at RT. After blocking, the membranes were sectioned and immunostained overnight at 4°C with an array of individual antibodies diluted in PBS-T, as listed in Table 11. Beta 1 tubulin (BTUB1) or GAPDH antibody was used as the loading control. The next day, the membranes were washed three times with PBS-T and

probed with the corresponding HRP-conjugated secondary antibodies diluted in 5% skim milk in PBS-T for 1 h at RT (Table 12). Bands were visualised and documented using SuperSignal™ West Pico Plus chemiluminescent substrate (Thermo Fischer Scientific) and an ImageQuant LAS 4000 (GE Healthcare Europe) imaging system. Densitometric analysis was performed using ImageJ software (version 2.9.2) and band densities were normalised to the corresponding loading control.

Table 11: Primary antibodies used for protein expression analysis

Antibody	Species	Dilution	Manufacturer
BTUB1 E7	mouse	1:10	deposited to the DSHB by Kawakami, A. (DSHB Hybridoma Product E7)
GAPDH sc-47724	mouse	1:2500	Santa Cruz Biotechnology; Dallas, Texas
LC3B 3868S	rabbit	1:1000	Cell Signaling Technology; Danvers, Massachusetts
TSPO affinity purified	rabbit	1:5000	Davids Biotechnologie; Regensburg, Germany
VDAC1 ab186321	Mouse	1:500	Abcam; Cambridge, UK

Table 12: Secondary antibodies used of protein expression analysis

Antibody	Species	Dilution	Manufacturer
Anti-mouse IgG HRP (ab97023)	rabbit	1:5000	Abcam; Cambridge, UK
Anti-rabbit IgG HRP (7074S)	goat	1:5000	Cell Signaling Technology; Danvers, Massachusetts

2.3.2 Cycloheximide protein degradation analysis

To block *de novo* protein biosynthesis and thus determine the protein half-life, iPSC-derived NPCs were treated with 100 µg/mL of the translational inhibitor cycloheximide (CHX) for the indicated time points. Proteins were separated by SDS-PAGE and immobilised onto nitrocellulose membranes. VDAC1 protein was detected using the VDAC1 ab186321 antibody, and BTUB1 was used as a loading control. VDAC1 band densities were quantified using ImageJ software (version 2.9.2) as a percentage of the initial VDAC1 protein level (0 h of CHX treatment) and normalised to the BTUB1 signal from the same blot.

2.4 Molecular biology techniques

2.4.1 mtDNA copy number analysis

To quantify the mtDNA copy number, primers for the mitochondrial encoded tRNA leucine 1 (mt-TL1) and the nuclear gene Beta-2 microtubulin (B2M) were used. Primer sequences are listed in Table 13.

Table 13: Primer sequences used for mtDNA copy number quantification

Gene	5‘3‘-Primer Sequence		Manufacturer
B2M	forward	TGCTGTCTCCATGTTTGATGTATCT	Metabion; Planegg, Germany
	reverse	TCTCTGCTCCCCACCTCTAAGT	
mt-TL1	forward	CACCCAAGAACAGGGTTTGT	Metabion; Planegg, Germany
	reverse	TGGCCATGGGTATGTTGTTA	

Quantitative real-time PCR was performed in technical duplicates from a minimum of three biological gDNA replicates extracted using the DNA RapidLyse Kit (MACHEREY-NAGEL), according to the manufacturer’s instructions. After elution in 30 µL distilled water, the gDNA yield was determined using a NanoDrop spectrophotometre (Thermo Fisher Scientific) and stored at -20°C until further use. qRT-PCR was performed on a RotorGeneQ (Qiagen) cycler using 1xTakyon SYBR Master Mix (Eurogentec) and specific intron-spanning primers. The reaction parameters included an initial phase at 95°C for 5 min, followed by 45 cycles of denaturation at 95°C for 15 s and 30 s annealing/extension at 61°C. The melting curve was assessed by increasing the temperature (1°C per 5 s) from 65 to 95°C. The results were analysed using RotorGeneQ software V2.3 (Qiagen) and Excel (Microsoft) with the following equation for quantification of mtDNA content relative to the diploid nuclear DNA:

$$mtDNA\ copy\ number = 2\ x\ E^{-\Delta\Delta Ct}$$

2.4.2 Quantification of gene expression

2.4.2.1 RNA isolation and reverse transcription into complementary DNA (cDNA)

For gene expression analysis, cell pellets from untreated astrocytes were used. Total RNA was isolated either directly after harvesting the cells or cell pellets were snap-frozen on dry ice and stored at –20°C for later use. RNA extraction was performed according to the manufacturer’s instructions using an RNA Plus Kit (MACHEREY-NAGEL). RNA was eluted using 24 µL of RNase-free water. The RNA concentration was measured using a Nanodrop spectrophotometre (Thermo Fischer Scientific) and stored thereafter at -80°C.

For each reverse transcription, 1 µg of total RNA was used and conducted using the QuantiTect Reverse Transcription Kit (Qiagen), following the manufacturer’s instructions. The obtained cDNA was used immediately for qRT-PCR analysis or stored at -20°C.

2.4.2.2 Quantitative real-time PCR

Quantitative real-time PCR was performed to determine mRNA expression levels of mitochondrial dynamics proteins *MFN1*, *OPA1*, and *DRP1*, the mitochondrial transcription factor *TFAM*, and the mitophagy proteins *PINK1* and *PARK2*. In addition to the genes of interest, one housekeeping gene, *HPRT*, was quantified to normalise the mRNA expression. An H_2O sample was used as a negative control. For each gene, a reaction mixture of 9 µL containing 1xTakyon SYBR Master Mix (Eurogentec), 3 µL H_2O, and X µM of forward and reverse primers (Table 14). All samples were analysed in duplicate using 50 ng/µL of cDNA. qRT-PCR was performed on a RotorGeneQ (Qiagen) cycler using a comparative experimental approach. The reaction parameters included an initial phase at 95°C for 5 min, followed by 45 cycles of denaturation at 95°C for 15 s and 30 s annealing/extension at 61°C. The melting curve was assessed by increasing the temperature (1°C per 5 s) from 65 to 95°C. The results were analysed using RotorGeneQ software V2.3 (Qiagen) and Excel (Microsoft) with the ΔΔCt method for relative quantification.

Table 14: Primer sequences used for gene expression analysis

Gene	5‘3‘-Primer Sequence		Manufacturer
HPRT	forward	TTGCTTTCCTTGGTCAGGCA	Metabion; Planegg, Germany
	reverse	ATCCAACACTTCGTGGGGTC	
DRP1	forward	TCAAGACAGTGTGCCAAAGG	IDT; Leuven, Belgium
	reverse	TGGCCTACTAGCTCACTCTGA	
MFN1	forward	AGGATGATTGTTAGCTCCACGA	IDT; Leuven, Belgium
	reverse	CACAGGCGAGCAAAAGTGG	
OP1	forward	ACTGAAGTTAGGCGATTAGAGAA	IDT; Leuven, Belgium
	reverse	CCAGTTGAACGCGTTTACCA	
Parkin	forward	AGAAAACCACCAAGCCCTGT	Metabion; Planegg, Germany
	reverse	CAGTTCCAGCACCACTCGAG	
PINK1	forward	GTACCAGTGCACCAGGAGAA	Metabion; Planegg, Germany
	reverse	AACCTGCCGAGATGTTCCAC	
TFAM	forward	CGCAGGAAAAGCTGAAGACTG	IDT; Leuven, Belgium
	reverse	TCGTCCTCTTTAGCATGCTGA	

2.5 Metabolic analysis

2.5.1 Mitochondrial Respiratory Function Analysis: Seahorse XF Flux analysis

Agilent Seahorse XF technology is a live-cell metabolic assay platform which simultaneously measures oxygen consumption rates (OCR) and extracellular acidification rates (ECAR) in real time in a multi-well plate, interrogating key cellular functions, such as mitochondrial respiration and glycolysis (Fig. 9A).

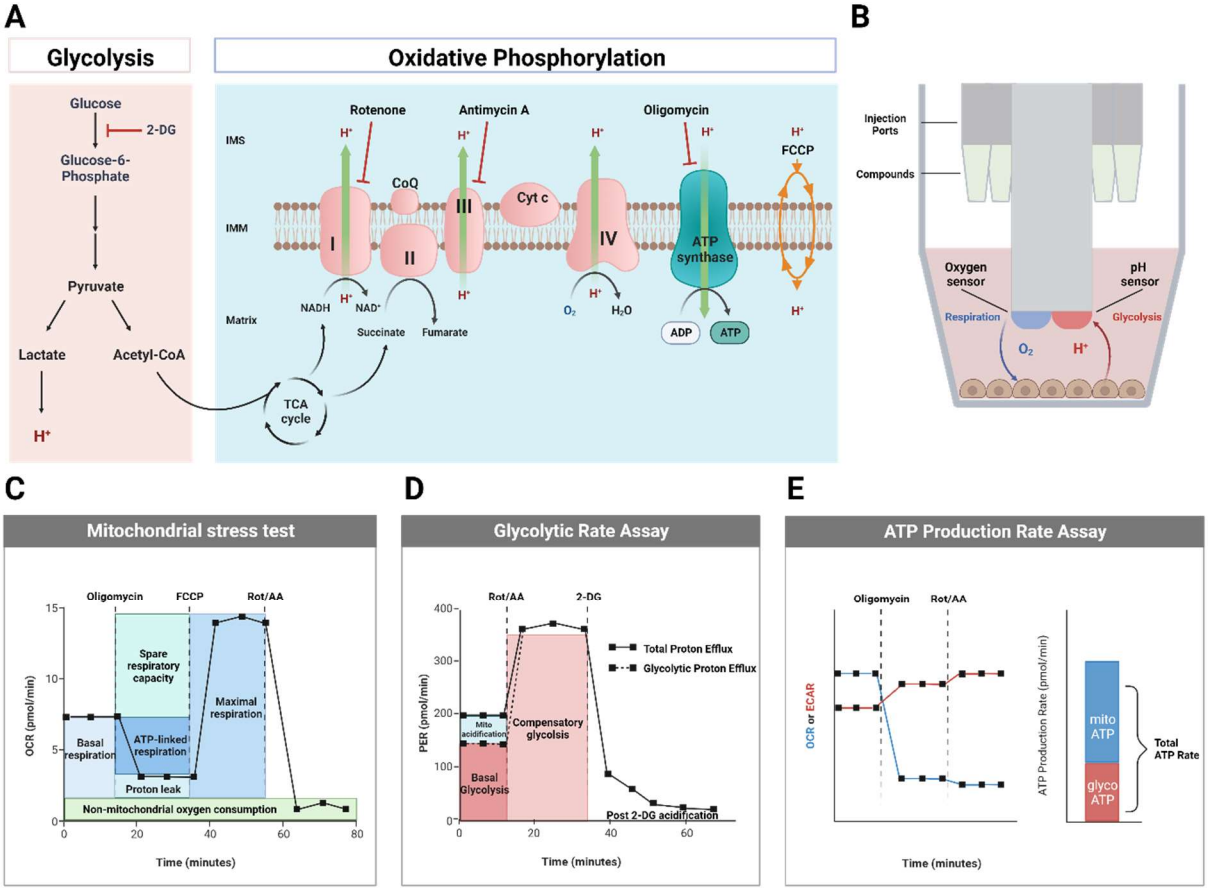

Figure 9: Measurement of cell metabolism using an XFp Extracellular Flux Analyser. (A) The assays reveal standard parameters of mitochondrial and glycolytic function by injecting different inhibitors: oligomycin, FCCP, a mixture of rotenone and antimycin A, and 2-deoxy-D-glucose (2-DG). **(B)** Agilent seahorse technology is a plate-based live-cell assay that allows nondestructive metabolic measurements in real time. Biologically compatible optical microsensors, integrated into the cartridge, contain two fluorophores which measure oxygen (O_2) and proton (H^+) concentrations in the extracellular medium without any dye. These sensors monitor changes in oxygen and proton concentrations during each measurement cycle and calculate oxygen consumption (OCR) and extracellular acidification rate (ECAR). **(C)** The Seahorse XF mitochondrial stress test determines the cells' mitochondrial respiration signature, consisting of basal respiration, ATP-related OCR, proton leak, maximal respiration, and spare respiratory capacity. **(D)** Glycolytic parameters are measured using the Seahorse XF Glycolytic Rate Assay which calculates the basal glycolytic rate and compensatory glycolysis following the injection of rotenone/antimycin A and 2-DG**. (E)** The Seahorse XF Real-Time ATP Rate Assay measures and quantifies the rate of ATP production from glycolysis and mitochondrial oxidative phosphorylation after serial addition of the mitochondrial inhibitors, oligomycin and rotenone/antimycin A. Created with BioRender.com

It is based on solid-state sensor probes containing polymer-embedded fluorophores which detect oxygen and proton levels in a small volume of culture medium above a cell monolayer. A decrease in the oxygen level indicates the extent of oxygen reduction to water during OXPHOS. An increase in proton concentration is an indicator of the glycolytic activity of cells.

An integrated drug delivery system allows the automated injection of up to four compounds during measurement (Fig. 9B). Seahorse XF assays were performed according to the manufacturer's instructions using an XFp Extracellular Flux Analyser (Seahorse Agilent).
The day prior to the assay, the cells were detached as described above and seeded at 80,000 NPCs/well or 30,000 astrocytes/well into a Matrigel-coated XFp Miniplate. The sensor cartridges were hydrated with Seahorse XF Calibrant in a non-CO_2 incubator overnight at 37°C. On the day of the assay, the cells were washed once and incubated with Seahorse XF Assay medium (buffered Seahorse XF DMEM supplemented with 10 mM glucose, 2 mM L-glutamine, and 1 mM pyruvate) in a non-CO_2 incubator for 45 min at 37°C. Meanwhile, the injection ports of the sensor cartridge were loaded with the appropriate assay compounds for either the Seahorse XF Mito Stress Test, the Seahorse XF Glycolytic Rate Assay, or the Seahorse XF Real-Time ATP Rate Assay. The sensor plate was calibrated in an XFp flux analyser prior to loading the cells and running the individual assay. For the Seahorse XF Glycolytic Rate and Real-Time ATP Rate Assays, the cells were washed once again with Seahorse XF Assay medium after incubation in a non-CO_2 incubator. The OCR is reported as pmol/min and mpH/min, respectively. For comparability, ECAR is expressed as the proton efflux rate (PER) [pmol/min]. Data were acquired and analysed using Wave software (Agilent). Following the assay, cells were fixed in 4% paraformaldehyde at RT for 15 min. After washing with PBS, the nuclei were stained with Hoechst (1:1000 in PBS) for 10 min in the dark and images of each well were captured using an Axio Observer Z1 fluorescence microscope (Zeiss, Oberkochen, Germany). With the help of an ImageJ macro (provided on request), nuclei were counted to normalise respiration data.

2.5.1.1.1 Seahorse XF Mito Stress Test

To test oxidative phosphorylation, the sensor plate was loaded with oligomycin (1 µM final), FCCP (1 µM final for NPCs and 2 µM final for astrocytes), and a combination of rotenone (0.5 µM final) and antimycin A (0.5 µM final). After four baseline measurements, OCR and ECAR were conducted four times after sequential injection of each compound to calculate the standard parameters defining the mitochondrial respiration signature of the cells (Fig. 9C):
Basal respiration is an indicator of basal OXPHOS and represents the oxygen consumption that meets the cell's endogenous ATP demand. Basal respiration comprises two processes: respiration, which drives ATP synthesis, and respiration, which is associated with mitochondrial proton leak pathways. Oligomycin leads to the inhibition of ATP synthase (complex V) and, consequently, to a decrease in OCR, which corresponds to mitochondrial respiration utilised for cellular ATP production (***ATP-related OCR***). The resulting proton congestion leads to reduced electron flow across the respiratory chain, thus reducing the oxygen consumption. ATP-related respiration is controlled by ATP utilisation, ATP synthesis,

substrate supply, and oxidation. The remaining mitochondrial respiration rate insensitive to oligomycin corresponds to ***proton leakage***, a measure of proton flux through the inner mitochondrial membrane, which occurs independently of ATP synthase. Proton leakage is caused by the incomplete coupling of electron transport and ATP synthase activity, but its molecular nature is not entirely understood. Injection of FCCP, an uncoupler of the respiratory chain, results in the breakdown of the proton gradient and collapse of the mitochondrial membrane potential. To maintain the mitochondrial membrane potential, substrate oxidation and ETC function increase, and FCCP mimics physiological "energy demand". FCCP shuttles protons across the inner membrane, thereby dissipating the proton motive force, and electron flow through the electron transport chain proceeds unimpeded, maximising oxygen consumption by complex IV (***maximal respiration***). Maximal respiration is dictated by substrate availability and oxidation, and changes in maximal respiration may indicate changes in mitochondrial biogenesis or cristae structure. The maximal increase in OCR can be used to calculate the ***spare respiratory capacity*** (SRC) of the cells. SRC is the mitochondrial reserve capacity, which indicates the ability of the cell to meet increased energy demands and respond to oxidative stress. Finally, the addition of rotenone (a complex I inhibitor) and antimycin A (a complex II inhibitor) leads to complete inhibition of mitochondrial respiration. The remaining oxygen consumption reflects the ***non-mitochondrial respiration*** of cells, which occurs outside the mitochondria. The calculation for each respiratory parameter is presented in Table 15.

Table 15: Mitochondrial respiration parameters determined using the Seahorse XF Mito Stress Test

Respiration Rate	Calculation
Basal respiration.	(Baseline OCR before addition of oligomycin) – (non-mitochondrial respiration)
Proton leak-linked respiration	(Minimal OCR after oligomycin addition but prior to FCCP injection) – (non-mitochondrial respiration)
ATP-related respiration	(basal respiration) – (proton leak)
Maximal respiration	(Maximal OCR after FCCP injection) – (non-mitochondrial respiration)
Spare respiratory capacity	(Maximal respiration) – (basal respiration)
Non-mitochondrial respiration	(Minimal OCR after rotenone/antimycin A injection)

2.5.1.1.2 Seahorse XF Glycolytic Rate Assay

For measuring the glycolytic rate by calculating and subtracting mitochondrial-produced acidification the mitochondrial inhibitors rotenone and antimycin A were used in a final concentration of 0.5 µM each as well as 50 mM 2-deoxy-D-glucose (2-DG) as a glycolytic

inhibitor. The Seahorse XF Glycolytic Rate Assay (Fig. 9D) uses both the ECAR and OCR measurements to report and calculate the following parameters (Table 16):
During glycolysis, glucose is converted to pyruvate and then to lactate in the cytoplasm. This breakdown of glucose results in proton efflux (***glycoPER***) and acidification of the extracellular medium, which is detected as ECAR by the Seahorse flux analyser. However, cells may also use glucose for energy production via oxidative phosphorylation. The TCA cycle, which fuels ETC, produces CO_2. This mitochondria-derived CO_2 hydrates the medium, resulting in additional extracellular acidification. The basal proton efflux rate (***basal PER***) indicates the total extracellular acidification and measures the protons secreted by cells under basal conditions. Injection of rotenone and antimycin A inhibits mitochondrial respiration and is used to calculate the contribution of non-mitochondrial respiration to the OCR and, subsequently, the proton efflux rate from mitochondrial TCA activity (***mitoPER***). Inhibition of OXPHOS drives compensatory changes in the cell to meet the cells' energy demands, resulting in increased glycolysis (***compensatory glycolysis***). The glucose analogue 2-DG stops glycolytic acidification through competitive binding of hexokinase, the first enzyme in the glycolytic pathway. This leads to a decrease in PER and confirms the pathway specificity. The remaining PER includes other sources of extracellular acidification (***post-2-DG acidification***), which are not attributed to glycolysis or mitochondrial TCA activity.

Table 16: Key glycolytic parameters determined using the Seahorse XF Glycolytic Rate Assay

Respiration Rate	Calculation
Basal PER.	Baseline PER prior to rotenone/antimycin A injection
mitoPER	Basal OCR * pre-determined CO_2 contribution factor
glycoPER	(basal PER) – (mitoPER)
Compensatorcy glycolysis	Mean PER after rotenone/antimycin A injection
Post-2-DG acidification	Mean PER after 2-DG injection

2.5.1.1.3 Seahorse XFp Real-Time ATP Rate Assay.

Glycolysis and OXPHOS pathways provide the majority of cellular ATP in mammalian cells, which is the ubiquitous, dominant energy currency for cells. To adjust for changes in ATP demand and subsequent changes in ATP production to maintain overall intracellular ATP levels, cells regulate their metabolism. While OXPHOS consumes oxygen, as indicated by the OCR, both pathways contribute to extracellular acidification of the assay medium, driving changes in ECAR. By obtaining both, OCR and ECAR, simultaneously under basal conditions and after serial addition of 1.5 µM oligomycin followed by 0.5 µM of each rotenone and antimycin A, pathway-specific ***mitoATP*** (associated with OXPHOS in the mitochondria) and ***glycoATP production rate*** (associated with the conversion of glucose to lactate during

glycolysis) and ***total ATP production rate*** (sum of mitochondrial ATP and glycolytic ATP production rates in live cells) can be measured (Table 17). Therefore, the Seahorse XFp Real-Time ATP Rate Assay (Fig. 9E) provides an overview of cellular bioenergetics and allows a quantitative comparison of energy engines under basal conditions.

Table 17: ATP production rates determined using the Seahorse XF Real-Time ATP Rate Assay

ATP Production Rate	Calculation
glycoATP production rate	glycoPER
mitoATP production rate	(OCR after Oligomycin injection) * 2(pmol O/pmol O_2) * P/O (pmol ATP/pmol O)
total ATP production rate	(glycoATP) + (mitoATP)

2.5.2 Total ATP content quantification

For the quantification of whole-cell ATP content, $1x10^6$ NPCs and $1x10^5$ astrocytes were collected in a 1.5 mL Eppendorf cup and stored at –20°C until use. ATP content was measured using the CellTiter-Glo® Luminescent Cell Viability Kit (Promega) based on an ATP-dependent luciferase reaction (Fig. 10). According to the manufacturer's instructions, CellTiter-Glo® Reagent containing CellTiter® Substrate and CellTiter® Buffer and ATP standards were thawed on ice. For the standard curve, ATP concentrations of 10 µM, 1 µM, 100 nM, 10 nM, and 1 nM in DPBS were used. The cell pellets were resuspended in 500 µL DPBS, heated at 100°C for 2 min to inactivate endogenous ATPases, and kept on ice afterwards. Fifty microlitres of each sample and standard were applied to a black 96-well plate in duplicate, together with 50 µL of CellTiter-Glo® reagent. After shaking for 2 min in the dark, absorption was measured with the VarioScan (Thermo Fisher Scientific) at an integration time of 1 s. The relative light unit (RLU) generated by the SkanIT Software was used to calculate the ATP concentrations in relation to the standard curve. ATP concentrations were normalised to µg/mL protein using a BCA assay (Thermo Fisher Scientific)

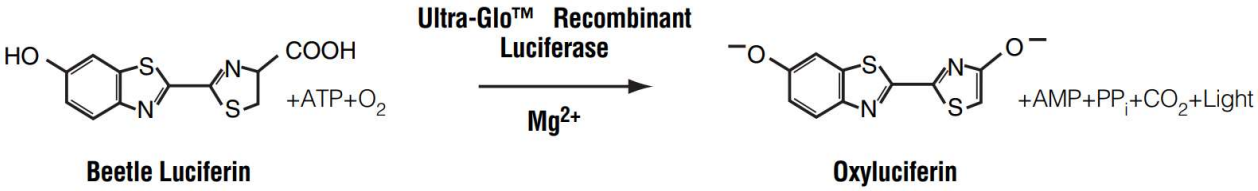

Figure 10: Luciferase reaction for total ATP quantification. Luciferin mono-oxygenation is catalysed by luciferase in the presence of Mg^{2+}, ATP, and molecular oxygen. CellTiter-Glo® Luminescent Cell Viability Assay Technical Bulletin, Promega.

2.5.3 Pregnenolone quantification

Pregnenolone quantification was performed using an enzyme-linked immunosorbent assay (ELISA) adapted from a previously published protocol (Germelli et al., 2021). Briefly, $1.5x10^5$ astrocytes/well were seeded in duplicate in a Matrigel-coated 24-well plate and maintained under standard culturing conditions for two days. On the day of the experiment, the culture medium was replaced with ELISA buffer (140 mM NaCl, 5 mM KCl, 1.8 mM $CaCl_2$, 1 mM $MgSO_4$, 10 mM glucose, 10 mM (HEPES)-NaOH, pH 7.4, and 0.1% BSA) containing inhibitors of pregnenolone metabolism trilostane (25 µM) and SU10603 (10 µM). To quantify pregnenolone accumulation, the supernatant was collected after 3 h of incubation at 37°C. The supernatant was analysed by ELISA according to the manufacturer's instructions (Pregnenolone ELISA, LDN, Nordhorn, Germany). The resulting absorbance intensity was quantified using a Tecan Spectra microplate reader (Tecan, Crailsheim, Germany) at 450 nm and then inversely related to the pg/mL of pregnenolone using the Magellan Data Analysis Software (Tecan). Quantified pregnenolone concentrations were normalised to the protein concentration of each sample, as determined using the Pierce BCA Protein Assay (Thermo Fisher Scientific), as described above.

2.6 Microscopy techniques

2.6.1 Immunocytochemical staining

For immunocytochemistry, cells were grown on either Geltrex- or Matrigel-coated glass coverslips (12 mm) and fixed in a 4% PFA solution for 15 min at RT. Neurons were fixed for immunostaining after live-cell fluorescent imaging on day 20 or 21 of differentiation. Fixed cells were washed and stored in PBS until further use. For certain antibodies, antigen retrieval was performed prior to staining to enhance the antibody intensity by unmasking epitopes. Therefore, coverslips were cooked for 15 min in citrate buffer (pH 6, Histo-Line) in a steamer (Braun) and allowed to cool to RT. Subsequently, cells were washed three times with DPBS and simultaneously permeabilised and blocked using a blocking solution containing 0.5% Triton X100 and 10% normal goat serum for 20 min. The indicated concentrations of the primary antibodies (Table 18) were incubated overnight at 4°C. The next day, coverslips were rinsed again three times with PBS, followed by a 2 h incubation at RT in the dark with species-specific fluorochrome-conjugated secondary antibodies (Table 19) and Hoechst to counterstain nuclei. Primary and secondary antibodies were diluted in antibody buffer. After three additional washing steps, the coverslips were mounted on glass slides with Dako fluorescent mounting medium overnight for long-term storage.

Table 18: Primary antibodies used for immunocytochemistry and respective protocol modifications

Antibody	Host	Dilution	Manufacturer	Protocol modification
ALDHL1 ab87117	rabbit	1:500	Abcam; Cambridge, UK	
EAAT1 ab416-1001	rabbit	1:200	Abcam; Cambridge, UK	
GFAP C53893	mouse	1:400	Sigma-Aldrich; St. Louis, Missouri	
MAP-2 ab5392	chicken	1:500	Abcam; Cambridge, UK	
NeuN ab177487	rabbit	1:1000	Abcam; Cambridge, UK	
PSD95 K28/43	mouse	1:250	UC Davis/NIH NeuroMab Facility; Davis, California	
PAX6	mouse	1:10	deposited to the DSHB by Kawakami, A. (DSHB Hybridoma Product PAX6)	
TSPO ab109497	rabbit	1:500	Abcam; Cambridge, UK	antigen retrieval
S100β S2532	mouse	1:1000	Sigma-Aldrich; St. Louis, Missouri	
SOX2 ab97959	rabbit	1:1000	Abcam; Cambridge, UK	
Synaptophysin ab52636	rabbit	1:250	Abcam; Cambridge, UK	
Tuj-1 G712A	mouse	1:2000	Promega; Madison, USA	
VDAC1 ab186321	mouse	1:500	Abcam; Cambridge, UK	antigen retrieval
VGLUT-1 ab180188	rabbit	1:250	Abcam; Cambridge, UK	

Table 19: Secondary antibodies used for immunocytochemistry

Antibody	Host	Dilution	Manufacturer
Alexa Fluor® 488 anti-rabbit A11008	goat	1:1000	Gibco by Life Technologies; Carlsbad, USA
CY3® anti-mouse A10521	goat	1:1000	Gibco by Life Technologies; Carlsbad, USA
CY5® anti-chicken ab97147	goat	1:1000	Abcam; Cambridge, UK

2.6.2 Fluorescent live-cell imaging

Live cell imaging experiments were conducted using an inverted Zeiss Axio Observer Z.1 microscope equipped with a Fluar 40/1.3 objective lens (Zeiss, Oberkochen, Germany). All recordings were taken at a magnification of 40X with oil and detected using an AxioCam MRm CCD camera (Zeiss, Oberkochen, Germany). Illumination control and image acquisition were performed using a Lambda DG-4 high-speed wavelength switcher (Sutter Instruments, Novato, California) and the ZEN 2012 imaging software. Analysis of the measurements in the regions of interest, manually drawn over selected cells in the visual field, was performed using ImageJ (version 2.9.2). The macros used for background subtraction and analysis will be provided on request.

2.6.2.1 Analysis of mitochondrial membrane potential

MMP of NPCs and neurons was assessed using the ratiometric fluorophore JC-1 (5,5',6,6'-tetrachloro-1,1',3,3'-tetraethylbenzimidazolylcarbocyanineiodide). It is a membrane-permeable cationic cyanine dye that accumulates in the mitochondria in a potential-dependent manner. Due to its dual emission properties, monomeric green fluorescence (530 nm) is the predominant form in cells exhibiting lower MMP, whereas red fluorescent aggregates of JC-1 (J-aggregates with an emission maximum at 596 nm) are found in cells with higher mitochondrial membrane potential. Consequently, mitochondrial depolarisation is indicated by a decrease in the ratio of red to green fluorescence intensity. This ratio depends only on the MMP and no other factors, such as the size, density, or shape of the mitochondria. Furthermore, the ratio signal is independent of dye concentration and intracellular distribution, dye leakage, photobleaching, and cell thickness, allowing MMP to be determined independently of these artefacts.

To investigate the mitochondrial membrane potential in astrocytes, the fluorescent dyes TMRE (tetramethylrhodamine, ethyl ester) in non-quenching mode and MitoTracker® Green (MTG) were used. TMRE is a lipophilic, cationic, red-orange fluorescent dye that accumulates in the mitochondria according to their MMP in a Nernstian fashion. Depolarised or inactive mitochondria with decreased MMP fail to sequester TMRE. MitoTracker® Green is a cell-permeable probe containing a mildly thiol-reactive chloromethyl moiety that allows mitochondrial labelling independent of MMP. The dye selectively accumulates in the mitochondrial matrix, where it reacts and covalently binds to the free thiol groups of cysteine residues of mitochondrial proteins.

2.6.2.1.1 Cell preparation and staining procedure

Approximately 1.8×10^6 NPCs and 1.2×10^5 astrocytes were grown on Matrigel-coated sterile glass coverslips (diameter 25 mm) overnight and loaded with 200 nM JC-1/Pluronic or 25 nM

TMRE/Pluronic and 200 nM MTG, respectively, in OptiMEM for 30 min at 37°C in humidified air and 5% CO_2. To improve solubilisation, the dyes were mixed at a ratio of 1:2 with the nonionic poloxamer Pluronic F-127. For imaging, the coverslips were washed three times with Ringer's solution containing glucose (300 mOsmol/kg) and placed in a measuring chamber under a microscope. Neurons were measured on day 20 of differentiation in imaging µ-dishes. The wavelength switcher allowed excitation of JC-1 at 480/36 nm, TMRE at 545/25 nm, and MitoTracker® Green at 470/40 nm. The emitted light was filtered at 537/42 nm and 620/60 nm for green or red JC-1 fluorescence and 605/70 nm and 525/50 nm for TMRE and MTG fluorescence, respectively. MMP was analysed as the ratio of red/green (JC-1) or as the ratio of TMRE/MTG fluorescence intensity in the regions of interest.

2.6.2.2 Analysis of intracellular and mitochondrial Ca^{2+} concentrations with Fura-2/AM and Rhod-2/AM dye

Cytosolic $[Ca^{2+}]_c$ calcium levels were quantified using the cell-permeable acetoxymethyl (AM) ester of Fura-2, which is a ratiometric fluorescent chelator selective for Ca^{2+} over other ions. Within the cell, cleavage of the ester group by cytosolic esterases leads to the release and polarisation of the Ca^{2+}-sensitive form, resulting in accumulation of active hydrophilic fluorescent Fura-2 in the cytoplasm. The excitation wavelength of Fura-2 depends on the free or Ca^{2+}-bound state of the dye. Unbound Fura-2 exhibits a maximum excitation wavelength (λ_{Ex}) of 363 nm. Upon binding of free Ca^{2+} ions, the excitation spectrum of the dye shifts to 335 nm, whereas the peak emission remains steady at approximately 510 nm. The intracellular Ca^{2+} concentration in NPCs, astrocytes, and neurons was assessed by measuring the emission fluorescence at 510 nm after excitation at 340 or 380 nm, as the ratio of emission fluorescence at $\lambda_{Ex}(340)/\lambda_{Ex}(380)$ is directly related to the amount of intracellular Ca^{2+}. Because the fluorescence intensity of Fura-2 increases at 340 nm and decreases at 380 nm with increasing Ca^{2+} binding, the ratio can be used as a direct measure of free $[Ca^{2+}]_c$ ($F_{ratio}340/380$). Rhod2-AM is a membrane-permeable rhodamine derivative, which is a positively charged fluorescent dye that allows the measurement of the mitochondrial $[Ca^{2+}]_m$ calcium concentration. Rhod-2/AM, a multivalent cation, effectively accumulates in negatively charged mitochondria due to the hydrolysis of acetoxymethyl groups. Rhod-2 is an intensity-based Ca^{2+} sensor that, unlike Fura-2, responds to increasing Ca^{2+} levels not by changes in its emission and excitation spectrum, but by an increase in fluorescence emission at 580 nm.

2.6.2.2.1 Cell preparation and staining procedure

Approximately $1.8x10^6$ NPCs and $2x10^5$ astrocytes were seeded onto Matrigel-coated 25 mm glass coverslips and incubated overnight in a humidified incubator at 37°C and 5% CO_2. The following day, the cells were simultaneously loaded with Fura-2/AM and Rhod-2/AM. To

improve solubilisation, the dyes were mixed at a ratio of 1:2 with the nonionic poloxamer Pluronic F-127, followed by further dilution to a final concentration of 2 µM in OptiMEM. After incubation for 30 min at 37°C, the cells were washed three times with Ringer's solution containing glucose (300 mosmol/kg). The coverslip was then mounted on an object holder, covered with Ringer's solution, and measured using an inverted microscope. Neurons were stained and measured likewise on day 21 of differentiation on imaging µ-dishes.
For intracellular Ca^{2+} signals, Fura-2/AM-loaded cells were excited with light at 340 nm and 380 nm (BP 340/HE, BP 387/15 HE), and fluorescence emission was detected at 510 nm (BP 510/90 HE and FT 409). Mitochondrial Ca^{2+} in Rhod-2/AM-loaded cells was excited at 545/25 nm and expressed as mean Rhod-2 fluorescence intensity using a 605/70 nm emission filter.

2.6.3 Electron microscopy

Astrocytes were grown on a Matrigel-coated 6-well plate until they reached 70 to 80% confluency. The culture medium was aspirated and the cells were washed with PBS and fixed with Karnovsky fixative for 4 h. Subsequently, the cells were scraped off the plate and centrifuged for 5 min at 800 rpm. The cell pellet was then convicted in cytoblock reagent (Epredia) and surrounded by 4% low-melting agarose. A LYNX microscopy tissue processor (Reichert-Jung, Wetzlar, Germany) was used for the embedding process (post-fixation with osmium tetroxide, dehydration, and infiltration with EPON). Semi-thin-sections (0,75 µm) for the selection of relevant areas and ultrathin sections (80 nm) were cut using a Reichert Ultracut S Microtome (Leica, Wetzlar, Germany). The grids were contrasted with aqueous 2% uranyl acetate, followed by a 2% lead citrate solution for 10 min each. Electron microscopic analysis was performed using a LEO 912AB transmission electron microscope (Zeiss, Oberkochen, Germany) by Heiko Siegmund. Mitochondrial morphology (i.e., area, perimeter, and sphericity) in the regions of interest, manually drawn over visible mitochondria, was analysed using RADIUS software (EMSIS GmbH, Münster, Germany)

2.7 Flow cytometry analyses

Flow cytometry was performed on a BD Biosciences FACS Celesta™, which was run using the Diva software v7.0 (BD Biosciences). The cytometer was equipped with violet (405 nm), blue (488 nm) and red (640 nm) lasers. Particle size and granularity were measured using forward scatter (FSC) and side scatter (SSC) detectors. The area, height, and width parameters of the FSC and SSC detectors were used for doublet exclusion. Compensation was not required. For each sample $0.15x10^6$ to $0.3x10^6$ (astrocytes) or $0.5x10^6$ to $1x10^6$ (NPCs) cells were harvested enzymatically with accutase and centrifuged at 1300 rpm for 7 min at 4°C. All tests were performed in at least three independent experiments. Data were acquired

immediately after staining using the FACS Celesta™ flow cytometer (BD Bioscience, capturing $1x10^5$ (NPCS) or $2x10^4$ (Astro) events per sample. FlowJo software (V10.8., Tree Star) was used for the analysis.

2.7.1 Cytosolic and mitochondrial reactive oxygen species/oxidative stress

Cytosolic ROS levels were determined by applying 10 µM 2',7'-dichlorofluorescein diacetate (H2DCFDA) for 20 min under standard culturing conditions in FACS buffer (DPBS supplemented with 2% FBS) in airtight tubes. To analyse mitochondrial ROS production, the cells were washed with Hank's Balanced Salt Solution (HBSS), stained with 5 µM MitoSOX™ Red Superoxide indicator in HBSS, and incubated in a humidified atmosphere at 37°C and 5% CO_2. Subsequently, the cells were washed with cold DPBS (cytosolic ROS) or FACS buffer (mitochondrial ROS), resuspended in 200-300 µL FACS buffer, and transferred into tubes using a cell strainer to ensure singularity.

2.7.2 Mitochondrial mass

Mitochondrial content was assessed by staining with 1 µM MitoTracker® Green in RPMI 1640 supplemented with 2 mM L-glutamine for 1 h at 37°C in a cell incubator. To prevent mitochondrial depolarization 1.5 µM cyclosporin A was added to prevent mitochondrial depolarisation. After washing and resuspension in 200-300 µL FACS buffer, the cells were filtered and immediately analysed by flow cytometry.

2.8 Statistical analysis

Graphical depictions and statistical analyses were performed using GraphPad Prism 9.5.1 (GraphPad Software) for at least three independent experiments. For all experiments, two to three technical replicates were calculated, and at least three biological replicates were averaged. Statistical outliers were identified using the ROUT-method and removed before the analysis. Normal distribution of the data was assessed using the D'Agostino-Pearson omnibus normality test. Nonparametric data that did not follow a Gaussian distribution were analysed using the Mann-Whitney U test (MW), whereas parametric data were analysed using independent samples t-test. The cut-off value for statistical significance was set at $p \leq 0.05$. Results are presented as mean ± standard error of the mean (SEM). The asterisks in the figures represent p-values as follows: * $p \leq 0.05$, ** $p < 0.01$, *** $p < 0.001$, and **** $p < 0.0001$.

3 Results

3.1 CRISPR/Cas9-mediated TSPO knockout and differentiation of human induced pluripotent stem cells into neural progenitors, astrocytes, and neurons

3.1.1 Validation of TSPO knockout in hiPSCs and off-target screening

To study the role and function of TSPO in neural cells, CRISPR/Cas9-mediated TSPO knockout variants were generated from hiPSCs, reprogrammed from primary skin fibroblasts of a healthy donor. The knockout was validated by DNA sequencing of PCR products and Western Blot analysis.

In one clone (KO1), the nucleofection of the cAB03 plasmid containing the sgRNA-targeting sequence #116 deleted a 17 bp fragment, which resulted in a shift in the open reading frame (ORF) after the amino acid V26 in allele 1. An additional 246 bp insertion in allele 2 generated a stop codon (*) after residue R24. A second clone (KO2) demonstrated a 26 bp deletion in allele 1 and a deletion of a 16 bp fragment in allele 2, resulting in a frameshift and generation of a non-functional *TSPO* gene. Electroporation of the hiPSCs with the cAB03 vector, including the #126 targeting sequence, generated a third clone (KO3), which lost the complete exon 2 and adjacent bases (286 bp) in allele 1. While the deletion of 19 bp in allele 2 led again to a shift in the ORF and a non-functional *TSPO* gene (Fig. 11A).

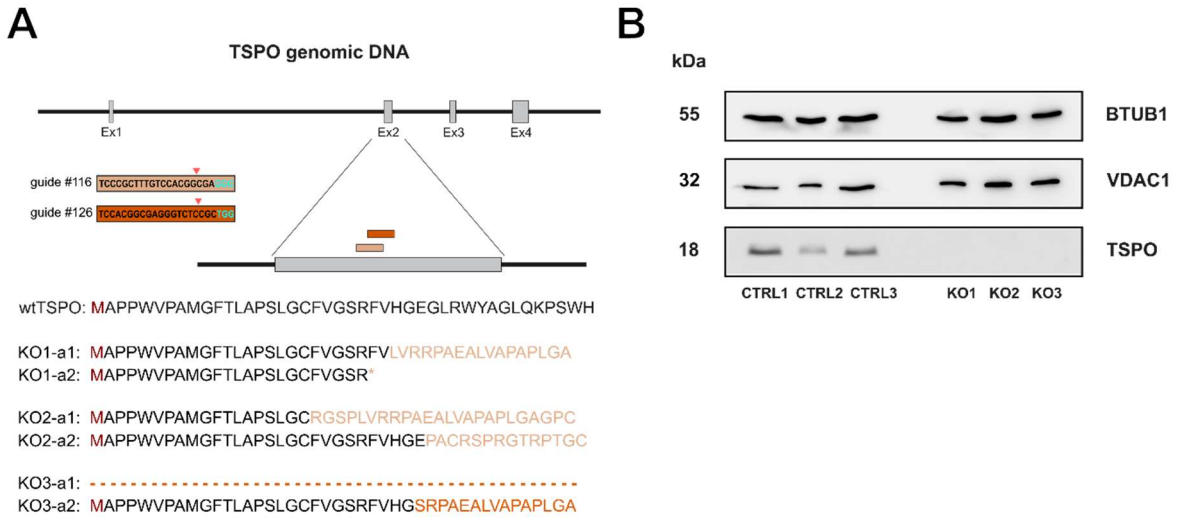

Figure 11: Translocator protein 18 kDa (TSPO) gene deletion in human induced pluripotent stem cells. (A) Schematic overview displaying the CRISPR/Cas9 sgRNA #116 and #126 targeting sites on exon 2 of the TSPO gene, along with their respective PAM sequences, indicated by cyan colour. Successful TSPO knockout in both alleles was confirmed using DNA sequencing. **(B)** Western Blot analysis of TSPO protein expression in hiPSC control (CTRL1, CTRL2, and CTRL3) and knockout (KO1, KO2, and KO3) cells, demonstrating a complete loss of TSPO. BTUB1 was used as a loading control.

Western Blot analysis of TSPO protein expression in all three clones revealed a complete loss of TSPO in the mutated cell lines KO1, KO2, and KO3, whereas the corresponding isogenic control cell lines CTRL1, CTRL2, and CTRL3 exhibited prominent TSPO expression at 18 kDa (Fig. 11B).

CRISPR/Cas9 genome editing is a promising tool in research. However, it can lead to undesired editing outcomes, both on-target at the intended editing site and off-target at other genomic loci. To ensure the reliability of the results and eliminate the possibility of biased outcomes due to potential off-target effects in a given clone, three independent isogenic clones were created. Additionally, three distinct isogenic control hiPSC lines were generated as a physiological reference.

To allow valid comparisons between edited cells and their non-edited isogenic controls, unintended alterations must be excluded. Therefore, guide RNAs with low predicted off-target scores were selected using the CRISPOR web tool. After genome editing, potential off-target sites were analysed by DNA sequencing of the top five off-target hits from the scoring algorithm. As shown in Table 20, the top five off-target candidates within the genome remained unaltered after CRISPR/Cas9 editing using sgRNAs #116 and #126.

Table 20: Off-target screening

sgRNA	Off-target Sequence	Locus description	Sequencing
#116	TCCTGTTTAGTCCACGGCAAAGG	chr9 intron: CTSV	✓
	TCCTGCTTTATCCACAGAGATGG	chrX intergenic: LL0XNC01-73E8.1-BEX1	✓
	TGCAGCTCTGTCCACGGTGAGGG	chr8 intron:DNAJC5B	✓
	TTCCTTTTTGTCCACAGCGAGGG	chr9 intron:RAPGEF1	✓
	TCCCTCTCAGTCCACGGCAAAGG	chr18 intergenic:Y_RNA-RP11-715C4.1	✓
#126	TTCTCAGCGAGGGTCTCCTCTGG	chr20 intergenic:RP5-984P4.4-PAX1	✓
	TCCATGGTGAGGATCTCTGCAGG	chr19 exon:SPC24	✓
	TCCACAGTCAGGGTCTCCTCTGG	chr1 exon:SH3D21	✓
	GCCACCGCTAGGGTCTCCACAGG	chrX exon:FAM127B	✓
	GCCACGGGCAGGGTCCCCGCAGG	chr7 intergenic:AC091729.9-UNCX	✓

3.1.2 Differentiation of hiPSCs into neural progenitor cells

Within seven days of changing the culture medium from mTeSR to neural induction medium, early neural progenitor cells (NPCs) were obtained by differentiating hiPSC colonies (Fig. 12A) derived from the three edited KO cell lines as well as the three corresponding isogenic CTRL cell lines. The NPCs were allowed to further mature for five passages before being stained with the neural progenitor markers SOX2 and PAX6 (Graham et al., 2003; X. Zhang et al., 2010) (Fig. 12B).

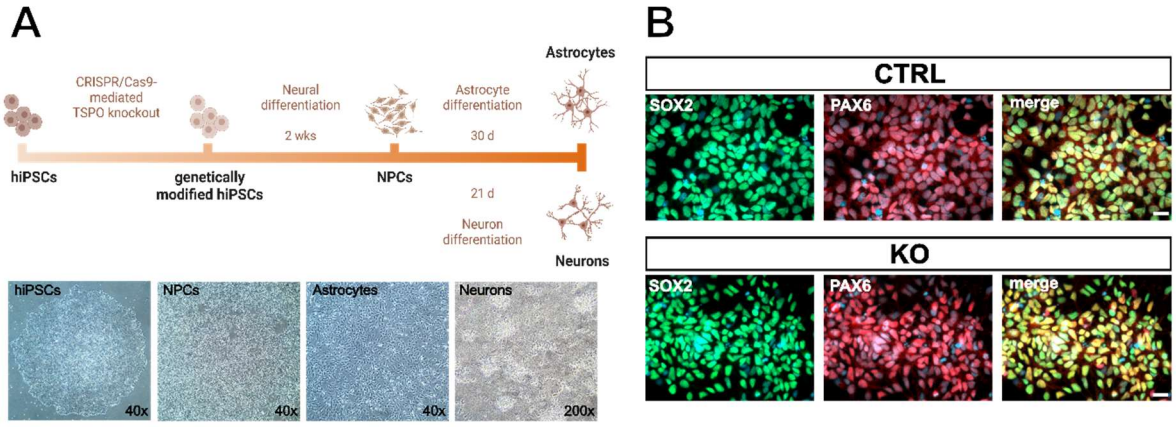

Figure 12: Generation of the hiPSC-based TSPO knockout model. (A) Schematic illustration depicting the experimental process. hiPSCs obtained from a healthy donor were differentiated into neural progenitor cells (NPCs), which were subsequently directed to differentiate into astrocytes or neurons. Images captured under a light microscope show the morphological characteristics of the resulting cell types. **(B)** Representative images of NPCs from both control and knockout groups showing the expression of the neural progenitor cell markers PAX6 and SOX2. Scale bar indicates 20 µm.

The percentage of cells positively labelled with the respective antibodies presented in Table 21 indicates that the majority of cells co-expressed both markers and could therefore be considered neural progenitors.

Table 21: Generation of PAX6/SOX2 positive hiPSC-derived NPC. Numbers represent proportion [%] of SOX2 and PAX6 positive cells in the analysed cultures.

Cell line	SOX2 positive [%]	PAX6 positive [%]
CTRL1	89.7	93.0
CTRL2	91.6	95.2
CTRL3	88.8	91.1
KO1	88.7	94.7
KO2	93.8	95.9
KO3	87.1	93.2

3.1.3 Differentiation of hiPSC-derived NPCs into astrocytes

Following the investigation of TSPO function in neural progenitor cells, astrocytes and induced cortical-like neurones were generated by differentiating NPCs, following the protocol described by (Tcw et al., 2017) and (Yan et al., 2013), respectively.

To identify and confirm the maturity of the astrocytes (Astro), the expression of specific markers was examined by immunostaining. Some of these astrocyte-specific markers include glial fibrillary acidic protein (GFAP), S100 calcium-binding protein B (S100β), glutamate transporter excitatory amino acid transporter 1 (EAAT-1) and aldehyde dehydrogenase 1 family member L1 (ALDH1L1) (Jurga et al., 2021; Verkhratsky et al., 2017). Within 30 days, hiPSC-derived astrocytes were immunopositive for the aforementioned astrocyte markers, as shown in Figure 13A.

Additionally, the functionality of mature astrocytes was verified by the presence of spontaneous and ATP-elicited Ca^{2+} transients, as previously described for astrocytes (Aguado et al., 2002; Barbar et al., 2020; Scemes & Giaume, 2006; Tcw et al., 2017; Volterra et al., 2014). The Ca^{2+} indicator Fura-2/AM was used to monitor Ca^{2+} signalling under basal conditions and in response to a pulse of extracellular ATP (100 µM) (Barbar et al., 2020). While some cells showed already spontaneous Ca^{2+} spikes (Fig. 13B), a single pulse of the gliotransmitter ATP produced a slow Ca^{2+} response in the majority of cells (Fig. 13C), suggesting a network of interconnected astrocytes with Ca^{2+} fluctuations serving as the signal by which they respond, integrate, and convey information (Scemes & Giaume, 2006).

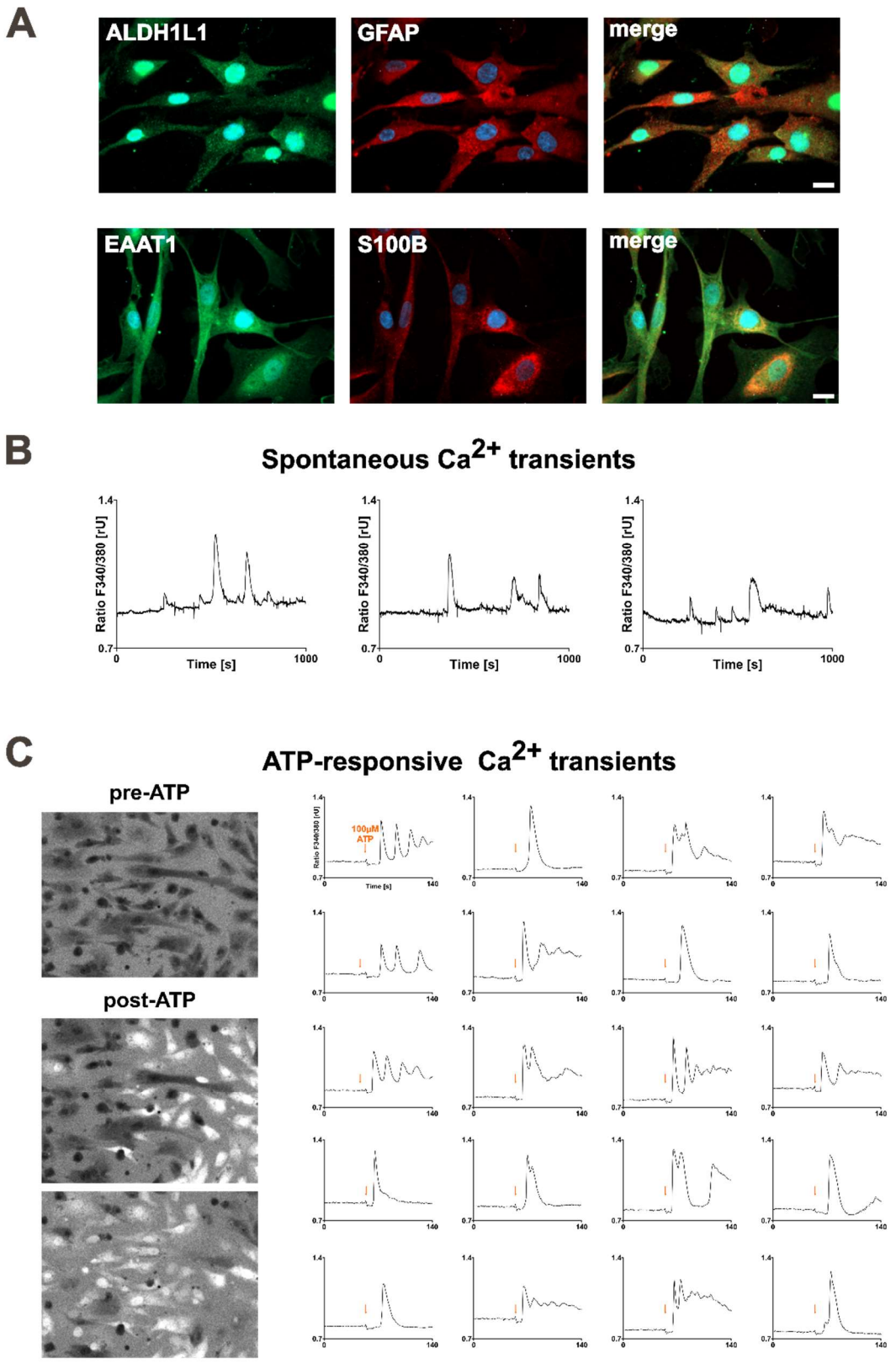

Figure 13: Validation of hiPSC-derived astrocytes. (A) Immunofluorescence stainings demonstrate the presence of mature astrocyte markers, including GFAP, ALDH1L1, S100β, and EAAT1. Scale bar represents 20 µm. Representative examples of **(B)** spontaneous and **(C)** ATP-responsive Ca^{2+} transients in astrocytes loaded with Fura-2/AM are shown. The curves depict spontaneous Ca^{2+} oscillations, a common feature of astrocytes, and ATP-responsive calcium transients in the recorded changes of the fluorescent Fura-2 ratio F_{340nm}/F_{380nm} [rU] over time in astrocyte somata. The gliotransmitter ATP was added at a final concentration of 100 µM to elicit a response. On the left, representative Fura-2 ratio images display brighter cells post-ATP treatment, indicating increased intracellular calcium levels. Scale bar indicates 50 µm.

3.1.4 Differentiation of hiPSC-derived NPCs into neurons

To characterise the identity of hiPSC-derived neurons, the expression of specific neuronal markers was investigated using immunocytochemical analysis. Somato-dendritic microtubule-associated protein 2 (MAP-2) and class III β-tubulin (Tuj-1)-positive neuronal cells were detected after 21 days of differentiation, representing the neurite network. Additionally, visualisation of the post-mitotic nuclei via the neuronal marker NeuN, co-localising with the nuclear-specific dye Hoechst, indicated a highly pure neuronal culture (Chalatsa et al., 2019). The induced neurons displayed mature synaptic terminals, as evidenced by distinct punctate labelling with antibodies against presynaptic (synaptophysin, VGLUT1) and postsynaptic (PSD95) markers (Fig. 14A). Vesicular glutamate transporters (VGLUTs) are essential for normal synaptic function by incorporating the excitatory neurotransmitter glutamate into synaptic vesicles (Martineau et al., 2017). The scaffolding postsynaptic density protein 95 (PSD95) is involved in orchestrating excitatory synapse maturation and specificity and regulates the trafficking and localisation of glutamate receptors (Prange et al., 2004; Yoo et al., 2019). Both proteins serve as distinctive biomarkers for glutamatergic synapses and neurons, and therefore, identify the differentiated cells as cortical-like glutamatergic neurons. To further visualise neuronal morphology, high-resolution electron micrographs were generated, revealing densely interconnected networks of neurites and protrusions (Fig. 14B). Excitability is a hallmark of neuronal function and is involved in both spontaneous and evoked neurotransmission as well as synaptic control. Spontaneous neuronal activity plays a crucial role in the maturation of the developing brain and is vital for processes such as neuronal migration, axonal and dendritic growth, and formation and refinement of neuronal connectivity and synapses (Aguado et al., 2002). Spontaneous activity, which refers to the firing of neurons in the absence of sensory input, represents a fundamental characteristic of the nervous system (Uddin, 2020). As changes and oscillations in intracellular Ca^{2+} concentrations through voltage-dependent Ca^{2+} channels, evoked by the electrical activity of individual neurons (Tada et al., 2014), are an important aspect of spontaneous activity, neuronal Ca^{2+} signalling was monitored in hiPSC-derived neurons to verify their functionality (Fig. 14C). Additionally, the occurrence of the first synchronous patterns of coactive neurons, contributing to the coordination of neural network activity (Aguado et al., 2002), further confirmed successful differentiation into neurons (Fig. 14D).

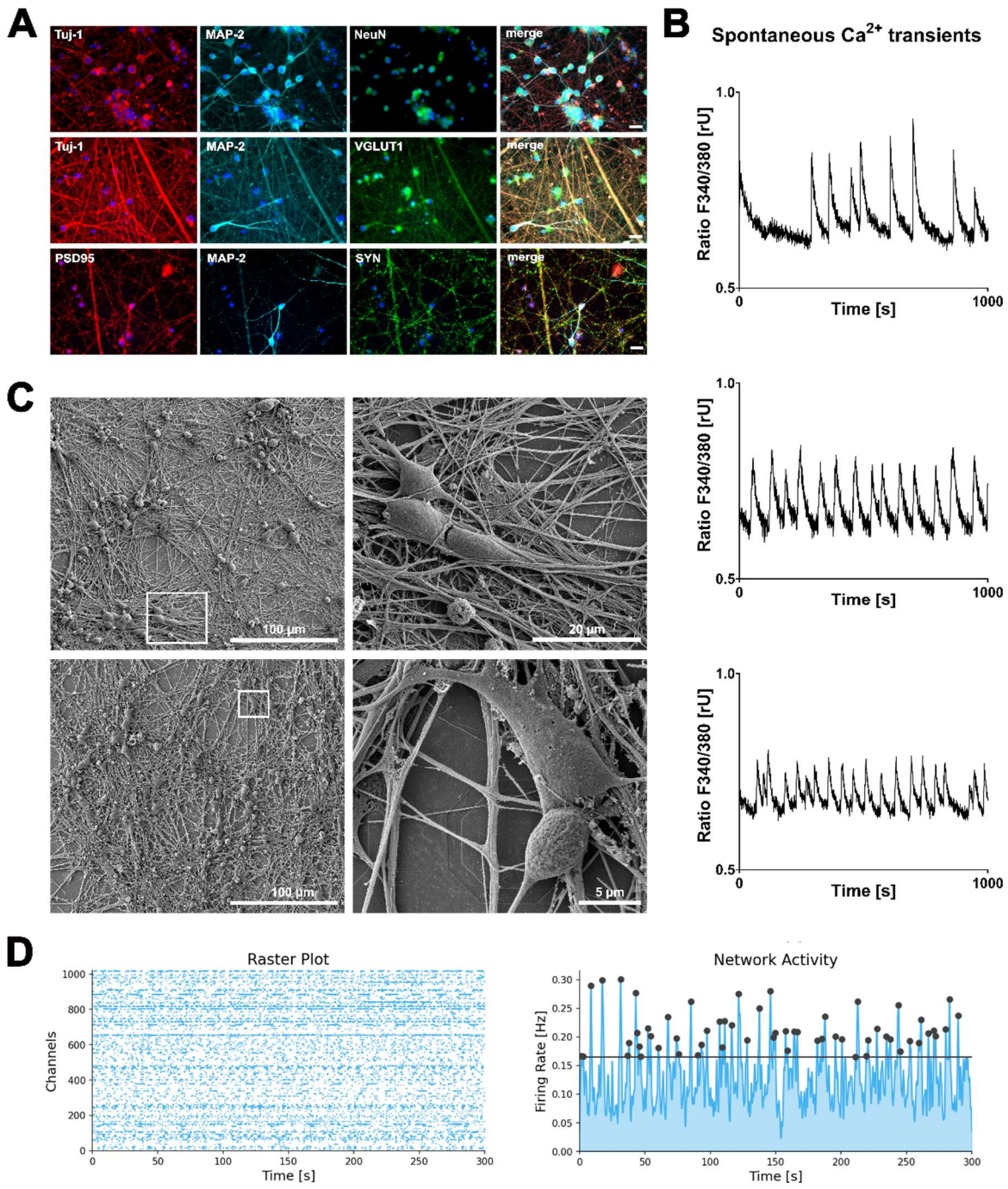

Figure 14: Validation of hiPSC-derived neurons. (A) Immunofluorescence stainings at day 21 of differentiation reveal the expression of neuronal markers in the induced neurons. The neurons display typical neuronal cytoskeleton proteins MAP-2 and Tuj-1, as well as the presynaptic synaptophysin (SYN) and postmitotic neuronal nuclear marker NeuN. Immunostaining for VGLUT1 and postsynaptic PSD95 indicates that the majority of induced neurons exhibit a glutamatergic phenotype. Scale bar indicates 20 µM. **(B)** Electron micrographs provide high-resolution visualisation of neuronal morphology after 21 days of differentiation. **(C)** Changes and oscillations in intracellular Ca^{2+} concentrations visualised via Fura-2/AM live-cell imaging demonstrate the spontaneous activity of induced neurons at day 21 of differentiation. **(D)** First signs of a synchronous activity pattern assessed with the HD-MEA system from Maxwell technologies at day 30 of differentiation.

3.1.5 Validation of TSPO knockout in NPCs, astrocytes, and neurons

TSPO knockout was validated in differentiated NPCs, astrocytes, and neurons using immunofluorescence. Anti-VDAC1 fluorescence clearly demonstrated the presence of a mitochondrial network in both the CTRL and KO cells. TSPO expression, as indicated by anti-

TSPO antibody staining, was only visible in CTRL cells, but was completely absent in KO cells, validating the loss of TSPO expression in mutated NPCs, astrocytes, and neurons. (Fig 15). Therefore, TSPO knockout cell lines are considered a viable and promising tool for studying the role of TSPO in different cell types derived from induced human neural cells.

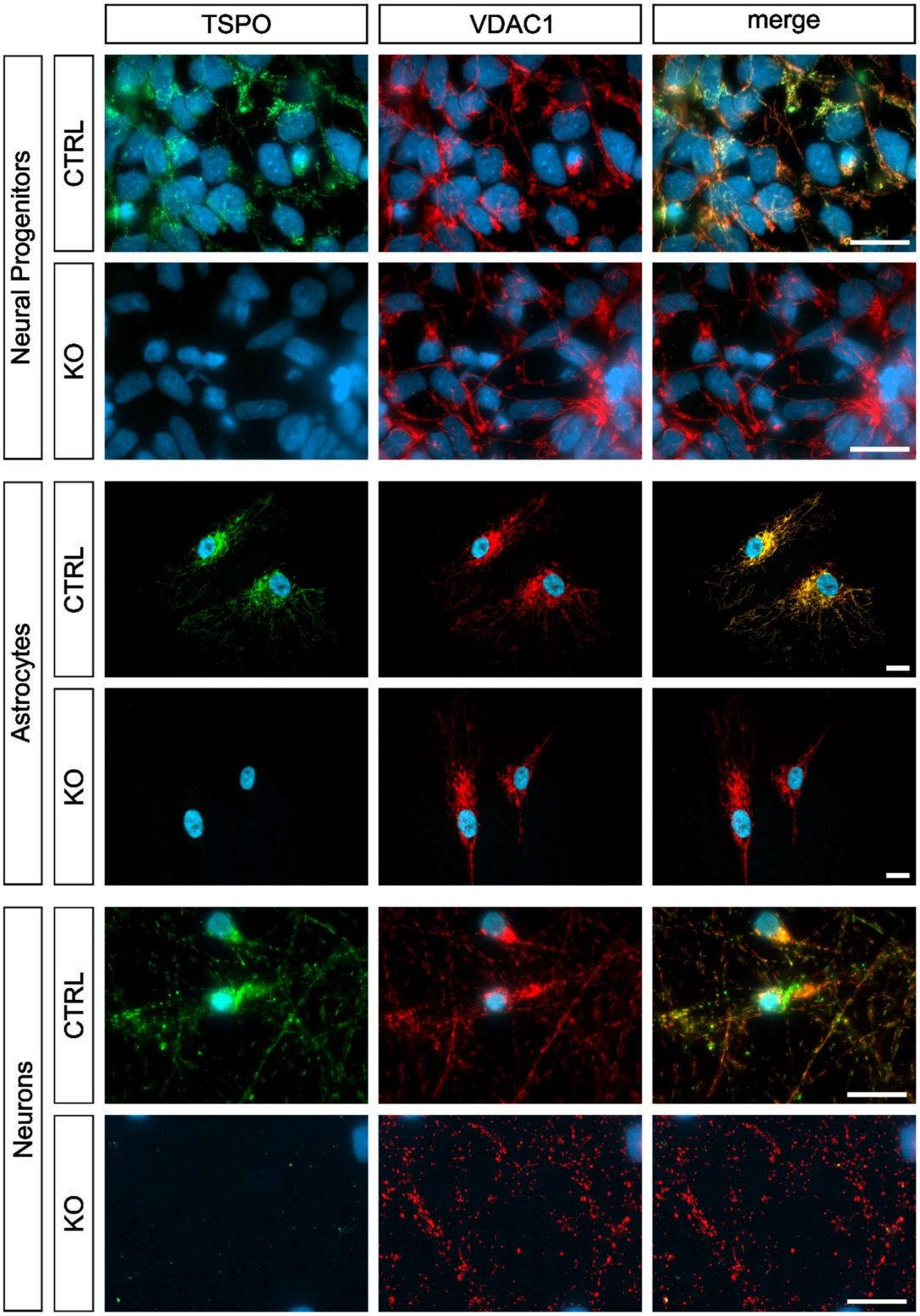

Figure 15: TSPO knockout in hiPSC-derived neural progenitors, astrocytes, and neurons. TSPO gene deletion was further confirmed by TSPO antibody co-staining, using VDAC1 as a mitochondrial marker. Scale bar indicates 20 µm.

3.2 Effect of TSPO expression on steroid synthesis in hiPSC-derived astrocytes

Neurosteroids act on the nervous system and therefore, play an important role in maintaining CNS homeostasis by regulating neural development, neural function, and the response of nervous tissue to injuries (Garcia-Segura & Melcangi, 2006). They are synthesised from cholesterol or other steroidal precursors by neurons and glial cells (Lloyd-Evans & Waller-Evans, 2020; Xu et al., 2022). The translocator protein, which is highly expressed in activated glial cells, has been reported to be involved in the mitochondrial cholesterol transport, thus making it a key regulator of pregnenolone synthesis (Bader et al., 2019; Barron et al., 2021; Costa et al., 2018; Papadopoulos et al., 2018; Rupprecht, Wetzel, et al., 2022; L. Wolf et al., 2015). Of all the potential physiological functions of TSPO, its role in the modulation of steroidogenesis is best characterised and studied. Thus, to evaluate the involvement of TSPO in neurosteroidogenesis, the concentration of pregnenolone in hiPSC-derived astrocytes was investigated using an ELISA assay. The supernatants collected from TSPO-knockout cells exhibited significantly lower concentrations of pregnenolone than those from CTRL cells (3.961±0.18 pg/µg/mL protein, n=17 vs. 5.144±0.33 pg/µg/mL protein, n=18, p=0.0031) after 3 h of incubation with the enzyme inhibitors trilostane (3β-hydroxysteroid dehydrogenase, HSD3B1) and SU10603 (17-OH-steroid hydroxylase, CYP17A1), which were used to prevent further metabolism of the newly synthesised pregnenolone (Fig. 16A). By omitting these inhibitors from the assay medium, the supernatants of both CTRL and TSPO$^{-/-}$ cells revealed a generally low basal rate of steroid production, indicating limited endogenous synthesis of steroids.

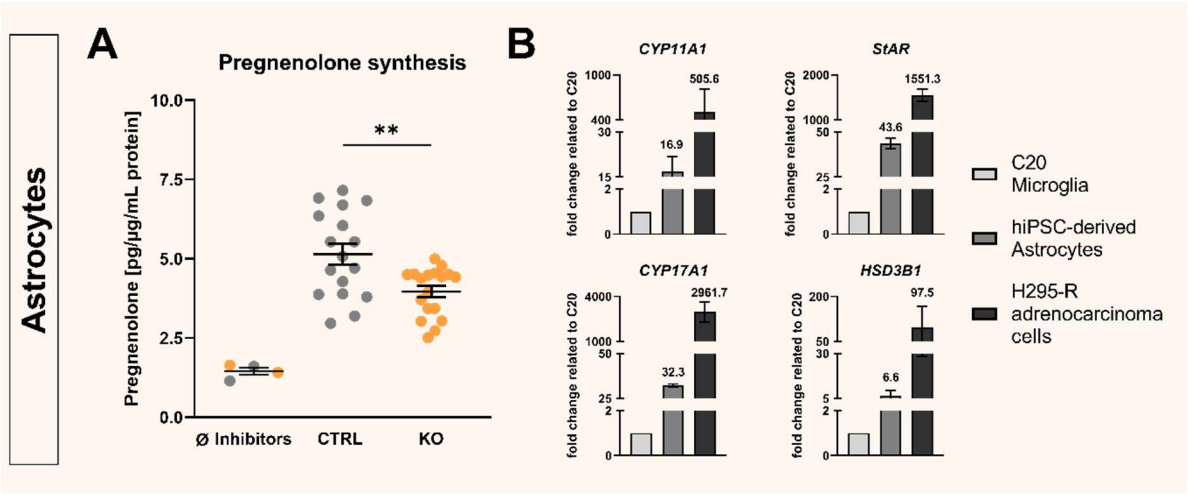

Figure 16: Pregnenolone synthesis in TSPO-knockout and control astrocytes. (A) TSPO knockout led to significantly lower basal pregnenolone production in hiPSC-derived astrocytes compared to CTRL cells**.** Dot blots represent normalized concentrations ± SEM using independent samples t-test. **(B)** Relative mRNA levels of key steroidogenic proteins (CYP11A1, CYP17A1, HSD3B1, and StAR) in hiPSC-derived astrocytes and the adrenocarcinoma cell line H295-R related to the very low gene expression in C20 microglial cells. Bar graphs represent the mean fold change ± SEM.

To gain insight into the steroid-synthesising capacity of hiPSC-derived astrocytes, quantitative analysis of gene expression was performed for key steroidogenic enzymes, including cytochrome P450 (*CYP11A1*), *HSD3B1*, and *CYP17A1*, which are crucial for the conversion of cholesterol to pregnenolone and subsequent pregnenolone and neurosteroid production, as well as steroidogenic acute regulatory protein (*StAR*), which is essential for cholesterol transport. As shown in Figure 16B, the results demonstrate higher mRNA transcript levels of these proteins in astrocytes than in the C20 microglial cell line, which does not produce substantial amounts of pregnenolone (Milenkovic et al., 2019). However, it is noteworthy that the mRNA levels observed in hiPSC-derived astrocytes were still considerably lower than those found in the steroidogenic adrenocarcinoma cell line H295-R, indicating a relatively low steroid-synthesising capacity of astrocytes. Nevertheless, these findings support the potential importance of TSPO in neurosteroidogenesis, as evidenced by the reduced pregnenolone concentration in the TSPO-knockout cells.

In a next step, the impact of TSPO on the modulation of mitochondrial homeostasis and function in hiPSC-derived neural progenitors, astrocytes, and neurons was investigated.

3.3 TSPO-deficient neural progenitors, astrocytes, and neurons show altered bioenergetic properties

3.3.1 Impact of TSPO expression on mitochondrial respiration

Mitochondria are crucial for generating and regulating cellular bioenergetics by providing nearly all of the cell's energy through OXPHOS facilitated by the mitochondrial respiratory chain. To investigate the functionality and performance of OXPHOS, the oxygen consumption rate (OCR) was measured using extracellular flux analysis. By using metabolism-altering reagents and selective enzyme inhibitors to evaluate the activity and capacity of the individual molecular respiratory complexes, the cellular metabolic profile can be characterised. To this end, the functions of ETC and OXPHOS in the mitochondria of both CTRL and KO cells were assessed. When examining TSPO-deficient knockout NPCs (Fig. 17A-C) and astrocytes (Fig. 17D-F) alongside their respective CTRL cells, it was discovered that TSPO expression had a significant impact on mitochondrial respiration. This resulted in almost all respiratory parameters being affected. Figures 17A and 17D show representative Seahorse measurements obtained using the Agilent Seahorse XF Cell Mito Stress Test, monitoring the oxygen consumption rates in different respiratory states. KO cells of both cell types showed significantly lower basal respiration than TSPO-expressing CTRL cells (**NPC**: p=0.0002; **Astro**: p=0.0022). Moreover, maximal respiration in the presence of the uncoupler FCCP and the resulting spare respiratory capacity, which reflects the cell's bioenergetic reserve and flexibility in meeting an energetic challenge or high energetic demand, were significantly

reduced in TSPO-deficient cells (maximal respiration: **NPC** p<0.0001; **Astro** p =0.0019; spare respiratory capacity: **NPC** p=0.0145; **Astro** p =0.0039).

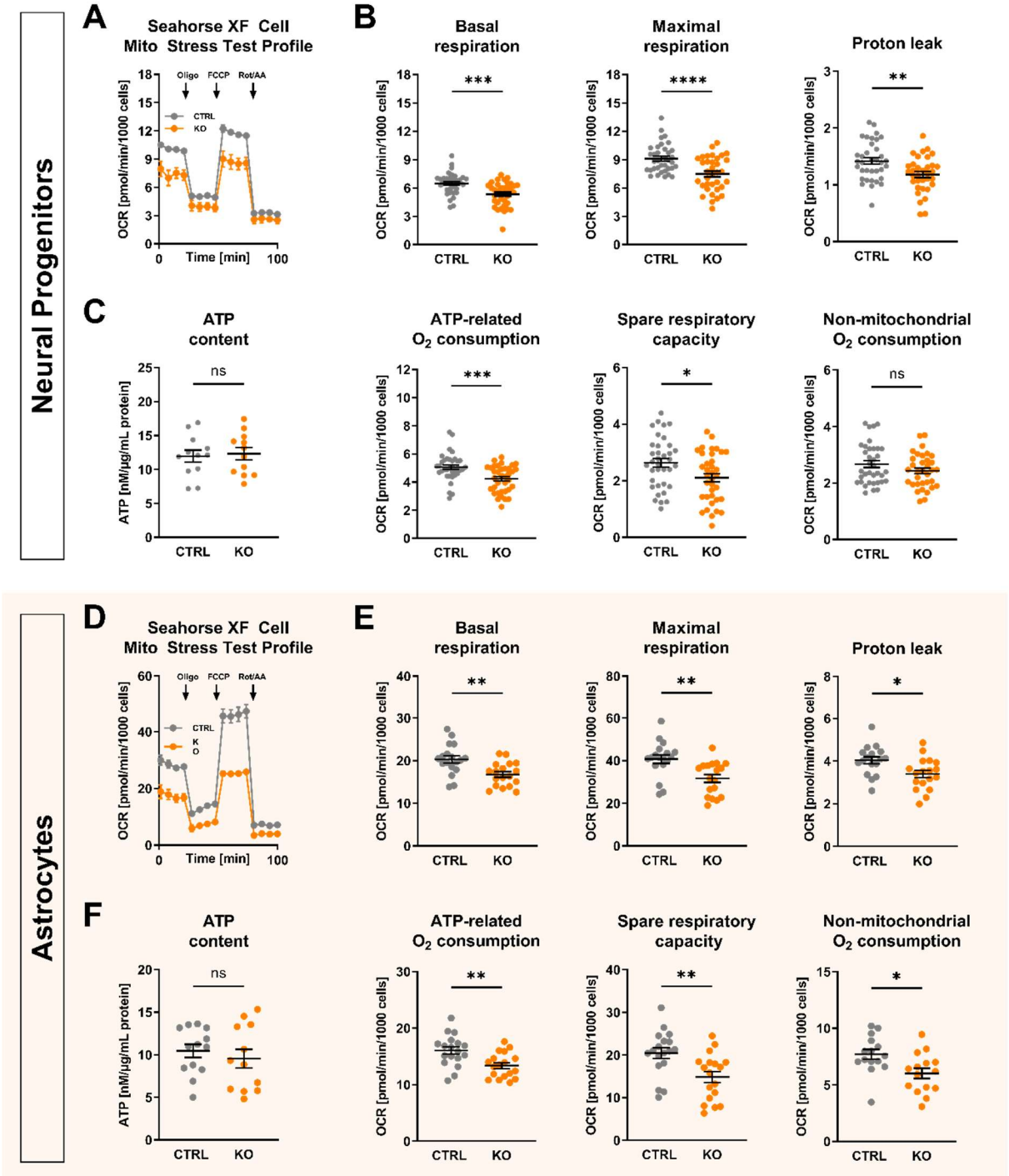

Figure 17: Mitochondrial respiration in TSPO-knockout and control cells. The oxygen consumption rate (OCR) was measured in TSPO KO and CTRL cells to assess the basal conditions and the effects of sequential injections of oligomycin (Oligo), carbonyl cyanide-4-(trifluoromethoxy)-phenylhydrazone (FCCP), and rotenone/antimycin A (Rot/AA) targeting different complexes of the electron transport chain. Representative examples of kinetic profiles of the Agilent Seahorse XF Mito Stress Test are shown for **(A)** NPCs and **(D)** astrocytes. Key respiratory parameters, including basal OCR, maximal respiration, proton leak, ATP-related oxygen consumption, spare respiratory capacity, and non-mitochondrial respiration, were compared between the KO and CTRL groups in **(B)** NPCs and **(E)** astrocytes. Total ATP content was quantified in **(C)** NPCs and **(F)** astrocytes using a bioluminescence assay. Dot plots display the normalised mean OCR values for NPCs and astrocytes. ATP levels in nM normalised to the total protein amount [µg/mL] are shown for the ATP content in NPCs and astrocytes. Data are presented as mean ± SEM using independent samples t-test.

Additionally, oxygen consumption related to ATP production differed significantly between KO and CTRL neural progenitors and astrocytes (**NPC** p=0.0004; **Astro** p=0.003). Proton leak, the flux of H^+ across the mitochondrial membrane independent of the ETC, was again significantly lower in the knockout group than in the CTRL group (**NPC** p=0.0031; **Astro** p=0.0123). Finally, non-mitochondrial respiration, which is caused by enzymatic reactions or oxygenases outside the mitochondria, was determined after the inhibition of mitochondrial respiration with Rotenone and Antimycin A. TSPO-KO astrocytes exhibited significantly decreased non-mitochondrial respiration (**Astro** p=0.0117), indicating an overall decrease in cellular metabolism, whereas, in NPCs, TSPO loss had no effect on non-mitochondrial respiration (**NPC** p=0.1311) (Fig. 17B and 17E).

Table 22: Mitochondrial respiration in TSPO-knockout and control cells

	Neural Progenitors		**Astrocytes**	
	CTRL	KO	CTRL	KO
Basal respiration [pmol/min/1000 cells]	6.47±0.19 n=36	5.33±0.22 n=35	20.28±0.84 n=18	16.76±0.66 n=18
	p=0.0002		p=0.0022	
Maximal respiration [pmol/min/1000 cells]	9.10±0.25 n=36	7.47±0.31 n=35	40.72±1.98 n=18	31.62±1.85 n=18
	p<0.0001		p=0.0019	
Proton leak [pmol/min/1000 cells]	1.42±0.06 n=36	1.18±0.06 n=34	4.03±0.17 n=17	3.39±0.17 n=18
	p=0.0031		p=0.0123	
ATP-related O_2 consumption [pmol/min/1000 cells]	5.05±0.16 n=36	4.22±0.16 n=36	16.02±0.65 n=18	13.36±0.52 n=18
	p=0.0004		p=0.003	
Spare respiratory capacity [pmol/min/1000 cells]	2.63±0.15 n=36	2.10±0.15 n=36	20.44±1.26 n=18	14.87±1.29 n=18
	p=0.0145		p=0.0039	
Non-mito. O_2 consumption [pmol/min/1000 cells]	2.67±0.12 n=36	2.43±0.11 n=34	7.67±0.43 n=15	6.02±0.45 n=15
	p=0.1311		p=0.0117	
ATP content [nM/µg/mL protein]	11.95±0.89 n=12	12.30±0.89 n=12	10.45±0.76 n=13	9.54±1.11 n=12
	p=0.7834		p=0.5011	

To provide a more comprehensive understanding of OXPHOS activity and to study the bioenergetic core function of mitochondrial metabolism – electron transport coupled with ATP synthesis – the total ATP levels within the cells were measured, since the Seahorse assay measures ATP production only indirectly by inhibiting the mitochondrial complex V. Surprisingly, in contrast to the Seahorse-derived data, there was no difference in cellular ATP content, either in TSPO-KO NPCs or astrocytes, compared with their respective controls (**NPC** p=0.7834; **Astro** p=0.5011) (Fig. 17C and 17F).

These findings provide comprehensive insights into the effects of TSPO on OXPHOS and mitochondrial respiration in neural cells. Altered respiratory parameters in TSPO-deficient cells highlight the significance of TSPO in regulating mitochondrial bioenergetics. Moreover, the unaffected ATP levels suggest compensatory mechanisms within $TSPO^{-/-}$ cells to maintain intracellular ATP levels, despite the potentially reduced energy production associated with decreased OXPHOS.

3.3.2 Role of TSPO in the modulation of mitochondrial membrane potential

During OXPHOS, a proton gradient across the IMM contributes to the formation of the MMP. The MMP represents the chemo-electrical potential difference between the mitochondrial matrix and the IMS, serving as an indicator of the bioenergetic state of mitochondria. This potential difference is generated through consecutive redox reactions and translocation of electrons and protons across the IMM via the ETC. The resulting proton gradient is the primary driving force for ATP synthesis, while active ATP synthase allows the backflow of protons into the matrix, which in turn diminishes the gradient. Thus, MMP provides valuable insights into mitochondrial function, metabolic activity, and potential imbalances arising from mitochondrial dysfunction.

To visualise the MMP in NPCs and neurons, mitochondria were labelled with the ratiometric cationic dye JC-1 (200 nM), which forms potential-dependent red fluorescent aggregates in highly energised mitochondria, whereas in response to the dissipation of the MMP, the dye molecules disaggregate into green fluorescent monomers. The MMP of hiPSC-derived astrocytes was assessed by loading the cells with a combination of the cationic dye TMRE (25 nM, non-quenching mode) and MitoTracker Green (MTG) (200 nM). TMRE also accumulates in negatively charged mitochondria to an extent that is dependent on the strength of the electric field. The mitochondria-specific dye MTG is nearly potential-independent and is used to normalise the TMRE fluorescence. The ratio of the fluorescence signals emitted by the two different states of JC-1 (red/green), as well as the ratio F_{TMRE}/F_{MTG}, is therefore a measure of the strength of the MMP (Chaudhuri et al., 2016).

TSPO deficiency in hiPSC-derived neural progenitors and astrocytes decreased the fluorescence ratio from 1.078±0.01 and 0.498±0.005 to 0.856±0.01 and 0.469±0.006,

respectively (p<0.0001). Given that the mitochondria residing in the soma or neurites of the neurons were located at different focal planes, separate images of JC-1 fluorescence of the relevant structures were captured.

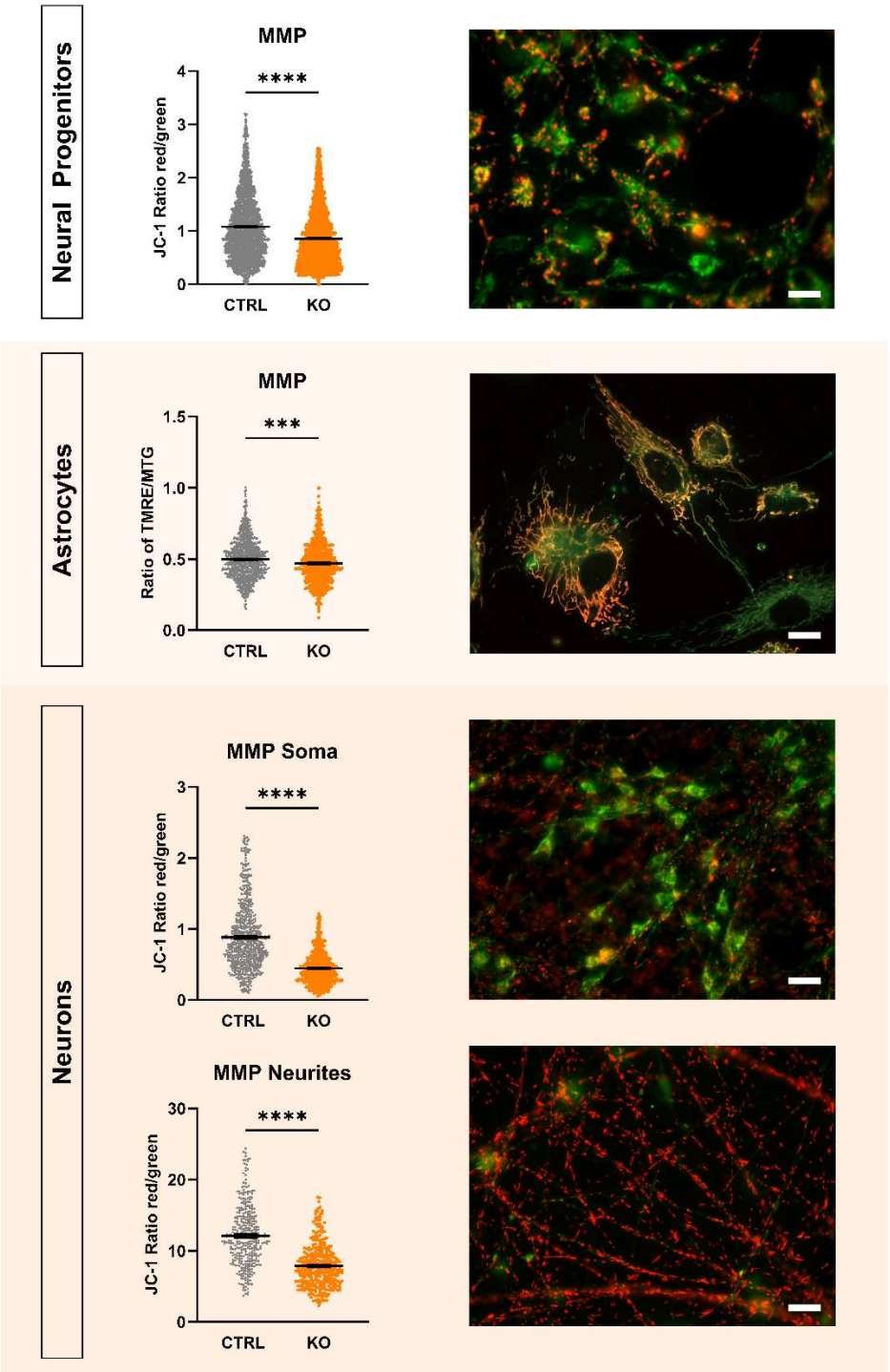

Figure 18 Effects of TSPO gene deletion on mitochondrial membrane potential. TSPO deficiency resulted in significant reduction of mitochondrial membrane potential in knockout cells of hiPSC-derived neural progenitors, astrocytes, and neurons (p<0.0001, Mann-Whitney U test (MW)). The MMP in NPCs and neurons is indicated by the JC-1 fluorescence ratio of red/green (JC-1 aggregates/monomers) and in astrocytes by the ratio of TMRE/MTG fluorescence. Dot plots show mean red/green or TMRE/MTG ratio ± SEM of n=3 biological replicates of several individual cell lines (NPC: CTRL n=3, KO n=3; Astro: CTRL n=2, KO n=2; Neuron: CTRL n=2, KO n=2). Representative fluorescence microscopy images of NPCs and neurons loaded with the cationic dye JC-1, and of astrocytes loaded with the cationic dye TMRE and the mitochondria-specific dye MitoTracker Green. Scale bar indicates 20 µm.

The TSPO-knockout neurons showed again a significantly reduced JC-1 ratio (p<0.0001), especially in the neurites, thereby indicating a less hyperpolarised membrane potential in the mitochondria devoid of TSPO (**Soma** 0.882±0.23 vs. 0.445±0.008; **Neurites** 12.07±0.23 vs. 7.85±0.16) (Fig. 18). Collectively, knocking out TSPO resulted in a robust and significant decline in the mitochondrial membrane potential across all examined cell types. This again indicates that the overall function of the ETC, the translocation of protons, and the parallel backflow of protons through the ATP synthase, which determines the mitochondrial membrane potential, is disrupted.

Table 23: Mitochondrial membrane potential in TSPO-knockout and control cells

	Neural Progenitors		Astrocytes		Neurons	
	CTRL	KO	CTRL	KO	CTRL	KO
MMP Soma [ratio]	1.078±0.01 n=3095	0.856±0.01 n=3032	0.498±0.005 n=930	0.469±0.006 n=643	0.882±0.02 n=694	0.445±0.008 n=747
	p<0.0001 (MW)		p=0.0001 (MW)		p<0.0001 (MW)	
MMP Neurite [ratio]					12.07±0.23 n=349	7.85±0.16 n=344
					p<0.0001 (MW)	

3.3.3 Involvement of TSPO in Ca^{2+} Homeostasis

Mitochondria play a critical role in Ca^{2+} homeostasis, which is essential for numerous signalling pathways, enzyme function, and cellular metabolism. Driven by their negative membrane potential, they attract and accumulate calcium ions within the mitochondrial matrix, thereby directly influencing and regulating cellular Ca^{2+} dynamics. With their capability to store or release calcium ions, mitochondria serve as calcium buffers with both beneficial and detrimental effects. The MMP, along with Ca^{2+}-conducting channels (e.g., voltage-dependent anion channel, VDAC) and the activity of Ca^{2+}-transporting proteins in the IMM (e.g., mitochondrial calcium uniporter, MCU), influence the extent of mitochondrial Ca^{2+} uptake.

Using Ca^{2+}-sensitive dyes, the cytosolic $[Ca^{2+}]_c$ and mitochondrial $[Ca^{2+}]_m$ levels, were investigated. Cytosolic Ca^{2+} concentrations were measured by loading the cells with the ratiometric dye Fura-2/AM, which is characterised by two excitation spectra depending on its Ca^{2+}-bound or Ca^{2+}-free state, and is directly related to the cytosolic amount of Ca^{2+}. For the assessment of the mitochondrial Ca^{2+} levels, the intensity-based dye Rhod-2/AM was used. Consistent within all analysed cell types, a significantly reduced Fura-2 ratio (F_{340nm}/F_{380nm}) was observed in the $TSPO^{-/-}$ cell lines compared to the respective CTRL cells, showing a decreased basal cytosolic Ca^{2+} concentration (p<0.0001) (Fig. 19A). While the Rhod-2 fluorescent

intensity showed a significant increase amongst all KO cell lines ($p<0.0001$) which may be a consequence of altered Ca^{2+} flux or active transport processes (Fig. 19B).

According to current hypotheses, TSPO plays a crucial role in coordinating and regulating the activity and expression of proteins within a multimeric complex. As a highly interactive protein, TSPO may function as a molecular hub of VDAC-containing supercomplexes, thereby contributing to the maintenance of intracellular Ca^{2+} homeostasis.

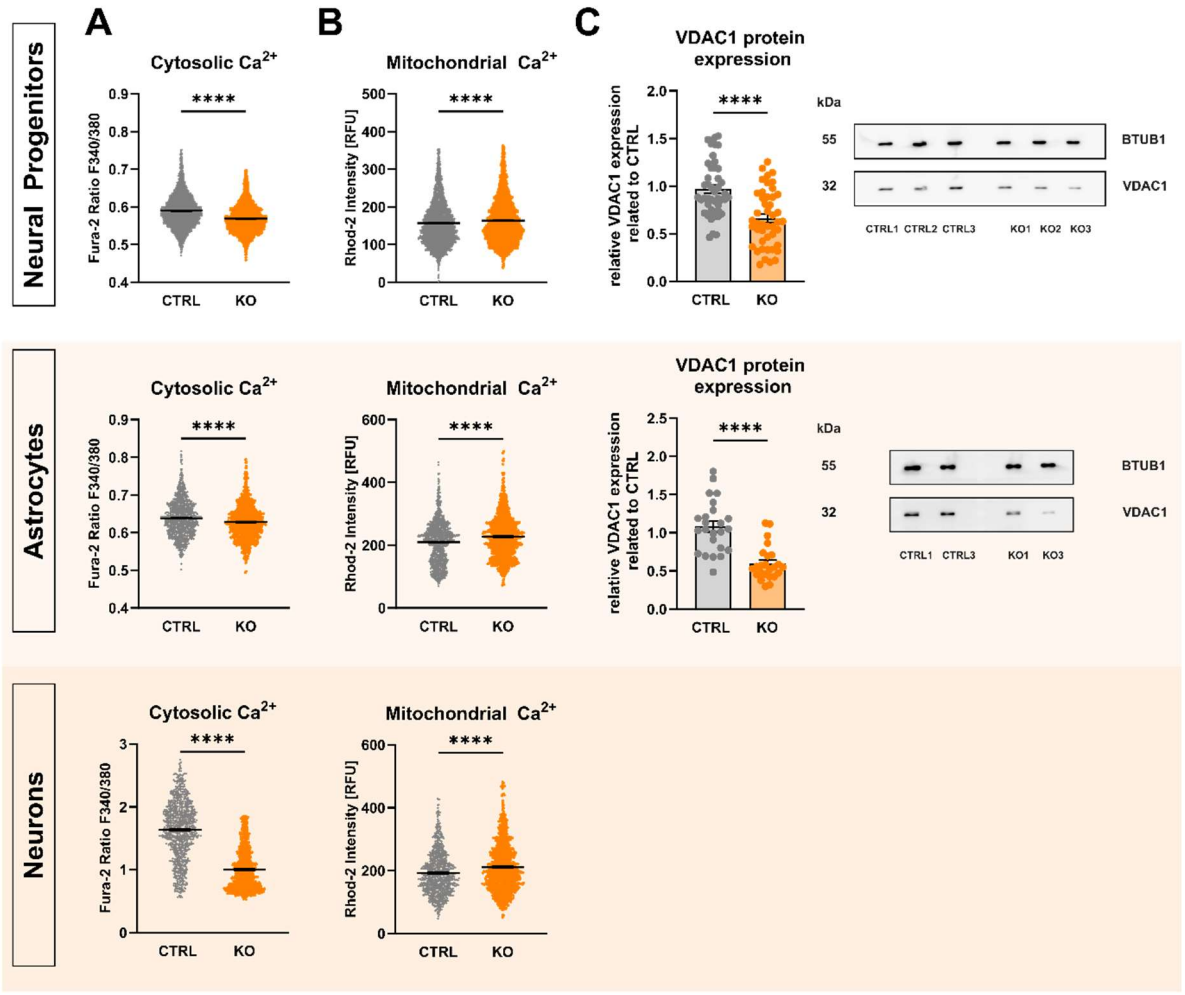

Figure 19: Impact of TSPO gene deletion on cytosolic and mitochondrial Ca^{2+} and on the expression of mitochondrial VDAC1 protein. (A) TSPO-knockout cells showed significantly reduced cytosolic Ca^{2+} levels, as indicated by the Fura-2 fluorescence ratio $F_{340/380}$. While the mitochondrial Ca^{2+} concentration was significantly increased in TSPO$^{-/-}$ NPCs, astrocytes, and neurons, as indicated by Rhod-2 mean fluorescence intensity (MFI) ± SEM. **(B)** Deletion of *TSPO* gene led to decreased expression of VDAC1 protein. Representative Western Blots depict the expression of housekeeper gene BTUB1 at 55 kDa and VDAC1 at 32 kDa in NPCs and astrocytes. Bar graphs show densitometric, relative mean of VDAC expression. Individual values were normalised to the respective expression level of BTUB1 and related to CTRL mean. Data are presented as mean ± SEM using Mann-Whitney U test (MW).

Table 24: Cytosolic and mitochondrial Ca^{2+} concentration in TSPO-knockout and control cells

	Neural Progenitors		Astrocytes		Neurons	
	CTRL	KO	CTRL	KO	CTRL	KO
$[Ca^{2+}]_c$ [ratio]	0.590±0.0008 n=5380	0.569±0.0005 n=5159	0.638±0.001 n=1206	0.628±0.001 n=1055	1.637±0.02 n=910	0.9984±0.01 n=1049
	p<0.0001 (MW)		p<0.0001 (MW)		p<0.0001 (MW)	
$[Ca^{2+}]_m$ [MFI]	156.7±0.88 n=4485	163.7±0.88 n=4550	209.7±1.95 n=1215	226.7±2.09 n=1065	192.2±2.23 n=961	210.8±2.38 n=1061
	p<0.0001 (MW)		p<0.0001 (MW)		p<0.0001 (MW)	

Western Blot analyses with an anti-VDAC1 antibody showed that TSPO deficiency in hiPSC-derived NPCs and astrocytes was accompanied by a 33.5±4.4% and 44.8±4.2% reduction in VDAC1 protein expression, respectively, compared to the respective control (p<0.0001, Mann-Whitney U test), as shown in Figure 19C. This finding supports the idea of functional and structural interactions between these two proteins. This altered VDAC1-expression suggests that changes in TSPO expression have a direct or indirect effect on key physiological aspects of mitochondrial function.

To gain insight into the underlying mechanisms, quantitative analysis of VDAC1 mRNA expression and protein stability was performed. qRT-PCR analysis indicated that the loss of TSPO expression had no effect on VDAC1 transcription (Fig. 20A).

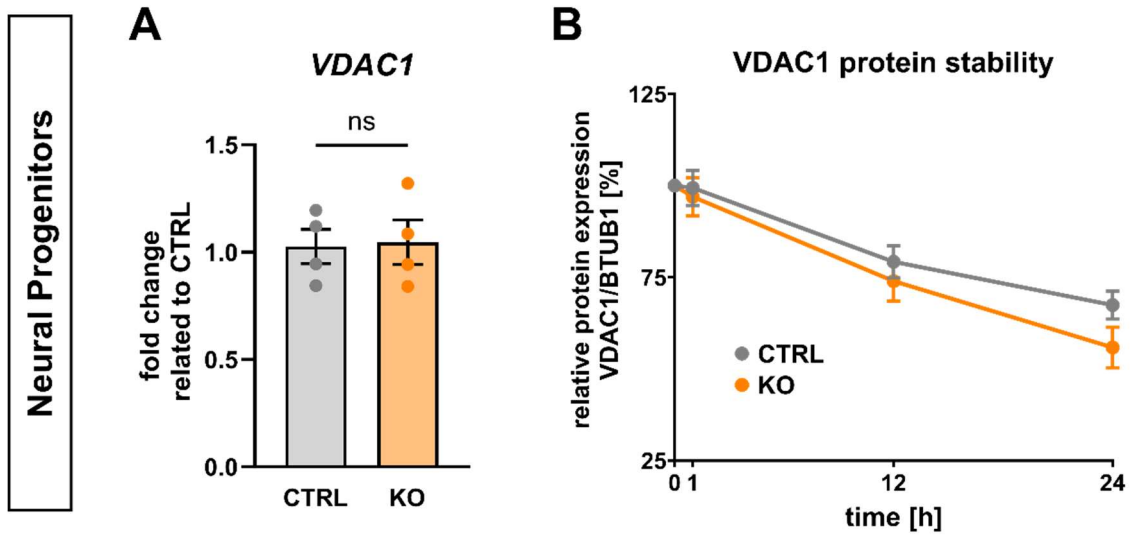

Figure 20: Effect of TSPO deficiency on VDAC1 gene expression and protein stability. (A) qRT-PCR analysis revealed no significant differences in mRNA transcript levels of VDAC1 in TSPO knockout NPCs compared to CTRL cells. Bar graphs show fold change ± SEM related to CTRL of n=2 biological replicates. **(B)** CTRL and KO cells were treated with cycloheximide (100 µg/mL) for the indicated times and endogenous VDAC1 was detected using a specific anti-VDAC1 antibody. Values were normalised to the expression level of BTUB1 and were related to the initial VDAC1 protein level (0 h of CHX) for each group. Data are shown as relative mean ± SEM of n=9 biological replicates.

To assess the stability of the endogenous VDAC1 protein, a cycloheximide (CHX) chase protein degradation assay was conducted. Therefore, neural progenitors were incubated with 100 µg/mL CHX, a well-known inhibitor of eukaryotic translation, for a maximum of 24 hours to evaluate VDAC1 protein levels at different time points after CHX treatment. VDAC1 protein expression was quantified as a percentage of the initial VDAC1 protein level (0 h of CHX treatment) and was normalised to BTUB1 expression. Findings indicate that the amount of VDAC1 protein in CTRL NPCs declined to 67.43±3.77% of the initial value after 24 h, while the KO cells showed higher protein degradation (55.89±5.55% of initial value), as shown in Fig. 20B.

3.3.4 Impact of TSPO on cellular bioenergetics and glycolysis

The proton gradient which constitutes the MMP, serves as a proton motive force that drives the activation of ATP synthase, resulting in ATP production. Most of the cell's ATP is produced during mitochondrial respiration. However, during glycolysis, the second pathway to provide ATP to meet the energy requirements of the cell, ATP is produced via the breakdown of glucose.

To measure glycolytic flux, the proton efflux rate (PER) of the TSPO KO and CTRL groups was analysed. Using the Agilent Seahorse Glycolytic Rate Assay, $TSPO^{-/-}$ neural progenitors (Fig. 21A), and astrocytes (Fig. 21B) showed significantly lower basal glycolysis (glycoPER) than CTRL (**NPC** $p<0.0001$; **Astro** $p=0.0023$). According to basal glycolysis, TSPO-deficient cells also had significantly reduced compensatory glycolysis (**NPC** $p<0.0001$; **Astro** $p=0.0002$), which is induced when mitochondrial ATP synthase is inhibited, thereby redirecting the cell to rely on glycolysis to meet its ATP requirements. In addition, the basal PER and post-2-DG acidification rate of KO cells also showed a statistically significant difference compared to that of CTRL cells (basal PER: **NPC** $p<0.0001$; **Astro** $p<0.001$; post-2-DG acidification: **NPC** $p=0.0005$; **Astro** $p=0.00238$). Conversely, the CTRL and KO groups did not differ significantly in their basal mitoOCR/glycoPER ratios (**NPC** $p=0.3124$; **Astro** $p=0.2965$).

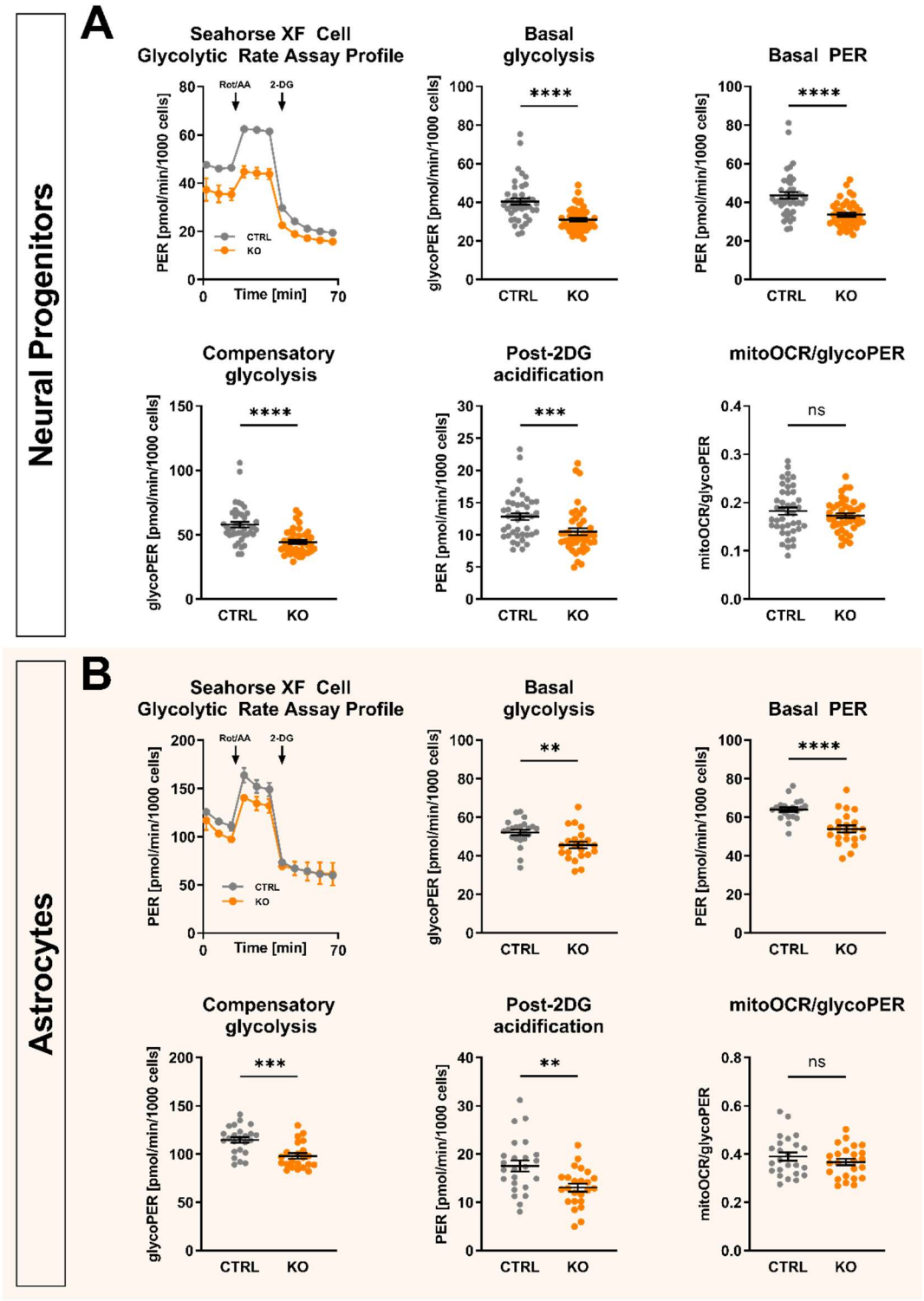

Figure 21: Glycolytic rates in TSPO-knockout and control cells. Oxygen consumption rate (OCR) and extracellular acidification rate (ECAR) were measured in TSPO KO and CTRL cells. Following basal measurement of OCR and ECAR, to determine the basal proton efflux rate (PER), rotenone and antimycin A (Rot/AA) were added to determine compensatory glycolysis and basal glycolysis (glycoPER) by blocking mitochondrial respiration. Subsequently, 2-deoxy-D-glucose (2-DG), an inhibitor of glycolysis by competitively binding hexokinase, was injected to ensure that the observed PER was caused by glycolysis. Representative kinetic profiles of the Agilent Seahorse Glycolytic Rate assay and key glycolytic parameters are shown for **(A)** neural progenitors (NPCs) and **(B)** astrocytes. Key glycolytic parameters, including basal glycolysis, basal PER, compensatory glycolysis, post-2DG acidification, and mitoOCR/glycoPER, were compared between KO and CTRL groups. Dot plots display normalised mean PER values ± SEM using independent samples t-test or Mann-Whitney U test (MW) for NPCs and astrocytes.

Table 25: Key glycolytic parameters of TSPO-knockout and control cells

	Neural Progenitors		Astrocytes	
	CTRL	KO	CTRL	KO
Basal glycolysis [pmol/min/1000 cells]	40.37±1.66 n=42	30.95±0.95 n=42	52.96±1.21 n=23	45.586±1.71 n=22
	p<0.0001 (MW)		p=0.0023 (MW)	
Basal PER [pmol/min/1000 cells]	43.54±1.75 n=42	33.60±1.01 n=42	63.93±1.17 n=21	53.93±1.79 n=22
	p<0.0001 (MW)		p<0.0001	
Compensatory glycolysis [pmol/min/1000 cells]	56.64±1.92 n=42	44.31±1.42 n=42	114.6±2.89 n=24	98.01±2.87 n=22
	p<0.0001 (MW)		p=0.0002	
Post-2DG acidification [pmol/min/1000 cells]	12.81±0.54 n=42	9.72±0.38 n=42	17.52±1.16 n=24	13.06±0.81 n=24
	p=0.0005 (MW)		p=0.0028	
mitoOCR/glycoPER [ratio]	0.18±0.008 n=42	0.17±0.005 n=42	0.3895±0.02 n=24	0.3670±0.01 n=24
	p=0.3124		p=0.2965	

Collectively, TSPO KO cells demonstrated lower basal respiration, spare respiratory capacity, glycolysis, and compensatory glycolysis in comparison with CTRL cells, but a similar mitoOCR/glycoPER ratio, indicating a lower metabolic flux in TSPO$^{-/-}$ cells.

Cells rely on energy to sustain their viability, growth, and normal functioning. ATP serves as the primary source of chemical energy within cells, and is predominantly generated via two pathways: glycolysis in the cytosol and oxidative phosphorylation in the mitochondria.

Measurement of cellular ATP production rate is an effective means of characterising cellular metabolism and can be quantitatively reflected by extracellular fluxes (Cumming et al., 2018; Mookerjee et al., 2017). Using the Agilent Seahorse XFp Real-Time ATP Rate Assay, the total ATP production rates as well as the fractions of ATP produced through mitochondrial OXPHOS and glycolysis of hiPSC-derived neural progenitors and astrocytes were analysed. As shown in Fig. 22 and consistent with the Seahorse Mito Stress Test, the mitochondrial-derived ATP production rate was significantly decreased in the TSPO$^{-/-}$ group of both cell types (basal mitoATP production rate) (**NPC** p=0.0035; **Astro** p<0.0001). Regarding the glycolysis-specific ATP rate fraction, only TSPO deficiency in NPCs resulted in a significant reduction compared to that in the control cells (**NPC** p<0.0001). The contribution of glycolysis to the total ATP production rate was not altered in KO and CTRL astrocytes (**Astro** p=0.1664).

However, consistent with the unchanged basal mitoOCR/glycoPER ratio, the overall metabolic flux, represented by the total ATP production rate, was lower in both TSPO-deficient NPCs

and astrocytes than in TSPO-expressing cells (**NPC** p<0.0001; **Astro** p=0.002). The XF ATP Rate Index, a metric for detecting changes or differences in metabolic phenotypes, showed a significant decrease in TSPO-KO astrocytes, indicating a less oxidative phenotype compared to CTRL cells (**Astro** p=0.0051). As both mitochondrial and glycolytic ATP rates decreased due to TSPO loss in NPCs, the XF ATP Rate Index remained unchanged (**NPC** p=0.2192).

Table 26: ATP production rate in TSPO-knockout and control cells

	Neural Progenitors		**Astrocytes**	
	CTRL	KO	CTRL	KO
Basal glycoATP production rate [pmol/min/1000 cells]	40.65±1.54 n=27	29.50±0.92 n=27	49.93±2.09 n=27	45.79±2.08 n=26
	p<0.0001		p=0.1664	
Basal mitoATP production rate [pmol/min/1000 cells]	28.42±1.80 n=27	21.34±0.82 n=27	97.72±3.72 n=25	72.68±2.61 n=26
	p=0.0035 (MW)		p<0.0001 (MW)	
Total ATP Production Rate [pmol/min/1000 cells]	69.08±2.97 n=27	50.85±1.57 n=27	143.3±6.27 n=27	118.5±4.22 n=26
	p<0.0001		p=0.002	
Basal ATP Rate Index [ratio]	0.6978±0.04 n=27	0.7274±0.02 n=27	1.874±0.07 n=27	1.606±0.06 n=27
	p=0.2192 (MW)		p=0.0051	

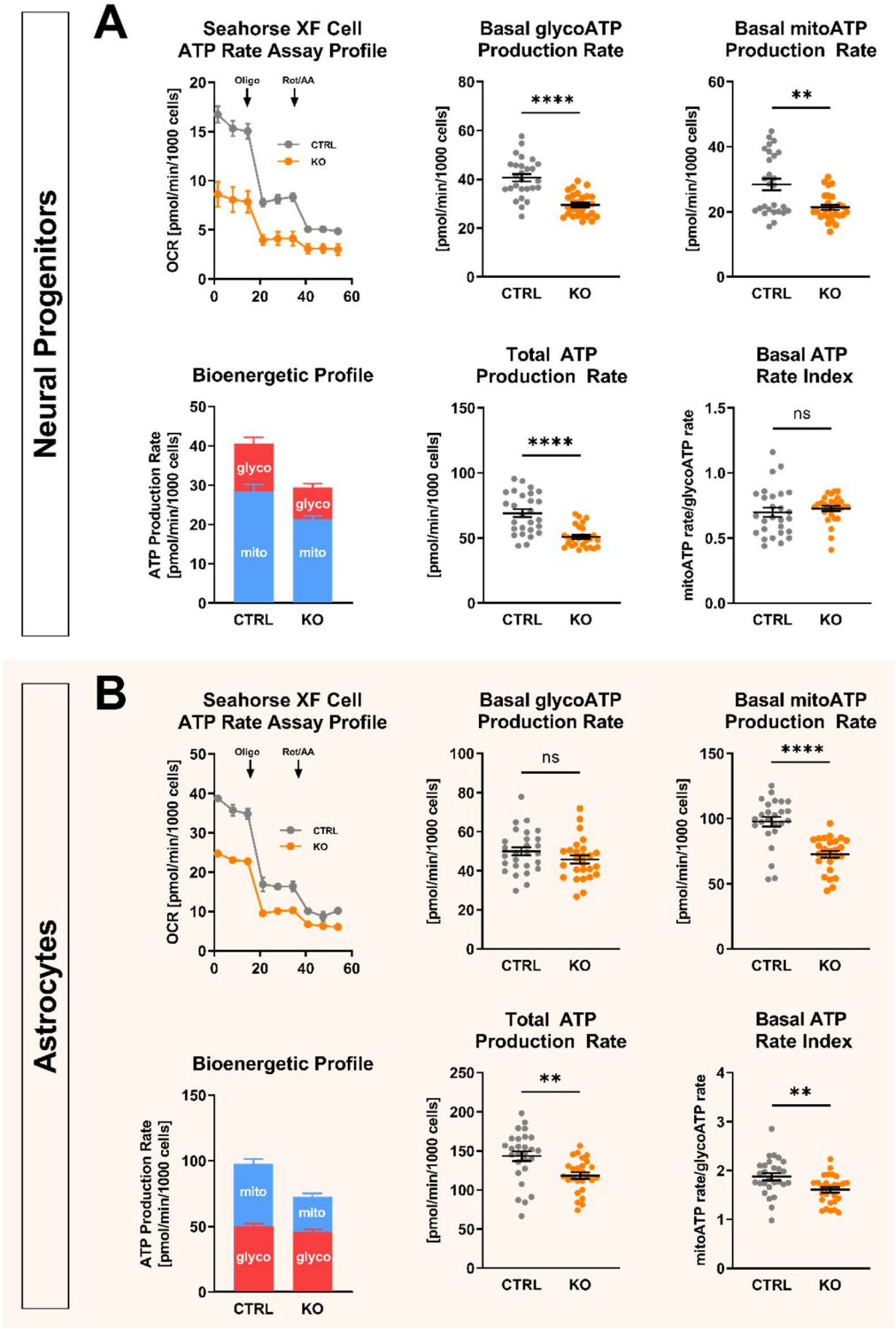

Figure 22: ATP production rates in TSPO-knockout and control cells. Oxygen consumption rate (OCR) and extracellular acidification rate (ECAR) were measured, and ATP production rates were calculated for TSPO KO and CTRL cells after sequential addition of the metabolic modulators oligomycin (oligo) and rotenone/antimycin A (Rot/AA). Representative kinetic profiles and ATP production rates conducted with the Agilent Seahorse XFp Real-time ATP Rate assay are shown for **(A)** NPCs and **(B)** astrocytes. Dot plots display normalised mean ATP production rate ± SEM for NPCs and astrocytes using independent samples t-test or Mann-Whitney U (MW) test.

Taken together, these findings demonstrate the impact of TSPO expression on the bioenergetic capacity of cells, and support the regulatory role of TSPO in cellular and mitochondrial energy homeostasis.

3.4 TSPO-deficient Neural Progenitors and astrocytes show oxidative stress

Mitochondria, as central organelles involved in cellular metabolism, exert a crucial role in maintaining the cell's redox homeostasis. Efficient functioning of the electron transport chain coupled with mitochondrial ATP production comes at the cost of reactive oxygen species (ROS), generated primarily at complexes I and III of the ETC. When maintained at low or moderate concentrations, ROS are involved in various cellular signalling pathways. However, an imbalance between the production and accumulation of reactive oxygen species causes oxidative stress, leading to molecular and cell damage. Cellular redox was analysed by flow cytometry using the fluorescent dyes DCFDA and MitoSOX^{TM} Red to detect global cytosolic hydrogen peroxide (H_2O_2) and peroxyl radicals (HO_2) and mitochondrial superoxide, respectively. As shown in Fig 23, both cytosolic and mitochondrial ROS were increased in TSPO-knockout neural progenitors (**cytosolic ROS** p=0.0028; **mitochondrial ROS** p=0.0131) (Fig. 23A), and astrocytes (**cytosolic ROS** p=0.0311; **mitochondrial ROS** p=0.0462) (Fig. 23B) compared with the respective controls, indicating oxidative stress and an imbalanced redox state of the cell.

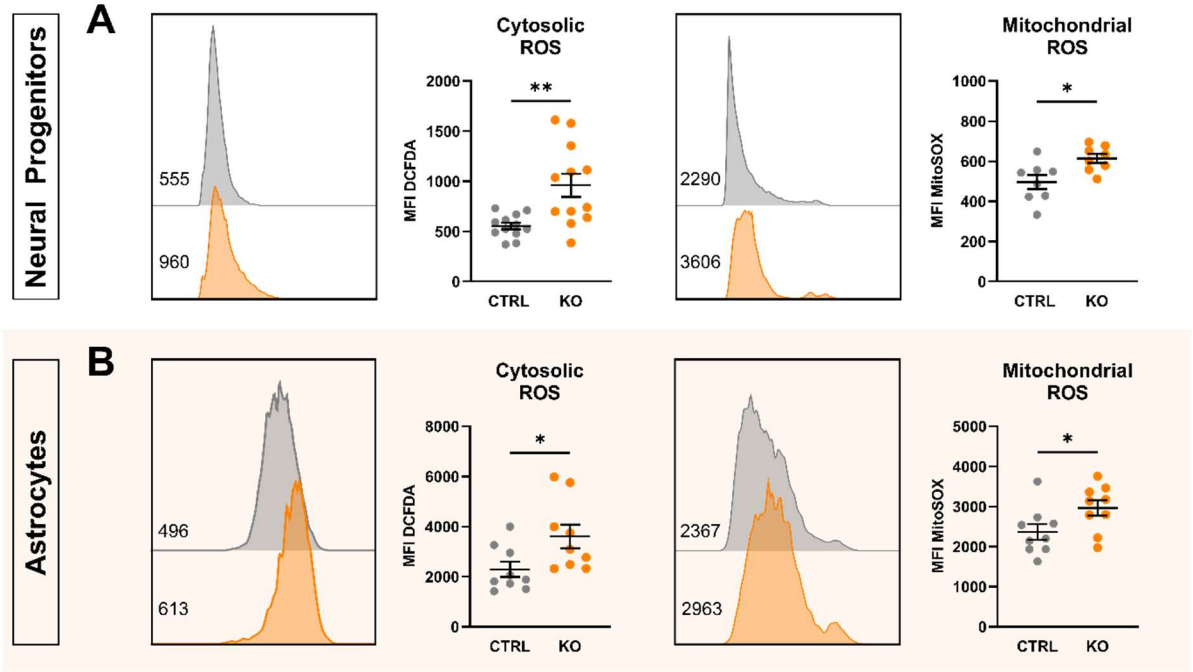

Figure 23: Oxidative stress indicators in TSPO-knockout and control cells. Cytosolic reactive oxygen species (ROS) and mitochondrial ROS (superoxide) were measured in **(A)** NPCs and **(B)** astrocytes by flow cytometry and are indicated by DCFDA and MitoSOX mean fluorescence intensity (MFI). Dot blots show MFI ± SEM using independent samples t-test. of n=4 individual experiments; $1x10^5$ and $2x10^4$ events were recorded for each replicate of NPCs and astrocytes, respectively.

Table 27: Cytosolic and mitochondrial ROS levels in TSPO-knockout and control cells

	Neural Progenitors		Astrocytes	
	CTRL	KO	CTRL	KO
Cytosolic ROS [MFI]	555.0±33.66 n=12	960.8±115.9 n=12	2290±298.6 n=8	3606±470.2 n=8
	p=0.0028		p=0.0311	
Mitochondrial ROS [MFI]	496.0±35.01 n=12	613.8±22.20 n=12	2367±195.9 n=8	2963±193.5 n=8
	p=0.0131		p=0.0462	

3.5 Effect of TSPO loss on mtDNA copy number, mitochondrial content and cell size

Mitochondria possess their own genetic material, mtDNA, which encodes rRNA, tRNA, and essential components of mitochondrial ETC that are involved in maintaining mitochondrial function. The dynamic equilibrium between mtDNA degradation and synthesis, which does not coincide with the cell cycle, determines the mtDNA copy number, ranging from 10^3 to 10^4 copies in different cells. The quantity and quality of mtDNA directly affect mitochondrial function, with mtDNA copy number serving as an indicator of mitochondrial integrity. Levels of mtDNA copy number are correlated with energy reserves, oxidative stress, and changes in MMP. Thus, altered mtDNA copy number can disrupt mitochondrial energy metabolism and contribute to diverse pathologies.

In order to evaluate whether the observed differences in the mitochondrial membrane potential and respiratory activity are related to lower mitochondrial content, the mtDNA copy number was determined in relation to the diploid genome in $TSPO^{-/-}$ and CTRL cells. Relative mtDNA content was quantified using quantitative polymerase chain reaction (qRT-PCR) targeting the mitochondrial-encoded gene tRNA leucine 1 (mt-TL1) and the nuclear-encoded single-copy gene beta-2-microglobulin (B2M).

Consistent with the observation of altered bioenergetic properties and oxidative stress, TSPO-deficient NPCs, astrocytes, and neurons contained significantly less mtDNA compared to their controls (**NPC** $p<0.0001$; **Astro** $p=0.0168$; **Neuron** $p<0.0001$) (Fig. 24A).

Reduced mitochondrial mass is an adaptive response to a decreased mtDNA copy number. Consequently, the mitochondrial content was determined by flow cytometry using the fluorescent dye MitoTracker Green. However, mitochondrial mass did not differ significantly between KO and CTRL cells (**NPC** $p=0.2576$; **Astro** $p=0.6665$) (Fig. 24B).

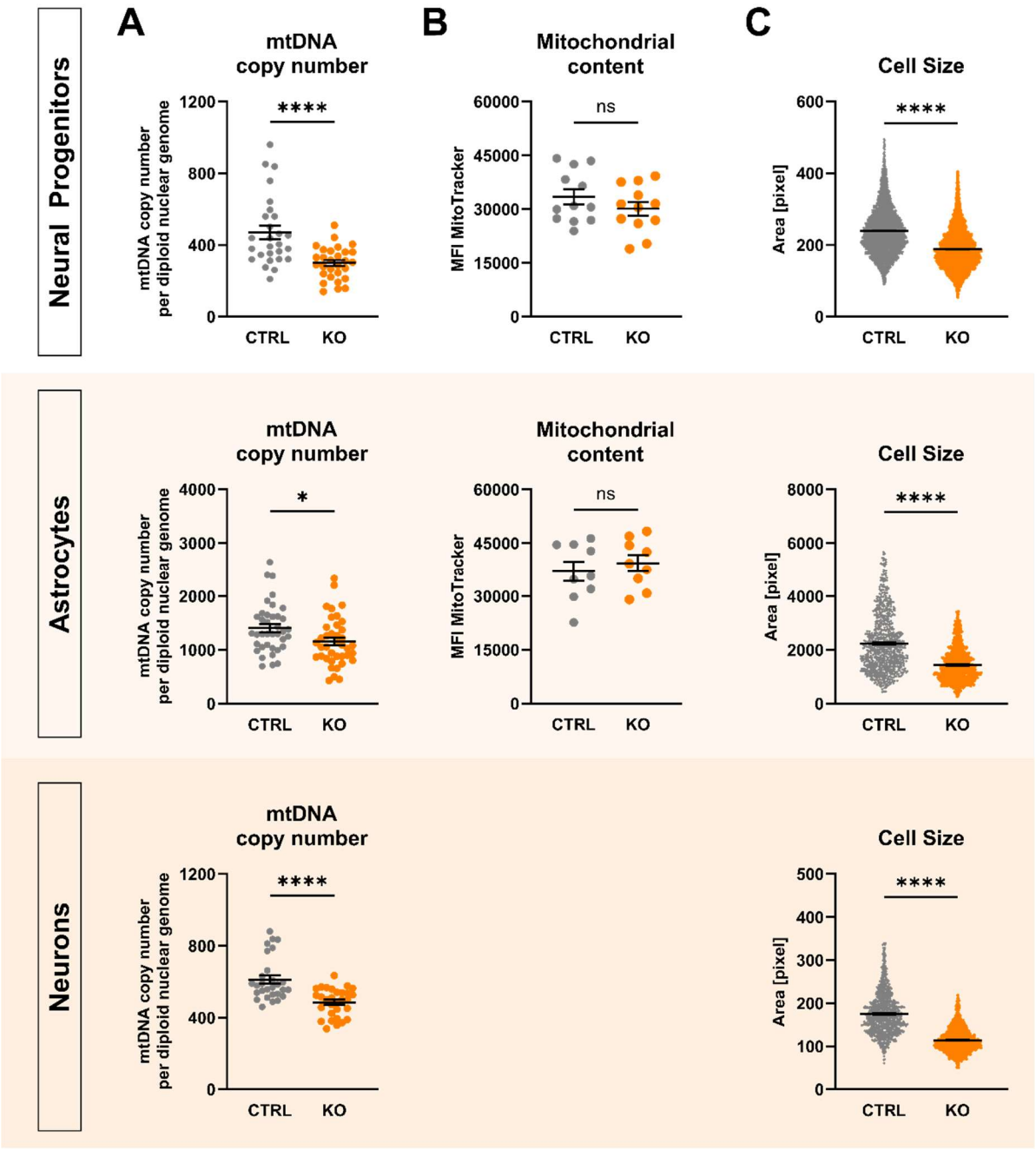

Figure 24: mtDNA copy number, mitochondrial content, and cell size in TSPO-knockout and control cells. **(A)** mtDNA copy numbers in TSPO$^{-/-}$ and CTRL cells are presented as single values of a minimum of three individual qRT-PCR of n=9 (NPCs), n=6 (astrocytes, neurons) biological replicates**. (B)** Mitochondrial content was measured by flow cytometry and is indicated by MitoTracker Green mean fluorescence intensity (MFI) of n=4 individual experiments; 1x10^5 and 2x10^4 events were recorded for each replicate of NPCs and astrocytes, respectively. **(C)** Cell size was analysed by assessing the area [pixels] of Fura-2/AM-loaded cells, and the dot plots show the number of pixels. Data are presented as mean ± SEM using independent samples t-test or Mann-Whitney U (MW) test.

Surprisingly, but consistently among all cell types examined, cells lacking TSPO protein exhibited a considerably reduced soma size ($p<0.0001$), as determined by pixel counting of the fluorescent area during Fura-2 imaging (Fig. 24C).

Table 28: mtDNA copy number, mitochondrial content, and cell size of TSPO-knockout and control cells

	Neural Progenitors		Astrocytes		Neurons	
	CTRL	KO	CTRL	KO	CTRL	KO
mtDNA copy number [a.u.]	470±37.3 n=27 p<0.0001 (MW)	298.8±16.76 n=29	1405±74.42 n=38 p=0.0168	1153±71.32 n=39	611.6±22.78 n=28 p<0.0001(MW)	485.6±14.13 n=30
Mito-chondrial content [MFI]	33416±2088 n=12 p=0.2576 (MW)	30140±1894 n=12	36996±2700 n=9 p=0.6665	39285±2281 n=9		
Cell size [pixel]	231.4±0.89 n=5983 p<0.0001 (MW)	181.4±0.71 n=6401	2367±45.79 n=822 p<0.0001 (MW)	1497±24.05 n=889	177.8±1.57 n=1106 p<0.0001 (MW)	114.3±0.74 n=1445

3.6 Impact of TSPO on mitochondrial dynamics and morphology

Mitochondrial dynamics and mitophagy play vital roles in maintaining mitochondrial function. By undergoing dynamic fusion and fission processes, mitochondria maintain their shape, size, and distribution, important for efficient cellular communication and energy transfer within the cell. Mitophagy selectively eliminates damaged or dysfunctional mitochondria, thereby preventing detrimental effects on cellular health. These processes collectively contribute to the integrity and functionality of the mitochondrial network, which is essential for sustaining cellular bioenergetics and overall homeostasis.

To investigate the impact of TSPO deficiency on mitochondrial dynamics, the mRNA expression levels of key fusion proteins, mitofusin 1 (*MFN1*) and optic atrophy protein 1 (*OPA1*), and fission protein dynamin-related protein 1 (*DRP1*) were analysed in hiPSC-derived astrocytes. Fig. 25A shows that TSPO knockout significantly reduced *MFN1* mRNA levels (p=0.0348), whereas *OPA1* and *DRP1* transcripts remained unchanged. Additionally, the gene expression of mitochondrial transcription factor A (*TFAM*), a crucial activator of mitochondrial transcription and regulator of mtDNA copy number, was examined. Consistent with the decreased mtDNA copy number, *TFAM* mRNA expression was significantly reduced in astrocytes lacking TSPO protein (p=0.05) (Fig. 25B). Furthermore, the role of TSPO in mitophagy was examined by gene and protein expression analyses. While PTEN-induced putative protein kinase 1 (*PINK1*) transcripts were not significantly different between TSPO$^{-/-}$ and CTRL cells parkin (*PARK2*) mRNA levels were considerably lower in TSPO-deficient astrocytes (p=0.0041) (Fig. 25C). Surprisingly, LC3B-II protein expression, the cleaved lipidated form of LC3B, which is tightly associated with the autophagosomal membrane and

indicates the degree of autophagic activation, was upregulated in TSPO-deficient NPCs and astrocytes. Western Blot analyses with an anti-LC3B antibody showed that TSPO deficiency in hiPSC-derived NPCs and astrocytes led to an increase of 42.1±10.3% and 49.9±14.3% in LC3B-II protein expression, compared to the respective control (**NPC** p=0.007; **Astro** p=0.0066), as shown in Figure 25D

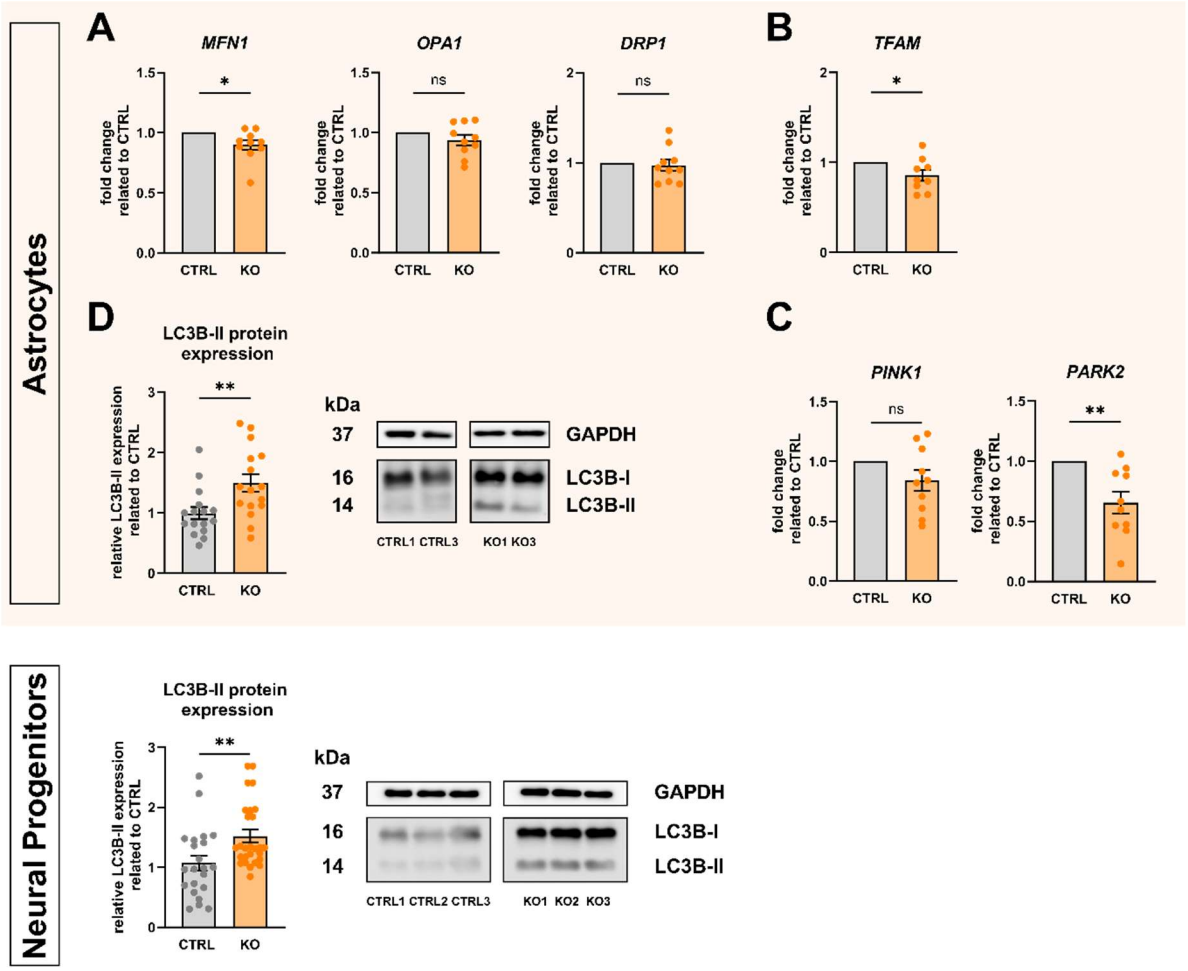

Figure 25: Relative gene and protein expression in TSPO-knockout and control cells. Gene expression of **(A)** mitochondrial fusion and fission proteins *MFN1*, *OPA1*, and *DRP1*; **(B)** mitochondrial transcription factor *TFAM*; and **(C)** mitophagy proteins *PINK1* and *PARK2*. mRNA levels of TSPO-deficient cells related to TSPO-expressing control cells. *MFN1*: 0.9097, p=0.0348; *OPA1*: 0.9393, p=0.1989; *DRP1*: 0.9703, p=0.6444; *TFAM*: 0.8581, p=0.05; *PINK1*: 0.8401, p=0.0988; *Parkin*: 0.6546, p=0.0041. Data are presented as mean single values of five qRT-PCR ± SEM (n=10), Welch's corrected t-test. **(D)** Deletion of TSPO led to increased expression of the lipidated form of LC3B protein (LC3B-II) in hiPSC-derived NPCs and astrocytes. Representative Western Blots show the expression of housekeeper gene GAPDH at 37 kDa and LC3B-I at 16 kDa and LC3B-II at 14 kDa. Bar graphs show densitometric, relative mean of LC3B-II expression levels. Individual values were normalised to the respective expression levels of GAPDH and were related to the CTRL mean. Data are presented as mean ± SEM using Mann-Whitney U test (Astro) and independent samples t-test (NPCs) of three biological replicates.

These findings suggest a role for TSPO in modulating mitochondrial dynamics, mitophagy, and the maintenance of the mitochondrial genome.

As mitochondrial morphology is regulated by the dynamic interplay between fusion and fission, ensuring mitochondrial network integrity and function, electron micrographs of hiPSC-derived astrocytes were quantified to investigate the influence of TSPO expression on mitochondrial morphology. Mitochondria devoid of TSPO were significantly smaller, as indicated by decreased surface area ($p<0.0001$) and perimeter ($p<0.0001$). Additionally, the sphericity of the mitochondria was significantly increased ($p=0.0306$) in TSPO KO astrocytes, indicating a rounder, less polymorphic shape, as depicted in Fig. 26.

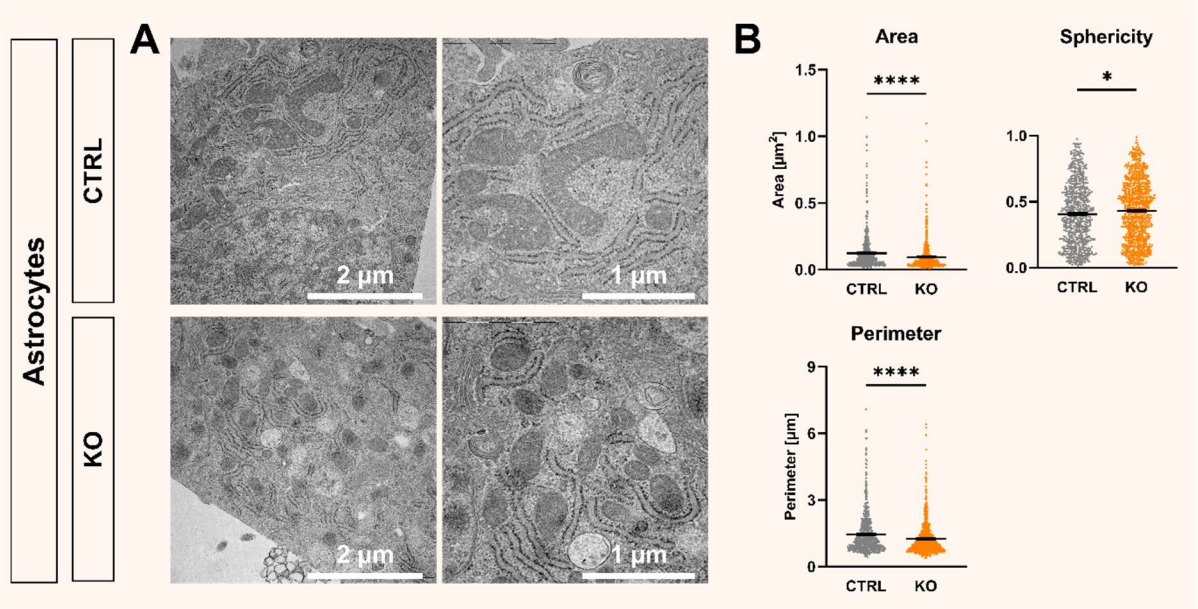

Figure 26: Analysis of mitochondrial structure by electron microscopy in TSPO-knockout and control astrocytes. (A) Representative images of mitochondria from astrocytes of both control and knockout groups (n=3 each). **(B)** Semi-quantitative analysis of mitochondrial area, perimeter, and sphericity. Dot plots display single values of TSPO-expressing (n=686) and TSPO-devoid (n=854) mitochondria. Data are presented as mean ± SEM using Mann-Whitney U test.

3.7 TSPO expression in Major Depressive Disorder

TSPO has been implicated in neurodegenerative and neuroinflammatory processes, as presumed by the observation of increased TSPO expression in various neuropathologies such as Alzheimer's disease, multiple sclerosis, Parkinson's disease, and major depressive disorder (MDD) (Rupprecht et al., 2010). Although the molecular pathomechanisms underlying MDD are still not fully understood, accumulating evidence suggests a link between mitochondrial dysfunction, bioenergetic imbalance, and the aetiology and pathology of depression (Kuffner et al., 2020; Triebelhorn et al., 2022). Thus, the protein expression of TSPO and VDAC1 was analysed in fibroblast cell lines derived from 16 MDD patients and sex- and age-matched controls. Surprisingly, the levels of both TSPO (Fig. 27A), and VDAC1 (Fig. 27B) proteins were significantly reduced (**TSPO** 76.03±4.94%, $p=0.0004$; **VDAC1** 76.48±3.92% $p=0.0028$) in patients with MDD, pointing towards a potential involvement of TSPO in the development of mitochondrial dysfunction and subsequent manifestation of MDD.

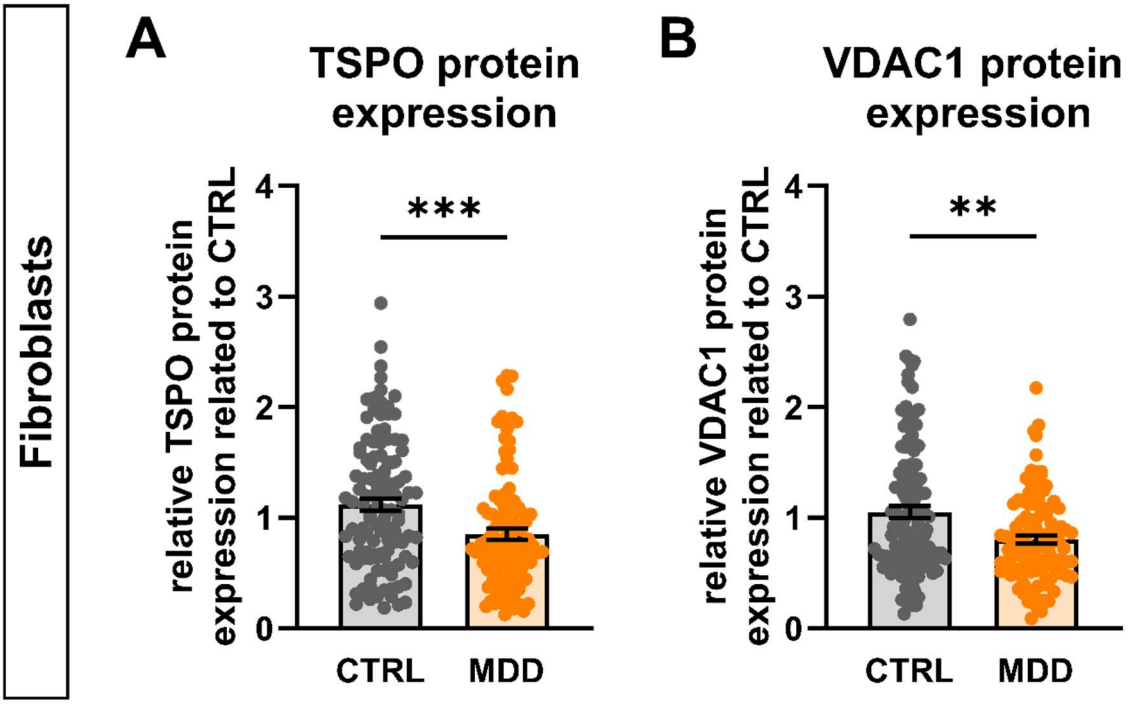

Figure 27: TSPO and VDAC1 protein expression in human primary fibroblasts of major depressive disorder (MDD) patients and healthy controls. Relative expression of **(A)** TSPO and **(B)** VDAC1 proteins normalised to the respective expression levels of BTUB1 and related to the CTRL mean. Bar graphs show densitometric, relative mean ± SEM using Mann-Whitney U test of three individual biological replicates of n=16 fibroblast cell lines.

These findings highlight the potential contribution of dysregulated TSPO and altered bioenergetics and redox homeostasis in the context of MDD.

4 Discussion

Since its discovery as a peripheral binding site for benzodiazepines in 1977, TSPO has been the subject of numerous studies that have revealed varying and sometimes conflicting functional roles. Despite decades of research, its involvement in regulating cellular and mitochondrial processes, such as steroid synthesis, oxidative stress, and mitochondrial bioenergetics, remains controversial, with no clear consensus on its specific physiological properties.

Under physiological conditions, TSPO expression in the central nervous system (CNS) is relatively low. Pathological conditions such as multiple sclerosis, Parkinson's disease, glioma, and major depressive disorder can lead to a marked and diagnostically relevant increase in TSPO expression. However, the underlying causality between elevated TSPO expression and disease onset remains a subject of debate, and its precise role in neuropathology is yet to be determined.

In this study, the effect of TSPO on cellular and mitochondrial homeostasis was investigated using a novel CRISPR/Cas9-mediated TSPO knockout model in human iPSCs. Despite its evolutionary conservation, the physiological significance of TSPO seems to be tissue- and cell type-specific. Thus, TSPO$^{-/-}$ and CTRL hiPSCs were differentiated into neural progenitor cells, astrocytes, and neurons to elucidate metabolic changes related to neurosteroid synthesis, cellular and mitochondrial bioenergetics, VDAC1 protein expression, redox and calcium homeostasis, and mitochondrial dynamics and morphology in the presence and absence of TSPO across different cell types.

4.1 Role of TSPO in neurosteroidogenesis

TSPO has long been considered essential for mitochondrial cholesterol import (Selvaraj et al., 2015), because of its localisation in the OMM, the specificity of the structural C-terminal CRAC domain with high affinity for cholesterol, and its particularly high expression in steroid-synthesising tissues. Thus, many studies using biochemical, pharmacological, and genetic experimental approaches have provided evidence for the important role of TSPO in steroid production (Costa et al., 2018; Hauet et al., 2005; Kelly-Hershkovitz et al., 1998; Mukhin et al., 1989; Papadopoulos, Amri, Li, et al., 1997; Papadopoulos et al., 1990, 2018, 2018). Although recent *in vivo* and *in vitro* TSPO knockout studies have refuted the role of TSPO in steroidogenesis (Banati et al., 2014; Morohaku et al., 2014; Tu et al., 2014), its specific role in neurosteroid synthesis is still largely unclear (Selvaraj & Tu, 2016).

To shed further light on this contradictory debate, pregnenolone concentration in the supernatants of CTRL and TSPO$^{-/-}$ hiPSC-derived astrocytes was measured using ELISA. A

significant decrease in pregnenolone levels in TSPO-deficient astrocytes was observed, supporting the potential importance of TSPO in neurosteroid synthesis. But generally, the amount of quantified pregnenolone was considerably low, ranging between 2.5 and 7.2 pg/µg/mL protein, indicating a low steroid-synthesising capacity of the hiPSC-derived astrocytes, similar to human C20 microglia (V. M. Milenkovic et al., 2019). While astrocytes showed higher P450scc (*CYP11A1*) transcripts compared to C20 microglial cells, the mRNA expression was still considerably lower than that found in the steroidogenic adrenocarcinoma cell line H295-R.

Neurosteroidogenesis occurs in both neurons and glia; however, the expression of steroidogenic enzymes in the CNS is specific to certain cell types and regions (Yilmaz et al., 2019). Recent results from a TSPO knockdown study in murine microglial BV-2 cells support a TSPO-related *de novo* neurosteroid synthesis pathway as well as a direct and TSPO-mediated effect of TSPO ligands on neurosteroidogenesis (Bader et al., 2019). In contrast, a study using human C20 microglial cells reported low pregnenolone synthesis, independent of TSPO depletion, which could not be stimulated by specific TSPO ligands or dibutyryl-cAMP (V. M. Milenkovic et al., 2019). Whereas, a more recent study not only confirmed the steroidogenic role of human microglia but also highlighted the explicit involvement of TSPO in this process (Germelli et al., 2021). Another study found that the human microglial cell line HMC3 and the human astrocyte cell line NHA produce pregnenolone in a TSPO-related manner, as pregnenolone production could be enhanced by XBD173 (Y. C. Lin et al., 2022). Moreover, Angeloni et al. suggested an essential autocrine control of neurosteroid synthesis in orchestrating cholesterol trafficking, since TSPO silencing, which is unable to promote native neurosteroidogenesis, resulted in impaired cholesterol homeostasis, leading to excessive cholesterol accumulation (Angeloni et al., 2023).

It has been discovered that murine and human microglia lack cholesterol-metabolising enzymes, that is exhibiting only low mRNA levels of StAR and no transcripts of P450scc, which are indispensable for *de novo* steroid synthesis (Gottfried-Blackmore et al., 2008; Owen, Narayan, et al., 2017). Instead, microglia are only able to metabolise androgens and oestrogens from available steroid precursors and convert dehydroepiandrosterone (DHEA) to 5-androstene-3-beta, 17-beta-diol, but lack the enzymes to synthesise progesterone and DHEA (Yilmaz et al., 2019).

On the contrary, astrocytes have been shown to be the most active steroidogenic cells in the brain producing pregnenolone, progesterone, DHEA, androstendion, testosterone, oestradiol and estrone (Zwain & Yen, 1999). Additionally, various studies have consistently indicated that elevated neurosteroid levels in hepatic encephalopathy, a neuropsychiatric syndrome, are linked to increased neurosteroid synthesis, and may be partly caused by the upregulation of TSPO in astrocytes (Bélanger et al., 2005; Bender & Norenberg, 1998; Itzhak et al., 1995). A

more recent study on primary rat hypothalamic astrocytes found that PKA-mediated activation of StAR and TSPO promoted neurosteroidogenesis following hormonal treatment (C. Chen et al., 2014). Another study conducted on an astrocytic model showed that stimulating TSPO using synthetic ligands could increase the expression level of the mitochondrial form of StAR, suggesting protein activation (Costa et al., 2020; Santoro et al., 2016).

Mellon and Deschepper discovered that the overall quantity of P450scc mRNA in the rat brain was only approximately 0.01% of that measured in the adrenal gland. Interestingly, they found vastly different ratios of P450scc mRNA and protein expression compared to the adrenal cortex, suggesting the importance of translational regulation or protein stability for P450scc activity in the brain (Mellon & Deschepper, 1993). This may indicate that only a small subpopulation of cells is capable of synthesising neurosteroids *de novo* (Selvaraj & Tu, 2016). However, Lin et al. demonstrated the ability of human microglia and astrocytes to produce pregnenolone despite low levels of P450scc mRNA and no detectable protein expression. They further provided evidence for a CYP11A1-independent pathway for pregnenolone synthesis and proposed the involvement of a CYP450 other than CYP11A1, responsible for producing pregnenolone in the human CNS (Y. C. Lin et al., 2022).

Although TSPO is highly expressed in microglia and astrocytes, it is less abundant in neurons. However, neurosteroidogenesis primarily occurs within principal neurons of various brain regions that possess the enzymatic machinery required to convert cholesterol into neuroactive steroids (Porcu et al., 2016). Single-cell transcriptomics and TSPO-antibody immunolabelling have confirmed low neuronal TSPO expression in rodent and human brains (Barron et al., 2021; Betlazar et al., 2018; Notter et al., 2021), which could be upregulated by neuronal activity (Notter et al., 2021). Moreover, Barron et al. demonstrated reduced depression-related behaviour, an effect caused by TSPO overexpression and dependent on steroidogenesis (Barron et al., 2021). Although these studies provide initial evidence of the functional importance of neuronal TSPO, further studies are required to verify the significance of these findings at physiological neuronal TSPO levels, which could be assessed using the novel TSPO knockout model in hiPSCs. Notably, nerve cells often possess only one steroidogenic enzyme, unlike classical endocrine steroidogenic cells which express multiple enzymes of the biosynthetic pathway. Consequently, the production of neurosteroids, such as DHEA or allopregnanolone, which requires the involvement of multiple enzymes, would necessitate the steroid precursor molecules to navigate from one type of nerve cell to another, and potentially even from glial cells to neurons, and *vice versa* (Do Rego et al., 2009). Furthermore, as opposed to peripheral steroidogenesis, which is predominantly regulated by pituitary hormones via the transcriptional regulation of StAR, neurosteroidogenesis is governed by neurotransmitters and neuropeptides (Barron et al., 2021).

Given the potential journey of steroids through different cell types, including their unique regulation, further investigation of the interactions between TSPO and other proteins involved in cholesterol transport and steroidogenesis may provide valuable insights into the complexity of neurosteroid synthesis in the brain.

Additionally, is has been indicated, that TSPO may have an impact on steroidogenesis beyond the immediate translocation of cholesterol into mitochondria. Studies have observed increased accumulation of lipid droplets in conditional TSPO-deficient ($TSPO^{\Delta/\Delta}$) Leydig cells (Fan et al., 2015) and primary murine microglia (Fairley et al., 2023), indicating a blockade of cholesterol utilisation. Furthermore, Fairley et al. observed TSPO-dependent transcriptional upregulation of genes associated with lipid synthesis in the hippocampi of TSPO-KO mice. Given the fact that *ACLY*, a key enzyme involved in the shift from carbohydrate metabolism via the TCA cycle to cholesterol and fatty acid synthesis, is upregulated, they proposed that TSPO deletion results in a switch to the conversion of glucose into lipids for storage. Hence, TSPO may regulate steroidogenesis by affecting the bioavailability of cholesterol for steroid production by influencing lipid synthesis from carbohydrate substrates (Fairley et al., 2023).

Taken together, in contrast to the periphery, where TSPO is not essential for maintaining baseline steroidogenesis except during aging or in response to stress (Barron et al., 2021), these findings suggest a critical role for TSPO in steroid production in the brain.

4.2 Impact of TSPO on the energetic status of the cell

4.2.1 Mitochondrial and cellular respiration

Mitochondria are often referred to as the powerhouse of the cell because they play a crucial role in providing cellular energy by generating ATP through oxidative phosphorylation. Quantification of mitochondrial respiration, which directly reflects electron transport impairment and depends on the oxidation of cytochrome c in complex IV leading to the consumption of molecular oxygen to form water, can serve as an indicator of OXPHOS functionality and efficiency (Triebelhorn et al., 2022; Yépez et al., 2018).

The involvement of TSPO in regulating the bioenergetic state of cells remains controversial. However, recent and growing literature on the evolving knowledge of TSPO functions (Betlazar et al., 2020) points to a central role of TSPO in modulating mitochondrial energetic processes. Therefore, respirometry measurements and analyses of functional bioenergetic parameters in hiPSC-derived CTRL and KO cells were performed using a Seahorse Extracellular Flux Analyser. Consistently, both TSPO-deficient NPCs and astrocytes showed reduced mitochondrial respiration, as indicated by lower basal and maximal respiration rates as well as decreased spare respiratory capacity and ATP-related respiration. Surprisingly, while the ATP content remained unchanged, the mitochondrial and total ATP production rates were significantly reduced in CTRL and $TSPO^{-/-}$ NPCs and astrocytes, indicating decreased

metabolic flux. An increased glycolytic activity of TSPO KO cells to compensate for decreased OXPHOS to maintain total intracellular ATP levels seemed likely. Thus, the Seahorse Glycolytic Rate assay was used to evaluate key glycolytic parameters. However, contrary to the presumption of increased glycolysis, basal and compensatory glycolysis were reduced in TSPO-deficient NPCs and astrocytes. Moreover, TSPO knockout in NPCs resulted in a lower glycolysis-specific ATP rate fraction.

Banati et al., provided the first evidence for a regulatory impact of TSPO in the metabolic activity of primary murine microglia from genetically modified TSPO knockout mice. In this context, loss of TSPO expression resulted in decreased basal oxygen consumption as well as ATP synthesis-related OCR (Banati et al., 2014). Since then, several groups have studied the role of TSPO in energy metabolism. Recent results using both rodent and human microglia suggest that TSPO and TSPO ligands may have differential effects on energy metabolism, some of which are specific or independent of TSPO expression. In the human C20 microglial cell line, basal and maximal respiration, as well as ATP-related oxygen consumption, were significantly reduced in TSPO-knockout cells compared to wild-type cells. Lentiviral overexpression of TSPO was able to rescue the impaired mitochondrial respiration in C20 knockout cells (V. M. Milenkovic et al., 2019). Similarly, TSPO deficiency in primary murine microglia restrained mitochondrial OXPHOS, as indicated by the lower basal and maximal OCR and subsequent ATP production, resulting in reduced mitochondrial ATP levels (Fairley et al., 2023; Yao et al., 2020). In a lentiviral TSPO knockdown model in the rodent microglial cell line BV-2, mitochondrial respiration was unchanged compared with that in SCR control cells. However, treatment with the specific TSPO-ligands PK11195 and Ro5-4864 stimulated basal and ATP-related oxygen consumption only in TSPO-expressing SCR microglia, in favour of a specific and TSPO-dependent effect on OXPHOS (Bader et al., 2019). Similarly, Fairley et al. observed a bioenergetic effect of Ro5-4864 in cultured BV-2 microglia, indicated by higher basal and maximal OCR (Fairley et al., 2023). Using murine TSPO-deficient glioma cells, TSPO knockdown patient-derived stem-like GBM1B cells and human glioma U87MG cells Fu et al. demonstrated, that TSPO deletion or silencing promoted glioma growth by suppressing mitochondrial function, i.e. mitochondrial respiration and global ATP production (Fu et al., 2019). Treatment of wild-type rodent glioma cells with the specific TSPO-antagonist PK11195 reduced mitochondrial function. Intriguingly, the TSPO-specific agonist Ro5-4864 also significantly decreased mitochondrial bioenergetic parameters (Fu et al., 2019). In contrast, human neuroblastoma SH-SY5Y cells treated with TSPO ligands showed increased ATP synthesis (Grimm et al., 2020; Lejri et al., 2019). However, conflicting results have been published regarding the effects of TSPO on glycolysis in primary murine microglia. Yao et al. observed a decrease in the extracellular acidification rate (ECAR), representing inhibited glycolytic function in TSPO-deficient microglia (Yao et al., 2020). Fairley et al. reported a

modest increase in glycolysis in TSPO$^{-/-}$ microglial cultures as measured by ECAR. Moreover, TSPO deletion in GL261 mouse glioma cells enhanced glycolysis, which could be reversed by restoring TSPO expression (Fu et al., 2019).

Although these findings suggest an effect of TSPO on the bioenergetic status of cells in the central nervous system, the underlying mechanisms remain to be elucidated.

Reduced mitochondrial respiration may be attributed to diminished mitochondrial respiratory chain activity or the limited availability of substrates or enzymes. If glucose or fatty acid substrates are restricted or enzymes involved in their metabolic breakdown malfunction, the levels of NADH/H$^+$ and $FADH_2$ reduction equivalents decrease. Moreover, the transport of these reduction equivalents into the mitochondria may be a limiting factor for ETC function (Leverve, 2007). Inhibition of complex I of ETC has been shown to affect the activity of complex II, as the tricarboxylic acid (TCA) cycle ceases succinate production in the absence of NADH/H$^+$ (Steinlechner-Maran et al., 1997).

The voltage-dependent anion channel VDAC, ubiquitously expressed in mammalian cells, is a crucial regulator of various mitochondrial functions. As the major pore of the OMM, VDAC1 facilitates the transport of respiratory chain substrates, such as ADP, ATP, NAD$^+$, and NADH. Furthermore, VDAC is involved in the regulation of metabolite diffusion, including glucose, pyruvate, glutamate, succinate, and citrate and cations, such as Ca^{2+} and Mg^{2+} (Shoshan-Barmatz et al., 2019). The association between TSPO and VDAC has been extensively studied, suggesting their involvement in an insufficiently characterised protein complex that exerts a joint influence on physiological functions.

Interestingly, TSPO deficiency was accompanied by reduced VDAC1 protein expression in hiPSC-derived NPCs and astrocytes. While the gene expression level was unchanged, protein stability assays using cycloheximide revealed higher protein degradation in TSPO$^{-/-}$ NPCs. This negative correlation between TSPO and VDAC expression has also been shown in a TSPO-knockout model of human C20 microglial cells (Bader et al., 2023; V. M. Milenkovic et al., 2019). Moreover, decreased VDAC expression in glioblastoma cancer cells resulted in a decline in TSPO expression (Arif et al., 2016), whereas patients with bipolar disorder showed highly increased expression levels of both TSPO and VDAC in their PBMCs (Scaini et al., 2019), further demonstrating the mutual dependence of TSPO and VDAC expression. Proteomic protein-protein interaction analysis identified the metabolic regulators 14-3-3 family scaffold adaptor and chaperone proteins as hubs in the TSPO-interactome network of the brain (Fairley et al., 2023). Notably, phosphoserine protein-binding motifs of 14-3-3 adaptors have been identified on functionally important sites of both TSPO and VDAC (Aghazadeh et al., 2012, 2014).

Mechanistically, TSPO has been associated with F_1F_o-ATP synthase of complex V, which is responsible for generating ATP. Studies on isolated rat brain mitochondria have demonstrated

that specific TSPO ligands PK11195, Ro5-4864, and protoporphyrin IX affect the phosphorylation of subunit *c* of F_1F_o-ATP synthase (Krestinina et al., 2009). Additionally, PK11195 was found to inhibit F_1F_o-ATPase activity in an oligomycin sensitivity-conferring protein-dependent manner, which decreased ATP synthesis and increased intracellular superoxide levels (Cleary et al., 2007). Seneviratne et al., showed that PK11195 is able to inhibit the activity of the F_1F_o-ATP synthase, similar to oligomycin, demonstrating a biological effect for PK11195 beyond TSPO binding (S.D. Seneviratne et al., 2012).

It is worth noting, that PAP 7, which can bind both TSPO and the regulatory protein kinase A (PKA) subunit RIα, may act as an endogenous TSPO ligand (Krestinina et al., 2009). Serving as a PKA-RIα-anchoring protein (J. Liu et al., 2003), PAP7, when associated with mitochondria, can be targeted by PKA in TSPO-expressing mitochondria influencing the phosphorylation/dephosphorylation of mitochondrial proteins (Krestinina et al., 2009). Phosphorylated F_1F_o-ATP subunit *c* can transmit signals to both the δ subunit and catalytic β subunit, which subsequently undergoes phosphorylation. Thus, TSPO ligands may regulate mitochondrial energy metabolism by regulating phosphorylation of F_1F_o-ATP subunit *c* (Krestinina et al., 2009). Additionally, ATP synthase, previously reported as an interactor with the TSPO-VDAC complex (Veenman et al., 2010) and regulated by 14-3-3 adaptor proteins, has recently been identified in the brain TSPO interactome. This interaction of both TSPO and ATP synthase with 14-3-3 adaptor proteins may provide an explanation for the contribution of TSPO to mitochondrial OXPHOS (Fairley et al., 2023).

The impact of TSPO on glycolysis may also be attributed to VDAC interactions. A study by Fairley et al. revealed that the higher glycolytic capacity observed in $TSPO^{-/-}$ microglia was caused by a compensatory increase in hexokinase II (HK2) activity, a key enzyme involved in glucose metabolism. This elevated HK activity was mediated by the recruitment of HK to the mitochondria, a process that has been shown to involve VDAC interaction (Roberts & Miyamoto, 2015). Moreover, mitochondrial HK recruitment is regulated by the phosphorylation of HK (Miyamoto et al., 2008) or VDAC (Das et al., 2008; Pastorino et al., 2005), and TSPO has been implicated in VDAC phosphorylation (Gatliff et al., 2014), suggesting a possible interaction between TSPO and HK activity (Fairley et al., 2023). A previous study also demonstrated the upregulation of HK2. Furthermore, hypoxia inducible factor 1 subunit α (HIF-1α), a key regulator of glycolysis, was found to be upregulated due to TSPO deficiency, which likely increased the expression of the key glycolysis-associated enzymes glucose transporter 1 (GLUT1) and lactate dehydrogenase (LDH) (Fu et al., 2019).

When cellular respiration is impaired, cells may have a “choice” to either maintain their mitochondrial membrane potential and consume ATP or to depolarise the mitochondria and preserve cellular ATP levels. The choice between these options may depend on the glycolytic capacity of the cells. However, it is unclear which option would be more beneficial for cell

survival, as allowing mitochondria to depolarise could lead to the release of pro-apoptotic molecules, triggering cell death (Campanella, Casswell, et al., 2008). Under any circumstances in which MMP is compromised, such as oxygen deprivation or damaged mitochondrial respiratory proteins, the enzymatic activity of ATP synthase can be reversed. The enzyme functions as a proton-motive ATPase, consuming ATP and pumping protons from the mitochondrial matrix to sustain MMP. However, inhibitor factor 1 (IF_1) can mitigate ATP hydrolysis by binding to the F_1F_o complex and inhibiting ATPase activity without affecting ATP synthesis during OXPHOS (Campanella, Casswell, et al., 2008). IF_1 activity may explain the observed MMP depolarisation and unchanged ATP levels in the hiPSC-derived TSPO-deficient cells. However, KO cells also exhibited reduced ATP-related OCR and total ATP production rates, suggesting a lower ATP demand and turnover. Thus, CTRL and TSPO knockout cells may consume ATP through different pathways. Previous studies have indicated the presence of a hierarchy of ATP-consuming reactions within a cell, and the utilisation of ATP can be determined by both ATP-producing and ATP-consuming processes. Hence, if the ATP supply is compromised, non-essential cellular processes are given up first, prioritising the preservation of critical functions vital for sustaining cellular ionic integrity (Buttgereit & Brand, 1995).

Cells conserve energy by converting ADP to ATP, similar to the function of rechargeable batteries. The energy released by the hydrolysis of ATP back to ADP is utilised to power most energy-dependent processes, including cell growth, division, communication, and movement (Hardie, 2018). Maintaining a balanced equilibrium between ATP production and consumption, represented by the ratio $\frac{[ATP+0.5*ADP]}{[ATP+ADP+AM\ ]}$, is crucial for proper cellular function. Although the mitochondrial and glycolytic pathways generate energy from various fuel sources, the phosphocreatine (PCr) shuttle is used to meet immediate energy requirements (Johnson et al., 2019). Mitochondrial creatine kinase, along with cytosolic isoenzymes, produces highly diffusible phosphocreatine for the temporal and spatial buffering of ATP levels to maintain cellular energy homeostasis (Schlattner et al., 2006). Interestingly, mitochondrial creatine kinase, has been identified in the brain TSPO interactome network (Fairley et al., 2023). Additionally, the coordinated actions of AMP deaminase (AMPD), AMP-activated protein kinase (AMPK), and adenylate kinase (AK) contribute to energy regulation. AMPK serves as an energy-charge sensor that modulates AMPD activity. AMPD converts AMP to IMP to maintain a higher energy charge and to facilitate the forward AK reaction, which generates ATP and AMP from two ADP molecules (Johnson et al., 2019).

Notably, reduced respiration in TSPO-knockout cells can be attributed to a reduced mitochondrial mass. However, the mitochondrial content measured by flow cytometry in TSPO-

knockout hiPSC-derived NPCs and astrocytes was unchanged compared with that in CTRL cells.

In summary, the reduced mitochondrial and cellular respiration observed in TSPO-deficient cells can be caused by various factors, including diminished ETC activity, restricted substrate or enzyme availability, malfunctioning of ETC complexes, and improper functioning of the TSPO-VDAC interactome. Further investigations are needed to fully understand the mechanisms underlying the regulatory role of TSPO in cellular and mitochondrial respiration.

4.2.2 Mitochondrial membrane potential and Ca^{2+} and redox homeostasis

The electrochemical proton gradient across the IMM, generated by the respiratory complexes of the ETC by pumping protons into the intermembrane space, forms a proton motive force. This driving force, which is composed of a pH gradient and mitochondrial membrane potential, is essential for mitochondrial respiration (Lodish et al., 2021). MMP and ATP synthesis are typically maintained at stable levels with minor temporary fluctuations. However, prolonged periods of MMP instability can lead to altered bioenergetic states, resulting in mitochondrial dysfunction and cell death (Ilkan & Akar, 2018; Zorova et al., 2018). Fluctuations in MMP triggered by local Ca^{2+} release from the endoplasmic reticulum are an indication of mitochondrial viability and functional capacity. Although mitochondria are largely autonomous organelles, their MMP can be modulated by their cellular environment and interactions with other organelles, particularly the ER (Keil et al., 2011). Thus, MMP serves as an important functional parameter for the bioenergetic state of mitochondria, influencing mitochondrial functions, such as Ca^{2+} homeostasis (V. M. Milenkovic et al., 2019), and provides information on the balance between energy supply and demand (Schmidt et al., 2021). A more negative or polarised MMP implies an increase in the coupling efficiency of OXPHOS, whereas a less negative or depolarised MMP suggests a decrease in efficiency or may result from rate limitations in the ETC or substrate oxidation (Schmidt et al., 2021).

Following respirometry analyses, MMP measurements were conducted to investigate its correlation with the observed metabolic changes in relation to the impact of TSPO on the cellular energy status. Consistent across all analysed cell types, TSPO-deficiency resulted in prominent depolarisation of MMP. This is in line with several studies reporting that inhibition of TSPO expression causes depolarisation of the mitochondria. In murine BV-2 microglial cells, RNA interference-mediated TSPO knockdown resulted in a lower MMP (Bader et al., 2019; Yao et al., 2020). Similarly, mitochondrial depolarisation has been observed in primary microglia isolated from genetically modified TSPO-knockout mice (Fairley et al., 2023; Yao et al., 2020). Moreover, CRISPR/Cas9-mediated knockout of TSPO in human C20 microglia caused a robust reduction in MMP (V. M. Milenkovic et al., 2019). A comprehensive study on the impact of TSPO on key mitochondrial functions reported similar results. TSPO-knockout

mouse glioma cells also showed lower MMP (Fu et al., 2019). In contrast, downregulation of TSPO expression in canine C35 epithelial cells resulted in hyperpolarised mitochondria (Gatliff et al., 2017), whereas TSPO deletion in murine MA-10 Leydig cells did not affect the MMP (Tu et al., 2016). However, in a recent study, TSPO-deficient MA-10 Leydig cells exhibited a significantly decreased MMP (Fan et al., 2018). Fan et al. attributed the depolarisation of MMP to the lack of regulation of VDAC/tubulin interaction caused by the loss of TSPO expression, as indicated by the reduced overlap of mitochondria and polymerised tubulin in TSPO-deficient cells (Fan et al., 2018). Tubulin, a cytoskeletal protein, has been shown to modulate VDAC function. Upon binding, the voltage sensitivity of VDAC increases, thereby inducing VDAC closure at low transmembrane potentials. This regulates ATP/ADP flux and limits mitochondrial metabolism and respiration, leading to alterations in MMP (Rostovtseva et al., 2008; Rostovtseva & Bezrukov, 2012). In cancer cells, MMP and concomitant VDAC conductance change depending on the amount of free tubulin present (Maldonado et al., 2010). Tubulin further controls VDAC conductance in a PKA-dependent manner. PKA agonists cause VDAC closure, which leads to reduced MMP levels. Conversely, antagonists reduce tubulin-dependent VDAC closure and MMP depolarisation (Maldonado & Lemasters, 2014). In turn, TSPO can modulate this tubulin/VDAC interaction by competitive binding and altering VDAC conductance (Gatliff & Campanella, 2012). The interaction between TSPO and ACBD3 leads to recruitment and complexation of ACBD3 with cAMP-dependent PKA. The resulting phosphorylation of VDAC regulates VDAC activity by decreasing its conductance (Gatliff et al., 2017).

Bioenergetic homeostasis and mitochondrial functionality are essential for energy supply. In respiring mitochondria, a negative MMP is a major driving force for the accumulation of Ca^{2+} ions. The concentration gradient between extracellular Ca^{2+} levels and cytosolic Ca^{2+} concentration $[Ca^{2+}]_c$ is essential for the induction of Ca^{2+}-dependent signalling cascades. Maintaining this gradient requires a significant amount of cellular energy, as extracellular Ca^{2+} levels are 20,000 times higher than $[Ca^{2+}]_c$ (Hopp, 2021). In the resting state, the mitochondrial matrix Ca^{2+} concentration $[Ca^{2+}]_m$ of approximately 100 nM is in equilibrium with the cytosol. Upon an increase in $[Ca^{2+}]_c$ due to its release from intracellular Ca^{2+} stores or influx from the extracellular space, Ca^{2+} uptake can increase $[Ca^{2+}]_m$ to more than 100 µM. This rapid and transient accumulation of Ca^{2+} ions allows mitochondria to contribute to the regulation of cytosolic Ca^{2+} transients and the maintenance of Ca^{2+} homeostasis as intracellular Ca^{2+} stores and buffers (Rostovtseva, 2017).

Limited evidence suggests a modulatory role of TSPO in maintaining cellular and mitochondrial Ca^{2+} homeostasis. However, the direct association and complex formation with VDAC, the main Ca^{2+} channel of the OMM, supports the involvement of TSPO in the regulation of intracellular Ca^{2+}. Furthermore, changes in MMP are closely related to changes in Ca^{2+}

homeostasis. Thus, basal cytosolic and mitochondrial Ca^{2+} levels were investigated in hiPSC-derived NPCs, astrocytes, and neurons. Consistently, all TSPO-knockout cells showed decreased cytosolic and increased mitochondrial Ca^{2+} levels. This is in line with a previous study that reported an ATP-induced increase in $[Ca^{2+}]_m$ and a decrease in $[Ca^{2+}]_c$ in TSPO-knockdown cells and reversed effects in TSPO-overexpressing cells from different species, suggesting a conserved mechanism of mitochondrial Ca^{2+} homeostasis. This mechanism involves TSPO, which limits the transport efficiency of Ca^{2+} ions into the mitochondria and controls mitochondrial Ca^{2+} uptake through VDAC (Gatliff et al., 2017). Consistently, treatment of isolated mitochondria with the endogenous ligand hemin (iron protoporphyrin IX) limited mitochondrial Ca^{2+} accumulation by reducing VDAC conductance (Tamse et al., 2008). In contrast, TSPO loss in human C20 microglia resulted in increased cytosolic Ca^{2+} levels (Bader et al., 2023; V. M. Milenkovic et al., 2019). However, $[Ca^{2+}]_m$ was also increased in microglia devoid of TSPO (Bader et al., 2023).

The ability of mitochondria to accumulate and release Ca^{2+}, which represents the Ca^{2+} buffering capacity, can be both beneficial and detrimental. It contributes to Ca^{2+} homeostasis by removing cytosolic Ca^{2+} ions, and modulates mitochondrial activity. Upon cytosolic Ca^{2+} rise, mitochondria take up Ca^{2+}, which regulates the activity of matrix dehydrogenases, triggering the generation of reducing equivalents that fuel ETC and ATP synthesis (Gherardi et al., 2020). Thus, the elevated $[Ca^{2+}]_m$ observed in hiPSC-derived $TSPO^{-/-}$ cells could be attributed to a regulatory response to decreased mitochondrial respiration and ATP production. Mild depolarisation significantly reduces Ca^{2+} efflux from the matrix, facilitated by the major mitochondrial Ca^{2+} efflux system, the mitochondrial sodium/calcium exchanger protein NCLX. As a result, the rise in $[Ca^{2+}]_m$ triggers the stimulation of OXPHOS (Dejos et al., 2020). Additionally, $[Ca^{2+}]_m$ regulates cAMP activation via a PKA-dependent pathway, and the subsequent increase in matrix cAMP levels, in turn, regulates mitochondrial ATP production capacity (Di Benedetto et al., 2013). However, according to a recent study by Malyala et al., the accumulation of mitochondrial Ca^{2+} as phosphate precipitates inhibits complex I of the ETC, resulting in decreased OXPHOS activity (Malyala et al., 2019).

Mitochondrial Ca^{2+} uptake occurs not only during a substantial global rise in cytosolic Ca^{2+} but also after stimulus-induced Ca^{2+} release from the ER. The efficiency of this uptake depends on the interaction between the mitochondria and ER at specialised contact sites known as mitochondria-associated membranes (MAMs). They are composed of specific proteins located in both organelles, serving as tethers for a physical interface, and allowing the release of Ca^{2+} at maximal proximity (Yang et al., 2021). The main mechanism of ER Ca^{2+} release is facilitated by the tethering complex between the ER-Ca^{2+} channel inositol-1,4,5-trsphosphate receptor (IP_3R) and VDAC1 in the OMM, which is supported by chaperone GRP75 (Betzer & Jensen, 2018). Notably, PKA plays an important role in Ca^{2+} signalling by modulating both IP_3R

(deSouza et al., 2002) and VDAC (Gatliff et al., 2017). PKA phosphorylation increases IP_3R channel activity (deSouza et al., 2002) and the on-rate of tubulin binding to VDAC, leading to a reversible cation-selective, closed state that favours Ca^{2+} influx (Sheldon et al., 2011).

Depletion of cytosolic Ca^{2+} triggers the active migration of mitochondria towards cellular Ca^{2+}, such as the ER. This promotes the formation of ER-mitochondrial contact sites through MAMs, and facilitates the uptake of mitochondrial Ca^{2+} (Panda et al., 2021). However, an increase in the number of MAMs results in mitochondrial Ca^{2+} overload (Arruda et al., 2014).

Notably, Ca^{2+} has been reported to regulate VDAC expression. Ca^{2+}-mobilising agents caused an increase in $[Ca^{2+}]_c$ and induced VDAC1 overexpression, whereas chelation of intracellular Ca^{2+} reduced VDAC1 expression (Weisthal et al., 2014).

Taken together, disruptions in cellular Ca^{2+} signalling cascades, such as altered Ca^{2+} release from intracellular Ca^{2+} stores, impaired Ca^{2+} sensing and buffering mechanisms, and dysregulation of Ca^{2+}-transporting proteins or channels, can affect mitochondrial function and compromise OXPHOS.

Although Ca^{2+} is required for ATP synthesis, excess influx of Ca^{2+} into the mitochondrial matrix can lead to increased ROS formation, which eventually induces MMP loss and may trigger mPTP opening, ultimately resulting in apoptosis (Panda et al., 2021). While low levels of ROS serve crucial signalling functions, excessive ROS accumulation leads to oxidative stress and molecular damage. Mitochondrial ETC, specifically complexes I and III, acts as the primary source of ROS and plays a key role in maintaining cellular redox homeostasis. Flow cytometry analysis of hiPSC-derived NPCs and astrocytes revealed a significant increase in cytosolic ROS and mitochondrial superoxide levels in TSPO-deficient cells. Similarly, TSPO-knockout murine glioma cells and TSPO-knockdown human microglial cells displayed significantly higher cytosolic ROS levels than wild-type cells, indicating a more hypoxic microenvironment (Angeloni et al., 2023; Fu et al., 2019). Interestingly, VDAC was also affected by hypoxic conditions. Hypoxia leads to HIF-1α-dependent cleavage of the C-terminal end of VDAC, reflecting the survival response of hypoxic cells to prevent apoptosis and permit the maintenance of ATP supply and cell survival (Brahimi-Horn et al., 2012, 2015).

The closed, low-conductance VDAC conformation has higher selectivity for cations than anions, thus facilitating Ca^{2+} influx. In addition, VDAC closure may prevent oxidative stress in the cytosol while simultaneously promoting intramitochondrial ROS accumulation by reducing the release of superoxide from the mitochondria (Tikunov et al., 2010). This in turn enhances ROS production through a positive feedback loop via ROS sensing and redox modifications of the MCU. Oxidation of cysteine residue Cys-97 in the MCU leads to increased MCU-mediated Ca^{2+} uptake, resulting in elevated $[Ca^{2+}]_m$ and subsequently enhanced mitochondrial ROS accumulation. Ultimately, this leads to disruption of cellular energy production, causing a

cellular bioenergetic crisis and mitochondrial Ca^{2+} overload-induced cell death (Dong et al., 2017).

TSPO knockdown in human SH-SY5Y neuroblastoma cells resulted in a significant increase in mitochondrial superoxide levels. Cytoplasmic superoxide was not affected, and global cellular hydrogen peroxide (H_2O_2) and peroxyl radicals (HO_2) were significantly lower than those in control cells. However, TSPO overexpression resulted in a heightened basal redox state (Frison et al., 2021). Gatliff et al. reported that dysregulation of mitochondrial Ca^{2+} signalling and the subsequent parallel increase in intracellular $[Ca^{2+}]_c$ in TSPO-overexpressing cells resulted in elevated mitochondrial ROS levels following the activation of Ca^{2+}-dependent NADPH oxidase (Gatliff et al., 2017). TSPO upregulation caused by anoxia/reoxygenation injury in cardiomyocytes has been found to increase oxidative stress (Meng et al., 2020). Conversely, downregulation of TSPO expression or administration of TSPO ligands reduced cellular ROS levels and increased antioxidant capacity, limiting oxidative stress (Biswas et al., 2018; Meng et al., 2020). Similarly, decreased ROS metabolism was coupled with high levels of reduced biologically active glutathione (GSH) in TSPO-knockdown cells (Gatliff et al., 2014). In summary, despite these controversial findings, TSPO appears to play a role in redox homeostasis and can alter ROS production and influence the signalling cascade.

4.3 Involvement of TSPO in mitochondrial dynamics and mitophagy

During the evolution of mitochondria, most genetic information has been lost or transferred to the nucleus. However, mitochondria have retained their own circular genome, which codes for 13 mitochondrial proteins essential for OXPHOS (Filograna et al., 2021). The proper functioning of mitochondria depends on the quantity and quality of mtDNA. Thus, the mtDNA copy number can serve as an indicator of mitochondrial integrity and function. Changes in mtDNA copy number can affect the cellular energy supply, oxidative stress response, and overall mitochondrial health, highlighting the significance of maintaining mtDNA copy number for cellular homeostasis (Castellani et al., 2020). In accordance with the observed impaired bioenergetic status, mtDNA copy number levels were significantly reduced in TSPO-knockout cells across all analysed cell types. Consistently, human $TSPO^{-/-}$ C20 microglial cells contained significantly less mtDNA than control cells (Bader et al., 2023). In contrast, Yao et al. demonstrated that although TSPO knockdown in BV-2 microglia resulted in decreased MMP and OXPHOS, the mtDNA copy number increased, in addition to a higher amount of released mtDNA, indicating IMM damage (Yao et al., 2020).

Within the mitochondrial matrix, mtDNA molecules are packed into DNA-protein structures called mitochondrial nucleoids. Along with mtDNA, mitochondrial nucleoids contain protein machinery responsible for mtDNA packaging, replication, transcription, and repair (Rostovtseva, 2017). Nuclear-encoded mitochondrial transcription factor A (TFAM), a major

structural element of these nucleoids, serves as a key activator of both transcription and replication and plays a crucial role in regulating mtDNA copy number (Campbell et al., 2012). TFAM knockdown cell models with reduced mtDNA copy numbers showed downregulation of mitochondrial transcription, lower respiratory enzyme activity, and reduced expression of mtDNA-coded complex proteins involved in OXPHOS (Jeng et al., 2008). Accordingly, TSPO-deficient hiPSC-derived astrocytes exhibited significantly lower *levels of TFAM* transcripts. In contrast, both knockdown and overexpression of TSPO protein did not affect *TFAM* gene expression (Gatliff et al., 2014).

A reduced mtDNA copy number has been correlated with increased oxidative stress caused by elevated ROS production. Chronic exposure to ROS may initiate a vicious cycle leading to mitochondrial dysfunction and further increase in oxidative stress, contributing to the accumulation of somatic mutations and oxidative damage to mtDNA (Lee & Wei, 2005). Mei et al. demonstrated that a reduced mtDNA copy number is accompanied by increased ROS levels, which results from the reduced expression of antioxidant genes (Mei et al., 2015).

The mitochondrial genome is sensitive to oxidative damage owing to the lack of protective histones and the high rate of ROS formation in the organelle. The displacement loop (D-loop), which is involved in the regulation of mtDNA replication and transcription, is particularly susceptible to mutations, possibly due to differential and inefficient repair capacity (Mambo et al., 2003) and somatic mutations in the D-loop are linked to decreased mtDNA copy number (Lee et al., 2004). Thus, persistent oxidative stress not only contributes to mtDNA mutations but also affects the mtDNA replication rate, resulting in impaired mitochondrial respiratory function (Lee & Wei, 2005). Zhang et al. further demonstrated that mitochondrial D-loop mutations and *TFAM* gene dysfunction cause reduced mtDNA copy numbers, leading to decreased mitochondrial ETC activity, membrane potential, and ATP production (Z. Zhang et al., 2022).

Interestingly, cAMP-dependent PKA phosphorylates TFAM, which impairs DNA-binding and subsequent transcription. Under physiological conditions, only DNA-free TFAM is degraded by the Lon protease. Thus, phosphorylation and proteolysis regulate TFAM function and abundance in mitochondria, which are vital for the maintenance and expression of the mitochondrial genome. However, in cells with severe mtDNA deficits, non-phosphorylated TFAM is degraded due to the lack of DNA binding (Lu et al., 2013).

Moreover, although mitochondrial fission is coordinated with DNA replication and is essential for mtDNA distribution during mitochondrial division (Lewis et al., 2016), it is not important to maintain mitochondrial genome abundance (Ishihara et al., 2009). In contrast, fusion is critical for preserving the mtDNA copy number, coordinating high rates of mtDNA replication, and promoting mitochondrial nucleoid distribution (Silva Ramos et al., 2019). Together, the OMM fusion proteins MFN1 and MFN2 coordinately control mitochondrial respiration, structure, and

mtDNA content by regulating TFAM-mediated mtDNA copy number and preventing TFAM loss (Sidarala et al., 2022; Silva Ramos et al., 2019). Loss of the OMM and IMM fusion causes a severe imbalance in replisome protein composition, which impairs mtDNA replication activity, ultimately resulting in mtDNA depletion (Silva Ramos et al., 2019).

Consistent with these findings, TSPO-knockout hiPSC-derived astrocytes contained significantly lower *MFN1* mRNA levels than CTRL cells, whereas *OPA1 and DRP1* transcripts were unaltered. TSPO-deficient mouse glioma cells also showed a dramatic reduction in MFN1 levels and no change in DRP1 protein expression. However, the mitochondrial fission proteins MFF and FIS1 and the fusion proteins MFN2 and OPA increased due to TSPO deficiency (Fu et al., 2019). In contrast, Gatliff et al. found no differences in the expression patterns of MFN1 and MFN2 in TSPO-knockdown, TSPO-overexpressing, and control cells (Gatliff et al., 2014).

Beyond the maintenance of mtDNA replication and distribution, mitochondrial fusion and fission modulate mitochondrial network morphology. These dynamic processes allow mitochondria to adapt their size in order to effectively respond to cellular requirements. Any disruption in the balance of mitochondrial dynamics can lead to cellular and mitochondrial dysfunction (H. Chen & Chan, 2009). Although only the mitochondrial fusion gene *MFN*1 was affected in TSPO-knockout astrocytes, mitochondria devoid of TSPO protein were significantly smaller and more rounded. TSPO-silenced mitochondria from hepatocellular carcinoma cells were found to have smaller mitochondria with fewer cristae (D. Zhang et al., 2023). Similarly, TSPO knockout in mouse GL261 glioma cells resulted in mitochondrial fragmentation, whereas wild-type cells contained more fused or elongated mitochondria (Fu et al., 2019). Moreover, treatment with the specific TSPO ligand PK11195 maintained the mitochondrial ultrastructure in tumor necrosis factor (TNF)-induced inflammation, suggesting that TSPO is a scaffold protein involved in the maintenance of cristae integrity (Issop et al., 2016). In contrast, analysis of mitochondrial morphology in human SH-SY5Y and canine CF35 cells revealed a more elongated and branched mitochondrial network in TSPO-knockdown cells (Frison et al., 2021; Gatliff et al., 2017). However, TSPO-depleted mitochondria are more susceptible to severe fragmentation when exposed to parkinsonian neurotoxins (Frison et al., 2021). Moreover, disruption of fusion leads to fragmentation of the usual tubular mitochondrial network, resulting in MMP depolarisation, lower activity of respiratory enzyme complexes, reduced growth rate, and increased susceptibility to cell death (H. Chen & Chan, 2005).

Mitochondrial dynamics, biogenesis, and mitophagy are crucial processes, tightly regulated and mutually dependent, for maintaining optimal mitochondrial morphology and function. Although mitochondrial fusion is linked to an increase in mitochondrial metabolism, fission has been suggested to be necessary for mitophagy (Ma et al., 2020). Mitophagy, a selective form of autophagy, is responsible for targeted degradation and recycling of damaged mitochondria. It acts as a quality control mechanism to maintain a healthy population of functional

mitochondria within cells, eliminating mitochondria with accumulated damage, oxidative stress, or mtDNA mutations. The canonical mitophagy pathway involves the accumulation of PINK1 on depolarised mitochondria, followed by the recruitment of parkin, and subsequent ubiquitination of OMM proteins. Ubiquitin-binding autophagy receptors p62/SQSTM1 are recruited to damaged mitochondria and bridge ubiquitinated mitochondria with autophagosomal LC3, directing them to proteolysis and mitophagic digestion.

Although *PARK2* mRNA levels were significantly decreased in TSPO$^{-/-}$ hiPSC-derived astrocytes, LC3B-II protein expression, the cleaved, lipidated form of LC3B, which is tightly associated with the autophagosomal membrane and indicates the degree of autophagic activation, was upregulated in TSPO-deficient NPCs and astrocytes. Gatliff et al. proposed an inhibitory function of TSPO via VDAC1 by limiting parkin-dependent ubiquitination. TSPO, VDAC1, and parkin may collectively serve as molecular platforms for regulating the autophagosome-mediated removal of mitochondria, depending on the homeostatic expression ratio of these proteins (Gatliff et al., 2014). Thus, reduced VDAC expression caused by TSPO deficiency may lead to increased autophagy through ubiquitination and degradation of mitochondrial proteins. It has been observed that cells expressing only low levels of TSPO show upregulation of mitochondrial ubiquitination and increased mitophagy, which is reliant on the depolarisation of MMP (Gatliff et al., 2014, 2017). TSPO silencing in SH-SY5Y cells induced a significant increase in mitophagy. Treatment with the mitochondrial uncoupler FCCP, which is commonly used to activate PINK1/parkin-mediated mitophagy due to MMP depolarisation, further increased the mitophagy index. In contrast, TSPO overexpression induced a reduction of mitophagy (Frison et al., 2021). Similarly, Atg12 protein expression, a fundamental component of the autophagosome, was significantly reduced in TSPO-overexpressing transgenic ALS mice (Magrì et al., 2023). PBMCs from patients with bipolar disorder showed upregulation of the TSPO-VDAC complex along with simultaneous downregulation of the mitophagic proteins parkin, p62, and LC3 (Scaini et al., 2019). Frison et al. further demonstrated that TSPO prevents ubiquitination of mitochondria by stabilising the deubiquitinating molecule USP30, thereby suppressing the processing of mitochondrial proteins required for mitophagy (Frison et al., 2021). According to a recent study, knocking down TSPO led to an increased number of autophagosomes and autolysosomes, as indicated by increased LC3B levels, while p62 levels decreased. The authors suggested that TSPO inhibits autophagy and p62 accumulation by directly interacting with p62 (D. Zhang et al., 2023). However, TSPO-silencing in CD34^{+} blood cells led to a decrease in PINK1 protein levels, while p62 was significantly accumulated, suggesting decreased recruitment of the autophagosome membrane to mitochondria (Moras et al., 2020). Additionally, it has been shown that pro-mitophagy stimuli and MMP depolarisation cause the externalization of the IMM phospholipid cardiolipin to the mitochondrial surface (Chu et al., 2013; Kagan et al., 2016).

The autophagy protein LC3 contains cardiolipin-binding sites, which are important for the engulfment of mitochondria by the autophagic system (Chu et al., 2013). Thus, the mitochondrial depolarisation observed in the iPSC-derived TSPO-knockout model may trigger cardiolipin redistribution, which acts as an “eat-me” signal for the elimination of damaged mitochondria, further increasing the mitophagic response.

In summary, these findings indicate that mitochondrial dysfunction induced by TSPO deletion can trigger the elimination of malfunctioning mitochondria, linking TSPO function to mitochondrial dynamics, mtDNA maintenance, and mitophagy.

TSPO-knockout NPCs, astrocytes, and neurons not only displayed impaired mitochondrial function but also exhibited a significant reduction in cellular size, which was also recently reported for human TSPO-deficient and -silenced C20 microglial cells (Angeloni et al., 2023; Bader et al., 2023). Typically, cellular organelles and protein content scale isometrically with cell size. However, mitochondrial content and functional scaling are uncoupled. Thus, mitochondrial activity, i.e., MMP and OXPHOS, is highest in cells of intermediate size. This nonlinearity of mitochondrial functionality results in an optimal cell size to maximise cellular fitness and proliferation capacity (Miettinen & Björklund, 2017). It has been shown that maintaining optimal cell size and scaling of mitochondrial functions depends on the normal morphology and dynamics of the mitochondria. Moreover, the mevalonate pathway, which produces plasma membrane components including cholesterol, affects mitochondrial dynamics and functionality scaling (Miettinen & Björklund, 2016). According to a study by Mourier et al., mitofusin knockout leads to decreased protein and metabolite levels in the mevalonate pathway (Mourier et al., 2015). Given the reduced *MFN1* gene expression and apparent increased mitochondrial fragmentation observed in TSPO$^{-/-}$ cells, TSPO-deficient cells appear to lose the ability to maintain their optimal cell size. However, the involvement of impaired mevalonate metabolism requires further investigation.

4.4 Possible Role for TSPO in mitochondrial dysfunction in depression

Mitochondrial dysfunction has emerged as an important factor in the pathophysiology of major depressive disorder (MDD). Reduced bioenergetic capability, oxidative stress, and impaired mitochondrial function render cells vulnerable to stress and may contribute to the development of MDD and other psychiatric disorders (Gardner & Boles, 2011; Klinedinst & Regenold, 2015; Manji et al., 2012). Malfunctioning mitochondria-related effects are not limited to neuronal cells, but have been reported in peripheral non-neuronal cells, such as fibroblasts (Garbett et al., 2015; Kuffner et al., 2020), muscle (Gardner, 2003), PBMCs (Karabatsiakis et al., 2014) and platelets (Hroudová et al., 2013; Sjövall et al., 2013) of depressed patients, highlighting the systemic nature of mitochondrial dysfunction in MDD. Thus, the regulation of mitochondrial function is emerging as a promising therapeutic approach for CNS diseases involving

mitochondrial dysfunction (Yao et al., 2020). Moreover, the inflammatory hypothesis of MDD suggests that cytokines and other inflammatory mediators modulate the hypothalamic-pituitary-adrenal gland (HPA) stress axis, metabolism of neurotransmitters, and multiple mechanisms of neuronal plasticity at the cellular and synaptic levels (Kéri, 2021; H. Li et al., 2018b).

TSPO has been linked to anxiety and depression disorders, making it a potential diagnostic and therapeutic target. Synthetic TSPO ligands are putative markers of neuroinflammation and microglial activation and have shown promising anxiolytic and antidepressant effects with minimal side effects (Kéri, 2021; X. Li et al., 2018; Rupprecht et al., 2010). Pharmacological studies have suggested that these neuropsychiatric benefits are mediated by TSPO-induced synthesis of 3α-reduced neurosteroid hormones directly within the brain (Barron et al., 2021). Neurosteroids such as allopregnanolone act as potent allosteric modulators of $GABA_A$ receptors (Rupprecht, Pradhan, et al., 2022), and imbalances in their brain levels have been observed in individuals with anxiety and depression (Schüle et al., 2014).

Various PET studies have reported increased TSPO binding in depression (Holmes et al., 2018; H. Li et al., 2018a; Setiawan et al., 2015), thought to reflect increased microglial TSPO expression and neuroinflammation, thereby linking immune-inflammatory activation with depressive disorders (Barron et al., 2021). Recent findings suggest that increased TSPO expression in humans reflects a higher density rather than the activation of microglia (Owen, Narayan, et al., 2017). Moreover, TSPO expression is lower in MDD patients receiving antidepressant medication than in unmedicated patients (Richards et al., 2018). TSPO binding is greater in patients with chronologically advanced MDD and a long duration of untreated depression (Setiawan et al., 2018).

Few studies have used human tissues to determine the cellular expression of TSPO in neuropsychiatric disorders to support TSPO-PET findings (Nutma et al., 2021). However, an early study described reduced TSPO density in platelets of depressed patients with adult separation anxiety (Chelli et al., 2008). Interestingly, a significant decrease in the expression levels of both TSPO and the TSPO-interacting protein VDAC1 was observed in fibroblasts obtained from depressed patients after remission and pharmacological treatment. Given the fact that TSPO deficiency in hiPSC-derived neural cells was accompanied by reduced VDAC1 protein levels and led to severe mitochondrial dysfunction, altered TSPO and VDAC expression may affect mitochondrial function, neurotransmitter signalling, and neurosteroidogenesis, thereby contributing to the aetiology of MDD pathogenesis. Additionally, the impact of TSPO knockout on mitochondrial bioenergetics closely resembles mitochondrial dysfunction observed in a human cellular model of depression (Kuffner et al., 2020; Triebelhorn et al., 2022).

TSPO loss impaired cellular energy metabolism, as evidenced by altered Ca^{2+} homeostasis, reduced OXPHOS, and depolarisation of MMP, suggesting that TSPO might be a promising treatment target for psychiatric disorders. However, correlation does not imply causation, and a deeper understanding of the mechanisms behind mitochondrial function and the disruption of mitochondrial bioenergetics in MDD in relation to TSPO expression and function is needed.

4.5 Conclusion

The role and mechanisms of action of TSPO continue to be intriguing and complex areas of study. Despite extensive research, our understanding of TSPO's exact function remains incomplete. TSPO is considered a key element in cellular and mitochondrial function and dysfunction because of its regulation under various pathological conditions. Thus, TSPO has been proposed as a diagnostic imaging tool and a promising therapeutic drug target in the nervous system (El Chemali et al., 2022). Different roles have been identified, which often seem unrelated and sometimes contradictory (F. Li et al., 2016). While earlier studies often used TSPO ligands to investigate function and pharmacological impact without considering potential off-target effects, recent studies have relied on the genetic deletion of TSPO, allowing the analysis of a well-defined TSPO-deficient phenotype.

To investigate the functional importance of TSPO in the CNS, a novel TSPO-knockout model was generated in hiPSCs, which provides valuable insights into the multifaceted role of TSPO and the consequences of TSPO deficiency on mitochondrial function.

Considering the different abundance of mitochondria in each tissue, TSPO expression does not necessarily correlate with the mitochondrial content. This suggests that tissue- and cell-specific factors regulate *TSPO* gene expression and drive TSPO content rather than factors influencing mitochondrial biogenesis (Nutma et al., 2021). Moreover, TSPO may hold a highly context-dependent function, which can vary depending on the specific cellular environment (Rostovtseva, 2017). Thus, hiPSC CTRL and TSPO-KO cells were differentiated into NPCs, astrocytes, and neurons, and further characterised with respect to TSPO functionality in mitochondrial metabolism.

The comprehensive functional investigation revealed severe mitochondrial dysfunction in TSPO-deficient cells, which encompassed various mutually dependent aspects of mitochondrial biology. The reduced pregnenolone synthesis observed in TSPO-knockout astrocytes confirms TSPO's contribution to the production of neurosteroids, such as progesterone and allopregnanolone, which are important modulators of neuronal activity and neurotransmission, necessary for normal brain function. The impaired cellular and mitochondrial bioenergetics in TSPO-deficient cells indicate the importance of TSPO in sustaining the energy-producing capacity of mitochondria. Reduced OXPHOS and glycolysis suggest disruptions in the metabolic processes necessary for cellular energy supply. The

altered mitochondrial morphology and dynamics observed in TSPO$^{-/-}$ astrocytes suggest the involvement of TSPO in regulating the dynamic structural integrity and functional organisation of mitochondria, which is important for preserving mitochondrial health and functionality. Moreover, increased mitophagy and a subsequent decrease in mtDNA copy number in TSPO-KO cells indicate a disturbance in the normal turnover and maintenance of mitochondria. This suggests that TSPO may be involved in modulating the removal of damaged mitochondria, thereby contributing to mitochondrial quality control. Overall, these findings highlight the intricate effects of TSPO on maintenance of mitochondrial integrity and function.

The precise molecular mechanisms underlying the effects of TSPO and the context-dependent nature of its action remain widely elusive. However, the interaction of TSPO with other mitochondrial and cellular proteins, forming complex molecular networks that regulate various processes, appears to be crucial for its function. The exact compositions of these functional complexes remain a subject of ongoing research. VDAC is the major pore in the OMM and plays a crucial role in mitochondrial homeostasis itself. Reduced VDAC expression in TSPO-knockout cells suggests a potential interaction between TSPO and VDAC. This positive correlation may contribute to the mechanism of action of TSPO in mitochondrial physiology.

The observed decrease in TSPO and VDAC protein expression in a human cellular model of depression raises intriguing possibilities regarding the role of TSPO in MDD pathophysiology. Further research on the function of TSPO and its physiologically relevant interaction partners will contribute to a deeper understanding of its role in maintaining cellular homeostasis. Moreover, these investigations may uncover new therapeutic targets for mitochondria-related disorders.

5 References

Aerts, L., Craessaerts, K., De Strooper, B., & Morais, V. A. (2015). PINK1 Kinase Catalytic Activity Is Regulated by Phosphorylation on Serines 228 and 402. *Journal of Biological Chemistry*, *290*(5), 2798–2811. https://doi.org/10.1074/jbc.M114.620906

Aghazadeh, Y., Martinez-Arguelles, D. B., Fan, J., Culty, M., & Papadopoulos, V. (2014). Induction of Androgen Formation in the Male by a TAT-VDAC1 Fusion Peptide Blocking 14-3-3ε Protein Adaptor and Mitochondrial VDAC1 Interactions. *Molecular Therapy*, *22*(10), 1779–1791. https://doi.org/10.1038/mt.2014.116

Aghazadeh, Y., Rone, M. B., Blonder, J., Ye, X., Veenstra, T. D., Hales, D. B., Culty, M., & Papadopoulos, V. (2012). Hormone-induced 14-3-3γ Adaptor Protein Regulates Steroidogenic Acute Regulatory Protein Activity and Steroid Biosynthesis in MA-10 Leydig Cells. *Journal of Biological Chemistry*, *287*(19), 15380–15394. https://doi.org/10.1074/jbc.M112.339580

Aghazadeh, Y., Zirkin, B. R., & Papadopoulos, V. (2015). Pharmacological Regulation of the Cholesterol Transport Machinery in Steroidogenic Cells of the Testis. In *Vitamins & Hormones* (Vol. 98, pp. 189–227). Elsevier. https://doi.org/10.1016/bs.vh.2014.12.006

Aguado, F., Espinosa-Parrilla, J. F., Carmona, M. A., & Soriano, E. (2002). Neuronal Activity Regulates Correlated Network Properties of Spontaneous Calcium Transients in Astrocytes *In Situ*. *The Journal of Neuroscience*, *22*(21), 9430–9444. https://doi.org/10.1523/JNEUROSCI.22-21-09430.2002

Alberts, B. (2015). *Molecular biology of the cell* (Sixth edition). Garland Science, Taylor and Francis Group.

Ammer, L.-M., Vollmann-Zwerenz, A., Ruf, V., Wetzel, C. H., Riemenschneider, M. J., Albert, N. L., Beckhove, P., & Hau, P. (2020). The Role of Translocator Protein TSPO in Hallmarks of Glioblastoma. *Cancers*, *12*(10), 2973. https://doi.org/10.3390/cancers12102973

Angeloni, E., Germelli, L., Marchetti, L., Da Pozzo, E., Tremolanti, C., Wetzel, C. H., Baglini, E., Taliani, S., Da Settimo, F., Martini, C., & Costa, B. (2023). The human microglial surveillant phenotype is preserved by de novo neurosteroidogenesis through the control of cholesterol homeostasis: Crucial role of 18 kDa Translocator Protein. *Biochimica et Biophysica Acta (BBA) - Molecular Basis of Disease*, *1869*(6), 166751. https://doi.org/10.1016/j.bbadis.2023.166751

Anholt, R. R., De Souza, E. B., Oster-Granite, M. L., & Snyder, S. H. (1985). Peripheral-type benzodiazepine receptors: Autoradiographic localization in whole-body sections of neonatal rats. *The Journal of Pharmacology and Experimental Therapeutics*, *233*(2), 517–526.

Archer, S. L. (2013). Mitochondrial Dynamics—Mitochondrial Fission and Fusion in Human Diseases. *New England Journal of Medicine*, *369*(23), 2236–2251. https://doi.org/10.1056/NEJMra1215233

Arguello, T., Peralta, S., Antonicka, H., Gaidosh, G., Diaz, F., Tu, Y.-T., Garcia, S., Shiekhattar, R., Barrientos, A., & Moraes, C. T. (2021). ATAD3A has a scaffolding role regulating mitochondria inner membrane structure and protein assembly. *Cell Reports*, *37*(12), 110139. https://doi.org/10.1016/j.celrep.2021.110139

Arif, T., Krelin, Y., & Shoshan-Barmatz, V. (2016). Reducing VDAC1 expression induces a non-apoptotic role for pro-apoptotic proteins in cancer cell differentiation. *Biochimica et Biophysica Acta (BBA) - Bioenergetics*, *1857*(8), 1228–1242. https://doi.org/10.1016/j.bbabio.2016.04.005

Arnaud, L., Benech, P., Greetham, L., Stephan, D., Jimenez, A., Jullien, N., García-González, L., Tsvetkov, P. O., Devred, F., Sancho-Martinez, I., Izpisua Belmonte, J. C., Baranger, K., Rivera, S., & Nivet, E. (2022). APOE4 drives inflammation in human astrocytes via TAGLN3 repression and NF-κB activation. *Cell Reports*, *40*(7), 111200. https://doi.org/10.1016/j.celrep.2022.111200

Arruda, A. P., Pers, B. M., Parlakgül, G., Güney, E., Inouye, K., & Hotamisligil, G. S. (2014). Chronic enrichment of hepatic endoplasmic reticulum–mitochondria contact leads to mitochondrial dysfunction in obesity. *Nature Medicine*, *20*(12), 1427–1435. https://doi.org/10.1038/nm.3735

Ashrafi, G., & Schwarz, T. L. (2015). PINK1- and PARK2-mediated local mitophagy in distal neuronal axons. *Autophagy*, *11*(1), 187–189. https://doi.org/10.1080/15548627.2014.996021

Austin, C. J. D., Kahlert, J., Kassiou, M., & Rendina, L. M. (2013). The translocator protein (TSPO): A novel target for cancer chemotherapy. *The International Journal of Biochemistry & Cell Biology*, *45*(7), 1212–1216. https://doi.org/10.1016/j.biocel.2013.03.004

Azarashvili, T., Grachev, D., Krestinina, O., Evtodienko, Y., Yurkov, I., Papadopoulos, V., & Reiser, G. (2007). The peripheral-type benzodiazepine receptor is involved in control of Ca2+-induced permeability transition pore opening in rat brain mitochondria. *Cell Calcium*, *42*(1), 27–39. https://doi.org/10.1016/j.ceca.2006.11.004

Azarashvili, T., Krestinina, O., Baburina, Y., Odinokova, I., Grachev, D., Papadopoulos, V., Akatov, V., Lemasters, J. J., & Reiser, G. (2015). Combined effect of G3139 and TSPO ligands on Ca2+-induced permeability transition in rat brain mitochondria. *Archives of Biochemistry and Biophysics*, *587*, 70–77. https://doi.org/10.1016/j.abb.2015.10.012

Backes, S., & Herrmann, J. M. (2017). Protein Translocation into the Intermembrane Space and Matrix of Mitochondria: Mechanisms and Driving Forces. *Frontiers in Molecular Biosciences*, *4*, 83. https://doi.org/10.3389/fmolb.2017.00083

Bader, S., Wolf, L., Milenkovic, V. M., Gruber, M., Nothdurfter, C., Rupprecht, R., & Wetzel, C. H. (2019). Differential effects of TSPO ligands on mitochondrial function in mouse microglia cells. *Psychoneuroendocrinology*, *106*, 65–76. https://doi.org/10.1016/j.psyneuen.2019.03.029

Bader, S., Würfel, T., Jahner, T., Nothdurfter, C., Rupprecht, R., Milenkovic, V. M., & Wetzel, C. H. (2023). Impact of Translocator Protein 18 kDa (TSPO) Deficiency on Mitochondrial Function and the Inflammatory State of Human C20 Microglia Cells. *Cells*, *12*(6), 954. https://doi.org/10.3390/cells12060954

Bae, K.-R., Shim, H.-J., Balu, D., Kim, S. R., & Yu, S.-W. (2014). Translocator Protein 18 kDa Negatively Regulates Inflammation in Microglia. *Journal of Neuroimmune Pharmacology*, *9*(3), 424–437. https://doi.org/10.1007/s11481-014-9540-6

Bagur, R., & Hajnóczky, G. (2017). Intracellular Ca2+ Sensing: Its Role in Calcium Homeostasis and Signaling. *Molecular Cell*, *66*(6), 780–788. https://doi.org/10.1016/j.molcel.2017.05.028

Balaban, R. S., Nemoto, S., & Finkel, T. (2005). Mitochondria, Oxidants, and Aging. *Cell*, *120*(4), 483–495. https://doi.org/10.1016/j.cell.2005.02.001

Banati, R. B., Middleton, R. J., Chan, R., Hatty, C. R., Wai-Ying Kam, W., Quin, C., Graeber, M. B., Parmar, A., Zahra, D., Callaghan, P., Fok, S., Howell, N. R., Gregoire, M., Szabo, A., Pham, T., Davis, E., & Liu, G.-J. (2014). Positron emission tomography and functional characterization of a complete PBR/TSPO knockout. *Nature Communications*, *5*(1), 5452. https://doi.org/10.1038/ncomms6452

Barata, A. G., & Dick, T. P. (2020). A role for peroxiredoxins in H2O2- and MEKK-dependent activation of the p38 signaling pathway. *Redox Biology*, *28*, 101340. https://doi.org/10.1016/j.redox.2019.101340

Barbar, L., Jain, T., Zimmer, M., Kruglikov, I., Sadick, J. S., Wang, M., Kalpana, K., Rose, I. V. L., Burstein, S. R., Rusielewicz, T., Nijsure, M., Guttenplan, K. A., Di Domenico, A., Croft, G., Zhang, B., Nobuta, H., Hébert, J. M., Liddelow, S. A., & Fossati, V. (2020). CD49f Is a Novel Marker of Functional and Reactive Human iPSC-Derived Astrocytes. *Neuron*, *107*(3), 436-453.e12. https://doi.org/10.1016/j.neuron.2020.05.014

Barcelos, I. P. de, Troxell, R. M., & Graves, J. S. (2019). Mitochondrial Dysfunction and Multiple Sclerosis. *Biology*, *8*(2), 37. https://doi.org/10.3390/biology8020037

Barron, A. M., Higuchi, M., Hattori, S., Kito, S., Suhara, T., & Ji, B. (2021). Regulation of Anxiety and Depression by Mitochondrial Translocator Protein-Mediated Steroidogenesis: The Role of

Neurons. *Molecular Neurobiology*, *58*(2), 550–563. https://doi.org/10.1007/s12035-020-02136-5

Barron, A. M., Ji, B., Kito, S., Suhara, T., & Higuchi, M. (2018). Steroidogenic abnormalities in translocator protein knockout mice and significance in the aging male. *Biochemical Journal*, *475*(1), 75–85. https://doi.org/10.1042/BCJ20170645

Batarseh, A., Barlow, K. D., Martinez-Arguelles, D. B., & Papadopoulos, V. (2012). Functional characterization of the human translocator protein (18kDa) gene promoter in human breast cancer cell lines. *Biochimica et Biophysica Acta (BBA) - Gene Regulatory Mechanisms*, *1819*(1), 38–56. https://doi.org/10.1016/j.bbagrm.2011.09.001

Batarseh, A., Giatzakis, C., & Papadopoulos, V. (2008). Phorbol-12-myristate 13-acetate acting through protein kinase Cepsilon induces translocator protein (18-kDa) TSPO gene expression. *Biochemistry*, *47*(48), 12886–12899. https://doi.org/10.1021/bi8012643

Batarseh, A., Li, J., & Papadopoulos, V. (2010). Protein kinase C epsilon regulation of translocator protein (18 kDa) Tspo gene expression is mediated through a MAPK pathway targeting STAT3 and c-Jun transcription factors. *Biochemistry*, *49*(23), 4766–4778. https://doi.org/10.1021/bi100020e

Batoko, H., Veljanovski, V., & Jurkiewicz, P. (2015). Enigmatic Translocator protein (TSPO) and cellular stress regulation. *Trends in Biochemical Sciences*, *40*(9), 497–503. https://doi.org/10.1016/j.tibs.2015.07.001

Beckers, L., Ory, D., Geric, I., Declercq, L., Koole, M., Kassiou, M., Bormans, G., & Baes, M. (2018). Increased Expression of Translocator Protein (TSPO) Marks Pro-inflammatory Microglia but Does Not Predict Neurodegeneration. *Molecular Imaging and Biology*, *20*(1), 94–102. https://doi.org/10.1007/s11307-017-1099-1

Bélanger, M., Desjardins, P., Chatauret, N., Rose, C., & Butterworth, R. F. (2005). Mild hypothermia prevents brain edema and attenuates up-regulation of the astrocytic benzodiazepine receptor in experimental acute liver failure. *Journal of Hepatology*, *42*(5), 694–699. https://doi.org/10.1016/j.jhep.2004.12.029

Bender, A. S., & Norenberg, M. D. (1998). Effect of benzodiazepines and neurosteroids on ammonia-induced swelling in cultured astrocytes. *Journal of Neuroscience Research*, *54*(5), 673–680. https://doi.org/10.1002/(SICI)1097-4547(19981201)54:5<673::AID-JNR12>3.0.CO;2-P

Benischke, A.-S., Vasanth, S., Miyai, T., Katikireddy, K. R., White, T., Chen, Y., Halilovic, A., Price, M., Price, F., Liton, P. B., & Jurkunas, U. V. (2017). Activation of mitophagy leads to decline in Mfn2 and loss of mitochondrial mass in Fuchs endothelial corneal dystrophy. *Scientific Reports*, *7*(1), 6656. https://doi.org/10.1038/s41598-017-06523-2

Bergman, S. A. (1986). The benzodiazepine receptor. *Anesthesia Progress*, *33*(5), 213–219.

Berridge, M. J. (2012). Calcium signalling remodelling and disease. *Biochemical Society Transactions*, *40*(2), 297–309. https://doi.org/10.1042/BST20110766

Betlazar, C., Harrison-Brown, M., Middleton, R., Banati, R., & Liu, G.-J. (2018). Cellular Sources and Regional Variations in the Expression of the Neuroinflammatory Marker Translocator Protein (TSPO) in the Normal Brain. *International Journal of Molecular Sciences*, *19*(9), 2707. https://doi.org/10.3390/ijms19092707

Betlazar, C., Middleton, R. J., Banati, R., & Liu, G.-J. (2020). The Translocator Protein (TSPO) in Mitochondrial Bioenergetics and Immune Processes. *Cells*, *9*(2), 512. https://doi.org/10.3390/cells9020512

Betzer, C., & Jensen, P. H. (2018). Reduced Cytosolic Calcium as an Early Decisive Cellular State in Parkinson's Disease and Synucleinopathies. *Frontiers in Neuroscience*, *12*, 819. https://doi.org/10.3389/fnins.2018.00819

Biswas, L., Farhan, F., Reilly, J., Bartholomew, C., & Shu, X. (2018). TSPO Ligands Promote Cholesterol Efflux and Suppress Oxidative Stress and Inflammation in Choroidal Endothelial

Cells. *International Journal of Molecular Sciences*, *19*(12), 3740. https://doi.org/10.3390/ijms19123740

Braestrup, C., Albrechtsen, R., & Squires, R. F. (1977). High densities of benzodiazepine receptors in human cortical areas. *Nature*, *269*(5630), 702–704. https://doi.org/10.1038/269702a0

Braestrup, C., & Squires, R. F. (1977). Specific benzodiazepine receptors in rat brain characterized by high-affinity (3H)diazepam binding. *Proceedings of the National Academy of Sciences*, *74*(9), 3805–3809. https://doi.org/10.1073/pnas.74.9.3805

Brahimi-Horn, M. C., Ben-Hail, D., Ilie, M., Gounon, P., Rouleau, M., Hofman, V., Doyen, J., Mari, B., Shoshan-Barmatz, V., Hofman, P., Pouysségur, J., & Mazure, N. M. (2012). Expression of a Truncated Active Form of VDAC1 in Lung Cancer Associates with Hypoxic Cell Survival and Correlates with Progression to Chemotherapy Resistance. *Cancer Research*, *72*(8), 2140–2150. https://doi.org/10.1158/0008-5472.CAN-11-3940

Brahimi-Horn, M. C., Lacas-Gervais, S., Adaixo, R., Ilc, K., Rouleau, M., Notte, A., Dieu, M., Michiels, C., Voeltzel, T., Maguer-Satta, V., Pelletier, J., Ilie, M., Hofman, P., Manoury, B., Schmidt, A., Hiller, S., Pouysségur, J., & Mazure, N. M. (2015). Local Mitochondrial-Endolysosomal Microfusion Cleaves Voltage-Dependent Anion Channel 1 To Promote Survival in Hypoxia. *Molecular and Cellular Biology*, *35*(9), 1491–1505. https://doi.org/10.1128/MCB.01402-14

Brand, M. D., Affourtit, C., Esteves, T. C., Green, K., Lambert, A. J., Miwa, S., Pakay, J. L., & Parker, N. (2004). Mitochondrial superoxide: Production, biological effects, and activation of uncoupling proteins. *Free Radical Biology and Medicine*, *37*(6), 755–767. https://doi.org/10.1016/j.freeradbiomed.2004.05.034

Braunersreuther, V., Montecucco, F., Ashri, M., Pelli, G., Galan, K., Frias, M., Burger, F., Quinderé, A. L. G., Montessuit, C., Krause, K.-H., Mach, F., & Jaquet, V. (2013). Role of NADPH oxidase isoforms NOX1, NOX2 and NOX4 in myocardial ischemia/reperfusion injury. *Journal of Molecular and Cellular Cardiology*, *64*, 99–107. https://doi.org/10.1016/j.yjmcc.2013.09.007

Bravo-Sagua, R., Parra, V., López-Crisosto, C., Díaz, P., Quest, A. F. G., & Lavandero, S. (2017). Calcium Transport and Signaling in Mitochondria. In R. Terjung (Ed.), *Comprehensive Physiology* (1st ed., pp. 623–634). Wiley. https://doi.org/10.1002/cphy.c160013

Burté, F., Carelli, V., Chinnery, P. F., & Yu-Wai-Man, P. (2015). Disturbed mitochondrial dynamics and neurodegenerative disorders. *Nature Reviews Neurology*, *11*(1), 11–24. https://doi.org/10.1038/nrneurol.2014.228

Buttgereit, F., & Brand, M. D. (1995). A hierarchy of ATP-consuming processes in mammalian cells. *Biochemical Journal*, *312*(1), 163–167. https://doi.org/10.1042/bj3120163

Camara, A. K. S., Zhou, Y., Wen, P.-C., Tajkhorshid, E., & Kwok, W.-M. (2017). Mitochondrial VDAC1: A Key Gatekeeper as Potential Therapeutic Target. *Frontiers in Physiology*, *8*, 460. https://doi.org/10.3389/fphys.2017.00460

Campanella, M., Casswell, E., Chong, S., Farah, Z., Wieckowski, M. R., Abramov, A. Y., Tinker, A., & Duchen, M. R. (2008). Regulation of Mitochondrial Structure and Function by the F1Fo-ATPase Inhibitor Protein, IF1. *Cell Metabolism*, *8*(1), 13–25. https://doi.org/10.1016/j.cmet.2008.06.001

Campanella, M., Szabadkai, G., & Rizzuto, R. (2008). Modulation of intracellular Ca2+ signalling in HeLa cells by the apoptotic cell death enhancer PK11195. *Biochemical Pharmacology*, *76*(11), 1628–1636. https://doi.org/10.1016/j.bcp.2008.09.034

Campbell, C. T., Kolesar, J. E., & Kaufman, B. A. (2012). Mitochondrial transcription factor A regulates mitochondrial transcription initiation, DNA packaging, and genome copy number. *Biochimica et Biophysica Acta (BBA) - Gene Regulatory Mechanisms*, *1819*(9–10), 921–929. https://doi.org/10.1016/j.bbagrm.2012.03.002

Casellas, P. (2002). Peripheral benzodiazepine receptors and mitochondrial function. *Neurochemistry International*, *40*(6), 475–486. https://doi.org/10.1016/S0197-0186(01)00118-8

Castellani, C. A., Longchamps, R. J., Sun, J., Guallar, E., & Arking, D. E. (2020). Thinking outside the nucleus: Mitochondrial DNA copy number in health and disease. *Mitochondrion*, *53*, 214–223. https://doi.org/10.1016/j.mito.2020.06.004

Cerella, C., Diederich, M., & Ghibelli, L. (2010). The Dual Role of Calcium as Messenger and Stressor in Cell Damage, Death, and Survival. *International Journal of Cell Biology*, *2010*, 1–14. https://doi.org/10.1155/2010/546163

Chalatsa, I., Arvanitis, D. A., Koulakiotis, N. S., Giagini, A., Skaltsounis, A. L., Papadopoulou-Daifoti, Z., Tsarbopoulos, A., & Sanoudou, D. (2019). The Crocus sativus Compounds trans-Crocin 4 and trans-Crocetin Modulate the Amyloidogenic Pathway and Tau Misprocessing in Alzheimer Disease Neuronal Cell Culture Models. *Frontiers in Neuroscience*, *13*, 249. https://doi.org/10.3389/fnins.2019.00249

Chan, D. C. (2006). Mitochondrial Fusion and Fission in Mammals. *Annual Review of Cell and Developmental Biology*, *22*(1), 79–99. https://doi.org/10.1146/annurev.cellbio.22.010305.104638

Chan, D. C. (2012). Fusion and Fission: Interlinked Processes Critical for Mitochondrial Health. *Annual Review of Genetics*, *46*(1), 265–287. https://doi.org/10.1146/annurev-genet-110410-132529

Chandel, N. S. (2015). *Navigating metabolism*. Cold Spring Harbor Laboratory Press.

Chaudhuri, D., Artiga, D. J., Abiria, S. A., & Clapham, D. E. (2016). Mitochondrial calcium uniporter regulator 1 (MCUR1) regulates the calcium threshold for the mitochondrial permeability transition. *Proceedings of the National Academy of Sciences*, *113*(13). https://doi.org/10.1073/pnas.1602264113

Chelli, B., Pini, S., Abelli, M., Cardini, A., Lari, L., Muti, M., Gesi, C., Cassano, G. B., Lucacchini, A., & Martini, C. (2008). Platelet 18 kDa Translocator Protein density is reduced in depressed patients with adult separation anxiety. *European Neuropsychopharmacology*, *18*(4), 249–254. https://doi.org/10.1016/j.euroneuro.2007.10.003

Chen, C., Kuo, J., Wong, A., & Micevych, P. (2014). Estradiol Modulates Translocator Protein (TSPO) and Steroid Acute Regulatory Protein (StAR) via Protein Kinase A (PKA) Signaling in Hypothalamic Astrocytes. *Endocrinology*, *155*(8), 2976–2985. https://doi.org/10.1210/en.2013-1844

Chen, H., & Chan, D. C. (2005). Emerging functions of mammalian mitochondrial fusion and fission. *Human Molecular Genetics*, *14*(suppl_2), R283–R289. https://doi.org/10.1093/hmg/ddi270

Chen, H., & Chan, D. C. (2009). Mitochondrial dynamics-fusion, fission, movement, and mitophagy-in neurodegenerative diseases. *Human Molecular Genetics*, *18*(R2), R169–R176. https://doi.org/10.1093/hmg/ddp326

Chen, H., Vermulst, M., Wang, Y. E., Chomyn, A., Prolla, T. A., McCaffery, J. M., & Chan, D. C. (2010). Mitochondrial fusion is required for mtDNA stability in skeletal muscle and tolerance of mtDNA mutations. *Cell*, *141*(2), 280–289. https://doi.org/10.1016/j.cell.2010.02.026

Chen, M.-K., & Guilarte, T. R. (2008). Translocator protein 18 kDa (TSPO): Molecular sensor of brain injury and repair. *Pharmacology & Therapeutics*, *118*(1), 1–17. https://doi.org/10.1016/j.pharmthera.2007.12.004

Christensen, A., & Pike, C. J. (2018). TSPO ligand PK11195 improves Alzheimer-related outcomes in aged female 3xTg-AD mice. *Neuroscience Letters*, *683*, 7–12. https://doi.org/10.1016/j.neulet.2018.06.029

Chu, C. T., Ji, J., Dagda, R. K., Jiang, J. F., Tyurina, Y. Y., Kapralov, A. A., Tyurin, V. A., Yanamala, N., Shrivastava, I. H., Mohammadyani, D., Qiang Wang, K. Z., Zhu, J., Klein-Seetharaman, J., Balasubramanian, K., Amoscato, A. A., Borisenko, G., Huang, Z., Gusdon, A. M., Cheikhi, A., … Kagan, V. E. (2013). Cardiolipin externalization to the outer mitochondrial membrane acts as an elimination signal for mitophagy in neuronal cells. *Nature Cell Biology*, *15*(10), 1197–1205. https://doi.org/10.1038/ncb2837

Cleary, J., Johnson, K. M., Opipari, A. W., & Glick, G. D. (2007). Inhibition of the mitochondrial F1F0-ATPase by ligands of the peripheral benzodiazepine receptor. *Bioorganic & Medicinal Chemistry Letters*, *17*(6), 1667–1670. https://doi.org/10.1016/j.bmcl.2006.12.102

Coskun, P., Wyrembak, J., Schriner, S. E., Chen, H.-W., Marciniack, C., LaFerla, F., & Wallace, D. C. (2012). A mitochondrial etiology of Alzheimer and Parkinson disease. *Biochimica et Biophysica Acta (BBA) - General Subjects*, *1820*(5), 553–564. https://doi.org/10.1016/j.bbagen.2011.08.008

Costa, B., Da Pozzo, E., & Martini, C. (2018). Translocator protein and steroidogenesis. *Biochemical Journal*, *475*(5), 901–904. https://doi.org/10.1042/BCJ20170766

Costa, B., Da Pozzo, E., & Martini, C. (2020). 18-kDa translocator protein association complexes in the brain: From structure to function. *Biochemical Pharmacology*, *177*, 114015. https://doi.org/10.1016/j.bcp.2020.114015

Da Pozzo, E., Costa, B., & Martini, C. (2012). Translocator Protein (TSPO) and Neurosteroids: Implications in Psychiatric Disorders. *Current Molecular Medicine*, *12*(4), 426–442. https://doi.org/10.2174/156652412800163451

Das, S., Wong, R., Rajapakse, N., Murphy, E., & Steenbergen, C. (2008). Glycogen Synthase Kinase 3 Inhibition Slows Mitochondrial Adenine Nucleotide Transport and Regulates Voltage-Dependent Anion Channel Phosphorylation. *Circulation Research*, *103*(9), 983–991. https://doi.org/10.1161/CIRCRESAHA.108.178970

Daugherty, D. J., Selvaraj, V., Chechneva, O. V., Liu, X., Pleasure, D. E., & Deng, W. (2013). A TSPO ligand is protective in a mouse model of multiple sclerosis. *EMBO Molecular Medicine*, *5*(6), 891–903. https://doi.org/10.1002/emmm.201202124

Davies, L. P., & Huston, V. (1981). Peripheral benzodiazepine binding sites in heart and their interaction with dipyridamole. *European Journal of Pharmacology*, *73*(2–3), 209–211. https://doi.org/10.1016/0014-2999(81)90092-3

De Stefani, D., Patron, M., & Rizzuto, R. (2015). Structure and function of the mitochondrial calcium uniporter complex. *Biochimica et Biophysica Acta (BBA) - Molecular Cell Research*, *1853*(9), 2006–2011. https://doi.org/10.1016/j.bbamcr.2015.04.008

Dejos, C., Gkika, D., & Cantelmo, A. R. (2020). The Two-Way Relationship Between Calcium and Metabolism in Cancer. *Frontiers in Cell and Developmental Biology*, *8*, 573747. https://doi.org/10.3389/fcell.2020.573747

Delavoie, F., Li, H., Hardwick, M., Robert, J.-C., Giatzakis, C., Péranzi, G., Yao, Z.-X., Maccario, J., Lacapère, J.-J., & Papadopoulos, V. (2003). In Vivo and in Vitro Peripheral-Type Benzodiazepine Receptor Polymerization: Functional Significance in Drug Ligand and Cholesterol Binding. *Biochemistry*, *42*(15), 4506–4519. https://doi.org/10.1021/bi0267487

deSouza, N., Reiken, S., Ondrias, K., Yang, Y., Matkovich, S., & Marks, A. R. (2002). Protein Kinase A and Two Phosphatases Are Components of the Inositol 1,4,5-Trisphosphate Receptor Macromolecular Signaling Complex. *Journal of Biological Chemistry*, *277*(42), 39397–39400. https://doi.org/10.1074/jbc.M207059200

Diaz, F., & Moraes, C. T. (2008). Mitochondrial biogenesis and turnover. *Cell Calcium*, *44*(1), 24–35. https://doi.org/10.1016/j.ceca.2007.12.004

Di Benedetto, G., Scalzotto, E., Mongillo, M., & Pozzan, T. (2013). Mitochondrial Ca2+ Uptake Induces Cyclic AMP Generation in the Matrix and Modulates Organelle ATP Levels. *Cell Metabolism*, *17*(6), 965–975. https://doi.org/10.1016/j.cmet.2013.05.003

Do Rego, J. L., Seong, J. Y., Burel, D., Leprince, J., Luu-The, V., Tsutsui, K., Tonon, M.-C., Pelletier, G., & Vaudry, H. (2009). Neurosteroid biosynthesis: Enzymatic pathways and neuroendocrine regulation by neurotransmitters and neuropeptides. *Frontiers in Neuroendocrinology*, *30*(3), 259–301. https://doi.org/10.1016/j.yfrne.2009.05.006

Doblado, L., Lueck, C., Rey, C., Samhan-Arias, A. K., Prieto, I., Stacchiotti, A., & Monsalve, M. (2021). Mitophagy in Human Diseases. *International Journal of Molecular Sciences*, *22*(8), 3903. https://doi.org/10.3390/ijms22083903

Dong, Z., Shanmughapriya, S., Tomar, D., Siddiqui, N., Lynch, S., Nemani, N., Breves, S. L., Zhang, X., Tripathi, A., Palaniappan, P., Riitano, M. F., Worth, A. M., Seelam, A., Carvalho, E., Subbiah, R., Jaña, F., Soboloff, J., Peng, Y., Cheung, J. Y., … Madesh, M. (2017). Mitochondrial Ca2+ Uniporter Is a Mitochondrial Luminal Redox Sensor that Augments MCU Channel Activity. *Molecular Cell*, *65*(6), 1014-1028.e7. https://doi.org/10.1016/j.molcel.2017.01.032

Duchen, M. R. (2000). Mitochondria and Ca2+in cell physiology and pathophysiology. *Cell Calcium*, *28*(5–6), 339–348. https://doi.org/10.1054/ceca.2000.0170

Duvvuri, B., & Lood, C. (2021). Mitochondrial Calcification. *Immunometabolism*, *3*(1). https://doi.org/10.20900/immunometab20210008

El Chemali, L., Akwa, Y., & Massaad-Massade, L. (2022). The mitochondrial translocator protein (TSPO): A key multifunctional molecule in the nervous system. *Biochemical Journal*, *479*(13), 1455–1466. https://doi.org/10.1042/BCJ20220050

Engel, S. R., & Grant, K. A. (2001). Neurosteroids and behavior. In *International Review of Neurobiology* (Vol. 46, pp. 321–348). Elsevier. https://doi.org/10.1016/S0074-7742(01)46067-3

Evans, C. S., & Holzbaur, E. L. (2020). Degradation of engulfed mitochondria is rate-limiting in Optineurin-mediated mitophagy in neurons. *ELife*, *9*, e50260. https://doi.org/10.7554/eLife.50260

Fairley, L. H., Lai, K. O., Wong, J. H., Chong, W. J., Vincent, A. S., D'Agostino, G., Wu, X., Naik, R. R., Jayaraman, A., Langley, S. R., Ruedl, C., & Barron, A. M. (2023). Mitochondrial control of microglial phagocytosis by the translocator protein and hexokinase 2 in Alzheimer's disease. *Proceedings of the National Academy of Sciences*, *120*(8), e2209177120. https://doi.org/10.1073/pnas.2209177120

Falkenberg, M. (2018). Mitochondrial DNA replication in mammalian cells: Overview of the pathway. *Essays in Biochemistry*, *62*(3), 287–296. https://doi.org/10.1042/EBC20170100

Falkenberg, M., Larsson, N.-G., & Gustafsson, C. M. (2007). DNA Replication and Transcription in Mammalian Mitochondria. *Annual Review of Biochemistry*, *76*(1), 679–699. https://doi.org/10.1146/annurev.biochem.76.060305.152028

Fan, J., Campioli, E., Midzak, A., Culty, M., & Papadopoulos, V. (2015). Conditional steroidogenic cell-targeted deletion of TSPO unveils a crucial role in viability and hormone-dependent steroid formation. *Proceedings of the National Academy of Sciences*, *112*(23), 7261–7266. https://doi.org/10.1073/pnas.1502670112

Fan, J., & Papadopoulos, V. (2012). Transcriptional Regulation of Translocator Protein (Tspo) via a SINE B2-Mediated Natural Antisense Transcript in MA-10 Leydig Cells1. *Biology of Reproduction*, *86*(5). https://doi.org/10.1095/biolreprod.111.097535

Fan, J., Wang, K., Zirkin, B., & Papadopoulos, V. (2018). CRISPR/Cas9–Mediated Tspo Gene Mutations Lead to Reduced Mitochondrial Membrane Potential and Steroid Formation in MA-10 Mouse Tumor Leydig Cells. *Endocrinology*, *159*(2), 1130–1146. https://doi.org/10.1210/en.2017-03065

Ferramosca, A. (2020). Mitochondrial Protein Network: From Biogenesis to Bioenergetics in Health and Disease. *International Journal of Molecular Sciences*, *22*(1), 1. https://doi.org/10.3390/ijms22010001

Ferzaz, B., Brault, E., Bourliaud, G., Robert, J.-P., Poughon, G., Claustre, Y., Marguet, F., Liere, P., Schumacher, M., Nowicki, J.-P., Fournier, J., Marabout, B., Sevrin, M., George, P., Soubrie, P., Benavides, J., & Scatton, B. (2002). SSR180575 (7-Chloro- *N* , *N* ,5-trimethyl-4-oxo-3-phenyl-3,5-dihydro-4 *H* -pyridazino[4,5- *b*]indole-1-acetamide), a Peripheral Benzodiazepine Receptor Ligand, Promotes Neuronal Survival and Repair. *Journal of Pharmacology and Experimental Therapeutics*, *301*(3), 1067–1078. https://doi.org/10.1124/jpet.301.3.1067

Filograna, R., Mennuni, M., Alsina, D., & Larsson, N. (2021). Mitochondrial DNA copy number in human disease: The more the better? *FEBS Letters*, *595*(8), 976–1002. https://doi.org/10.1002/1873-3468.14021

Friedman, J. R., Lackner, L. L., West, M., DiBenedetto, J. R., Nunnari, J., & Voeltz, G. K. (2011). ER Tubules Mark Sites of Mitochondrial Division. *Science*, *334*(6054), 358–362. https://doi.org/10.1126/science.1207385

Frison, M., Faccenda, D., Abeti, R., Rigon, M., Strobbe, D., England-Rendon, B. S., Cash, D., Barnes, K., Sadeghian, M., Sajic, M., Wells, L. A., Xia, D., Giunti, P., Smith, K., Mortiboys, H., Turkheimer, F. E., & Campanella, M. (2021). The translocator protein (TSPO) is prodromal to mitophagy loss in neurotoxicity. *Molecular Psychiatry*, *26*(7), 2721–2739. https://doi.org/10.1038/s41380-021-01050-z

Frison, M., Mallach, A. K., Kennedy, E., & Campanella, M. (2017). The 18 kDa Translocator Protein (TSPO): Cholesterol Trafficking and the Biology of a Prognostic and Therapeutic Mitochondrial Target. In T. K. Rostovtseva (Ed.), *Molecular Basis for Mitochondrial Signaling* (pp. 285–315). Springer International Publishing. https://doi.org/10.1007/978-3-319-55539-3_11

Fu, Y., Wang, D., Wang, H., Cai, M., Li, C., Zhang, X., Chen, H., Hu, Y., Zhang, X., Ying, M., He, W., & Zhang, J. (2019). TSPO deficiency induces mitochondrial dysfunction, leading to hypoxia, angiogenesis, and a growth-promoting metabolic shift toward glycolysis in glioblastoma. *Neuro-Oncology*, noz183. https://doi.org/10.1093/neuonc/noz183

Garbett, K. A., Vereczkei, A., Kálmán, S., Wang, L., Korade, Ž., Shelton, R. C., & Mirnics, K. (2015). Fibroblasts from patients with major depressive disorder show distinct transcriptional response to metabolic stressors. *Translational Psychiatry*, *5*(3), e523–e523. https://doi.org/10.1038/tp.2015.14

Garcia-Segura, L. M., & Melcangi, R. C. (2006). Steroids and glial cell function. *Glia*, *54*(6), 485–498. https://doi.org/10.1002/glia.20404

Gardner, A. (2003). Alterations of mitochondrial function and correlations with personality traits in selected major depressive disorder patients. *Journal of Affective Disorders*, *76*(1–3), 55–68. https://doi.org/10.1016/S0165-0327(02)00067-8

Gardner, A., & Boles, R. G. (2011). Beyond the serotonin hypothesis: Mitochondria, inflammation and neurodegeneration in major depression and affective spectrum disorders. *Progress in Neuro-Psychopharmacology and Biological Psychiatry*, *35*(3), 730–743. https://doi.org/10.1016/j.pnpbp.2010.07.030

Garnier, M., Boujrad, N., Oke, B. O., Brown, A. S., Riond, J., Ferrara, P., Shoyab, M., Suarez-Quian, C. A., & Papadopoulos, V. (1993). Diazepam binding inhibitor is a paracrine/autocrine regulator of Leydig cell proliferation and steroidogenesis: Action via peripheral-type benzodiazepine receptor and independent mechanisms. *Endocrinology*, *132*(1), 444–458. https://doi.org/10.1210/endo.132.1.8380386

Gatliff, J., & Campanella, M. (2012). The 18 kDa Translocator Protein (TSPO): A New Perspective in Mitochondrial Biology. *Current Molecular Medicine*, *12*(4), 356–368. https://doi.org/10.2174/1566524011207040356

Gatliff, J., & Campanella, M. (2016). TSPO: Kaleidoscopic 18-kDa amid biochemical pharmacology, control and targeting of mitochondria. *Biochemical Journal*, *473*(2), 107–121. https://doi.org/10.1042/BJ20150899

Gatliff, J., East, D. A., Singh, A., Alvarez, M. S., Frison, M., Matic, I., Ferraina, C., Sampson, N., Turkheimer, F., & Campanella, M. (2017). A role for TSPO in mitochondrial Ca2+ homeostasis and redox stress signaling. *Cell Death & Disease*, *8*(6), e2896–e2896. https://doi.org/10.1038/cddis.2017.186

Gatliff, J., East, D., Crosby, J., Abeti, R., Harvey, R., Craigen, W., Parker, P., & Campanella, M. (2014). TSPO interacts with VDAC1 and triggers a ROS-mediated inhibition of mitochondrial quality control. *Autophagy*, *10*(12), 2279–2296. https://doi.org/10.4161/15548627.2014.991665

Gavioli, E. C., Duarte, F. S., Bressan, E., Ferrara, P., Farges, R. C., & De Lima, T. C. M. (2003). Antidepressant-like effect of Ro5-4864, a peripheral-type benzodiazepine receptor ligand, in forced swimming test. *European Journal of Pharmacology*, *471*(1), 21–26. https://doi.org/10.1016/S0014-2999(03)01789-8

Gavish, M., Bachman, I., Shoukrun, R., Katz, Y., Veenman, L., Weisinger, G., & Weizman, A. (1999). Enigma of the peripheral benzodiazepine receptor. *Pharmacological Reviews*, *51*(4), 629–650.

Geisler, S., Holmström, K. M., Skujat, D., Fiesel, F. C., Rothfuss, O. C., Kahle, P. J., & Springer, W. (2010). PINK1/Parkin-mediated mitophagy is dependent on VDAC1 and p62/SQSTM1. *Nature Cell Biology*, *12*(2), 119–131. https://doi.org/10.1038/ncb2012

Germelli, L., Da Pozzo, E., Giacomelli, C., Tremolanti, C., Marchetti, L., Wetzel, C. H., Barresi, E., Taliani, S., Da Settimo, F., Martini, C., & Costa, B. (2021). De novo Neurosteroidogenesis in Human Microglia: Involvement of the 18 kDa Translocator Protein. *International Journal of Molecular Sciences*, *22*(6), 3115. https://doi.org/10.3390/ijms22063115

Gherardi, G., Monticelli, H., Rizzuto, R., & Mammucari, C. (2020). The Mitochondrial Ca2+ Uptake and the Fine-Tuning of Aerobic Metabolism. *Frontiers in Physiology*, *11*, 554904. https://doi.org/10.3389/fphys.2020.554904

Giatzakis, C., Batarseh, A., Dettin, L., & Papadopoulos, V. (2007). The Role of Ets Transcription Factors in the Basal Transcription of the Translocator Protein (18 kDa). *Biochemistry*, *46*(16), 4763–4774. https://doi.org/10.1021/bi062208o

Giatzakis, C., & Papadopoulos, V. (2004). Differential Utilization of the Promoter of Peripheral-Type Benzodiazepine Receptor by Steroidogenic Versus Nonsteroidogenic Cell Lines and the Role of Sp1 and Sp3 in the Regulation of Basal Activity. *Endocrinology*, *145*(3), 1113–1123. https://doi.org/10.1210/en.2003-1330

Girard, C., Liu, S., Adams, D., Lacroix, C., Sinéus, M., Boucher, C., Papadopoulos, V., Rupprecht, R., Schumacher, M., & Groyer, G. (2012). Axonal Regeneration and Neuroinflammation: Roles for the Translocator Protein 18 kDa: TSPO as a target for neuroregeneration. *Journal of Neuroendocrinology*, *24*(1), 71–81. https://doi.org/10.1111/j.1365-2826.2011.02215.x

Goldschen-Ohm, M. P. (2022). Benzodiazepine Modulation of GABAA Receptors: A Mechanistic Perspective. *Biomolecules*, *12*(12), 1784. https://doi.org/10.3390/biom12121784

Gong, J., Szego, É. M., Leonov, A., Benito, E., Becker, S., Fischer, A., Zweckstetter, M., Outeiro, T., & Schneider, A. (2019). Translocator Protein Ligand Protects against Neurodegeneration in the MPTP Mouse Model of Parkinsonism. *The Journal of Neuroscience*, *39*(19), 3752–3769. https://doi.org/10.1523/JNEUROSCI.2070-18.2019

Gottfried-Blackmore, A., Sierra, A., Jellinck, P. H., McEwen, B. S., & Bulloch, K. (2008). Brain microglia express steroid-converting enzymes in the mouse. *The Journal of Steroid Biochemistry and Molecular Biology*, *109*(1–2), 96–107. https://doi.org/10.1016/j.jsbmb.2007.12.013

Gottschalk, B., Klec, C., Waldeck-Weiermair, M., Malli, R., & Graier, W. F. (2018). Intracellular Ca2+ release decelerates mitochondrial cristae dynamics within the junctions to the endoplasmic reticulum. *Pflügers Archiv - European Journal of Physiology*, *470*(8), 1193–1203. https://doi.org/10.1007/s00424-018-2133-0

Graham, V., Khudyakov, J., Ellis, P., & Pevny, L. (2003). SOX2 Functions to Maintain Neural Progenitor Identity. *Neuron*, *39*(5), 749–765. https://doi.org/10.1016/S0896-6273(03)00497-5

Greene, A. W., Grenier, K., Aguileta, M. A., Muise, S., Farazifard, R., Haque, M. E., McBride, H. M., Park, D. S., & Fon, E. A. (2012). Mitochondrial processing peptidase regulates PINK1 processing, import and Parkin recruitment. *EMBO Reports*, *13*(4), 378–385. https://doi.org/10.1038/embor.2012.14

Griffiths, E. J., & Rutter, G. A. (2009). Mitochondrial calcium as a key regulator of mitochondrial ATP production in mammalian cells. *Biochimica et Biophysica Acta (BBA) - Bioenergetics*, *1787*(11), 1324–1333. https://doi.org/10.1016/j.bbabio.2009.01.019

Grimm, A., Lejri, I., Hallé, F., Schmitt, M., Götz, J., Bihel, F., & Eckert, A. (2020). Mitochondria modulatory effects of new TSPO ligands in a cellular model of tauopathies. *Journal of Neuroendocrinology*, *32*(1). https://doi.org/10.1111/jne.12796

Guilarte, T. R. (2019). TSPO in diverse CNS pathologies and psychiatric disease: A critical review and a way forward. *Pharmacology & Therapeutics*, *194*, 44–58. https://doi.org/10.1016/j.pharmthera.2018.09.003

Guilarte, T. R., Loth, M. K., & Guariglia, S. R. (2016). TSPO Finds NOX2 in Microglia for Redox Homeostasis. *Trends in Pharmacological Sciences*, *37*(5), 334–343. https://doi.org/10.1016/j.tips.2016.02.008

Guo, Y., Kalathur, R. C., Liu, Q., Kloss, B., Bruni, R., Ginter, C., Kloppmann, E., Rost, B., & Hendrickson, W. A. (2015). Structure and activity of tryptophan-rich TSPO proteins. *Science*, *347*(6221), 551–555. https://doi.org/10.1126/science.aaa1534

Gureev, A. P., Shaforostova, E. A., & Popov, V. N. (2019). Regulation of Mitochondrial Biogenesis as a Way for Active Longevity: Interaction Between the Nrf2 and PGC-1α Signaling Pathways. *Frontiers in Genetics*, *10*, 435. https://doi.org/10.3389/fgene.2019.00435

Gustafsson, C. M., Falkenberg, M., & Larsson, N.-G. (2016). Maintenance and Expression of Mammalian Mitochondrial DNA. *Annual Review of Biochemistry*, *85*(1), 133–160. https://doi.org/10.1146/annurev-biochem-060815-014402

Hardie, D. G. (2018). Keeping the home fires burning: AMP-activated protein kinase. *Journal of The Royal Society Interface*, *15*(138), 20170774. https://doi.org/10.1098/rsif.2017.0774

Harvey, A. J. (2019). Mitochondria in early development: Linking the microenvironment, metabolism and the epigenome. *Reproduction*, *157*(5), R159–R179. https://doi.org/10.1530/REP-18-0431

Hauet, T., Yao, Z.-X., Bose, H. S., Wall, C. T., Han, Z., Li, W., Hales, D. B., Miller, W. L., Culty, M., & Papadopoulos, V. (2005). Peripheral-Type Benzodiazepine Receptor-Mediated Action of Steroidogenic Acute Regulatory Protein on Cholesterol Entry into Leydig Cell Mitochondria. *Molecular Endocrinology*, *19*(2), 540–554. https://doi.org/10.1210/me.2004-0307

Herst, P. M., Rowe, M. R., Carson, G. M., & Berridge, M. V. (2017). Functional Mitochondria in Health and Disease. *Frontiers in Endocrinology*, *8*, 296. https://doi.org/10.3389/fendo.2017.00296

Hirsch, J. D., Beyer, C. F., Malkowitz, L., Beer, B., & Blume, A. J. (1989). Mitochondrial benzodiazepine receptors mediate inhibition of mitochondrial respiratory control. *Molecular Pharmacology*, *35*(1), 157–163.

Hiser, C., Montgomery, B. L., & Ferguson-Miller, S. (2021). TSPO protein binding partners in bacteria, animals, and plants. *Journal of Bioenergetics and Biomembranes*, *53*(4), 463–487. https://doi.org/10.1007/s10863-021-09905-4

Holmes, S. E., Hinz, R., Conen, S., Gregory, C. J., Matthews, J. C., Anton-Rodriguez, J. M., Gerhard, A., & Talbot, P. S. (2018). Elevated Translocator Protein in Anterior Cingulate in Major Depression and a Role for Inflammation in Suicidal Thinking: A Positron Emission Tomography Study. *Biological Psychiatry*, *83*(1), 61–69. https://doi.org/10.1016/j.biopsych.2017.08.005

Holmström, K. M., & Finkel, T. (2014). Cellular mechanisms and physiological consequences of redox-dependent signalling. *Nature Reviews Molecular Cell Biology*, *15*(6), 411–421. https://doi.org/10.1038/nrm3801

Hong, S. H., Choi, H. B., Kim, S. U., & McLarnon, J. G. (2006). Mitochondrial ligand inhibits store-operated calcium influx and COX-2 production in human microglia. *Journal of Neuroscience Research*, *83*(7), 1293–1298. https://doi.org/10.1002/jnr.20829

Hopp, S. C. (2021). Targeting microglia L-type voltage-dependent calcium channels for the treatment of central nervous system disorders. *Journal of Neuroscience Research*, *99*(1), 141–162. https://doi.org/10.1002/jnr.24585

Hroudová, J., Fišar, Z., Kitzlerová, E., Zvěřová, M., & Raboch, J. (2013). Mitochondrial respiration in blood platelets of depressive patients. *Mitochondrion*, *13*(6), 795–800. https://doi.org/10.1016/j.mito.2013.05.005

Ilkan, Z., & Akar, F. G. (2018). The Mitochondrial Translocator Protein and the Emerging Link Between Oxidative Stress and Arrhythmias in the Diabetic Heart. *Frontiers in Physiology*, *9*, 1518. https://doi.org/10.3389/fphys.2018.01518

Ishihara, N., Nomura, M., Jofuku, A., Kato, H., Suzuki, S. O., Masuda, K., Otera, H., Nakanishi, Y., Nonaka, I., Goto, Y., Taguchi, N., Morinaga, H., Maeda, M., Takayanagi, R., Yokota, S., & Mihara, K. (2009). Mitochondrial fission factor Drp1 is essential for embryonic development and synapse formation in mice. *Nature Cell Biology*, *11*(8), 958–966. https://doi.org/10.1038/ncb1907

Issop, L., Ostuni, M. A., Lee, S., Laforge, M., Péranzi, G., Rustin, P., Benoist, J.-F., Estaquier, J., Papadopoulos, V., & Lacapère, J.-J. (2016). Translocator Protein-Mediated Stabilization of Mitochondrial Architecture during Inflammation Stress in Colonic Cells. *PLOS ONE*, *11*(4), e0152919. https://doi.org/10.1371/journal.pone.0152919

Itzhak, Y., Roig-Cantisano, A., Dombro, R. S., & Norenberg, M. D. (1995). Acute liver failure and hyperammonemia increase peripheral-type benzodiazepine receptor binding and pregnenolone synthesis in mouse brain. *Brain Research*, *705*(1–2), 345–348. https://doi.org/10.1016/0006-8993(95)01244-3

Jaipuria, G., Leonov, A., Giller, K., Vasa, S. K., Jaremko, Ł., Jaremko, M., Linser, R., Becker, S., & Zweckstetter, M. (2017). Cholesterol-mediated allosteric regulation of the mitochondrial translocator protein structure. *Nature Communications*, *8*(1), 14893. https://doi.org/10.1038/ncomms14893

Jaremko, Ł., Jaremko, M., Giller, K., Becker, S., & Zweckstetter, M. (2014). Structure of the Mitochondrial Translocator Protein in Complex with a Diagnostic Ligand. *Science*, *343*(6177), 1363–1366. https://doi.org/10.1126/science.1248725

Jaremko, Ł., Jaremko, M., Giller, K., Becker, S., & Zweckstetter, M. (2015). Conformational Flexibility in the Transmembrane Protein TSPO. *Chemistry – A European Journal*, *21*(46), 16555–16563. https://doi.org/10.1002/chem.201502314

Jaremko, M., Jaremko, Ł., Jaipuria, G., Becker, S., & Zweckstetter, M. (2015). Structure of the mammalian TSPO/PBR protein. *Biochemical Society Transactions*, *43*(4), 566–571. https://doi.org/10.1042/BST20150029

Jeng, J.-Y., Yeh, T.-S., Lee, J.-W., Lin, S.-H., Fong, T.-H., & Hsieh, R.-H. (2008). Maintenance of mitochondrial DNA copy number and expression are essential for preservation of mitochondrial function and cell growth. *Journal of Cellular Biochemistry*, *103*(2), 347–357. https://doi.org/10.1002/jcb.21625

Johnson, T. A., Jinnah, H. A., & Kamatani, N. (2019). Shortage of Cellular ATP as a Cause of Diseases and Strategies to Enhance ATP. *Frontiers in Pharmacology*, *10*, 98. https://doi.org/10.3389/fphar.2019.00098

Johri, A., & Beal, M. F. (2012). Mitochondrial Dysfunction in Neurodegenerative Diseases. *Journal of Pharmacology and Experimental Therapeutics*, *342*(3), 619–630. https://doi.org/10.1124/jpet.112.192138

Joo, H. K., Lee, Y. R., Kang, G., Choi, S., Kim, C.-S., Ryoo, S., Park, J. B., & Jeon, B. H. (2015). The 18-kDa Translocator Protein Inhibits Vascular Cell Adhesion Molecule-1 Expression via Inhibition of Mitochondrial Reactive Oxygen Species. *Molecules and Cells*, *38*(12), 1064–1070. https://doi.org/10.14348/molcells.2015.0165

Joo, H. K., Lee, Y. R., Lim, S. Y., Lee, E. J., Choi, S., Cho, E. J., Park, M. S., Ryoo, S., Park, J. B., & Jeon, B. H. (2012). Peripheral benzodiazepine receptor regulates vascular endothelial activations via suppression of the voltage-dependent anion channel-1. *FEBS Letters*, *586*(9), 1349–1355. https://doi.org/10.1016/j.febslet.2012.03.049

Joseph-Liauzun, E., Delmas, P., Shire, D., & Ferrara, P. (1998). Topological Analysis of the Peripheral Benzodiazepine Receptor in Yeast Mitochondrial Membranes Supports a Five-transmembrane

Structure. *Journal of Biological Chemistry*, *273*(4), 2146–2152. https://doi.org/10.1074/jbc.273.4.2146

Jurga, A. M., Paleczna, M., Kadluczka, J., & Kuter, K. Z. (2021). Beyond the GFAP-Astrocyte Protein Markers in the Brain. *Biomolecules*, *11*(9), 1361. https://doi.org/10.3390/biom11091361

Kagan, V. E., Jiang, J., Huang, Z., Tyurina, Y. Y., Desbourdes, C., Cottet-Rousselle, C., Dar, H. H., Verma, M., Tyurin, V. A., Kapralov, A. A., Cheikhi, A., Mao, G., Stolz, D., St. Croix, C. M., Watkins, S., Shen, Z., Li, Y., Greenberg, M. L., Tokarska-Schlattner, M., … Schlattner, U. (2016). NDPK-D (NM23-H4)-mediated externalization of cardiolipin enables elimination of depolarized mitochondria by mitophagy. *Cell Death & Differentiation*, *23*(7), 1140–1151. https://doi.org/10.1038/cdd.2015.160

Kamer, K. J., & Mootha, V. K. (2015). The molecular era of the mitochondrial calcium uniporter. *Nature Reviews Molecular Cell Biology*, *16*(9), 545–553. https://doi.org/10.1038/nrm4039

Kane, L. A., Lazarou, M., Fogel, A. I., Li, Y., Yamano, K., Sarraf, S. A., Banerjee, S., & Youle, R. J. (2014). PINK1 phosphorylates ubiquitin to activate Parkin E3 ubiquitin ligase activity. *Journal of Cell Biology*, *205*(2), 143–153. https://doi.org/10.1083/jcb.201402104

Karabatsiakis, A., Böck, C., Salinas-Manrique, J., Kolassa, S., Calzia, E., Dietrich, D. E., & Kolassa, I.-T. (2014). Mitochondrial respiration in peripheral blood mononuclear cells correlates with depressive subsymptoms and severity of major depression. *Translational Psychiatry*, *4*(6), e397–e397. https://doi.org/10.1038/tp.2014.44

Karlstetter, M., Nothdurfter, C., Aslanidis, A., Moeller, K., Horn, F., Scholz, R., Neumann, H., Weber, B. H. F., Rupprecht, R., & Langmann, T. (2014). Translocator protein (18 kDa) (TSPO) is expressed in reactive retinal microglia and modulates microglial inflammation and phagocytosis. *Journal of Neuroinflammation*, *11*(1), 3. https://doi.org/10.1186/1742-2094-11-3

Keil, V. C., Funke, F., Zeug, A., Schild, D., & Müller, M. (2011). Ratiometric high-resolution imaging of JC-1 fluorescence reveals the subcellular heterogeneity of astrocytic mitochondria. *Pflügers Archiv - European Journal of Physiology*, *462*(5), 693–708. https://doi.org/10.1007/s00424-011-1012-8

Kelly-Hershkovitz, E., Weizman, R., Spanier, I., Leschiner, S., Lahav, M., Weisinger, G., & Gavish, M. (1998). Effects of Peripheral-type Benzodiazepine Receptor Antisense Knockout on MA-10 Leydig Cell Proliferation and Steroidogenesis. *Journal of Biological Chemistry*, *273*(10), 5478–5483. https://doi.org/10.1074/jbc.273.10.5478

Kéri, S. (2021). Translocator protein (18 kDa TSPO) binding in depression. In *The Neuroscience of Depression* (pp. 189–196). Elsevier. https://doi.org/10.1016/B978-0-12-817935-2.00030-1

Kim, J., Wei, Y., & Sowers, J. R. (2008). Role of Mitochondrial Dysfunction in Insulin Resistance. *Circulation Research*, *102*(4), 401–414. https://doi.org/10.1161/CIRCRESAHA.107.165472

King, L., & Plun-Favreau, H. (2017). Mitophagy. In *Parkinson's Disease* (pp. 139–177). Elsevier. https://doi.org/10.1016/B978-0-12-803783-6.00005-5

Kinnally, K. W., Peixoto, P. M., Ryu, S.-Y., & Dejean, L. M. (2011). Is mPTP the gatekeeper for necrosis, apoptosis, or both? *Biochimica et Biophysica Acta (BBA) - Molecular Cell Research*, *1813*(4), 616–622. https://doi.org/10.1016/j.bbamcr.2010.09.013

Kita, A., Kohayakawa, H., Kinoshita, T., Ochi, Y., Nakamichi, K., Kurumiya, S., Furukawa, K., & Oka, M. (2004). Antianxiety and antidepressant-like effects of AC-5216, a novel mitochondrial benzodiazepine receptor ligand: Antianxiety and antidepressant effects of AC-5216. *British Journal of Pharmacology*, *142*(7), 1059–1072. https://doi.org/10.1038/sj.bjp.0705681

Klinedinst, N. J., & Regenold, W. T. (2015). A mitochondrial bioenergetic basis of depression. *Journal of Bioenergetics and Biomembranes*, *47*(1–2), 155–171. https://doi.org/10.1007/s10863-014-9584-6

Knez, J., Winckelmans, E., Plusquin, M., Thijs, L., Cauwenberghs, N., Gu, Y., Staessen, J. A., Nawrot, T. S., & Kuznetsova, T. (2016). Correlates of Peripheral Blood Mitochondrial DNA Content in a

General Population. *American Journal of Epidemiology*, *183*(2), 138–146. https://doi.org/10.1093/aje/kwv175

Koller, A., Fazzini, F., Lamina, C., Rantner, B., Kollerits, B., Stadler, M., Klein-Weigel, P., Fraedrich, G., & Kronenberg, F. (2020). Mitochondrial DNA copy number is associated with all-cause mortality and cardiovascular events in patients with peripheral arterial disease. *Journal of Internal Medicine*, *287*(5), 569–579. https://doi.org/10.1111/joim.13027

Kondapalli, C., Kazlauskaite, A., Zhang, N., Woodroof, H. I., Campbell, D. G., Gourlay, R., Burchell, L., Walden, H., Macartney, T. J., Deak, M., Knebel, A., Alessi, D. R., & Muqit, M. M. K. (2012). PINK1 is activated by mitochondrial membrane potential depolarization and stimulates Parkin E3 ligase activity by phosphorylating Serine 65. *Open Biology*, *2*(5), 120080. https://doi.org/10.1098/rsob.120080

Korkhov, V. M., Sachse, C., Short, J. M., & Tate, C. G. (2010). Three-Dimensional Structure of TspO by Electron Cryomicroscopy of Helical Crystals. *Structure*, *18*(6), 677–687. https://doi.org/10.1016/j.str.2010.03.001

Kowaltowski, A. J., de Souza-Pinto, N. C., Castilho, R. F., & Vercesi, A. E. (2009). Mitochondria and reactive oxygen species. *Free Radical Biology and Medicine*, *47*(4), 333–343. https://doi.org/10.1016/j.freeradbiomed.2009.05.004

Krestinina, O. V., Grachev, D. E., Odinokova, I. V., Reiser, G., Evtodienko, Yu. V., & Azarashvili, T. S. (2009). Effect of peripheral benzodiazepine receptor (PBR/TSPO) ligands on opening of Ca2+-induced pore and phosphorylation of 3.5-kDa polypeptide in rat brain mitochondria. *Biochemistry (Moscow)*, *74*(4), 421–429. https://doi.org/10.1134/S0006297909040105

Krueger, K. E., & Papadopoulos, V. (1990). Peripheral-type benzodiazepine receptors mediate translocation of cholesterol from outer to inner mitochondrial membranes in adrenocortical cells. *The Journal of Biological Chemistry*, *265*(25), 15015–15022.

Kuffner, K., Triebelhorn, J., Meindl, K., Benner, C., Manook, A., Sudria-Lopez, D., Siebert, R., Nothdurfter, C., Baghai, T. C., Drexler, K., Berneburg, M., Rupprecht, R., Milenkovic, V. M., & Wetzel, C. H. (2020). Major Depressive Disorder is Associated with Impaired Mitochondrial Function in Skin Fibroblasts. *Cells*, *9*(4), 884. https://doi.org/10.3390/cells9040884

Kühlbrandt, W. (2015). Structure and function of mitochondrial membrane protein complexes. *BMC Biology*, *13*(1), 89. https://doi.org/10.1186/s12915-015-0201-x

Kuznetsov, A., & Margreiter, R. (2009). Heterogeneity of Mitochondria and Mitochondrial Function within Cells as Another Level of Mitochondrial Complexity. *International Journal of Molecular Sciences*, *10*(4), 1911–1929. https://doi.org/10.3390/ijms10041911

Lacapère, J.-J., Delavoie, F., Li, H., Péranzi, G., Maccario, J., Papadopoulos, V., & Vidic, B. (2001). Structural and Functional Study of Reconstituted Peripheral Benzodiazepine Receptor. *Biochemical and Biophysical Research Communications*, *284*(2), 536–541. https://doi.org/10.1006/bbrc.2001.4975

Lacapère, J.-J., & Papadopoulos, V. (2003). Peripheral-type benzodiazepine receptor: Structure and function of a cholesterol-binding protein in steroid and bile acid biosynthesis. *Steroids*, *68*(7–8), 569–585. https://doi.org/10.1016/S0039-128X(03)00101-6

Larcher, J.-C., Vayssiere, J.-L., Le Marquer, F. J., Cordeau, L. R., Keane, P. E., Bachy, A., Gross, F., & Croizat, B. P. (1989). Effects of peripheral benzodiazepines upon the O2 consumption of neuroblastoma cells. *European Journal of Pharmacology*, *161*(2–3), 197–202. https://doi.org/10.1016/0014-2999(89)90843-1

Lavisse, S., Guillermier, M., Herard, A.-S., Petit, F., Delahaye, M., Van Camp, N., Ben Haim, L., Lebon, V., Remy, P., Dolle, F., Delzescaux, T., Bonvento, G., Hantraye, P., & Escartin, C. (2012). Reactive Astrocytes Overexpress TSPO and Are Detected by TSPO Positron Emission Tomography Imaging. *Journal of Neuroscience*, *32*(32), 10809–10818. https://doi.org/10.1523/JNEUROSCI.1487-12.2012

Lazarou, M., Sliter, D. A., Kane, L. A., Sarraf, S. A., Wang, C., Burman, J. L., Sideris, D. P., Fogel, A. I., & Youle, R. J. (2015). The ubiquitin kinase PINK1 recruits autophagy receptors to induce mitophagy. *Nature*, *524*(7565), 309–314. https://doi.org/10.1038/nature14893

Lee, H.-C., Li, S.-H., Lin, J.-C., Wu, C.-C., Yeh, D.-C., & Wei, Y.-H. (2004). Somatic mutations in the D-loop and decrease in the copy number of mitochondrial DNA in human hepatocellular carcinoma. *Mutation Research*, *547*(1–2), 71–78. https://doi.org/10.1016/j.mrfmmm.2003.12.011

Lee, H.-C., & Wei, Y.-H. (2005). Mitochondrial biogenesis and mitochondrial DNA maintenance of mammalian cells under oxidative stress. *The International Journal of Biochemistry & Cell Biology*, *37*(4), 822–834. https://doi.org/10.1016/j.biocel.2004.09.010

Lejri, I., Grimm, A., Hallé, F., Abarghaz, M., Klein, C., Maitre, M., Schmitt, M., Bourguignon, J.-J., Mensah-Nyagan, A. G., Bihel, F., & Eckert, A. (2019). TSPO Ligands Boost Mitochondrial Function and Pregnenolone Synthesis. *Journal of Alzheimer's Disease*, *72*(4), 1045–1058. https://doi.org/10.3233/JAD-190127

Leverve, X. M. (2007). Mitochondrial function and substrate availability: *Critical Care Medicine*, *35*(Suppl), S454–S460. https://doi.org/10.1097/01.CCM.0000278044.19217.73

Lewis, S. C., Uchiyama, L. F., & Nunnari, J. (2016). ER-mitochondria contacts couple mtDNA synthesis with mitochondrial division in human cells. *Science*, *353*(6296), aaf5549. https://doi.org/10.1126/science.aaf5549

Li, F., Liu, J., Liu, N., Kuhn, L. A., Garavito, R. M., & Ferguson-Miller, S. (2016). Translocator Protein 18 kDa (TSPO): An Old Protein with New Functions? *Biochemistry*, *55*(20), 2821–2831. https://doi.org/10.1021/acs.biochem.6b00142

Li, H., & Papadopoulos, V. (1998). Peripheral-Type Benzodiazepine Receptor Function in Cholesterol Transport. Identification of a Putative Cholesterol Recognition/Interaction Amino Acid Sequence and Consensus Pattern [1]. *Endocrinology*, *139*(12), 4991–4997. https://doi.org/10.1210/endo.139.12.6390

Li, H., Sagar, A. P., & Kéri, S. (2018a). Microglial markers in the frontal cortex are related to cognitive dysfunctions in major depressive disorder. *Journal of Affective Disorders*, *241*, 305–310. https://doi.org/10.1016/j.jad.2018.08.021

Li, H., Sagar, A. P., & Kéri, S. (2018b). Translocator protein (18 kDa TSPO) binding, a marker of microglia, is reduced in major depression during cognitive-behavioral therapy. *Progress in Neuro-Psychopharmacology and Biological Psychiatry*, *83*, 1–7. https://doi.org/10.1016/j.pnpbp.2017.12.011

Li, M., Ren, H., Sheth, K. N., Shi, F., & Liu, Q. (2017). A TSPO ligand attenuates brain injury after intracerebral hemorrhage. *The FASEB Journal*, *31*(8), 3278–3287. https://doi.org/10.1096/fj.201601377RR

Li, X., Liu, A., Yang, L., Zhang, K., Wu, Y., Zhao, M., & Liu, S. (2018). Antidepressant-like effects of translocator protein (18 kDa) ligand ZBD-2 in mouse models of postpartum depression. *Molecular Brain*, *11*(1), 12. https://doi.org/10.1186/s13041-018-0355-x

Liang, J., Martinez, A., Lane, J. D., Mayor, U., Clague, M. J., & Urbé, S. (2015). USP 30 deubiquitylates mitochondrial P arkin substrates and restricts apoptotic cell death. *EMBO Reports*, *16*(5), 618–627. https://doi.org/10.15252/embr.201439820

Liesa, M., Palacín, M., & Zorzano, A. (2009). Mitochondrial Dynamics in Mammalian Health and Disease. *Physiological Reviews*, *89*(3), 799–845. https://doi.org/10.1152/physrev.00030.2008

Lin, H., Xu, H., Liang, F.-Q., Liang, H., Gupta, P., Havey, A. N., Boulton, M. E., & Godley, B. F. (2011). Mitochondrial DNA Damage and Repair in RPE Associated with Aging and Age-Related Macular Degeneration. *Investigative Opthalmology & Visual Science*, *52*(6), 3521. https://doi.org/10.1167/iovs.10-6163

Lin, R., Rittenhouse, D., Sweeney, K., Potluri, P., & Wallace, D. C. (2015). TSPO, a Mitochondrial Outer Membrane Protein, Controls Ethanol-Related Behaviors in Drosophila. *PLOS Genetics*, *11*(8), e1005366. https://doi.org/10.1371/journal.pgen.1005366

Lin, Y. C., Cheung, G., Porter, E., & Papadopoulos, V. (2022). The neurosteroid pregnenolone is synthesized by a mitochondrial P450 enzyme other than CYP11A1 in human glial cells. *Journal of Biological Chemistry*, *298*(7), 102110. https://doi.org/10.1016/j.jbc.2022.102110

Liu, G.-J., Middleton, R. J., Kam, W. W.-Y., Chin, D. Y., Hatty, C. R., Chan, R. H. Y., & Banati, R. B. (2017). Functional gains in energy and cell metabolism after *TSPO* gene insertion. *Cell Cycle*, *16*(5), 436–447. https://doi.org/10.1080/15384101.2017.1281477

Liu, J., Li, H., & Papadopoulos, V. (2003). PAP7, a PBR/PKA-RIα-associated protein: A new element in the relay of the hormonal induction of steroidogenesis. *The Journal of Steroid Biochemistry and Molecular Biology*, *85*(2–5), 275–283. https://doi.org/10.1016/S0960-0760(03)00213-9

Lloyd-Evans, E., & Waller-Evans, H. (2020). Biosynthesis and signalling functions of central and peripheral nervous system neurosteroids in health and disease. *Essays in Biochemistry*, *64*(3), 591–606. https://doi.org/10.1042/EBC20200043

Lodish, H. F., Berk, A., Kaiser, C., Krieger, M., Bretscher, A., Ploegh, H. L., Martin, K. C., Yaffe, M. B., & Amon, A. (2021). *Molecular cell biology* (Ninth edition, loose-leaf student edition). Macmillan Learning.

Loth, M. K., Guariglia, S. R., Re, D. B., Perez, J., de Paiva, V. N., Dziedzic, J. L., Chambers, J. W., Azzam, D. J., & Guilarte, T. R. (2020). A Novel Interaction of Translocator Protein 18 kDa (TSPO) with NADPH Oxidase in Microglia. *Molecular Neurobiology*, *57*(11), 4467–4487. https://doi.org/10.1007/s12035-020-02042-w

Lu, B., Lee, J., Nie, X., Li, M., Morozov, Y. I., Venkatesh, S., Bogenhagen, D. F., Temiakov, D., & Suzuki, C. K. (2013). Phosphorylation of Human TFAM in Mitochondria Impairs DNA Binding and Promotes Degradation by the AAA+ Lon Protease. *Molecular Cell*, *49*(1), 121–132. https://doi.org/10.1016/j.molcel.2012.10.023

Ma, K., Chen, G., Li, W., Kepp, O., Zhu, Y., & Chen, Q. (2020). Mitophagy, Mitochondrial Homeostasis, and Cell Fate. *Frontiers in Cell and Developmental Biology*, *8*, 467. https://doi.org/10.3389/fcell.2020.00467

Magrì, A., Lipari, C. L. R., Risiglione, P., Zimbone, S., Guarino, F., Caccamo, A., & Messina, A. (2023). ERK1/2-dependent TSPO overactivation associates with the loss of mitophagy and mitochondrial respiration in ALS. *Cell Death & Disease*, *14*(2), 122. https://doi.org/10.1038/s41419-023-05643-0

Mailloux, R. J. (2018). Mitochondrial Antioxidants and the Maintenance of Cellular Hydrogen Peroxide Levels. *Oxidative Medicine and Cellular Longevity*, *2018*, 7857251. https://doi.org/10.1155/2018/7857251

Maldonado, E. N., & Lemasters, J. J. (2014). ATP/ADP ratio, the missed connection between mitochondria and the Warburg effect. *Mitochondrion*, *19*, 78–84. https://doi.org/10.1016/j.mito.2014.09.002

Maldonado, E. N., Patnaik, J., Mullins, M. R., & Lemasters, J. J. (2010). Free Tubulin Modulates Mitochondrial Membrane Potential in Cancer Cells. *Cancer Research*, *70*(24), 10192–10201. https://doi.org/10.1158/0008-5472.CAN-10-2429

Malik, A. N., & Czajka, A. (2013). Is mitochondrial DNA content a potential biomarker of mitochondrial dysfunction? *Mitochondrion*, *13*(5), 481–492. https://doi.org/10.1016/j.mito.2012.10.011

Malyala, S., Zhang, Y., Strubbe, J. O., & Bazil, J. N. (2019). Calcium phosphate precipitation inhibits mitochondrial energy metabolism. *PLOS Computational Biology*, *15*(1), e1006719. https://doi.org/10.1371/journal.pcbi.1006719

Mambo, E., Gao, X., Cohen, Y., Guo, Z., Talalay, P., & Sidransky, D. (2003). Electrophile and oxidant damage of mitochondrial DNA leading to rapid evolution of homoplasmic mutations.

Proceedings of the National Academy of Sciences, *100*(4), 1838–1843. https://doi.org/10.1073/pnas.0437910100

Mammucari, C., Gherardi, G., & Rizzuto, R. (2017). Structure, Activity Regulation, and Role of the Mitochondrial Calcium Uniporter in Health and Disease. *Frontiers in Oncology*, *7*, 139. https://doi.org/10.3389/fonc.2017.00139

Manji, H., Kato, T., Di Prospero, N. A., Ness, S., Beal, M. F., Krams, M., & Chen, G. (2012). Impaired mitochondrial function in psychiatric disorders. *Nature Reviews Neuroscience*, *13*(5), 293–307. https://doi.org/10.1038/nrn3229

Marangos, P. J., Patel, J., Boulenger, J. P., & Clark-Rosenberg, R. (1982). Characterization of peripheral-type benzodiazepine binding sites in brain using [3H]Ro 5-4864. *Molecular Pharmacology*, *22*(1), 26–32.

Marchi, S., Giorgi, C., Suski, J. M., Agnoletto, C., Bononi, A., Bonora, M., De Marchi, E., Missiroli, S., Patergnani, S., Poletti, F., Rimessi, A., Duszynski, J., Wieckowski, M. R., & Pinton, P. (2012). Mitochondria-ros crosstalk in the control of cell death and aging. *Journal of Signal Transduction*, *2012*, 329635. https://doi.org/10.1155/2012/329635

Martineau, M., Guzman, R. E., Fahlke, C., & Klingauf, J. (2017). VGLUT1 functions as a glutamate/proton exchanger with chloride channel activity in hippocampal glutamatergic synapses. *Nature Communications*, *8*(1), 2279. https://doi.org/10.1038/s41467-017-02367-6

McBride, H. M., Neuspiel, M., & Wasiak, S. (2006). Mitochondria: More Than Just a Powerhouse. *Current Biology*, *16*(14), R551–R560. https://doi.org/10.1016/j.cub.2006.06.054

McCarron, J. G., Wilson, C., Sandison, M. E., Olson, M. L., Girkin, J. M., Saunter, C., & Chalmers, S. (2013). From structure to function: Mitochondrial morphology, motion and shaping in vascular smooth muscle. *Journal of Vascular Research*, *50*(5), 357–371. https://doi.org/10.1159/000353883

McCormack, J. G., Halestrap, A. P., & Denton, R. M. (1990). Role of calcium ions in regulation of mammalian intramitochondrial metabolism. *Physiological Reviews*, *70*(2), 391–425. https://doi.org/10.1152/physrev.1990.70.2.391

Mei, H., Sun, S., Bai, Y., Chen, Y., Chai, R., & Li, H. (2015). Reduced mtDNA copy number increases the sensitivity of tumor cells to chemotherapeutic drugs. *Cell Death & Disease*, *6*(4), e1710–e1710. https://doi.org/10.1038/cddis.2015.78

Mellon, S. H., & Deschepper, C. F. (1993). Neurosteroid biosynthesis: Genes for adrenal steroidogenic enzymes are expressed in the brain. *Brain Research*, *629*(2), 283–292. https://doi.org/10.1016/0006-8993(93)91332-M

Memon, A. A., Zöller, B., Hedelius, A., Wang, X., Stenman, E., Sundquist, J., & Sundquist, K. (2017). Quantification of mitochondrial DNA copy number in suspected cancer patients by a well optimized ddPCR method. *Biomolecular Detection and Quantification*, *13*, 32–39. https://doi.org/10.1016/j.bdq.2017.08.001

Meng, Y., Tian, M., Yin, S., Lai, S., Zhou, Y., Chen, J., He, M., & Liao, Z. (2020). Downregulation of TSPO expression inhibits oxidative stress and maintains mitochondrial homeostasis in cardiomyocytes subjected to anoxia/reoxygenation injury. *Biomedicine & Pharmacotherapy*, *121*, 109588. https://doi.org/10.1016/j.biopha.2019.109588

Midzak, A., & Papadopoulos, V. (2016). Adrenal Mitochondria and Steroidogenesis: From Individual Proteins to Functional Protein Assemblies. *Frontiers in Endocrinology*, *7*. https://doi.org/10.3389/fendo.2016.00106

Midzak, A. S., Chen, H., Aon, M. A., Papadopoulos, V., & Zirkin, B. R. (2011). ATP Synthesis, Mitochondrial Function, and Steroid Biosynthesis in Rodent Primary and Tumor Leydig Cells1. *Biology of Reproduction*, *84*(5), 976–985. https://doi.org/10.1095/biolreprod.110.087460

Miettinen, T. P., & Björklund, M. (2016). Cellular Allometry of Mitochondrial Functionality Establishes the Optimal Cell Size. *Developmental Cell*, *39*(3), 370–382. https://doi.org/10.1016/j.devcel.2016.09.004

Miettinen, T. P., & Björklund, M. (2017). Mitochondrial Function and Cell Size: An Allometric Relationship. *Trends in Cell Biology*, *27*(6), 393–402. https://doi.org/10.1016/j.tcb.2017.02.006

Milenkovic, V. M., Slim, D., Bader, S., Koch, V., Heinl, E.-S., Alvarez-Carbonell, D., Nothdurfter, C., Rupprecht, R., & Wetzel, C. H. (2019). CRISPR-Cas9 Mediated TSPO Gene Knockout alters Respiration and Cellular Metabolism in Human Primary Microglia Cells. *International Journal of Molecular Sciences*, *20*(13), 3359. https://doi.org/10.3390/ijms20133359

Milenkovic, V., Rupprecht, R., & Wetzel, C. (2015). The Translocator Protein 18 kDa (TSPO) and Its Role in Mitochondrial Biology and Psychiatric Disorders. *Mini-Reviews in Medicinal Chemistry*, *15*(5), 366–372. https://doi.org/10.2174/1389557515666150324122642

Miller, W. L. (2013). Steroid hormone synthesis in mitochondria. *Molecular and Cellular Endocrinology*, *379*(1–2), 62–73. https://doi.org/10.1016/j.mce.2013.04.014

Mirończuk-Chodakowska, I., Witkowska, A. M., & Zujko, M. E. (2018). Endogenous non-enzymatic antioxidants in the human body. *Advances in Medical Sciences*, *63*(1), 68–78. https://doi.org/10.1016/j.advms.2017.05.005

Mishra, J., Jhun, B. S., Hurst, S., O-Uchi, J., Csordás, G., & Sheu, S.-S. (2017). The Mitochondrial Ca2+ Uniporter: Structure, Function, and Pharmacology. In H. Singh & S.-S. Sheu (Eds.), *Pharmacology of Mitochondria* (Vol. 240, pp. 129–156). Springer International Publishing. https://doi.org/10.1007/164_2017_1

Mishra, P., & Chan, D. C. (2016). Metabolic regulation of mitochondrial dynamics. *Journal of Cell Biology*, *212*(4), 379–387. https://doi.org/10.1083/jcb.201511036

Miyamoto, S., Murphy, A. N., & Brown, J. H. (2008). Akt mediates mitochondrial protection in cardiomyocytes through phosphorylation of mitochondrial hexokinase-II. *Cell Death & Differentiation*, *15*(3), 521–529. https://doi.org/10.1038/sj.cdd.4402285

Modesti, L., Danese, A., Angela Maria Vitto, V., Ramaccini, D., Aguiari, G., Gafà, R., Lanza, G., Giorgi, C., & Pinton, P. (2021). Mitochondrial Ca2+ Signaling in Health, Disease and Therapy. *Cells*, *10*(6), 1317. https://doi.org/10.3390/cells10061317

Moras, M., Hattab, C., Gonzalez-Menendez, P., Martino, S., Larghero, J., Le Van Kim, C., Kinet, S., Taylor, N., Lefevre, S. D., & Ostuni, M. A. (2020). Downregulation of Mitochondrial TSPO Inhibits Mitophagy and Reduces Enucleation During Human Terminal Erythropoiesis. *International Journal of Molecular Sciences*, *21*(23), 9066. https://doi.org/10.3390/ijms21239066

Morohaku, K., Pelton, S. H., Daugherty, D. J., Butler, W. R., Deng, W., & Selvaraj, V. (2014). Translocator Protein/Peripheral Benzodiazepine Receptor Is Not Required for Steroid Hormone Biosynthesis. *Endocrinology*, *155*(1), 89–97. https://doi.org/10.1210/en.2013-1556

Morohaku, K., Phuong, N. S., & Selvaraj, V. (2013). Developmental Expression of Translocator Protein/Peripheral Benzodiazepine Receptor in Reproductive Tissues. *PLoS ONE*, *8*(9), e74509. https://doi.org/10.1371/journal.pone.0074509

Mourier, A., Motori, E., Brandt, T., Lagouge, M., Atanassov, I., Galinier, A., Rappl, G., Brodesser, S., Hultenby, K., Dieterich, C., & Larsson, N.-G. (2015). Mitofusin 2 is required to maintain mitochondrial coenzyme Q levels. *Journal of Cell Biology*, *208*(4), 429–442. https://doi.org/10.1083/jcb.201411100

Mukhin, A. G., Papadopoulos, V., Costa, E., & Krueger, K. E. (1989). Mitochondrial benzodiazepine receptors regulate steroid biosynthesis. *Proceedings of the National Academy of Sciences*, *86*(24), 9813–9816. https://doi.org/10.1073/pnas.86.24.9813

Muller, F. L., Liu, Y., & Van Remmen, H. (2004). Complex III Releases Superoxide to Both Sides of the Inner Mitochondrial Membrane. *Journal of Biological Chemistry*, *279*(47), 49064–49073. https://doi.org/10.1074/jbc.M407715200

Murphy, M. P. (2009). How mitochondria produce reactive oxygen species. *Biochemical Journal*, *417*(1), 1–13. https://doi.org/10.1042/BJ20081386

Narendra, D. P., Jin, S. M., Tanaka, A., Suen, D.-F., Gautier, C. A., Shen, J., Cookson, M. R., & Youle, R. J. (2010). PINK1 is selectively stabilized on impaired mitochondria to activate Parkin. *PLoS Biology*, *8*(1), e1000298. https://doi.org/10.1371/journal.pbio.1000298

Nasrallah, C. M., & Horvath, T. L. (2014). Mitochondrial dynamics in the central regulation of metabolism. *Nature Reviews Endocrinology*, *10*(11), 650–658. https://doi.org/10.1038/nrendo.2014.160

Nimse, S. B., & Pal, D. (2015). Free radicals, natural antioxidants, and their reaction mechanisms. *RSC Advances*, *5*(35), 27986–28006. https://doi.org/10.1039/C4RA13315C

Notter, T., Schalbetter, S. M., Clifton, N. E., Mattei, D., Richetto, J., Thomas, K., Meyer, U., & Hall, J. (2021). Neuronal activity increases translocator protein (TSPO) levels. *Molecular Psychiatry*, *26*(6), 2025–2037. https://doi.org/10.1038/s41380-020-0745-1

Nunnari, J., & Suomalainen, A. (2012). Mitochondria: In sickness and in health. *Cell*, *148*(6), 1145–1159. https://doi.org/10.1016/j.cell.2012.02.035

Nutma, E., Ceyzériat, K., Amor, S., Tsartsalis, S., Millet, P., Owen, D. R., Papadopoulos, V., & Tournier, B. B. (2021). Cellular sources of TSPO expression in healthy and diseased brain. *European Journal of Nuclear Medicine and Molecular Imaging*, *49*(1), 146–163. https://doi.org/10.1007/s00259-020-05166-2

Okatsu, K., Oka, T., Iguchi, M., Imamura, K., Kosako, H., Tani, N., Kimura, M., Go, E., Koyano, F., Funayama, M., Shiba-Fukushima, K., Sato, S., Shimizu, H., Fukunaga, Y., Taniguchi, H., Komatsu, M., Hattori, N., Mihara, K., Tanaka, K., & Matsuda, N. (2012). PINK1 autophosphorylation upon membrane potential dissipation is essential for Parkin recruitment to damaged mitochondria. *Nature Communications*, *3*(1), 1016. https://doi.org/10.1038/ncomms2016

Ordureau, A., Sarraf, S. A., Duda, D. M., Heo, J.-M., Jedrychowski, M. P., Sviderskiy, V. O., Olszewski, J. L., Koerber, J. T., Xie, T., Beausoleil, S. A., Wells, J. A., Gygi, S. P., Schulman, B. A., & Harper, J. W. (2014). Quantitative Proteomics Reveal a Feedforward Mechanism for Mitochondrial PARKIN Translocation and Ubiquitin Chain Synthesis. *Molecular Cell*, *56*(3), 360–375. https://doi.org/10.1016/j.molcel.2014.09.007

Ory, D., Celen, S., Verbruggen, A., & Bormans, G. (2014). PET Radioligands for In Vivo Visualization of Neuroinflammation. *Current Pharmaceutical Design*, *20*(37), 5897–5913. https://doi.org/10.2174/1381612820666140613120212

Ostuni, M. A., Ducroc, R., Péranzi, G., Tonon, M.-C., Papadopoulos, V., & Lacapere, J.-J. (2007). Translocator protein (18 kDa) ligand PK 11195 induces transient mitochondrial Ca2+ release leading to transepithelial Cl− secretion in HT-29 human colon cancer cells. *Biology of the Cell*, *99*(11), 639–647. https://doi.org/10.1042/BC20070048

Owen, D. R., Fan, J., Campioli, E., Venugopal, S., Midzak, A., Daly, E., Harlay, A., Issop, L., Libri, V., Kalogiannopoulou, D., Oliver, E., Gallego-Colon, E., Colasanti, A., Huson, L., Rabiner, E. A., Suppiah, P., Essagian, C., Matthews, P. M., & Papadopoulos, V. (2017). TSPO mutations in rats and a human polymorphism impair the rate of steroid synthesis. *The Biochemical Journal*, *474*(23), 3985–3999. https://doi.org/10.1042/BCJ20170648

Owen, D. R., Narayan, N., Wells, L., Healy, L., Smyth, E., Rabiner, E. A., Galloway, D., Williams, J. B., Lehr, J., Mandhair, H., Peferoen, L. A., Taylor, P. C., Amor, S., Antel, J. P., Matthews, P. M., & Moore, C. S. (2017). Pro-inflammatory activation of primary microglia and macrophages increases 18 kDa translocator protein expression in rodents but not humans. *Journal of Cerebral Blood Flow & Metabolism*, *37*(8), 2679–2690. https://doi.org/10.1177/0271678X17710182

Pagliuso, A., Cossart, P., & Stavru, F. (2018). The ever-growing complexity of the mitochondrial fission machinery. *Cellular and Molecular Life Sciences*, *75*(3), 355–374. https://doi.org/10.1007/s00018-017-2603-0

Pallafacchina, G., Zanin, S., & Rizzuto, R. (2021). From the Identification to the Dissection of the Physiological Role of the Mitochondrial Calcium Uniporter: An Ongoing Story. *Biomolecules*, *11*(6), 786. https://doi.org/10.3390/biom11060786

Panda, S., Behera, S., Alam, M. F., & Syed, G. H. (2021). Endoplasmic reticulum & mitochondrial calcium homeostasis: The interplay with viruses. *Mitochondrion*, *58*, 227–242. https://doi.org/10.1016/j.mito.2021.03.008

Papadopoulos, V., Aghazadeh, Y., Fan, J., Campioli, E., Zirkin, B., & Midzak, A. (2015). Translocator protein-mediated pharmacology of cholesterol transport and steroidogenesis. *Molecular and Cellular Endocrinology*, *408*, 90–98. https://doi.org/10.1016/j.mce.2015.03.014

Papadopoulos, V., Amri, H., Boujrad, N., Cascio, C., Culty, M., Garnier, M., Hardwick, M., Li, H., Vidic, B., Brown, A. S., Reversa, J. L., Bernassau, J. M., & Drieu, K. (1997). Peripheral benzodiazepine receptor in cholesterol transport and steroidogenesis. *Steroids*, *62*(1), 21–28. https://doi.org/10.1016/S0039-128X(96)00154-7

Papadopoulos, V., Amri, H., Li, H., Boujrad, N., Vidic, B., & Garnier, M. (1997). Targeted Disruption of the Peripheral-type Benzodiazepine Receptor Gene Inhibits Steroidogenesis in the R2C Leydig Tumor Cell Line. *Journal of Biological Chemistry*, *272*(51), 32129–32135. https://doi.org/10.1074/jbc.272.51.32129

Papadopoulos, V., Baraldi, M., Guilarte, T. R., Knudsen, T. B., Lacapère, J.-J., Lindemann, P., Norenberg, M. D., Nutt, D., Weizman, A., Zhang, M.-R., & Gavish, M. (2006). Translocator protein (18kDa): New nomenclature for the peripheral-type benzodiazepine receptor based on its structure and molecular function. *Trends in Pharmacological Sciences*, *27*(8), 402–409. https://doi.org/10.1016/j.tips.2006.06.005

Papadopoulos, V., Berkovich, A., Krueger, K. E., Costa, E., & Guidotti, A. (1991). Diazepam Binding Inhibitor and Its Processing Products Stimulate Mitochondrial Steroid Biosynthesis via an Interaction with Mitochondrial Benzodiazepine Receptors *. *Endocrinology*, *129*(3), 1481–1488. https://doi.org/10.1210/endo-129-3-1481

Papadopoulos, V., Fan, J., & Zirkin, B. (2018). Translocator protein (18 kDa): An update on its function in steroidogenesis. *Journal of Neuroendocrinology*, *30*(2), e12500. https://doi.org/10.1111/jne.12500

Papadopoulos, V., & Lecanu, L. (2009). Translocator protein (18 kDa) TSPO: An emerging therapeutic target in neurotrauma. *Experimental Neurology*, *219*(1), 53–57. https://doi.org/10.1016/j.expneurol.2009.04.016

Papadopoulos, V., Mukhin, A. G., Costa, E., & Krueger, K. E. (1990). The peripheral-type benzodiazepine receptor is functionally linked to Leydig cell steroidogenesis. *The Journal of Biological Chemistry*, *265*(7), 3772–3779.

Pasdois, P., Parker, J. E., Griffiths, E. J., & Halestrap, A. P. (2011). The role of oxidized cytochrome *c* in regulating mitochondrial reactive oxygen species production and its perturbation in ischaemia. *Biochemical Journal*, *436*(2), 493–505. https://doi.org/10.1042/BJ20101957

Pastorino, J. G., Hoek, J. B., & Shulga, N. (2005). Activation of Glycogen Synthase Kinase 3β Disrupts the Binding of Hexokinase II to Mitochondria by Phosphorylating Voltage-Dependent Anion Channel and Potentiates Chemotherapy-Induced Cytotoxicity. *Cancer Research*, *65*(22), 10545–10554. https://doi.org/10.1158/0008-5472.CAN-05-1925

Pathak, T., & Trebak, M. (2018). Mitochondrial Ca2+ signaling. *Pharmacology & Therapeutics*, *192*, 112–123. https://doi.org/10.1016/j.pharmthera.2018.07.001

Patron, M., Granatiero, V., Espino, J., Rizzuto, R., & De Stefani, D. (2019). MICU3 is a tissue-specific enhancer of mitochondrial calcium uptake. *Cell Death & Differentiation*, *26*(1), 179–195. https://doi.org/10.1038/s41418-018-0113-8

Pavlov, E., Grigoriev, S. M., Dejean, L. M., Zweihorn, C. L., Mannella, C. A., & Kinnally, K. W. (2005). The mitochondrial channel VDAC has a cation-selective open state. *Biochimica et Biophysica Acta (BBA) - Bioenergetics*, *1710*(2–3), 96–102. https://doi.org/10.1016/j.bbabio.2005.09.006

Pekkurnaz, G., & Wang, X. (2022). Mitochondrial heterogeneity and homeostasis through the lens of a neuron. *Nature Metabolism*, *4*(7), 802–812. https://doi.org/10.1038/s42255-022-00594-w

Pfanner, N., Warscheid, B., & Wiedemann, N. (2019). Mitochondrial proteins: From biogenesis to functional networks. *Nature Reviews. Molecular Cell Biology*, *20*(5), 267–284. https://doi.org/10.1038/s41580-018-0092-0

Pizzo, P., & Pozzan, T. (2007). Mitochondria–endoplasmic reticulum choreography: Structure and signaling dynamics. *Trends in Cell Biology*, *17*(10), 511–517. https://doi.org/10.1016/j.tcb.2007.07.011

Pizzorno, J. (2014). Mitochondria-Fundamental to Life and Health. *Integrative Medicine (Encinitas, Calif.)*, *13*(2), 8–15.

Porcu, P., Barron, A. M., Frye, C. A., Walf, A. A., Yang, S.-Y., He, X.-Y., Morrow, A. L., Panzica, G. C., & Melcangi, R. C. (2016). Neurosteroidogenesis Today: Novel Targets for Neuroactive Steroid Synthesis and Action and Their Relevance for Translational Research. *Journal of Neuroendocrinology*, *28*(2). https://doi.org/10.1111/jne.12351

Porporato, P. E., Filigheddu, N., Pedro, J. M. B.-S., Kroemer, G., & Galluzzi, L. (2018). Mitochondrial metabolism and cancer. *Cell Research*, *28*(3), 265–280. https://doi.org/10.1038/cr.2017.155

Prange, O., Wong, T. P., Gerrow, K., Wang, Y. T., & El-Husseini, A. (2004). A balance between excitatory and inhibitory synapses is controlled by PSD-95 and neuroligin. *Proceedings of the National Academy of Sciences*, *101*(38), 13915–13920. https://doi.org/10.1073/pnas.0405939101

Quinlan, C. L., Gerencser, A. A., Treberg, J. R., & Brand, M. D. (2011). The mechanism of superoxide production by the antimycin-inhibited mitochondrial Q-cycle. *The Journal of Biological Chemistry*, *286*(36), 31361–31372. https://doi.org/10.1074/jbc.M111.267898

Ran, F. A., Hsu, P. D., Wright, J., Agarwala, V., Scott, D. A., & Zhang, F. (2013). Genome engineering using the CRISPR-Cas9 system. *Nature Protocols*, *8*(11), 2281–2308. https://doi.org/10.1038/nprot.2013.143

Rhee, S. G. (2006). H_2O_2, a Necessary Evil for Cell Signaling. *Science*, *312*(5782), 1882–1883. https://doi.org/10.1126/science.1130481

Richards, E. M., Zanotti-Fregonara, P., Fujita, M., Newman, L., Farmer, C., Ballard, E. D., Machado-Vieira, R., Yuan, P., Niciu, M. J., Lyoo, C. H., Henter, I. D., Salvadore, G., Drevets, W. C., Kolb, H., Innis, R. B., & Zarate Jr, C. A. (2018). PET radioligand binding to translocator protein (TSPO) is increased in unmedicated depressed subjects. *EJNMMI Research*, *8*(1), 57. https://doi.org/10.1186/s13550-018-0401-9

Roberts, D. J., & Miyamoto, S. (2015). Hexokinase II integrates energy metabolism and cellular protection: Akting on mitochondria and TORCing to autophagy. *Cell Death & Differentiation*, *22*(2), 248–257. https://doi.org/10.1038/cdd.2014.173

Romero-Garcia, S., & Prado-Garcia, H. (2019). Mitochondrial calcium: Transport and modulation of cellular processes in homeostasis and cancer (Review). *International Journal of Oncology*. https://doi.org/10.3892/ijo.2019.4696

Rone, M. B., Midzak, A. S., Issop, L., Rammouz, G., Jagannathan, S., Fan, J., Ye, X., Blonder, J., Veenstra, T., & Papadopoulos, V. (2012). Identification of a Dynamic Mitochondrial Protein Complex Driving Cholesterol Import, Trafficking, and Metabolism to Steroid Hormones. *Molecular Endocrinology*, *26*(11), 1868–1882. https://doi.org/10.1210/me.2012-1159

Rong, Z., Tu, P., Xu, P., Sun, Y., Yu, F., Tu, N., Guo, L., & Yang, Y. (2021). The Mitochondrial Response to DNA Damage. *Frontiers in Cell and Developmental Biology*, *9*, 669379. https://doi.org/10.3389/fcell.2021.669379

Rossier, M. (2006). T channels and steroid biosynthesis: In search of a link with mitochondria. *Cell Calcium*, *40*(2), 155–164. https://doi.org/10.1016/j.ceca.2006.04.020

Rostovtseva, T. K. (Ed.). (2017). *Molecular Basis for Mitochondrial Signaling*. Springer International Publishing. https://doi.org/10.1007/978-3-319-55539-3

Rostovtseva, T. K., & Bezrukov, S. M. (2012). VDAC inhibition by tubulin and its physiological implications. *Biochimica et Biophysica Acta (BBA) - Biomembranes*, *1818*(6), 1526–1535. https://doi.org/10.1016/j.bbamem.2011.11.004

Rostovtseva, T. K., Sheldon, K. L., Hassanzadeh, E., Monge, C., Saks, V., Bezrukov, S. M., & Sackett, D. L. (2008). Tubulin binding blocks mitochondrial voltage-dependent anion channel and regulates respiration. *Proceedings of the National Academy of Sciences*, *105*(48), 18746–18751. https://doi.org/10.1073/pnas.0806303105

Rupprecht, R., di Michele, F., Hermann, B., Ströhle, A., Lancel, M., Romeo, E., & Holsboer, F. (2001). Neuroactive steroids: Molecular mechanisms of action and implications for neuropsychopharmacology. *Brain Research Reviews*, *37*(1–3), 59–67. https://doi.org/10.1016/S0165-0173(01)00123-0

Rupprecht, R., Papadopoulos, V., Rammes, G., Baghai, T. C., Fan, J., Akula, N., Groyer, G., Adams, D., & Schumacher, M. (2010). Translocator protein (18 kDa) (TSPO) as a therapeutic target for neurological and psychiatric disorders. *Nature Reviews Drug Discovery*, *9*(12), 971–988. https://doi.org/10.1038/nrd3295

Rupprecht, R., Pradhan, A. K., Kufner, M., Brunner, L. M., Nothdurfter, C., Wein, S., Schwarzbach, J., Puig, X., Rupprecht, C., & Rammes, G. (2022). Neurosteroids and translocator protein 18 kDa (TSPO) in depression: Implications for synaptic plasticity, cognition, and treatment options. *European Archives of Psychiatry and Clinical Neuroscience*. https://doi.org/10.1007/s00406-022-01532-3

Rupprecht, R., Rammes, G., Eser, D., Baghai, T. C., Schüle, C., Nothdurfter, C., Troxler, T., Gentsch, C., Kalkman, H. O., Chaperon, F., Uzunov, V., McAllister, K. H., Bertaina-Anglade, V., La Rochelle, C. D., Tuerck, D., Floesser, A., Kiese, B., Schumacher, M., Landgraf, R., … Kucher, K. (2009). Translocator Protein (18 kD) as Target for Anxiolytics Without Benzodiazepine-Like Side Effects. *Science*, *325*(5939), 490–493. https://doi.org/10.1126/science.1175055

Rupprecht, R., Wetzel, C. H., Dorostkar, M., Herms, J., Albert, N. L., Schwarzbach, J., Schumacher, M., & Neumann, I. D. (2022). Translocator protein (18kDa) TSPO: A new diagnostic or therapeutic target for stress-related disorders? *Molecular Psychiatry*, *27*(7), 2918–2926. https://doi.org/10.1038/s41380-022-01561-3

Ryu, J. K., Choi, H. B., & McLarnon, J. G. (2005). Peripheral benzodiazepine receptor ligand PK11195 reduces microglial activation and neuronal death in quinolinic acid-injected rat striatum. *Neurobiology of Disease*, *20*(2), 550–561. https://doi.org/10.1016/j.nbd.2005.04.010

Saano, V. (1988). Central-type and peripheral-type benzodiazepine receptors. *Annals of Clinical Research*, *20*(5), 348–355.

Sanchis-Gomar, F., Garcia-Gimenez, J., Gomez-Cabrera, M., & Pallardo, F. (2014). Mitochondrial Biogenesis in Health and Disease. Molecular and Therapeutic Approaches. *Current Pharmaceutical Design*, *20*(35), 5619–5633. https://doi.org/10.2174/1381612820666140306095106

Santoro, A., Mattace Raso, G., Taliani, S., Da Pozzo, E., Simorini, F., Costa, B., Martini, C., Laneri, S., Sacchi, A., Cosimelli, B., Calignano, A., Da Settimo, F., & Meli, R. (2016). TSPO-ligands prevent oxidative damage and inflammatory response in C6 glioma cells by neurosteroid synthesis. *European Journal of Pharmaceutical Sciences*, *88*, 124–131. https://doi.org/10.1016/j.ejps.2016.04.006

Scaini, G., Barichello, T., Fries, G. R., Kennon, E. A., Andrews, T., Nix, B. R., Zunta-Soares, G., Valvassori, S. S., Soares, J. C., & Quevedo, J. (2019). TSPO upregulation in bipolar disorder and concomitant downregulation of mitophagic proteins and NLRP3 inflammasome activation. *Neuropsychopharmacology*, *44*(7), 1291–1299. https://doi.org/10.1038/s41386-018-0293-4

Scarpulla, R. C. (2006). Nuclear control of respiratory gene expression in mammalian cells. *Journal of Cellular Biochemistry*, *97*(4), 673–683. https://doi.org/10.1002/jcb.20743

Scarpulla, R. C., Vega, R. B., & Kelly, D. P. (2012). Transcriptional integration of mitochondrial biogenesis. *Trends in Endocrinology & Metabolism*, *23*(9), 459–466. https://doi.org/10.1016/j.tem.2012.06.006

Scemes, E., & Giaume, C. (2006). Astrocyte calcium waves: What they are and what they do. *Glia*, *54*(7), 716–725. https://doi.org/10.1002/glia.20374

Scherz-Shouval, R., Shvets, E., Fass, E., Shorer, H., Gil, L., & Elazar, Z. (2007). Reactive oxygen species are essential for autophagy and specifically regulate the activity of Atg4. *The EMBO Journal*, *26*(7), 1749–1760. https://doi.org/10.1038/sj.emboj.7601623

Schiaffarino, O., Valdivieso González, D., García-Pérez, I. M., Peñalva, D. A., Almendro-Vedia, V. G., Natale, P., & López-Montero, I. (2022). Mitochondrial membrane models built from native lipid extracts: Interfacial and transport properties. *Frontiers in Molecular Biosciences*, *9*, 910936. https://doi.org/10.3389/fmolb.2022.910936

Schiffer, L., Barnard, L., Baranowski, E. S., Gilligan, L. C., Taylor, A. E., Arlt, W., Shackleton, C. H. L., & Storbeck, K.-H. (2019). Human steroid biosynthesis, metabolism and excretion are differentially reflected by serum and urine steroid metabolomes: A comprehensive review. *The Journal of Steroid Biochemistry and Molecular Biology*, *194*, 105439. https://doi.org/10.1016/j.jsbmb.2019.105439

Schlattner, U., Tokarska-Schlattner, M., & Wallimann, T. (2006). Mitochondrial creatine kinase in human health and disease. *Biochimica et Biophysica Acta (BBA) - Molecular Basis of Disease*, *1762*(2), 164–180. https://doi.org/10.1016/j.bbadis.2005.09.004

Schmidt, C. A., Fisher-Wellman, K. H., & Neufer, P. D. (2021). From OCR and ECAR to energy: Perspectives on the design and interpretation of bioenergetics studies. *Journal of Biological Chemistry*, *297*(4), 101140. https://doi.org/10.1016/j.jbc.2021.101140

Scholz, R., Caramoy, A., Bhuckory, M. B., Rashid, K., Chen, M., Xu, H., Grimm, C., & Langmann, T. (2015). Targeting translocator protein (18 kDa) (TSPO) dampens pro-inflammatory microglia reactivity in the retina and protects from degeneration. *Journal of Neuroinflammation*, *12*(1), 201. https://doi.org/10.1186/s12974-015-0422-5

Schüle, C., Nothdurfter, C., & Rupprecht, R. (2014). The role of allopregnanolone in depression and anxiety. *Progress in Neurobiology*, *113*, 79–87. https://doi.org/10.1016/j.pneurobio.2013.09.003

S.D. Seneviratne, M., Faccenda, D., De Biase, V., & Campanella, M. (2012). PK11195 Inhibits Mitophagy Targeting the F1Fo-ATPsynthase in Bcl-2 Knock-Down Cells. *Current Molecular Medicine*, *12*(4), 476–482. https://doi.org/10.2174/156652412800163406

Selvaraj, V., & Stocco, D. M. (2015). The changing landscape in translocator protein (TSPO) function. *Trends in Endocrinology & Metabolism*, *26*(7), 341–348. https://doi.org/10.1016/j.tem.2015.02.007

Selvaraj, V., Stocco, D. M., & Tu, L. N. (2015). Minireview: Translocator Protein (TSPO) and Steroidogenesis: A Reappraisal. *Molecular Endocrinology*, *29*(4), 490–501. https://doi.org/10.1210/me.2015-1033

Selvaraj, V., & Tu, L. N. (2016). Current status and future perspectives: TSPO in steroid neuroendocrinology. *Journal of Endocrinology*, *231*(1), R1–R30. https://doi.org/10.1530/JOE-16-0241

Sena, L. A., & Chandel, N. S. (2012). Physiological roles of mitochondrial reactive oxygen species. *Molecular Cell*, *48*(2), 158–167. https://doi.org/10.1016/j.molcel.2012.09.025

Serasinghe, M. N., & Chipuk, J. E. (2017). Mitochondrial Fission in Human Diseases. *Handbook of Experimental Pharmacology*, *240*, 159–188. https://doi.org/10.1007/164_2016_38

Serrat, R., Oliveira-Pinto, A., Marsicano, G., & Pouvreau, S. (2022). Imaging mitochondrial calcium dynamics in the central nervous system. *Journal of Neuroscience Methods*, *373*, 109560. https://doi.org/10.1016/j.jneumeth.2022.109560

Setiawan, E., Attwells, S., Wilson, A. A., Mizrahi, R., Rusjan, P. M., Miler, L., Xu, C., Sharma, S., Kish, S., Houle, S., & Meyer, J. H. (2018). Association of translocator protein total distribution volume

with duration of untreated major depressive disorder: A cross-sectional study. *The Lancet Psychiatry*, *5*(4), 339–347. https://doi.org/10.1016/S2215-0366(18)30048-8

Setiawan, E., Wilson, A. A., Mizrahi, R., Rusjan, P. M., Miler, L., Rajkowska, G., Suridjan, I., Kennedy, J. L., Rekkas, P. V., Houle, S., & Meyer, J. H. (2015). Role of Translocator Protein Density, a Marker of Neuroinflammation, in the Brain During Major Depressive Episodes. *JAMA Psychiatry*, *72*(3), 268. https://doi.org/10.1001/jamapsychiatry.2014.2427

Shang, C., Yao, R.-M., Guo, Y., Ding, Z.-C., Sun, L.-J., Ran, Y.-H., Xue, R., Wang, H.-S., Zhang, J.-M., Zhang, Y.-Z., Zhang, L.-M., & Li, Y.-F. (2020). Translocator protein–mediated fast-onset antidepressant-like and memory-enhancing effects in chronically stressed mice. *Journal of Psychopharmacology*, *34*(4), 441–451. https://doi.org/10.1177/0269881119896304

Sheldon, K. L., Maldonado, E. N., Lemasters, J. J., Rostovtseva, T. K., & Bezrukov, S. M. (2011). Phosphorylation of Voltage-Dependent Anion Channel by Serine/Threonine Kinases Governs Its Interaction with Tubulin. *PLoS ONE*, *6*(10), e25539. https://doi.org/10.1371/journal.pone.0025539

Shoshan-Barmatz, V., N. Maldonado, E., & Krelin, Y. (2017). VDAC1 at the crossroads of cell metabolism, apoptosis and cell stress. *Cell Stress*, *1*(1), 11–36. https://doi.org/10.15698/cst2017.10.104

Shoshan-Barmatz, V., Pittala, S., & Mizrachi, D. (2019). VDAC1 and the TSPO: Expression, Interactions, and Associated Functions in Health and Disease States. *International Journal of Molecular Sciences*, *20*(13), 3348. https://doi.org/10.3390/ijms20133348

Sidarala, V., Zhu, J., Levi-D'Ancona, E., Pearson, G. L., Reck, E. C., Walker, E. M., Kaufman, B. A., & Soleimanpour, S. A. (2022). Mitofusin 1 and 2 regulation of mitochondrial DNA content is a critical determinant of glucose homeostasis. *Nature Communications*, *13*(1), 2340. https://doi.org/10.1038/s41467-022-29945-7

Šileikytė, J., Blachly-Dyson, E., Sewell, R., Carpi, A., Menabò, R., Di Lisa, F., Ricchelli, F., Bernardi, P., & Forte, M. (2014). Regulation of the Mitochondrial Permeability Transition Pore by the Outer Membrane Does Not Involve the Peripheral Benzodiazepine Receptor (Translocator Protein of 18 kDa (TSPO)). *Journal of Biological Chemistry*, *289*(20), 13769–13781. https://doi.org/10.1074/jbc.M114.549634

Silva Ramos, E., Motori, E., Brüser, C., Kühl, I., Yeroslaviz, A., Ruzzenente, B., Kauppila, J. H. K., Busch, J. D., Hultenby, K., Habermann, B. H., Jakobs, S., Larsson, N.-G., & Mourier, A. (2019). Mitochondrial fusion is required for regulation of mitochondrial DNA replication. *PLOS Genetics*, *15*(6), e1008085. https://doi.org/10.1371/journal.pgen.1008085

Simon-O'Brien, E., Gauthier, D., Riban, V., & Verleye, M. (2016). Etifoxine improves sensorimotor deficits and reduces glial activation, neuronal degeneration, and neuroinflammation in a rat model of traumatic brain injury. *Journal of Neuroinflammation*, *13*(1), 203. https://doi.org/10.1186/s12974-016-0687-3

Simula, L., Nazio, F., & Campello, S. (2017). The mitochondrial dynamics in cancer and immune-surveillance. *Seminars in Cancer Biology*, *47*, 29–42. https://doi.org/10.1016/j.semcancer.2017.06.007

Sjövall, F., Ehinger, J. K. H., Marelsson, S. E., Morota, S., Åsander Frostner, E., Uchino, H., Lundgren, J., Arnbjörnsson, E., Hansson, M. J., Fellman, V., & Elmér, E. (2013). Mitochondrial respiration in human viable platelets—Methodology and influence of gender, age and storage. *Mitochondrion*, *13*(1), 7–14. https://doi.org/10.1016/j.mito.2012.11.001

Smith, A. L. M., Whitehall, J. C., & Greaves, L. C. (2022). Mitochondrial DNA mutations in ageing and cancer. *Molecular Oncology*, *16*(18), 3276–3294. https://doi.org/10.1002/1878-0261.13291

Smith, R. A. J., Hartley, R. C., Cochemé, H. M., & Murphy, M. P. (2012). Mitochondrial pharmacology. *Trends in Pharmacological Sciences*, *33*(6), 341–352. https://doi.org/10.1016/j.tips.2012.03.010

Soustiel, J. F., Zaaroor, M., Vlodavsky, E., Veenman, L., Weizman, A., & Gavish, M. (2008). Neuroprotective effect of Ro5-4864 following brain injury. *Experimental Neurology*, *214*(2), 201–208. https://doi.org/10.1016/j.expneurol.2008.08.008

Spinelli, J. B., & Haigis, M. C. (2018). The multifaceted contributions of mitochondria to cellular metabolism. *Nature Cell Biology*, *20*(7), 745–754. https://doi.org/10.1038/s41556-018-0124-1

Srivastava, S. (2017). The Mitochondrial Basis of Aging and Age-Related Disorders. *Genes*, *8*(12), 398. https://doi.org/10.3390/genes8120398

Stanga, S., Caretto, A., Boido, M., & Vercelli, A. (2020). Mitochondrial Dysfunctions: A Red Thread across Neurodegenerative Diseases. *International Journal of Molecular Sciences*, *21*(10), 3719. https://doi.org/10.3390/ijms21103719

Steinlechner-Maran, R., Eberl, T., Kunc, M., Schr??cksnadel, H., Margreiter, R., & Gnaiger, E. (1997). RESPIRATORY DEFECT AS AN EARLY EVENT IN PRESERVATION-REOXYGENATION INJURY OF ENDOTHELIAL CELLS1: *Transplantation*, *63*(1), 136–142. https://doi.org/10.1097/00007890-199701150-00025

St-Pierre, J., Drori, S., Uldry, M., Silvaggi, J. M., Rhee, J., Jäger, S., Handschin, C., Zheng, K., Lin, J., Yang, W., Simon, D. K., Bachoo, R., & Spiegelman, B. M. (2006). Suppression of Reactive Oxygen Species and Neurodegeneration by the PGC-1 Transcriptional Coactivators. *Cell*, *127*(2), 397–408. https://doi.org/10.1016/j.cell.2006.09.024

Szymański, J., Janikiewicz, J., Michalska, B., Patalas-Krawczyk, P., Perrone, M., Ziółkowski, W., Duszyński, J., Pinton, P., Dobrzyń, A., & Więckowski, M. (2017). Interaction of Mitochondria with the Endoplasmic Reticulum and Plasma Membrane in Calcium Homeostasis, Lipid Trafficking and Mitochondrial Structure. *International Journal of Molecular Sciences*, *18*(7), 1576. https://doi.org/10.3390/ijms18071576

Tada, M., Takeuchi, A., Hashizume, M., Kitamura, K., & Kano, M. (2014). A highly sensitive fluorescent indicator dye for calcium imaging of neural activity *in vitro* and *in vivo*. *European Journal of Neuroscience*, *39*(11), 1720–1728. https://doi.org/10.1111/ejn.12476

Takeuchi, A., Kim, B., & Matsuoka, S. (2015). The destiny of Ca2+ released by mitochondria. *The Journal of Physiological Sciences*, *65*(1), 11–24. https://doi.org/10.1007/s12576-014-0326-7

Tamse, C. T., Lu, X., Mortel, E. G., Cabrales, E., Feng, W., & Schaefer, S. (2008). The peripheral benzodiazepine receptor modulates Ca2+ transport through the VDAC in rat heart mitochondria. *J Clin Basic Cardiol*, *11*(1–4), 24–29.

Tanaka, A., Cleland, M. M., Xu, S., Narendra, D. P., Suen, D.-F., Karbowski, M., & Youle, R. J. (2010). Proteasome and p97 mediate mitophagy and degradation of mitofusins induced by Parkin. *Journal of Cell Biology*, *191*(7), 1367–1380. https://doi.org/10.1083/jcb.201007013

Tang, M. Y., Vranas, M., Krahn, A. I., Pundlik, S., Trempe, J.-F., & Fon, E. A. (2017). Structure-guided mutagenesis reveals a hierarchical mechanism of Parkin activation. *Nature Communications*, *8*(1), 14697. https://doi.org/10.1038/ncomms14697

Tcw, J., Wang, M., Pimenova, A. A., Bowles, K. R., Hartley, B. J., Lacin, E., Machlovi, S. I., Abdelaal, R., Karch, C. M., Phatnani, H., Slesinger, P. A., Zhang, B., Goate, A. M., & Brennand, K. J. (2017). An Efficient Platform for Astrocyte Differentiation from Human Induced Pluripotent Stem Cells. *Stem Cell Reports*, *9*(2), 600–614. https://doi.org/10.1016/j.stemcr.2017.06.018

Tikunov, A., Johnson, C. B., Pediaditakis, P., Markevich, N., Macdonald, J. M., Lemasters, J. J., & Holmuhamedov, E. (2010). Closure of VDAC causes oxidative stress and accelerates the Ca2+-induced mitochondrial permeability transition in rat liver mitochondria. *Archives of Biochemistry and Biophysics*, *495*(2), 174–181. https://doi.org/10.1016/j.abb.2010.01.008

Trewin, A. J., Berry, B. J., & Wojtovich, A. P. (2018). Exercise and Mitochondrial Dynamics: Keeping in Shape with ROS and AMPK. *Antioxidants (Basel, Switzerland)*, *7*(1), 7. https://doi.org/10.3390/antiox7010007

Triebelhorn, J., Cardon, I., Kuffner, K., Bader, S., Jahner, T., Meindl, K., Rothhammer-Hampl, T., Riemenschneider, M. J., Drexler, K., Berneburg, M., Nothdurfter, C., Manook, A., Brochhausen,

C., Baghai, T. C., Hilbert, S., Rupprecht, R., Milenkovic, V. M., & Wetzel, C. H. (2022). Induced neural progenitor cells and iPS-neurons from major depressive disorder patients show altered bioenergetics and electrophysiological properties. *Molecular Psychiatry*. https://doi.org/10.1038/s41380-022-01660-1

Tu, L. N., Morohaku, K., Manna, P. R., Pelton, S. H., Butler, W. R., Stocco, D. M., & Selvaraj, V. (2014). Peripheral Benzodiazepine Receptor/Translocator Protein Global Knock-out Mice Are Viable with No Effects on Steroid Hormone Biosynthesis. *Journal of Biological Chemistry*, *289*(40), 27444–27454. https://doi.org/10.1074/jbc.M114.578286

Tu, L. N., Zhao, A. H., Hussein, M., Stocco, D. M., & Selvaraj, V. (2016). Translocator Protein (TSPO) Affects Mitochondrial Fatty Acid Oxidation in Steroidogenic Cells. *Endocrinology*, *157*(3), 1110–1121. https://doi.org/10.1210/en.2015-1795

Uddin, L. Q. (2020). Bring the Noise: Reconceptualizing Spontaneous Neural Activity. *Trends in Cognitive Sciences*, *24*(9), 734–746. https://doi.org/10.1016/j.tics.2020.06.003

Ureshino, Erustes, Bassani, Wachilewski, Guarache, Nascimento, Costa, Smaili, & Pereira. (2019). The Interplay between Ca2+ Signaling Pathways and Neurodegeneration. *International Journal of Molecular Sciences*, *20*(23), 6004. https://doi.org/10.3390/ijms20236004

Veenman, L., Alten, J., Linnemannstöns, K., Shandalov, Y., Zeno, S., Lakomek, M., Gavish, M., & Kugler, W. (2010). Potential involvement of F0F1-ATP(synth)ase and reactive oxygen species in apoptosis induction by the antineoplastic agent erucylphosphohomocholine in glioblastoma cell lines: A mechanism for induction of apoptosis via the 18 kDa mitochondrial translocator protein. *Apoptosis*, *15*(7), 753–768. https://doi.org/10.1007/s10495-010-0460-5

Veenman, L., Vainshtein, A., Yasin, N., Azrad, M., & Gavish, M. (2016). Tetrapyrroles as Endogenous TSPO Ligands in Eukaryotes and Prokaryotes: Comparisons with Synthetic Ligands. *International Journal of Molecular Sciences*, *17*(6), 880. https://doi.org/10.3390/ijms17060880

Veenman, Vassilios Papadopoulos, & Moshe Gavish. (2007). Channel-Like Functions of the 18-kDa Translocator Protein (TSPO): Regulation of Apoptosis and Steroidogenesis as Part of the Host-Defense Response. *Current Pharmaceutical Design*, *13*(23), 2385–2405. https://doi.org/10.2174/138161207781368710

Veiga, S., Azcoitia, I., & Garcia-Segura, L. M. (2005). Ro5-4864, a peripheral benzodiazepine receptor ligand, reduces reactive gliosis and protects hippocampal hilar neurons from kainic acid excitotoxicity. *Journal of Neuroscience Research*, *80*(1), 129–137. https://doi.org/10.1002/jnr.20430

Verkhratsky, A., Zorec, R., & Parpura, V. (2017). Stratification of astrocytes in healthy and diseased brain. *Brain Pathology (Zurich, Switzerland)*, *27*(5), 629–644. https://doi.org/10.1111/bpa.12537

Vicente, B., Saldivia, S., Hormazabal, N., Bustos, C., & Rubí, P. (2020). Etifoxine is non-inferior than clonazepam for reduction of anxiety symptoms in the treatment of anxiety disorders: A randomized, double blind, non-inferiority trial. *Psychopharmacology*, *237*(11), 3357–3367. https://doi.org/10.1007/s00213-020-05617-6

Volterra, A., Liaudet, N., & Savtchouk, I. (2014). Astrocyte Ca2+ signalling: An unexpected complexity. *Nature Reviews Neuroscience*, *15*(5), 327–335. https://doi.org/10.1038/nrn3725

Vyas, S., Zaganjor, E., & Haigis, M. C. (2016). Mitochondria and Cancer. *Cell*, *166*(3), 555–566. https://doi.org/10.1016/j.cell.2016.07.002

Wacquier, B., Combettes, L., & Dupont, G. (2020). Dual dynamics of mitochondrial permeability transition pore opening. *Scientific Reports*, *10*(1), 3924. https://doi.org/10.1038/s41598-020-60177-1

Wang, X., Winter, D., Ashrafi, G., Schlehe, J., Wong, Y. L., Selkoe, D., Rice, S., Steen, J., LaVoie, M. J., & Schwarz, T. L. (2011). PINK1 and Parkin target Miro for phosphorylation and degradation to arrest mitochondrial motility. *Cell*, *147*(4), 893–906. https://doi.org/10.1016/j.cell.2011.10.018

Wauer, T., Simicek, M., Schubert, A., & Komander, D. (2015). Mechanism of phospho-ubiquitin-induced PARKIN activation. *Nature*, *524*(7565), 370–374. https://doi.org/10.1038/nature14879

Weisthal, S., Keinan, N., Ben-Hail, D., Arif, T., & Shoshan-Barmatz, V. (2014). Ca2+-mediated regulation of VDAC1 expression levels is associated with cell death induction. *Biochimica et Biophysica Acta (BBA) - Molecular Cell Research*, *1843*(10), 2270–2281. https://doi.org/10.1016/j.bbamcr.2014.03.021

Werry, E. L., Bright, F. M., Piguet, O., Ittner, L. M., Halliday, G. M., Hodges, J. R., Kiernan, M. C., Loy, C. T., Kril, J. J., & Kassiou, M. (2019). Recent Developments in TSPO PET Imaging as A Biomarker of Neuroinflammation in Neurodegenerative Disorders. *International Journal of Molecular Sciences*, *20*(13), 3161. https://doi.org/10.3390/ijms20133161

West, A. P., Shadel, G. S., & Ghosh, S. (2011). Mitochondria in innate immune responses. *Nature Reviews Immunology*, *11*(6), 389–402. https://doi.org/10.1038/nri2975

Westermann, B. (2010). Mitochondrial fusion and fission in cell life and death. *Nature Reviews Molecular Cell Biology*, *11*(12), 872–884. https://doi.org/10.1038/nrm3013

Westermann, B. (2012). Bioenergetic role of mitochondrial fusion and fission. *Biochimica et Biophysica Acta (BBA) - Bioenergetics*, *1817*(10), 1833–1838. https://doi.org/10.1016/j.bbabio.2012.02.033

Wolf, A., Herb, M., Schramm, M., & Langmann, T. (2020). The TSPO-NOX1 axis controls phagocyte-triggered pathological angiogenesis in the eye. *Nature Communications*, *11*(1), 2709. https://doi.org/10.1038/s41467-020-16400-8

Wolf, D. M., Segawa, M., Kondadi, A. K., Anand, R., Bailey, S. T., Reichert, A. S., Bliek, A. M., Shackelford, D. B., Liesa, M., & Shirihai, O. S. (2019). Individual cristae within the same mitochondrion display different membrane potentials and are functionally independent. *The EMBO Journal*, *38*(22). https://doi.org/10.15252/embj.2018101056

Wolf, L., Bauer, A., Melchner, D., Hallof-Buestrich, H., Stoertebecker, P., Haen, E., Kreutz, M., Sarubin, N., Milenkovic, V., Wetzel, C., Rupprecht, R., & Nothdurfter, C. (2015). Enhancing Neurosteroid Synthesis – Relationship to the Pharmacology of Translocator Protein (18 kDa) (TSPO) Ligands and Benzodiazepines. *Pharmacopsychiatry*, *48*(02), 72–77. https://doi.org/10.1055/s-0034-1398507

Wolf, S. A., Boddeke, H. W. G. M., & Kettenmann, H. (2017). Microglia in Physiology and Disease. *Annual Review of Physiology*, *79*(1), 619–643. https://doi.org/10.1146/annurev-physiol-022516-034406

Wu, Y., Chen, M., & Jiang, J. (2019). Mitochondrial dysfunction in neurodegenerative diseases and drug targets via apoptotic signaling. *Mitochondrion*, *49*, 35–45. https://doi.org/10.1016/j.mito.2019.07.003

Xu, J., Zhou, Y., Yan, C., Wang, X., Lou, J., Luo, Y., Gao, S., Wang, J., Wu, L., Gao, X., & Shao, A. (2022). Neurosteroids: A novel promise for the treatment of stroke and post-stroke complications. *Journal of Neurochemistry*, *160*(1), 113–127. https://doi.org/10.1111/jnc.15503

Yan, Y., Shin, S., Jha, B. S., Liu, Q., Sheng, J., Li, F., Zhan, M., Davis, J., Bharti, K., Zeng, X., Rao, M., Malik, N., & Vemuri, M. C. (2013). Efficient and rapid derivation of primitive neural stem cells and generation of brain subtype neurons from human pluripotent stem cells. *Stem Cells Translational Medicine*, *2*(11), 862–870. https://doi.org/10.5966/sctm.2013-0080

Yang, D., Ying, J., Wang, X., Zhao, T., Yoon, S., Fang, Y., Zheng, Q., Liu, X., Yu, W., & Hua, F. (2021). Mitochondrial Dynamics: A Key Role in Neurodegeneration and a Potential Target for Neurodegenerative Disease. *Frontiers in Neuroscience*, *15*, 654785. https://doi.org/10.3389/fnins.2021.654785

Yao, R., Pan, R., Shang, C., Li, X., Cheng, J., Xu, J., & Li, Y. (2020). Translocator Protein 18 kDa (TSPO) Deficiency Inhibits Microglial Activation and Impairs Mitochondrial Function. *Frontiers in Pharmacology*, *11*, 986. https://doi.org/10.3389/fphar.2020.00986

Yépez, V. A., Kremer, L. S., Iuso, A., Gusic, M., Kopajtich, R., Koňaříková, E., Nadel, A., Wachutka, L., Prokisch, H., & Gagneur, J. (2018). OCR-Stats: Robust estimation and statistical testing of mitochondrial respiration activities using Seahorse XF Analyzer. *PLOS ONE*, *13*(7), e0199938. https://doi.org/10.1371/journal.pone.0199938

Yilmaz, C., Karali, K., Fodelianaki, G., Gravanis, A., Chavakis, T., Charalampopoulos, I., & Alexaki, V. I. (2019). Neurosteroids as regulators of neuroinflammation. *Frontiers in Neuroendocrinology*, *55*, 100788. https://doi.org/10.1016/j.yfrne.2019.100788

Yoo, K.-S., Lee, K., Oh, J.-Y., Lee, H., Park, H., Park, Y. S., & Kim, H. K. (2019). Postsynaptic density protein 95 (PSD-95) is transported by KIF5 to dendritic regions. *Molecular Brain*, *12*(1), 97. https://doi.org/10.1186/s13041-019-0520-x

Zapico, S. (2013). MtDNA Mutations and Their Role in Aging, Diseases and Forensic Sciences. *Aging and Disease*, *4*(6), 364–380. https://doi.org/10.14336/AD.2013.0400364

Zhang, D., Man, D., Lu, J., Jiang, Y., Ding, B., Su, R., Tong, R., Chen, J., Yang, B., Zheng, S., Chen, D., & Wu, J. (2023). Mitochondrial TSPO Promotes Hepatocellular Carcinoma Progression through Ferroptosis Inhibition and Immune Evasion. *Advanced Science*, *10*(15), 2206669. https://doi.org/10.1002/advs.202206669

Zhang, H., Wang, H., Gao, F., Yang, J., Xu, Y., Fu, Y., Cai, M., Zhang, X., Yang, Q., Tong, K., Hu, Y., Chen, H., Ma, C., He, W., & Zhang, J. (2021). TSPO deficiency accelerates amyloid pathology and neuroinflammation by impairing microglial phagocytosis. *Neurobiology of Aging*, *106*, 292–303. https://doi.org/10.1016/j.neurobiolaging.2021.06.020

Zhang, L.-M., Zhao, N., Guo, W.-Z., Jin, Z.-L., Qiu, Z.-K., Chen, H.-X., Xue, R., Zhang, Y.-Z., Yang, R.-F., & Li, Y.-F. (2014). Antidepressant-like and anxiolytic-like effects of YL-IPA08, a potent ligand for the translocator protein (18 kDa). *Neuropharmacology*, *81*, 116–125. https://doi.org/10.1016/j.neuropharm.2013.09.016

Zhang, S., Rao, S., Yang, M., Ma, C., Hong, F., & Yang, S. (2022). Role of Mitochondrial Pathways in Cell Apoptosis during He-Patic Ischemia/Reperfusion Injury. *International Journal of Molecular Sciences*, *23*(4), 2357. https://doi.org/10.3390/ijms23042357

Zhang, X., Huang, C. T., Chen, J., Pankratz, M. T., Xi, J., Li, J., Yang, Y., LaVaute, T. M., Li, X.-J., Ayala, M., Bondarenko, G. I., Du, Z.-W., Jin, Y., Golos, T. G., & Zhang, S.-C. (2010). Pax6 Is a Human Neuroectoderm Cell Fate Determinant. *Cell Stem Cell*, *7*(1), 90–100. https://doi.org/10.1016/j.stem.2010.04.017

Zhang, Z., Yang, D., Zhou, B., Luan, Y., Yao, Q., Liu, Y., Yang, S., Jia, J., Xu, Y., Bie, X., Wang, Y., Li, Z., Li, A., Zheng, H., & He, Y. (2022). Decrease of MtDNA copy number affects mitochondrial function and involves in the pathological consequences of ischaemic stroke. *Journal of Cellular and Molecular Medicine*, *26*(15), 4157–4168. https://doi.org/10.1111/jcmm.17262

Zick, M., Rabl, R., & Reichert, A. S. (2009). Cristae formation—Linking ultrastructure and function of mitochondria. *Biochimica et Biophysica Acta (BBA) - Molecular Cell Research*, *1793*(1), 5–19. https://doi.org/10.1016/j.bbamcr.2008.06.013

Zorova, L. D., Popkov, V. A., Plotnikov, E. Y., Silachev, D. N., Pevzner, I. B., Jankauskas, S. S., Babenko, V. A., Zorov, S. D., Balakireva, A. V., Juhaszova, M., Sollott, S. J., & Zorov, D. B. (2018). Mitochondrial membrane potential. *Analytical Biochemistry*, *552*, 50–59. https://doi.org/10.1016/j.ab.2017.07.009

Zwain, I. H., & Yen, S. S. C. (1999). Neurosteroidogenesis in Astrocytes, Oligodendrocytes, and Neurons of Cerebral Cortex of Rat Brain. *Endocrinology*, *140*(8), 3843–3852. https://doi.org/10.1210/endo.140.8.6907

Appendix

List of abbreviations

ACBD3	acyl-CoA binding domain-containing protein 3
ADP	adenosine diphosphate
ALS	Amyotrophic Lateral Sclerosis
AMP	adenosine monophosphate
AP1	activator protein 1
ATAD3A	ATPase family AAA domain-containing protein 3A
ATP	adenosine triphosphate
B2M	beta-2-microglobulin
BCA	bichinoic acid
BDNF	brain-derived neurotrophic factor
cAMP	cyclic AMP
Cas9	CRISPR-associated protein 9
CBR	central benzodiazepine receptor
CNS	central nervous system
CoA	coenzyme A
CRAC	cholesterol recognition amino acid consensus
CRISPR	clustered regularly interspaced short palindromic repeats
CTRL	control
Cyt	cytochrome
DHEA	dehydroepiandrosterone
DNA	desoxiribonucleic acid
DRP1	dynamin-related protein 1
e^-	electron
ECAR	extracellular consumption rate
EM	electron microscopy
EMRE	essential MCU regulator
ERK	extracellular signal-regulated kinase
ER	endoplasmic reticulum
ETC	electron transport chain
ETS	V-ets erythroblastosis virus E26 oncogene homologue
$FAD^+/FADH_2$	flavin adenine dinucleotide
FAO	fatty acid oxidation
FCCP	carbonyl cyanide-*4*-(trifluoromethoxy)phenylhydrazone
FCS	fetal calf serum
Fig	figure
FIS1	mitochondrial fission 1 protein
$GABA_A$	gamma-aminobutric-acid type A
GPx	glutathione peroxidase
GTP	guanosintripohosphate
GTPase	GTPase activating protein
H^+	proton

H_2O	water
H_2O_2	hydrogen peroxide
HCX	H^+/Ca^{2+} exchanger
hiPSC	human induced pluripotent stem cell
HPA axis	Hypothalamus-Pituitary-Adrenal axis
H-strand	heavy strand
IMM	inner mitochondrial membrane
IMS	intermembrane space
KO	knockout
LC3	microtubule-associated protein 1A/1B-light chain 3
LC3B-II	LC3B-phosphatidylethanolamine conjugate
LPS	lipopolysaccharide
L-strand	light strand
MAM	mitochondria-associated membrane
MAPK	mitogen-activated protein kinase
MCU_{CX}	MCU holocomplex
MCU	mitochondrial Ca^{2+} uniporter
MCUR1	MCU regulator 1
MDD	Major Depressive Disorder
MFF	mitochondrial fission factor
MFN1/2	mitofusin 1/2
MICU	mitochondrial Ca^{2+} uptake protein
MID49/51	mitochondrial dynamics proteins of 49 and 51 kDa
MMP/Δψm	mitochondrial membrane potential
mPTP	mitochondrial permeability transition pore
mRNA	messenger RNA
mtDNA	mitochondrial DNA
mt	mitochondrial
mtSSB	mitochondrial single-stranded DNA-binding protein
MW	Mann-Whitney U test
Mt-TL1	mitochondrially encoded tRNA leucine 1
NAD^+/NADH	nicotinamide adenine dinucleotide
NCLX	$Na^+/Ca^{2+}/Li^+$ exchanger
NMDA	*N*-Methyl-D-aspartic acid
NOX	NADPH oxidase
NPC	neural progenitor cell
NRF1/NRF2	nuclear respiratory factor 1/2
O_2	oxygen
O_2^-	superoxide
OCR	oxygen consumption rate
O_H	origin of the H-strand
O_L	origin of the L-strand
OMM	outer mitochondrial membrane
OPA1	optic atrophy protein 1
OXPHOS	oxidative phosphorylation

P450scc	cytochrome P450/cholesterol side-chain cleavage enzyme
p62/SQSTM1	ubiquitin-binding protein p62/sequestosome-1
PBMC	peripheral blood mononuclear cell
PBR	peripheral-type benzodiazepine receptor
PBS	phosphate buffered saline
PET	positron emission tomography
P_i	phosphate
PPIX	protoporphyrin IX
PKA	protein kinase A
PKCε	protein kinase C epsilon type
Q	ubiquinone/ubiquinol
PFA	paraformaldehyde
PGC-1α	proliferator-activated receptor γ co-activator 1α
pH	potential of hydrogen
PINK	PTEN-induced putative protein kinase 1
POLγ	DNA polymerase γ
PTEN	phosphatase and tensin homologue
RET	reverse electron transport
RNA	ribonucleic acid
ROS	reactive oxygen species
rRNA	ribosomal RNA
qRT-PCR	quantitative real-time polymerase chain reaction
SEM	standard error of the mean
SINE B2	seven intron-based short interspersed repetitive elements B2
SOD	superoxide dismutase
SP	specificity proteins
StAR	steroidogenic acute regulatory protein
STAT3	signal transducer and activator of transcription 3
TCA	tricarboxylic acid cycle
TFAM	mitochondrial transcription factor A
TM	transmembrane domain
TNF	tumour necrosis factor
tRNA	transfer RNA
TSPO	translocator protein 18 kDa
TWINKLE	twinkle mtDNA helicase
Ub	ubiquitin
UCP	uncoupling protein
VDAC	voltage-dependent anion channel

List of units

%	percentage
A	Ampere
°C	degree Celcius
Da	Dalton
g	gram
h	hour
min	minute
s	second
L	liter
m	meter
M	molar concentration in mol L^{-1}
mol	mole
rpm	rounds per minute
t	timer
T	temperature
V	volt

List of dimensions

k	kilo (10^{3})
m	milli (10^{-3})
µ	micro (10^{-6})
n	nano (10^{-9})
p	pico (10^{-12})

List of figures

List of tables

Acknowledgements

Ohne die Unterstützung und Ermutigung meiner Kollegen, Freunde und Familie hätte ich meine Promotion nicht abschließen können, und dafür bin ich unendlich dankbar.

Mein besonderer Dank gilt dabei meinem Doktorvater Prof. Dr. Christian Wetzel. Lieber Christian, vielen Dank, dass du mir erneut die Möglichkeit gegeben hast Teil deines wunderbaren Teams zu sein. Trotz der anfänglichen Schwierigkeiten hast du nie aufgehört an mich und meine Fähigkeiten zu glauben. Danke für all deine Unterstützung, Ratschläge und das entgegengebrachte Vertrauen. Ohne dich und deine Begeisterung für die Wissenschaft wäre diese Arbeit nicht das, was sie heute ist.

Ein großer Dank geht auch an Prof. Dr. Peter Hau für die bereitwillige Übernahme des Zweitgutachtens und Prof. Dr. Richard Warth für die Übernahme des Prüfungsvorsitzes. Bedanken möchte ich mich auch bei Prof. Dr. Oliver Bosch und PD Dr. Markus Reichold, die ebenfalls Teil meiner Prüfungskommission sind, sowie bei Prof. Dr. Rainer Rupprecht als Leiter des Lehrstuhls für Psychiatrie und Psychotherapie.

Ein herzliches Dankeschön geht an meine Kollegen der AG Wetzel, AG Nothdurfter und AG Di Benedetto, die mich auf diesem Weg begleitet haben, insbesondere an Dr. Vladimir Milenkovic, Tatjana Jahner, Iseline Cardon, Doris Melchner und Anett Dörfelt, die nicht nur Kollegen, sondern Freunde geworden sind.
Ihr seid ein tolles Team – bleibt so wie ihr seid, ich werde euch vermissen!
Danke, Vladi, für die Weitergabe deiner technischen und wissenschaftlichen Expertise, aber auch für deinen Humor, die Ermutigungen und Ratschläge.
Liebe Tati, vielen Dank für alles, was ich von dir lernen durfte, für jede Unterstützung und deine absolute Hilfsbereitschaft.
Vielen Dank liebe Doris und liebe Anett für euer unbezahlbares Engagement und für die unzählige Hilfe mit all den ELISAs, Western Blots, qPCRs und den administrativen Schwierigkeiten.
Dir, liebe Iseline, möchte ich herzlich danken. Du hast mich während unserer gemeinsamen Promotionszeit stets unterstützt und bist mir eine echte Freundin geworden. Dein fachlicher Rat, deine aufmunternden Worte und unsere zahlreichen Gespräche und Diskussionen haben mir geholfen die Herausforderungen dieser Promotion zu meistern.

Ein besonderer Dank geht an meinen Partner Simon. Danke für deine Liebe, dein Vertrauen und deine Geduld. Aber auch vielen Dank an deine Familie für ihre Unterstützung und vor allem die gute Verpflegung.

Zu guter Letzt möchte ich mich von ganzem Herzen bei meiner Familie bedanken, die mich immer bedingungslos unterstützt hat. Danke für euren Rückhalt, eure Ermutigungen und eure Liebe. Danke, dass ihr immer für mich da seid!